

TECHNISCHE UNIVERSITÄT MÜNCHEN

Lehrstuhl für Biotechnologie

Chaperone mechanism of the small heat shock protein Hsp26

Titus Marcellus Franzmann

Vollständiger Abdruck der von der Fakultät für Chemie der Technischen Universität München zur Erlangung des akademischen Grades eines

Doktors der Naturwissenschaften

genehmigten Dissertation.

Vorsitzender: Univ.-Prof. Dr. Horst Kessler

Prüfer der Dissertation:

1. Univ.-Prof. Dr. Johannes Buchner
2. Univ.-Prof. Dr. Thomas Kiefhaber
3. Univ.-Prof. Dr. Matthias Rief

Die Dissertation wurde am 20.05.2008 bei der Technischen Universität München eingereicht und durch die Fakultät für Chemie am 18.08.2008 angenommen.

To those who I love

1 Summary / Zusammenfassung

Die biologisch aktive dreidimensionale Struktur von Proteinen ist sensibel auf Änderungen der Umgebungstemperatur. Unter Hitzeschock können viele Proteine ihre natürliche Struktur verlieren und werden in eine für Proteinaggregation anfällige Konformation überführt. Eine Erhöhung der Außentemperatur stellt demnach eine Bedrohung für alle Lebewesen dar. Um der Proteinaggregation in der Zelle entgegenzuwirken, nehmen Zellen Temperaturunterschiede autonom wahr und antworten auf Hitzestress mit der Expression von Hitzeschockgenen. Die Produkte dieser Hitzeschockantwort sind die Hitzeschockproteine (Hsps), von denen viele als molekulare Chaperone identifiziert wurden. Molekulare Chaperone erkennen nicht-native Proteinstrukturen, binden diese spezifisch und verhindern durch Ausbildung eines Chaperon-Substrate-Komplexes Proteinaggregation. Viele Chaperone binden und hydrolysieren ATP. Die freiwerdende Energie wird oft dazu verwendet, das Chaperon von einem hochaffinen in einen niederaffinen Zustand für das Substrate zu überführen und somit die Substratfreisetzung zu ermöglichen.

Kleine Hitzeschockproteine (engl. small heat shock proteins, sHsps) sind molekulare Chaperone. sHsps binden entfaltete Proteine, bilden mit diesen stabile Substratkomplexe und verhindern so deren Aggregation. Im Gegensatz zu den ATP-abhängigen Chaperonklassen binden und hydrolysieren sHsps kein ATP. Ihre Aktivität wird durch andere Strategien, wie z.B. durch Hitze, oder

Veränderungen des zellulären Redoxpotentials reguliert. Ein Vertreter der temperaturkontrollierten sHsps ist Hsp26 aus der Bäckerhefe.

Hsp26 ist das generelle kleine Hitzeschockprotein in der Bäckerhefe, *Saccharomyces cerevisiae*. Strukturuntersuchungen haben gezeigt, dass Hsp26 Homooligomere aus 24 Untereinheiten bildet, die sich zu einer ca. 600 kDa Hohlkugel zusammenlagern. Sequenzvergleiche zwischen sHsps haben gezeigt, dass sich die Hsp26 Domänenstruktur aus einer N-terminalen Domäne, einer einzigartigen Mitteldomäne, der strukturell konservierten α -Kristallindomäne und einer C-terminalen Extension zusammensetzt. Biochemische Analysen haben gezeigt, dass die N-terminale Region von sHsps generell eine wichtige Funktion für die Substraterkennung darstellt. Dies konnte ebenfalls für Hsp26 gezeigt werden. Eine Hsp26 Variante, der die ersten 30 Aminosäuren fehlen, wies reduzierte Chaperonaktivität auf und eine Variante, der die ersten 95 Reste fehlten war chaperoninaktiv. Während die α -Kristallindomäne sowie die C-terminale Extension verantwortlich für die Oligomerisierung von Hsp26 sind, war die Funktion der Mitteldomäne bislang unbekannt.

Eine Besonderheit von Hsp26 ist, dass es autonom Temperaturänderungen wahrnehmen kann und seine Chaperonaktivität temperaturabhängig ist. Erst unter Hitzeschockbedingungen, z.B. 45°C, ist Hsp26 in der Lage die Aggregation von Substraten zu verhindern, während es bei 25°C die Substrataggregation nicht unterdrückt. Mechanistische Untersuchungen haben gezeigt, dass die Temperaturaktivierung der Hsp26-Chaperonfunktion gleichzeitig die Oligomerstabilität herabsetzt. In analytischen Gelfiltrationsexperimenten konnte gezeigt werden, dass die temperatur-induzierte Destabilisierung der Oligomere zur Dissoziation in Dimere führt. Gleichzeitig haben elektronenmikroskopische Untersuchungen gezeigt, dass Hsp26-Substratkomplexe grundsätzlich eine andere Struktur aufwiesen als Hsp26 in Abwesenheit von Substraten. Diese

Beobachtungen haben zu einem mechanistischen Model geführt, in dem das Hsp26 Oligomer eine Speichergruppe darstellt, die unter Hitzeschock in aktive Dimere dissoziiert. Diese Dimere binden entfaltete Substrate Moleküle und reassoziieren zu Hsp26-Substrate-Komplexen. Die mechanistischen Details dieses Regulationsprinzips blieben jedoch bislang ungeklärt.

Um weitere Details über den Hsp26 Chaperonmechanismus zu erlangen, wurden der Hsp26 Temperaturaktivierungsmechanismus und die damit verbundenen temperatur-induzierten Strukturänderungen thermodynamisch und kinetisch untersucht. Dazu wurden Hsp26 Varianten hergestellt, die sich spektroskopisch vom Wildtyp (wt) Protein unterschieden. Zum einen wurden Hsp26 Cysteinvarianten hergestellt, in denen jeweils ein Serinrest in der N-terminalen Domäne (Hsp26S4C), Mitteldomäne (Hsp26S82C) sowie in der C-terminalen Extension (Hsp26S210C) durch Cystein ersetzt wurde. Desweiteren wurden Tryptophanvarianten hergestellt, bei denen das Tryptophan der Mitteldomäne (W72) und das der C-terminalen Extension (W211) durch Tyrosin ersetzt wurden.

Redoxanalysen haben gezeigt, dass Hsp26S4C und Hsp26S210C, jedoch nicht wt Hsp26 und Hsp26S82C, Disulfidbrücken bilden können. Die Ausbildung von Disulfidbrücken zwischen den N-terminalen Domänen, sowie den C-terminalen Extensionen innerhalb eines Oligomers hatte weder Einfluss auf die Sekundär- oder Tertiärstruktur noch auf die thermodynamische Stabilität. Jedoch wurden die Oligomere durch die Ausbildung von Disulfidbrücken zwischen Untereinheiten innerhalb eines Oligomers signifikant stabilisiert, so dass eine Dissoziation in Dimere nicht mehr beobachtet wurde. Untersuchungen zur Dynamik der Oligomere zeigten, dass wt Hsp26 in wässriger Lösung kontinuierlich Untergruppen austauscht, dieser Austausch jedoch vollständig inhibiert wurde, wenn die Oligomere durch Disulfidbrücken kovalent verknüpft

wurden. Interessanterweise war die Chaperonaktivität dieser kovalent verknüpften Hsp26 Varianten unbeeinträchtigt. Weder die Effizienz noch die Temperaturabhängigkeit der Chaperonfunktion waren verändert. Diese Experimente korrigierten das bislang gängige Arbeitsmodell und zeigten eindeutig, dass weder die Dissoziation in Dimere noch die Fähigkeit Untergruppen austauschen zu können essentielle Schritte im Hsp26 Aktivierungsmechanismus darstellen. Vielmehr konnte gezeigt werden, dass eine intrinsische Konformationsänderung innerhalb des Hsp26 Oligomers zur Aktivierung seiner Chaperonfunktion führt.

Um diese Konformationsänderung in einem weiteren mechanistischen Detail zu untersuchen, wurden die Hsp26 Cysteinvarianten mit Fluoreszenzfarbstoffen modifiziert und mittels Fluoreszenz-Resonanz-Energie-Transfer (FRET) untersucht. Bei FRET wird die Energie eines angeregten Donorchromophors auf einen in der Nähe befindlichen Akzeptorchromophor strahlenlos übertragen. Dieser Prozess ist Distanzabhängig und ermöglicht so die Entfernungsmessung zwischen zwei Domänen. Die starke Distanzabhängigkeit macht FRET zu einem sensitiven spektroskopischen Werkzeug, das besonders gut geeignet ist, relative Änderungen zu beobachten. So konnte unter Verwendung der Einzelcysteinvarianten eine Serie von unterschiedlich gelabelten Hsp26 Oligomeren hergestellt werden und ermöglichte so eine ortsspezifische Strukturanalyse von inaktivem und chaperonaktivem Hsp26 mittels FRET. Interessanterweise hatte die Temperaturaktivierung von Hsp26 wenig Einfluss auf die FRET Effizienz zwischen N-terminal und C-terminal gelabelten Hsp26 Molekülen. Wenn Hsp26, das an der Mitteldomäne gelabelt war, untersucht wurde, änderten sich die FRET Effizienz jedoch deutlich. Gleichmaßen änderte sich auch die FRET Effizienz, wenn spektroskopische Heterooligomere, bestehend aus Mitteldomänen gelabelten Protein mit N- oder C-terminal

gelabeltem Protein, gemessen wurden. Dies zeigt, dass sich spezifisch die Konformation der Mitteldomäne, nicht jedoch die der anderen Bereiche von Hsp26, temperaturabhängig ändert. Die kinetische Analyse der Konformationsänderung sowie der Chaperonaktivität ermöglichte die Bestimmung der Energiebarriere, die inaktives Hsp26 von aktivem trennt. Dabei ist klar geworden, dass die Mitteldomäne ihre Konformation temperaturabhängig verändert und dadurch Hsp26 vom seinem inaktiven in den chaperonaktiven Zustand überführt. Die Ergebnisse dieser Arbeit zeigen, dass die Hsp26 Mitteldomäne ein Thermosensor und der intrinsische Regulator der Hsp26 Chaperonaktivität ist. Eine große Energiebarriere ermöglicht dabei, dass Hsp26 bei niedrigen Temperaturen seine inaktive Konformation einnehmen kann und unter Hitzeschock schnell und unabhängig von anderen Faktoren aktiviert wird.

<u>1</u>	<u>Summary / Zusammenfassung</u>	<u>5</u>
<u>2</u>	<u>Introduction</u>	<u>17</u>
2.1	Protein folding and molecular chaperones	17
2.2	Molecular chaperones	20
2.3	Hsp60 chaperones	22
2.4	Hsp70 chaperones	25
2.5	Hsp90 chaperones	28
2.6	Hsp100 chaperones	31
2.7	Small heat shock proteins (sHsps)	34
2.7.1	The structure of sHsps	36
2.7.2	Chaperone function of sHsps	39
2.7.3	Regulation of the heat shock response and sHsp chaperone function	43
2.7.4	Hsp26 is a sHsp from <i>S. cerevisiae</i>	46
2.8	Objective	50

3.1	Strains	53
3.2	Vectors and Plasmids	54
3.3	Chemicals	57
3.4	Fluorophores	58
3.5	Size and molecular mass standard kits	59
3.6	Proteins	59
3.7	Antibodies	59
3.8	Chromatography	60
3.9	Additional materials	61
3.10	Media and antibiotics	61
3.11	Buffers for molecular biological methods	62
3.12	Buffers for protein chemical methods	62
	3.12.1 Buffers for purification of Hsp26	63
3.13	Devices	64
	3.13.1 Absorptions spectrophotometer	64
3.14	Circular dichroism spectropolarimeter	64
3.15	Fluorescence Spectrophotometer	64
3.16	Analytical ultracentrifuge	65
3.17	Chromatography devices	65
3.18	HPLC devices	65
3.19	Gel electrophoresis und blotting devices	66
3.20	Scales	66
3.21	Centrifuges	66
3.22	Additional devices	67
3.23	Computer programs	68

3.24	Molecular methods	69
3.24.1	Cultivation and storage of <i>E. coli</i>	69
3.24.2	Cultivation and storage of <i>S. cerevisiae</i>	69
3.24.3	Amplification and cloning of Hsp26 variants	70
3.25	Protein chemical methods	76
3.25.1	SDS polyacrylamid gel electrophoresis	76
3.25.2	Western blotting	77
3.26	Purification of Hsp26	77
3.27	Spectroscopy	80
3.27.1	Absorbance spectroscopy (UV-VIS)	80
3.27.2	Fluorescence spectroscopy (FL)	81
3.27.3	Circular dichroism spectroscopy (CD)	82
3.27.4	Thermal unfolding and refolding of Hsp26	84
3.27.5	Chemical unfolding and refolding of Hsp26	85
3.27.6	Kinetic analysis of temperature-induced changes in Hsp26	85
3.27.7	Fluorescence quenching	87
3.27.8	Fluorescence resonance energy transfer (FRET)	88
3.27.9	Subunit exchange (SX)	94
3.28	Analytical gel filtration (SEC-HPLC)	94
3.29	Sedimentation equilibrium analytical ultracentrifugation (SE)	95
3.30	Sedimentation velocity analytical ultracentrifugation (SV)	97
3.31	Dynamic light scattering (DLS)	99
3.32	Chaperone assays	101
3.32.1	Thermal-induced aggregation of citrate synthase (CS)	101
3.32.2	Thermal-induced aggregation of glutamate dehydrogenase (GDH)	101
3.32.3	Aggregation of chemically denatured CS	102
3.32.4	Aggregation of chemically denatured GDH	102

4.1	wt Hsp26 and Hsp26 variants	103
4.2	Redox analysis of Hsp26	108
4.3	Secondary structure analysis by CD spectroscopy	110
4.3.1	Secondary structure analysis	110
4.3.2	Temperature-induced secondary structure changes	113
4.4	Tertiary structure analysis of Hsp26	117
4.4.1	Tertiary structure analysis by near UV CD spectroscopy	117
4.4.2	Tertiary structure analysis by fluorescence	121
4.5	Quaternary structure of Hsp26	125
4.5.1	Quaternary structure analysis by analytical gel filtration	125
4.5.2	Quaternary structure analysis by dynamic light scattering	128
4.5.3	Quaternary structure analysis by analytical ultracentrifugation	131
4.5.4	Species distribution of inactive and chaperone-active Hsp26	134
4.6	Site-specific conformational changes upon Hsp26 temperature activation	139
4.6.1	Topology changes monitored by FRET	139
4.6.2	Conformational changes monitored by fluorescence quenching	144
4.7	Kinetic analysis of the temperature-induced structural changes in Hsp26	145
4.7.1	Kinetic analysis of temperature-induced structural changes	146
4.7.2	Kinetic analysis of the Hsp26 subunit exchange (SX)	152
4.7.3	Influences of salt on the kinetics of structural changes and subunit exchange	157
4.8	Chaperone activity of Hsp26	160
4.9	Kinetic analysis of Hsp26 chaperone activation	165
4.10	Hsp26 in the Cell – Simulating molecular crowding	170

<u>5</u>	<u>Discussion</u>	<u>175</u>
5.1	Structural changes	176
5.2	The middle domain changes its conformation upon temperature shift	180
5.3	A large energy barrier controls the chaperone activity of Hsp26	182
5.4	Subunit exchange of Hsp26	185
5.5	Hypothesis about substrate binding by Hsp26	188
5.6	Hsp26 in the cell	191
<u>6</u>	<u>References</u>	<u>195</u>
<u>7</u>	<u>Acknowledgments</u>	<u>219</u>
<u>8</u>	<u>Appendix</u>	<u>221</u>
8.1	Supplemental data: Structure analysis of the Hsp26 thermosensor domain	221
8.2	Supplemental data for FRET distance analysis	222
8.3	Supplemental data for fluorescence quenching	225
<u>9</u>	<u>Declaration</u>	<u>227</u>
<u>10</u>	<u>Publications</u>	<u>229</u>

2 Introduction

Proteins are polymers that are synthesized by the ribosome from activated amino acids (McQuillen et al., 1959). The linear information for the polypeptides is stored in base triplets in the genome of an organism. Transcription of the genomic DNA into complementary mRNA by mRNA-polymerase and translation of this mRNA into a chain of amino acids enable cells to synthesize proteins based on the genomic information. The product of translation is a linear polypeptide chain that has to adopt a three dimensional structure to gain biological activity. This sophisticated process is termed protein folding and its product is a folded protein structure corresponding to the “native” or “folded state”.

2.1 Protein folding and molecular chaperones

In 1972 Christian Anfinsen was awarded the Nobel Prize for demonstrating that folding of a polypeptide chain to its native state is an autonomous process. He provided the first evidence that the information of the three dimensional structure of a protein is intrinsically encoded in the amino acid sequence. In his key experiments, Anfinsen showed that chemically unfolded RNaseA can be refolded to its native state *in vitro*, demonstrating that refolding of a polypeptide chain under optimized conditions does not require extrinsic factors (Anfinsen, 1973; Anfinsen et al., 1961).

The unfolded state resembles an ensemble of conformational states with high energies and flexibility, whereas the native state of a protein usually corresponds to a single, compact structure with an energy minimum on the conformational landscape (Creighton, 1990). This difference in the energetic potential allows protein folding to occur spontaneously. During the folding process, non-covalent interactions between atoms of the protein side chains have to form specific contacts. These do not only stabilize the native structure, but also guide the folding polypeptide through its folding pathway (Figure 1). Especially hydrophobic interactions between side chains seem to play an important role (Kauzmann, 1959). Based on hydrophobic interactions, polypeptide chains can associate in polar environment. However, one distinguishes between the specific association of polypeptides to form defined oligomers and the deleterious, unspecific aggregation of polypeptides that lead to amorphous assembly forms (Figure 1). As proteins expose a considerable amount of hydrophobic residues on their way from the unfolded to the folded state, they can easily undergo non-specific interactions with each other and form non-productive structures, aggregates. Accordingly, in the native state hydrophobic residues are usually buried inside of the protein. Since association is a second- or higher-order reaction, the concentration plays an important role in determining whether aggregation or productive folding will predominate (Kiefhaber et al., 1991). For a given protein, *in vitro* the condition can be adjusted so that refolding dominates (Bosse-Doenecke et al., 2008; De Bernardez et al., 1999; Patil et al., 2008; Rudolph and Lilie, 1996; Rudolph et al., 1979; Zettlmeissl et al., 1979).

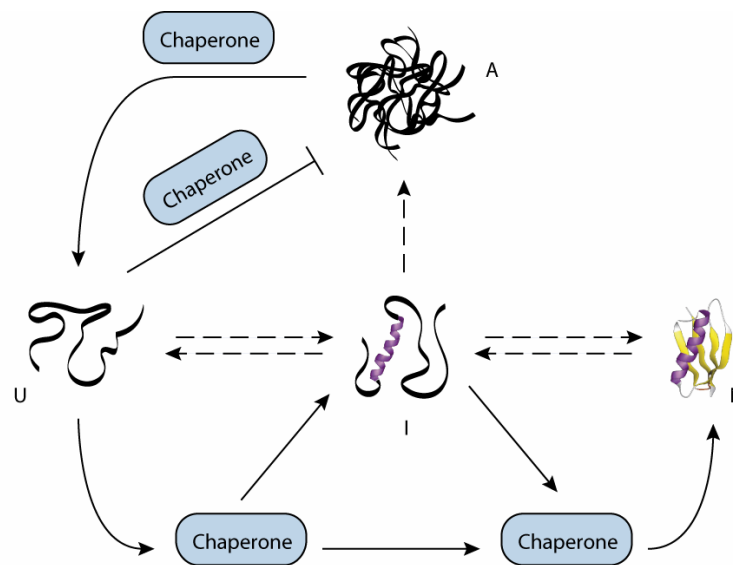


Figure 1 Schematic overview of protein folding and the interplay with molecular chaperones. U: unfolded state, I: intermediate state, N: native state, A: aggregate state of a polypeptide chain.

But *in vivo*, all proteins have to adopt their native conformation under the same set of conditions and the cellular milieu seems to be counterproductive, as the relatively high temperature and high protein concentration disfavor protein folding (Bukau et al., 2000; Gething and Sambrook, 1992; Jaenicke, 1991; Kiefhaber et al., 1991). It appears that cells have developed several strategies to avoid extensive protein aggregation. On the one hand, proteins with simple folding mechanism have been selected. On the other hand, cells express a certain set of proteins that specifically prevent non-native interactions between proteins. These proteins are collectively termed “molecular chaperones” (Lindquist, 1986; Lindquist and Craig, 1988). Like their human counterparts, molecular chaperones prevent the non-productive interaction between their clients, preventing aggregation (Bukau and Horwich, 1998; Hendrick and Hartl, 1993; Walter and Buchner, 2002). The native structure of a protein is sensitive to changes in the cellular environment. Elevated temperatures destabilize the native state and thus

proteins expose an increased amount of hydrophobic residues (Foss, 1961; Joseph and Nagaraj, 1992; Privalov et al., 1989). Molecular chaperones specifically recognize and bind to these unfolding intermediates to form chaperone-substrate-complexes and assist in protein folding (Figure 1). However, molecular chaperones do not provide information about the folding pathway of their clients, but rather isolate the polypeptide chains, thereby prevent aggregation (Walter and Buchner, 2002; Walter et al., 1996). Cells express a broad variety of molecular chaperone, many of which have been identified in response to temperature stress (Lindquist, 1981; Velazquez et al., 1980). Accordingly, many chaperones identified so far also belong to the family of heat shock proteins (HSPs).

2.2 Molecular chaperones

According to their molecular mass, molecular chaperones have been classified into five classes; Hsp100, Hsp90, Hsp70, Hsp60 and small heat shock proteins (sHsps) (Figure 2). They specifically bind to and stabilize unstable protein conformers and facilitate the proper folding of their clients (Buchner, 1996; Gething and Sambrook, 1992; Hartl, 1996). To this end, chaperones recognize structural elements that are not exposed in the native state, yet become accessible to the chaperone when the client adopts a non-native structure. Binding is often established through hydrophobic interactions (Walter and Buchner, 2002). However, many other proteins, which do not belong to the family of molecular chaperones, also expose hydrophobic areas, bind to non-native protein conformations and thus may also prevent aggregation (Beissinger and Buchner, 1998; Hendrick and Hartl, 1995). What sets chaperones apart from these scavenger proteins? Chaperones form defined chaperone-substrate-complexes.

These are established through the controlled binding and release of the substrate. To this end, chaperones switch between conformational states with different affinities for polypeptides. Binding of a substrate will stabilize the high affinity state and thus the release requires additional input of energy (Walter and Buchner, 2002). Many chaperones exploit ATP binding and hydrolysis to cycle between their functional conformations. Usually ATP hydrolysis delivers the energy to trigger substrate release. So far there is no direct evidence that ATP binding or hydrolysis is required to induce a distinct conformational change in the clients, yet it appears to be required to switch the chaperone from the high to its low affinity state and the controlled release of the bound substrate. It was shown recently that GroEL transfers unfolding force onto a trapped polypeptide (Lin et al., 2008). Yet, it is unclear, whether this feature reflects an essential step in the functional GroE chaperone cycle. One explanation might be that GroE unfolds trapped polypeptides in a first step, allowing them to escape from an energetic minimum and allowing chaperone-assisted refolding from an extended unfolded state. Beside these ATP-dependent mechanisms, other strategies have developed that trigger conformational rearrangements to switch a chaperone between its low and high affinity state. Two outstanding examples are Hsp26 from *S. cerevisiae*, a thermally-regulated chaperone, and Hsp33 from *E. coli*, which in addition to temperature, seems to be redox-regulated (Haslbeck et al., 1999; Ruddock and Klappa, 1999). In the following section, a short overview of the different classes of chaperones, their structures and their individual mechanisms is given.



Figure 2 Schematic overview of the five chaperone families. From left to right: Hsp100, Hsp90, Hsp70 with its co-chaperone Hsp40 shown in pink, Hsp60 with its co-chaperone Hsp10 shown in green, and a sHsp. Substrate polypeptides are shown in black.

2.3 Hsp60 chaperones

The *groE* genes of *E. coli* encode for the two proteins GroEL and GroES (Zeilstra-Ryalls et al., 1991). The large GroEL (57 kDa) subunit, comprises 14 subunits and forms a barrel-shaped cylinder with two open ends at both sides (Figure 3) (Braig et al., 1994; Xu et al., 1997). The two rings, each of which consists of seven GroEL molecules, are stacked together back to back, forming two separated cavities with an inner diameter of 45 Å (Braig et al., 1994). The monomer can be dissected into three distinct domains: The equatorial domains provides the connection interface of both seven-rings and all inter-subunit contacts within one ring. The domains bind and hydrolyze ATP. The apical domains are located on the outside of each side and comprise the substrate binding sites (Fenton et al., 1994). Both domains are interconnected by an intermediate domain, which serves as a hinge allowing large conformational changes that are important for the functional cycle of GroE chaperone system (Sigler and Horwich, 1995; Xu et al., 1997).

The co-chaperone GroES (11 kDa) forms dome-shaped heptamers (Hunt et al., 1996). Binding of GroES to GroEL is established through the so called “mobile loops”, a stretch of 16 amino acids that loll out of the structure (Landry et al., 1993). However, only when ATP or ADP is present in the respective equatorial domains of the GroEL subunit binding can occur (Saibil et al., 1991). Binding of

GroES to the GroEL apical domains closes the GroEL cavity thereby encapsulating the polypeptide and allowing folding inside of the cavity (Chen et al., 2001; Saibil, 2000; Saibil et al., 2001).

The GroE chaperone cycle can be divided into three steps, capture, folding and release (Thirumalai and Lorimer, 2001). In the capture step, a polypeptide is trapped on the apical domains (Elad et al., 2007). Binding of ATP to the same subunit induces a conformational rearrangement that buries the hydrophobic substrate interaction sites inside of the GroEL cylinder wall and triggers the release of the unfolded polypeptide into the folding cage (Horwich et al., 2006). At the same time, GroES binds to the apical domains via its mobile loops and closes the folding compartment. ATP hydrolysis of GroE is in the range of 15-30 seconds and sets a timer for the folding of the polypeptide inside of the folding compartment (Fenton and Horwich, 1997). Binding of ATP to the *trans*-ring induces a second conformational change that primes GroEL for the release of GroES and releases the polypeptide irrespective of its folding stage (Weissman et al., 1994). An outstanding feature of the GroE system is that substrate folding takes place in a folding cage that prevents association of polypeptides, as GroES blocks the entry.

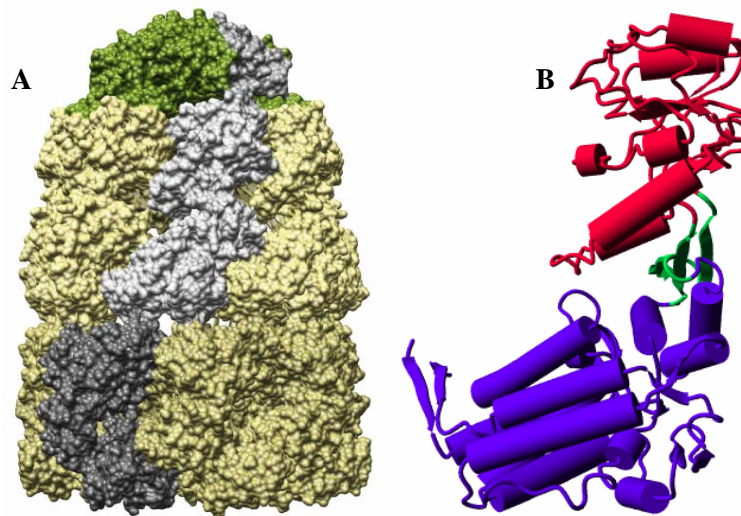


Figure 3 A: Crystal structure of the GroEL/GroES complex (Xu et al., 1997). The heptameric co-chaperone GroES (green) is bound to the apical domain of the heptameric cis-ring of the GroEL subunit (yellow). A single GroEL subunit is depicted in light grey. Shown in dark grey, a single GroEL subunit trans-ring (dark yellow) without co-chaperone. B: Structure of a single GroEL subunit. The apical domain is depicted in red, the flexible intermediate domain is depicted in green and the equatorial domain is shown in blue.

Several monomeric proteins can reach the native state during a single reaction GroE cycle (Chen et al., 2001; Elad et al., 2007). However, not all proteins have simple and fast folding mechanisms and many form oligomers. These candidates are released from GroE in a committed state that can rebind to GroE and undergo a second reaction cycle (Rye et al., 1999).

For reasons of function and homology, the class of Hsp60 chaperones can be subdivided into two classes (Horwich et al., 2007). The bacterial GroEL belongs to the class I Hsp60 chaperonins. These consist of seven subunits per ring and require co-chaperones, such as GroES. The class II chaperonins consist of eight or nine subunits per ring and do not have co-chaperones. Whereas class I chaperones are usually located in the bacterial cytosol or in eukaryotic

organelles, such as chloroplasts or mitochondria, class II chaperones are found in the eukaryotic or archeal cytosol.

2.4 Hsp70 chaperones

The Hsp70 chaperone family comprises a ubiquitous class of proteins associated with a broad variety of cellular functions, including protein synthesis, mitochondrial import, protein degradation and protein refolding after stress (Bukau and Horwich, 1998; Hartl, 1996). Alike the GroE chaperone system, the best studied member of Hsp70 chaperones is the bacterial DnaK from *E. coli* (Hartl, 1996).

Hsp70 consists of two domains, an N-terminal ATPase domain and a C-terminal substrate binding domain (Figure 4). ATP binding and hydrolysis determines the peptide binding properties of Hsp70 and switches the chaperone between its low and high affinity states (Schmid et al., 1994). In the ATP-bound state, substrate binding of Hsp70 is very dynamic and the overall affinity to substrate is low (Buchberger et al., 1995; McCarty et al., 1995). In the nucleotide-free or ADP bound state, substrate binding is less dynamic and Hsp70 exhibits high affinity for its substrates. Crystal structures of the individual domains and also of the substrate binding domain in complex with a substrate peptide bound to it, are available (Harrison et al., 1997; Zhu et al., 1996). The peptide binding domain consists of a β -sandwich covered by an α -helical domain sitting on top of it (Figure 4). In the chaperone-peptide-complex, the peptide is bound to a hydrophobic groove located within the β -sandwich (Figure 4) (Zhu et al., 1996). The α -helical domain seems to function as a lid closing the structure thereby trapping the peptide (Groemping et al., 2001; Popp et al., 2005). This “closed” structure already explains the high affinity state of Hps70, as the peptide is

trapped between the substrate binding cleft and the lid. Hsp70 preferentially binds to hydrophobic residues, peptide sequences typically found in the core of a protein, implying that a substrate protein must be considerably unfolded (Bukau and Horwich, 1998; Mayer et al., 2000; Rüdiger et al., 1997a; Rüdiger et al., 1997b).

Besides the thermodynamic affinities for unfolded polypeptides, also the binding kinetics of DnaK are important. In general, to prevent protein aggregation binding of Hsp70 to unfolded polypeptides must be at least as fast as the kinetics for aggregation. However, complex formation is limited by the slow conversion of the low affinity/ATP state to the high affinity/ADP state by ATP hydrolysis, which takes place with a rate of 0.1 s^{-1} (Gamer et al., 1996). This conversion is too slow to compete with the fast aggregation and explains why Hsp70 is not very potent in preventing protein aggregation also *in vitro* (Langer et al., 1992; Schröder et al., 1993). Thus it does not come as a surprise that DnaK functionally interacts with two co-chaperones, DnaJ and GrpE, both of which regulate the Hsp70 chaperone cycle (Langer et al., 1992; Schröder et al., 1993).

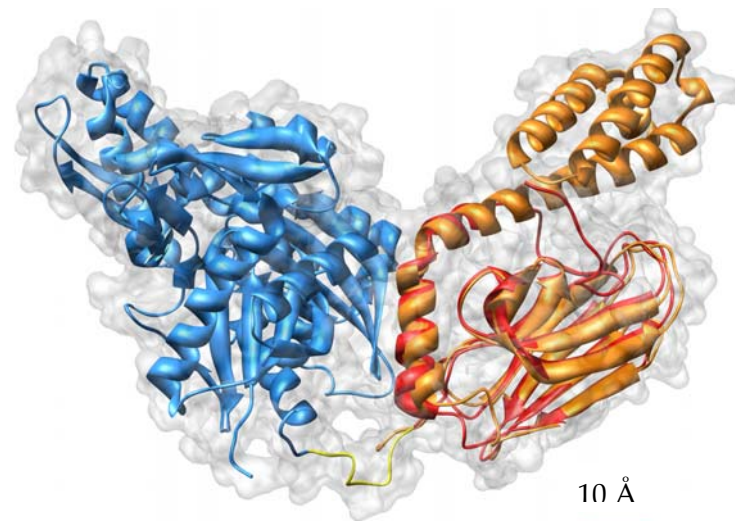


Figure 4 Structure model of Hsp70 based on the crystal structures of the N-terminal ATPase domain of bovine Hsp70 (blue) and C-terminal substrate binding domain of bovine Hsp70 (red) overlaid with the substrate binding domain of *E. coli* DnaK (orange) (Harrison et al., 1997; Zhu et al., 1996). The disordered linker connecting both subunits is depicted in yellow. Adapted from Otmar Hainzl.

DnaJ belongs to the class of Hsp40 proteins. A characteristic of these proteins is the presence of a conserved J-domain, a 75 amino acid stretch that mediates the interaction with Hsp70 (Schröder et al., 1993; Suh et al., 1998). It serves as a scavenger that prevents aggregation and delivers unfolded polypeptides to open Hsp70 substrate cleft (Schröder et al., 1993). At the same time it accelerates ATP hydrolysis and converts Hsp70 into its high affinity state, locking the peptide in the Hsp70 substrate binding domain (Liberek et al., 1991b).

The second co-chaperone, GrpE, accelerates nucleotide exchange of Hsp70 (Harrison et al., 1997; Liberek et al., 1991a). Since ATP hydrolysis is stimulated by substrate transfer from DnaJ to DnaK, Hsp70 resides in this stable high affinity/ADP state and apparently substrate release requires energy input (Walter and Buchner, 2002). GrpE exhibits high affinity to empty Hsp70, yet low affinity

for the ADP bound form (Harrison et al., 1997; Packschies et al., 1997). Binding of GrpE to Hsp70 displaces ADP and allows replacement by ATP and resets Hsp70 for a new chaperone cycle (Packschies et al., 1997).

2.5 Hsp90 chaperones

The Hsp90 chaperone system is present, yet dispensable in prokaryotes, and appears to be a complex chaperone machinery that has particularly evolved for the function in eukaryotes where it is essential (Klaus Richter, 2008). In the eukaryotic cytosol, Hsp90 interacts with a large number of co-chaperones and co-factors and is the most complex chaperone machinery known so far (Buchner, 1999; Riggs et al., 2004). The Hsp90 monomer consists of three domains, an N-terminal ATPase domain, a middle domain and a C-terminal dimerization domain (Figure 5) (Ali et al., 2006). It forms an elongated rod-like homodimer, which undergo large conformational changes during the chaperone cycle (Ali et al., 2006; Dollins et al., 2007; Phillips et al., 2007; Richter et al., 2006; Richter et al., 2008; Shiau et al., 2006). Although a large number of clients and especially co-chaperones have been identified so far, information about substrate binding and how Hsp90 co-chaperones manipulate substrate maturation remains largely unknown (Buchner, 1999; Vaughan et al., 2006). At present, it appears that Hsp90 does not play a major role in *de novo* protein folding (Walter and Buchner, 2002). In contrast to the Hsp60 and Hsp70 chaperones, substrates can also be recognized in a fairly folded state (Jakob et al., 1995; Vaughan et al., 2006). A well characterized example is the maturation of steroid hormone receptors (Pratt et al., 2004; Pratt et al., 1996). Here, the receptor adopts a collapsed, yet folded state but is unable to function as a transcription factor. However, in the presence of chaperones, the receptor becomes hormone binding-competent and exhibits

signaling activity (Dittmar and Pratt, 1997). Detailed analysis revealed that receptor maturation also requires the interaction with Hsp70 (Dittmar and Pratt, 1997). Receptor transfer from Hsp70 to Hsp90 is mediated via a ternary complex containing the partner protein Hop (Hsp organizing protein) that links both chaperone systems (Dittmar and Pratt, 1997; Wegele et al., 2004). Binding of Hsp90 to many of its co-regulators is established through its acidic C-terminal tail that binds to a specialized binding domain of the partner protein, so called tetratricopeptide repeats (TPR). An outstanding feature of these co-regulators is that many of them also function as chaperones (Bose et al., 1996). Besides HOP, also peptidyl-prolyl isomerases (PPIases) have been identified as Hsp90 partner proteins (Pratt and Toft, 1997). These catalyze the cis/trans isomerization of proline residues. However, it is so far unclear whether PPIases affect the Hsp90 or the client conformation (Pirkl and Buchner, 2001).

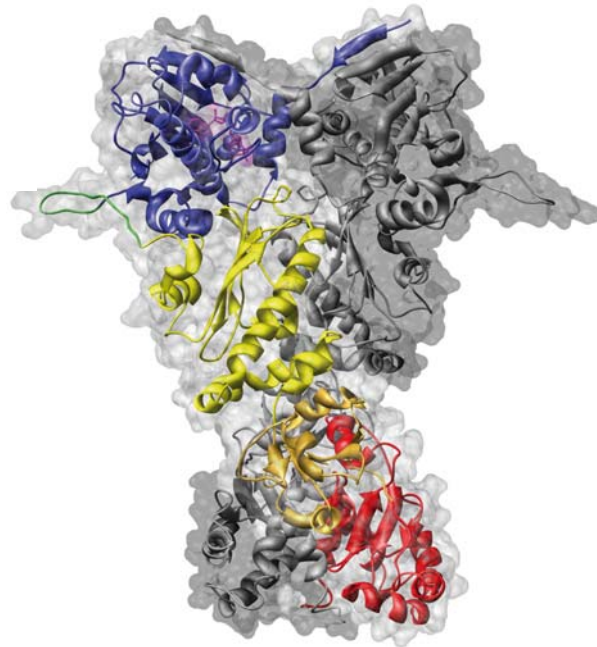


Figure 5 Crystal structure of the N-terminally closed state of *S. cerevisiae* Hsp82. N-terminal dimerization was induced by AMP-PNP binding, mimicking the ATP-bound state (Ali et al., 2006). Blue: N-terminal ATPase domain, Green: Interdomain linker connecting the ATPase domain with the middle domain, Yellow: First subdomain of the middle domain, Orange: Second subdomain of the middle domain, Red: C-terminal dimerization domain. The second protomer of the Hsp90 dimer is depicted in grey.

In yeast, an ATPase-deficient Hsp90 mutant causes lethality, demonstrating that ATP hydrolysis is essential for the Hsp90 chaperone function (Obermann et al., 1998; Panaretou et al., 1998). Recent data suggest that the ATP cycle drives its large conformational rearrangements and it is yet unclear, whether the energy is required for substrate release or its manipulation (Prodromou et al., 2000; Weikl et al., 2000).

2.6 Hsp100 chaperones

To prevent deleterious effects of stress on the proteome, cells express molecular chaperones that specifically bind to unfolded polypeptides and mediate their proper folding. But what if the extent of stress-induced protein unfolding is massive and overwhelms the chaperone systems? Protein aggregation is normally an irreversible process and apparently proteins are lost through means of aggregation. In the early 90ies it was shown that a specialized chaperone machinery reverses this fatal consequence in the cell (Parsell et al., 1994).

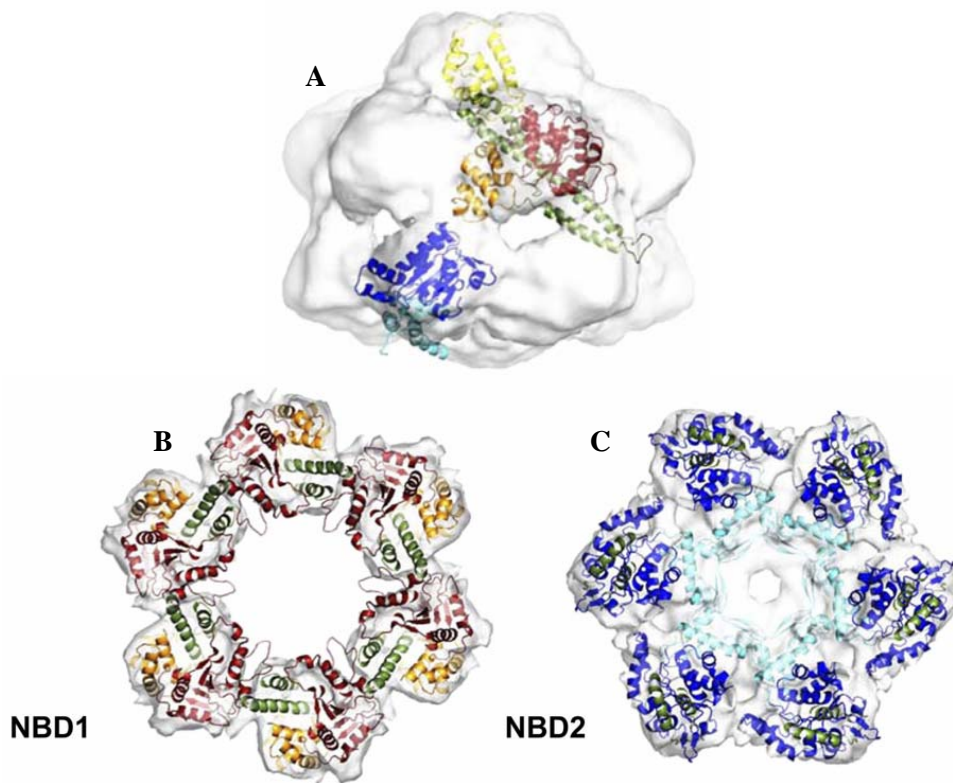


Figure 6 Cryo EM density map of the AAA+ disaggregase Hsp104 from *S. cerevisiae* (Wendler et al., 2007). A: Side view of the Hsp104 hexamer with a fitted single crystal structure subunit of the homolog ClpB from *E. coli*. Yellow: N-terminal domain, Red: NBD1 (Nucleotide binding domain1), Green: Flexible helical linker, which connects NBD1 and NBD2. Blue: NBD2, Cyan: C-terminal extension. B: Top view of the Cryo EM density map of the hexameric NBD1-ring with the fitted crystal structure of ClpB NBD1 (red/orange). The helical linker is depicted in green. C: Top view of the hexameric NBD2-ring with the fitted crystal structure of ClpB NBD2.

Members of the Hsp100 chaperone class are able to dissolve protein aggregates in an ATP-dependent manner and reestablish protein homeostasis. Two well characterized members are ClpB from *E. coli* and Hsp104 from *S. cerevisiae* (Figure 6).

Both chaperones belong to the super family of AAA+ proteins (ATPases associated with various cellular activities). Structure analysis of these and other

AAA+ proteins revealed that in general they associate into ring-shaped hexamers with a central channel (Bosl et al., 2006; Massey et al., 2006; Mogk and Bukau, 2004; Wendler et al., 2007). In the case of ClpB and Hsp104, the monomers consist of an N-terminal domain, which is postulated to establish the first contact with unfolded polypeptides, and two individual ATPase domains separated by a linker/middle domain (Haslberger et al., 2007; Wendler et al., 2007). Activity of both ATPase domains is required for the disaggregation function, yet the detailed information about the individual contribution of each ATPase domain is currently under debate (Bosl et al., 2005, 2006; Doyle et al., 2007). An essential function has been assigned to the linker domain, as its deletion from the protein cause a loss in disaggregation activity *in vivo*. Apparently, ClpB/Hsp104 act after heat shock and *in vitro* they do not efficiently prevent protein aggregation (Parsell et al., 1994). Thus it does not come as a surprise that both chaperones functionally interact with other chaperones to mediate protein refolding (Glover and Lindquist, 1998; Motohashi et al., 1999; Sanchez et al., 1993). In a current model an unfolded polypeptide is extracted from an aggregate and is threaded through the central channel (Haslberger et al., 2007; Weibezahn et al., 2004). The processed polypeptide exits the ClpB/Hsp104 in an unfolded state, well suited for the interaction with the Hsp70/Hsp40 chaperone system (Bosl et al., 2005; Schaupp et al., 2007). It is currently unclear, whether Hsp70 itself extracts polypeptides from aggregates and then feeds them to Hsp104 for further unfolding, or whether Hsp70 acts also downstream (Bosl et al., 2006). In another model, the crowbar model, aggregates are peered apart into smaller units by ClpB/Hsp104 and further processing is carried out by Hsp70 (Glover and Lindquist, 1998). Although both models are under debate, recent publications strongly support the threading model (Haslberger et al., 2007; Lum et al., 2004; Mogk et al., 2008; Schaupp et al., 2007). It could be demonstrated that the

complex of a modified ClpB protein, to which a binding site for the protease ClpP was engineered, efficiently degrades model substrates (Weibezahn et al., 2004). By electron microscopic analysis it was shown, that the protease ClpP sits at the exit tunnel of ClpB, strongly suggesting that in a first step ClpB binds to aggregates, extracts polypeptides that are subsequently thread through its central channel and handed over for degradation by ClpP (Weibezahn et al., 2004). Other chaperones that have been shown to interact with the ClpB/Hsp104 systems belong to the class of sHsps (Cashikar et al., 2005; Haslbeck et al., 2005b; Mogk et al., 2003a; Mogk et al., 2003b). These appear to incorporate into aggregates and loosen the tight packing of unfolded polypeptides. Aggregates that also include sHsps can be resolved more efficiently by ClpB/Hsp104 than pure aggregates (Cashikar et al., 2005; Haslbeck et al., 2005b; Mogk et al., 2003b). However, it is currently unclear, whether Hsp100 chaperones physically interact with the Hsp70 chaperones or sHsps or whether the cooperation with these chaperone systems is only on a functional level. Nonetheless, the emerging picture strongly suggests that all chaperone systems cooperate to some extent in a complex cellular multi-chaperone network to maintain protein homeostasis.

2.7 Small heat shock proteins (sHsps)

A deviation from the so far introduced chaperone systems constitutes the ubiquitous class of sHsps. In contrast to the other chaperone classes, sHsps are divergent and show a characteristic heterogeneity in sequence, structure and size. Their distinguishing feature is the presence of the structurally conserved α -crystallin domain in the C-terminal part of the proteins, named after the most renowned member of sHsps, the α -crystallin of the vertebrate eye lens. sHsps have been found in all kingdoms of life and many organisms express several

members in one compartment (Narberhaus, 2002). According to their cellular function as molecular chaperones, sHsps bind to non-native polypeptides and maintain them in a refolding-competent state (Figure 7).

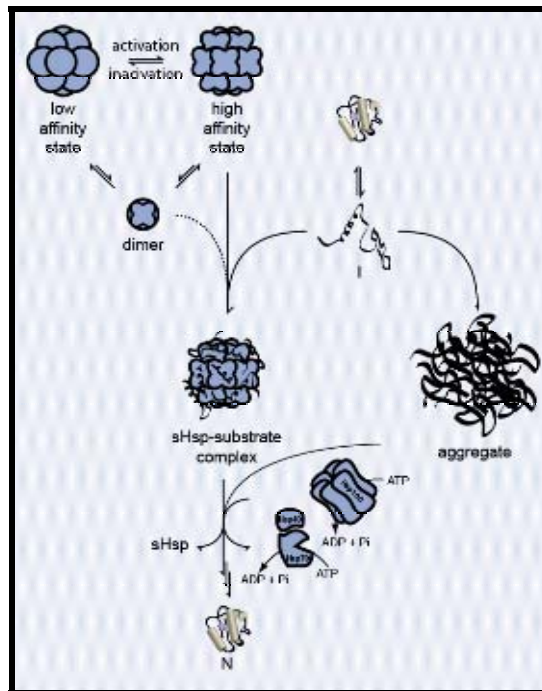


Figure 7 sHsps in the cellular multi chaperone network. Under heat shock conditions, proteins unfold and become prone to aggregation. Simultaneously, some sHsps become activated and bind to these unfolding intermediates to form stable substrate complexes, thus preventing deleterious protein aggregation. After the cell has re-entered its physiological environmental conditions, sHsp-bound polypeptides can be released and refolded by ATP-dependent chaperones, involving the Hsp100 and Hsp70/40 chaperones.

(Ehrnsperger et al., 1997b; Ehrnsperger et al., 1998; Lee et al., 1997). However, sHsps function independent from ATP binding and hydrolysis and lack refolding activity. Trapped polypeptides can be released and refolded by the cooperative interplay with ATP-dependent chaperone systems, such as Hsp70/40 system (Cashikar et al., 2005; Haslbeck et al., 2005b; Lee and Vierling, 2000; Mogk et al., 2003a; Mogk et al., 2003b). What sets sHsps apart from all other chaperone machines is that they can absorb multiple unfolded polypeptides per functional

unit at once and that their overall activity is regulated by other strategies, such as changes in the temperature or redox potential (Haslbeck et al., 1999; Jakob et al., 1999).

2.7.1 The structure of sHsps

The primary structure of sHsps consists of three distinct regions; a conserved α -crystallin domain located among a divergent N-terminal region and a moderately conserved C-terminal extension. The α -crystallin domain consists of approximately 80-100 amino acids and is located in the C-terminal part of the monomer. Phylogenetic analysis revealed that sHsps are sequence-related, yet distinct from each other. Only few amino acids within the α -crystallin domain are conserved throughout the family and form a consensus motif (A-x-x-x-n-G-v-L) at the end of the domain (Narberhaus, 2002). Although classification of sHsps relies on the α -crystallin domain, the domain itself is moderately conserved. Even between closely related organisms the domain sequence varies between 10-20% and up to 50-60% between non-related (De Jong et al., 1998). Even the closely related α -crystallins, α A and α B-crystallin from the vertebrate eye lens exhibit only 60% sequence identity. Another conserved motif is formed by the residues IXI/E located in the C-terminal extensions of many sHsps. The most divergent region of sHsps is the N-terminal part that varies strongly in sequence, amino acid composition and length. Whereas the N-terminal region of Hsp16.5 from *Methanocaldococcus jannaschii* comprises 44 amino acids, this region comprises 64 residues in α A-crystallin and 65 in α B-crystallin. Exceptionally long N-terminal regions are found in Hsp26 and Hsp42 from *S. cerevisiae*, which exhibit 95 and 213 residues, respectively.

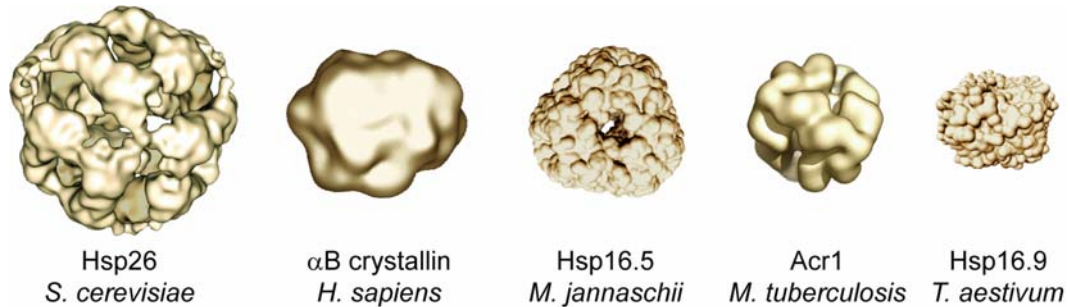


Figure 8 Structural comparison of sHsps (Haslbeck et al., 2005a). The structures for yeast Hsp26, human α B-crystallin and Acr1 from *Mycoplasmata tuberculosis* were resolved by high resolution cryo electron microscopy. The crystal structures for Hsp16.5 and Hsp16.9 were resolved by x-ray diffraction. All structures are drawn to scale.

According to their monomer molecular mass, which ranges between 10-40 kDa, sHsps are referred to as “small” heat shock proteins (Jakob et al., 1993). However, sHsps monomers selforganize to form large oligomers (Figure 8). In most cases these oligomers consist of 12 or 24 subunits and constitute large chaperones complexes with molecular mass up to the MDalton mass range. The crystal structure of the archeal Hsp16.5 from *M. jannaschii* revealed 24 subunits assembled to form a ~400 kDa shell with octahedral symmetry (Figure 9) (Kim et al., 1998). In the case of Hsp16.9 from *T. aestivum*, the 200 kDa oligomer consists of 12 subunits that form an open barrel (van Montfort et al., 2001). Recently, structures for Hsp16.3 (200 kDa) from *M. tuberculosis* and Hsp26 (600 kDa) from *S. cerevisiae* were solved by high resolution cryo electron microscopy (Kennaway et al., 2005; White et al., 2006). Both structures differ in the number of subunits and symmetry. Whereas the Hsp16.3 oligomer consists of 12 subunits and forms a shell with octahedral symmetry, the Hsp26 oligomer contains 24 subunits arranged to form a shell with tetrahedral symmetry (Kennaway et al., 2005; White et al., 2006). Furthermore, negative-stain electron microscopy on Hsp18.2

and Hsp25 revealed globular complexes with diameters of 10-25 nm, and low resolution cryo electron microscopic studies carried out on human α B-crystallin and Hsp27 revealed that these assemble into similar shaped hollow spheres (Ehrnsperger et al., 1997a; Ehrnsperger et al., 1999; Haley et al., 2000; Van Montfort et al., 2002).

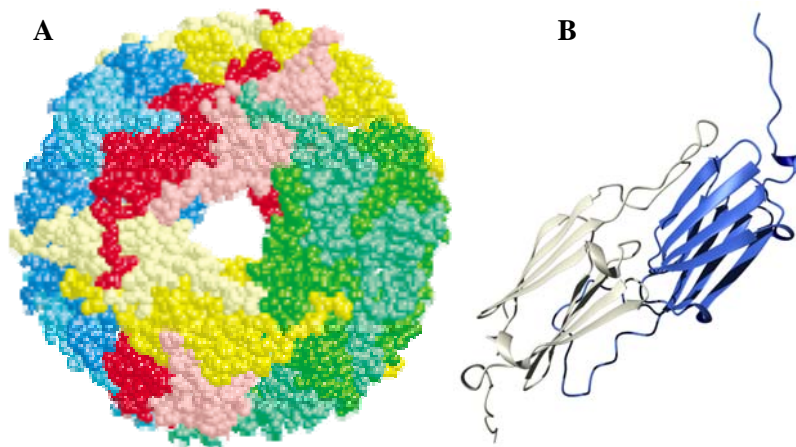


Figure 9 A: Crystal structure of the oligomeric Hsp16.5 from *M. Jannaschii* (Kim et al., 1998). The oligomer consists of 12 dimeric subunits. Each dimer is depicted in an individual color. B: Crystal structure of a dimeric subunit of Hsp16.5 with secondary structure elements. The monomers are depicted in white and blue, respectively.

All three parts of sHsps appear to be important for oligomerization. The crystal structures of Hsp16.5 and Hsp16.9 indicate that sHsp monomers associate to form anti-parallel dimers that presumably form the building block from which the oligomer is assembled (Figure 9) (Kim et al., 1998; van Montfort et al., 2001). Comparison of sHsps structures suggests that the N-terminal region protrudes into the interior of the oligomeric complexes and is important for oligomer stability. Deletion of the N-terminal region from α B-crystallin and Hsp26 resulted in dimeric protein and truncation of the N-terminal region of Hsp26 by 30 amino acids produced destabilized oligomers (Feil et al., 2001; Haslbeck et al.,

2004; Stromer et al., 2004). The assembly of a Hsp26 deletion variant lacking the first 30 amino acids and the C-terminal extension stopped on the level of a dimer, demonstrating that both terminal regions contribute to the oligomerization (Franzmann et al., 2008). A mutant of α A-crystallin lacking the last 17 amino acids was found to be sensitive to aggregation itself and truncation of the C-termini of various small heat shock proteins, including Hsp30 from *Xenopus*, pea Hsp17.7, as well as several chaperones from plants, displayed great structural anomalies (Kirschner et al., 2000; Smulders et al., 1996). Interestingly, in many cases deficiencies in oligomerization also impairs chaperone function, suggesting that selforganization of sHsps into larger complexes plays an essential role for the chaperone mechanism.

2.7.2 Chaperone function of sHsps

In vivo, protein synthesis produces 30,000 polypeptide chains per *E. coli* cell, per ribosome, within 20 min (Bukau et al., 2000). The synthesis of proteins competes with protein degradation, yet the protein concentration remains high, reaching up to 20 mg/ml (Bukau et al., 2000). An increase in ambient temperature poses a threat to any living cell, because many proteins unfold under these conditions in the cell. Temperature-induced protein unfolding causes exposition of hydrophobic residues, which are usually buried in the protein inner core, and renders proteins prone to aggregation. Molecular chaperones act on these proteins, preventing irreversible protein aggregation.

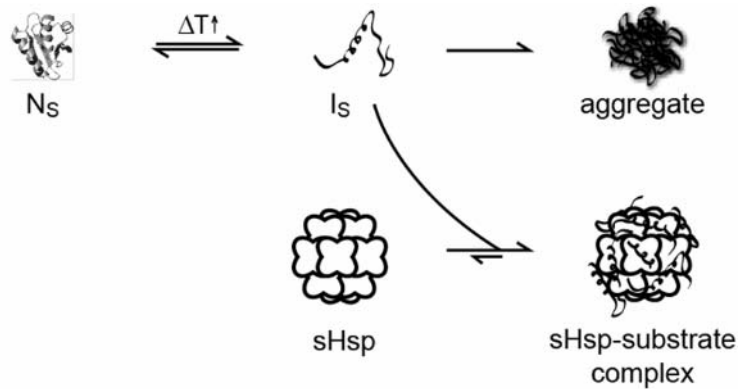


Figure 10 sHsps chaperone mechanism. An increase in ambient temperature destabilizes the native conformation of proteins and renders them prone to aggregation. sHsps bind to unfolding intermediates to form substrate complexes and hence prevent protein aggregation.

sHsps occupy a specific position in the multi-chaperone network. In contrast to all other chaperones, which keep substrates biologically active under exceptional conditions, sHsps provide shelter and host proteins until the cell re-enters physiological conditions (Figure 10). Substrates are bound in a refolding-competent state, allowing them to be reactivated by ATP-dependent chaperones (Cashikar et al., 2005; Ehrnsperger et al., 1997b; Haslbeck et al., 2005b; Lee and Vierling, 2000; Mogk et al., 2003a; Mogk et al., 2003b). Their binding efficiency is striking. While GroE accommodates one or two substrates per 14 subunits, sHsps bind multiple substrates per subunit (Hartl, 1996). Hsp16.5 was shown to bind 0.25 molecules of citrate synthase per monomer at 85°C (Lee et al., 1997). For others, substrates stoichiometries were found to be 1:2 (insulin, 5.7 kDa and α -Lactalbumin, 14 kDa), 1:8 (BSA, 66 kDa) and 1:10 (Ovotransferrin, 78 kDa), suggesting that the binding capacity is strongly correlated with the molecular mass of the substrate (Basha et al., 2004b; Lee et al., 1997; Lindner et al., 1998).

It remains to be elucidated which structural elements mediate chaperone activity. Investigations carried out on various sHsps, including sHsps from prokaryotes, plants and vertebrates, suggest that all domains contribute to the holdase

function. And oligomerization and the dynamic quaternary structure of small heat shock proteins appear to play a key role for efficient chaperone activity. The N-terminal regions of sHsps contain a high content of hydrophobic residues and a low, but significant amount of α -helical secondary structure, making them a likely site for substrate interaction (Stromer et al., 2003; Van Montfort et al., 2002; van Montfort et al., 2001). ANS-titration experiments carried out on α A- and α B-crystallin confirm that both proteins contain a high degree of hydrophobicity (Datta and Rao, 1999). At elevated temperature, both proteins displayed higher chaperone activity, coinciding with increased hydrophobicity, indicating conformational changes (Raman et al., 1995; Raman and Rao, 1997; Sun et al., 1997). Substitution of two conserved Phe residues in the N-terminus of pea Hsp18.1 caused a total loss of chaperone activity without affecting its quaternary structure and deleting the first 30 amino acids of yeast Hsp26 diminished its chaperone activity, coinciding with loss of hydrophobicity and few α -helical elements (Haslbeck et al., 2004; Plater et al., 1996). Strong evidence for a role of the N-terminal region in substrate binding came from single point mutants of Hsp16.6 from *Synechocystis spec.* generated by random mutagenesis that fail to mediate thermotolerance (Giese et al., 2005). Interestingly, the mutations clustered within the N-terminal arm of the sHsp. And a chimeric protein consisting of the N-terminal region of pea Hsp18.1 and the C-terminal region of Hsp16.9 from wheat possesses chaperone activity like the natural pea Hsp18.1 protein, whereas the vice versa chimera consisting of the N-terminal region of Hsp16.9 and the C-terminal part of Hsp18.1 does not exhibit chaperone activity, as the wt Hsp16.9 does not (Basha et al., 2006).

Surprisingly, the proposed substrate binding site in Hsp16.5 from *M. jannaschii* was mapped within the α -crystallin domain, compromising a structurally conserved loop connecting two β -strands (Kim et al., 1998; Narberhaus, 2002). It

was known from the crystal structure that this loop is surface-exposed, thus well suited for substrate interaction (Kim et al., 1998). For α B-crystallin, synthetic peptides of the α -crystallin domain, as well as of the N-terminal region and the C-terminal extension were identified to bind to substrate (Bhattacharyya et al., 2006; Sharma et al., 1997; Sharma et al., 2000). Site-directed mutagenesis of a single amino acid within the α -crystallin domain of α A- and α B-crystallin, substituting R116 and R120, respectively, by glycine caused changes in the quaternary structure along with a dramatic decrease in chaperone activity (Bova et al., 1999; Koteiche and McHaourab, 2006). At least in these cases, the substrate binding was attributed to the α -crystallin domain.

The functional role of the C-terminal extension remains unclear. Recent findings and the comparison of plant to vertebrate sHsps suggest that the structurally conserved element may play different roles. The C-terminal extension of mammalian α -crystallin was reported to be highly flexible, whereas the extensions of the bacterial and plant representatives remains rigid (Carver and Lindner, 1998; Kim et al., 1998; van Montfort et al., 2001). Bacterial and plant sHsps appeared to be more susceptible to alterations, whereas the quaternary structure and chaperone function were barely affected in vertebrate sHsps. Plant and bacterial sHsps displayed great anomalies concerning quaternary structure assembly and chaperone function. In contrast, C-terminally truncated mouse Hsp25 displayed a normal quaternary structure and normal chaperone activity towards heat-induced substrate unfolding (Lindner et al., 2000). However, the deletion protein was unable to prevent chemically induced aggregation of substrates, indicating that different regions of the protein are responsible for these two chaperone effects. Interestingly, the deletion protein produced larger and especially insoluble substrate-complexes, suggesting a role of solubilization of the C-terminus. C-terminally truncated Hsp16.2 from *C. elegans* displayed

similar properties (Leroux et al., 1997). Oligomerization and chaperone activity were rarely affected, yet the protein was sensible to aggregation, supporting the role for solubility. In contrast, assembly of bacterial and plant sHsps was reported to strongly depend on the C-terminal extension. Truncated pea Hsp17.7 was unable to assemble into normal size oligomers, but displayed normal chaperone activity, suggesting a structural role for the C-terminal extension of bacteria and plants (Kirschner et al., 2000).

2.7.3 Regulation of the heat shock response and sHsp chaperone function

To assist protein folding, chaperones must recognize and bind to non-native protein conformations specifically. Typically, non-native polypeptides expose hydrophobic amino acids and are thus recognized by chaperones. However, newly synthesized polypeptides emerging from the ribosomal tunnel may also expose residues recognized by chaperones and may thus become potential substrates. It appears reasonable that the level of chaperones in the cytosol must be strictly controlled as both limited, as well as excessive amounts of chaperone can compromise the fitness of the cell. In most cases, the chaperone activity is primarily controlled on the transcriptional level (Lindquist, 1986). Several strategies have been described to regulate the heat shock response, yet the phenomenon itself appears to be conserved throughout all kingdoms. Commonly, its trigger is an increase of unfolded polypeptides. In the case of many bacteria, transcriptional regulation of the heat shock genes is through the use of alternative transcription factors, so called sigma-factors (Ishihama, 1993; Stover et al., 2000). A sigma-factor is a regulatory subunit of RNA-polymerase that confers specificity to the promoter region. E.g. σ_{32} or σ_{54} regulate the transcription of two sHsp genes, *IbpA* and *IbpB*, respectively, as well as other heat shock genes of

E. coli under heat shock conditions (Allen et al., 1992; Yura et al., 1990). The σ^{32} concentration increases transiently, which is otherwise low under physiological conditions, and activates gene transcription (Bukau, 1993). A variation to the theme was found in many other bacteria. Here, the regulation of the heat shock response is controlled through transcriptional repression. In *Streptomyces albus*, RheA binds to the promoter region and thus inhibits transcription (Servant et al., 1999). As a result of a temperature-induced conformational change, the repressor becomes binding-incompetent, and apparently activates transcription of heat shock genes (Servant et al., 2000). The conformational conversion is fully reversible and RheA acts as an intra-cellular thermosensor, controlling the transcription of heat shock genes in *S. albus* (Servant et al., 2000).

In contrast to bacteria, lower eukaryotes and plants, animals usually experience less pronounced changes in ambient temperature, as they can easily return to a more favorable habitate. Here, the regulation of the heat shock response requires additional principles. In eukaryotes, transcriptional regulation of the heat shock response is mainly mediated through the heat shock transcription factor HSF1. Upon stress, inactive HSF1 is converted into a transcription-competent activator that binds to its heat shock element HSE within the promoter region of heat shock genes (Morimoto, 1998). Activation goes along with oligomerization and phosphorylation of HSF1 (Morimoto, 1998).

In addition to the regulation on the transcriptional level, the activity of some sHsps has been reported to occur on the protein level. Although controversially discussed in literature, human Hsp27 and α -crystallin, as well as mouse Hsp25 were reported to exhibit modulated chaperone activity when phosphorylated (Benndorf et al., 1994; Engel et al., 1995; Gaestel et al., 1992; Ito et al., 2001; Kato et al., 2001; Lambert et al., 1999; Rogalla et al., 1999). Additionally, α B-crystallin was shown to undergo a conformational change upon temperature shift that leads to

increased chaperone activity (Raman et al., 1995; Raman and Rao, 1997). In yeast, Hsp26 was shown to exhibit chaperone activity only under heat shock conditions (Haslbeck et al., 1999). The gain of Hsp26 chaperone function was shown to correlate with the dissociation of the oligomer into dimers (Haslbeck et al., 1999; Stromer et al., 2004). The chaperone activity of *Synchocystis spec.* Hsp16.6 was also shown to be temperature-dependent (Giese and Vierling, 2002; Lee et al., 2000). This suggests that at least for some sHsps a rise in ambient temperature triggers activation of sHsp chaperone function, whereas other sHsps appear to be constitutively active or at least controlled by other means, such as phosphorylation.

sHsps oligomers are dynamic structure. *In vitro*, sHsps oligomer can exchange subunit, a phenomenon termed subunit exchange. α A- and α B-crystallin subunit exchange increases with increasing temperature and these related sHsps can form hetero complexes consisting of α A and α B-crystallin *in vitro* (Bova et al., 1997; Bova et al., 2000). α A-crystallin is able to form heterooligomers with Hsp27, suggesting that both are structurally compatible (Bova et al., 2000). Yet, one should bear in mind that the α A-crystallin expression is restricted to the mammalian eye-lens, whereas Hsp27 was found in other tissues. α B-crystallin is expressed throughout the tissues and might form heterooligomers with Hsp27 *in vivo*, giving rise to the speculation that these complexes may exhibit a different substrate specificity compared to that of the homooligomers (MacRae, 2000). Subunit exchange of the archeal and mesophilic *M. jannaschii* Hsp16.5 was detected only above temperatures of 58°C and as expected its rate increased with a further increase in the temperature (Bova et al., 2002). Changes in the subunit exchange rate have been proposed to correlate with changes in the chaperone activity. Taken together these observations led to the generally accepted notion, that subunit exchange and oligomer dissociation are mechanistically linked to the

chaperone function of sHsps (Bova et al., 1997; Bova et al., 2002; Bova et al., 2000; Ehrnsperger et al., 1999; Giese and Vierling, 2002, 2004; Gu et al., 2002; Haslbeck et al., 1999; Ito et al., 2001; Lentze et al., 2004; Rogalla et al., 1999; Sobott et al., 2002; Stromer et al., 2004).

2.7.4 Hsp26 is a sHsp from *S. cerevisiae*

Hsp26 is the principal sHsp of *S. cerevisiae* (Susek and Lindquist, 1989). It exhibits sequence homology to other sHsps in the C-terminal region, especially to sHsps from plants and lower eukaryotes (Petko and Lindquist, 1986). Its expression depends on the growth phase and the cells' condition. Especially when yeast passes from the logarithmic into the stationary growth phase, as well as during sporulation and other cellular stress, such as starvation or heat shock, Hsp26 expression is enhanced (Petko and Lindquist, 1986). Gene disruption did not reveal an obvious phenotype under any of these stress conditions, but Hsp26 seems to facilitate cell recovery after severe heat shock (Cashikar et al., 2005). Cell recovery itself depends on the presence of the protein disaggregase Hsp104, yet the synthetic knock out of Hsp26 and Hsp104 revealed a 5fold reduced survival rate after severe heat shock compared to when Hsp26 was present (Cashikar et al., 2005).

Hsp26 forms shell-like particles composed of 24 subunits (Figure 11) (White et al., 2006). The primary structure of Hsp26 reveals an exceptionally long N-terminal region that can be subdivided into a N-terminal domain (NTD) and a unique middle domain (MD). Whereas the NTD appears to be critical for oligomer stability, the function of the MD was unknown up to now (Haslbeck et al., 2004). A Hsp26 truncation variant, lacking the NTD (Hsp26dN30), formed destabilized oligomers and deletion of the entire N-terminal region from Hsp26

(Hsp26dN) produced dimers (Haslbeck et al., 2004; Stromer et al., 2004). The assembly of a deletion variant lacking NTD and the C-terminal extension (CTE) stopped on the level of a dimer, indicating that MD itself is not sufficient to mediate oligomerization and apparently the CTE is the critical oligomerization element (Franzmann et al., 2008). Taken together these results suggest that dimerization is mediated by the α -crystallin domain, whereas the CTE and NTD are required to form stable Hsp26 oligomers.

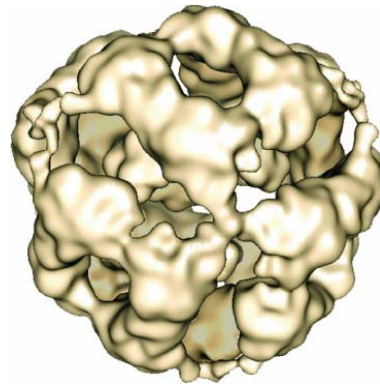


Figure 11 Cryo electron microscopy density map of oligomeric Hsp26 (White et al., 2006).

One of the most remarkable features of Hsp26 is that its activity is temperature-dependent (Haslbeck et al., 1999). At 25°C, Hsp26 does not interact with substrates, while it displays a strong affinity for unfolded polypeptides under conditions of thermal stress, e.g. at 45°C (Franzmann et al., 2008; Franzmann et al., 2005). The molecular basis of this temperature regulation was unknown, but it was shown previously that the gain of chaperone function correlates with the destabilization of the oligomer and the appearance of dimers under special conditions (Figure 12).

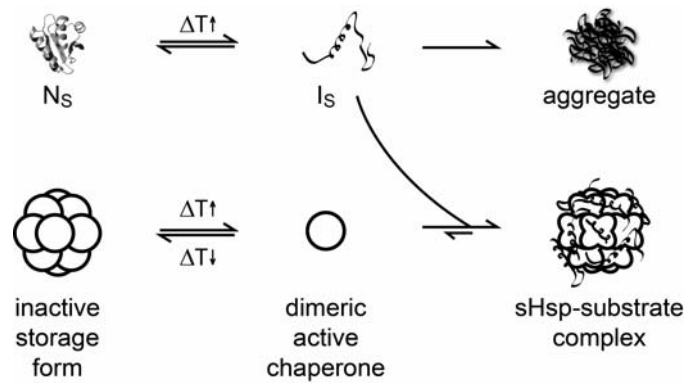


Figure 12 Current opinion: Model of the Hsp26 chaperone mechanism. Upon heat shock, the native structure of polypeptides is destabilized and proteins unfold. Simultaneously, temperature-regulated Hsp26 dissociates into small chaperone active species (dimer) and binds to the unfolding intermediates to form large substrate complexes.

sHsps form stable substrate complexes (Basha et al., 2004a; Ehrnsperger et al., 1997b; Ehrnsperger et al., 1998; Friedrich et al., 2004; Stromer et al., 2003). These vary in size and shape, depending on the substrate. Hsp26 substrate complexes with the model substrate citrate synthase (CS) appeared as regular and round-shaped structures with diameters of ~50 nm, when analysed by transmission electromicroscopy (Figure 13) (Stromer et al., 2003). Using rhodanase, insulin and α -glucosidase as substrates revealed particles with diameters between 30-50 nm, as well rod-like structures, indicating that the substrate may dictate the shape and size of the complex (Stromer et al., 2003). Similare observations were made with Hsp25, but a comparison between Hsp16.6 and Hsp18.1 revealed that luciferase substrate complexes also differ in size and shape, depending on the sHsp (Friedrich et al., 2004; Stromer et al., 2003).

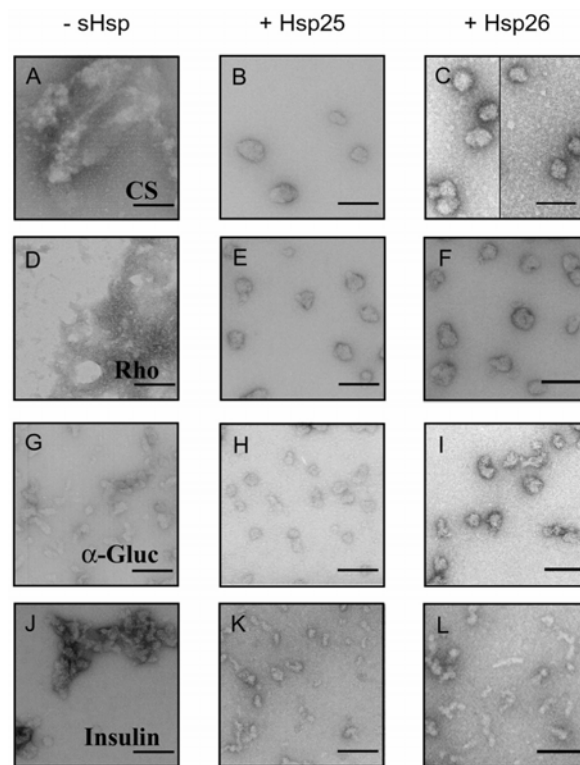


Figure 13 Negative stain electron micrographs of temperature aggregated A: citrate synthase, D: rhodanese, G: α -glucosidase and J: insulin. and in the presence of Hsp25 (B, E, H, K), and in the presence of Hsp26 (C, F, I, L) (Stromer et al., 2003).

2.8 Objective

Temperature-sensing is a crucial feature that allows cells to respond to environmental changes. This is especially important for heat shock proteins (Hsps) which have to be active under non-physiological temperatures. sHsps are molecular chaperones which specifically bind to non-native proteins and prevent them from irreversible aggregation (Horwitz, 1992; Jakob et al., 1993). A key trait of sHsps is their existence as dynamic oligomers (Bova et al., 1997; Bova et al., 2002; Bova et al., 2000; Gu et al., 2002; Lentze et al., 2004; Sobott et al., 2002). Hsp26 from *Saccharomyces cerevisiae* is an oligomer consisting of 24 identical subunits that becomes activated under heat shock conditions. It forms large, stable substrate complexes with unfolded polypeptides (Haslbeck et al., 1999; Stromer et al., 2003; White et al., 2006). This activation coincides with the destabilization of the oligomer and the appearance of dimers in gel filtration experiments (Haslbeck et al., 1999; Stromer et al., 2004). Apparently, Hsp26 is able to sense temperature autonomously, yet the underlying mechanism of its regulation by temperature has remained enigmatic. To gain a better understanding of the chaperone mechanism of sHsps it is crucial to analyze the relationship between chaperone activity, conformational changes and stability of the oligomer. To this end, the thermodynamic and kinetic parameters of the structural changes controlling the Hsp26 activation process were identified. Hsp26 variants with altered spectroscopic properties were generated, allowing to follow the structural changes controlling the activation process in real-time by fluorescence spectroscopy. Additionally, single and double Cys variants were generated allowing site-specific fluorescence labelling of Hsp26 domains for

subsequent fluorescence resonance energy transfer (FRET) distance analysis. Hence, a topological distance pattern of Hsp26 was revealed, allowing detection of site-specific conformational differences between inactive and chaperone active Hsp26. Analysis of the kinetics of these structural rearrangements allowed identification of the energy barrier controlling the chaperones activity state.

3 Materials and Methods

3.1 Strains

Strains	Geno- / Phenotype	Source / Reference
<i>E. coli</i> XL1 Blue	<i>recA1 endA1 gyrA96 thi-1 hsdR17 supE44 relA1 lac</i> [F'proAB <i>lacIq</i> ZDM15 Tn10 (<i>TetR</i>)]	Stratagene, La Jolla, USA
<i>E. coli</i> XL1 DH10B	F- <i>mcrA</i> Δ (<i>mrr-hsdRMS-mcrBC</i>) Φ 80 <i>lacZ</i> Δ M15 Δ <i>lacX74 recA1 endA1 araD139 Δ(<i>ara, leu</i>)7697 <i>galU galK</i> λ: <i>rpsL nupG tonA</i></i>	
<i>E. coli</i> BL21 (DE3)	F- <i>ompT hsdS</i> (rB- mB-) <i>dcm+</i> <i>Tetr gal 1</i> (DE3) <i>endA Hte</i> [<i>argU ileY leuW CamR</i>]	Stratagene, La Jolla, USA
<i>S. cerevisiae</i> BY4741	MATa; <i>his3D1; leu2D0; met15D0; ura3D0</i>	Euroscarf
<i>S. cerevisiae</i> BY4742	MAT α ; <i>his3D1; leu2D0; met15D0; ura3D0</i>	Euroscarf
<i>S. cerevisiae</i> BY4741 Δ Hsp26	BY4741; Mat a; <i>his3D1; leu2D0; met15D0; ura3D0; YBR072w::kanMX4</i>	Euroscarf
<i>S. cerevisiae</i> BY4742 Δ Hsp26	BY4742; Mat α ; <i>his3D1; leu2D0; lys2D0; ura3D0; YBR072w::kanMX4</i>	Euroscarf

3.2 Vectors and Plasmids

Vector / Plasmid	Construct	Origin / Reference	Cloning site
pET28b+		Merck Biosciences GmbH (Schwalbach, Germany)	
pGEX-6P1		GE Healthcare (Freiburg, Germany)	
p2 μ GPD		S. Lindquist, (Boston, USA)	
pTMF8	pET28b+Hsp26 Δ N30-195C	Parent vector: pET28b+, Diploma thesis Titus M. Franzmann (2004)	Nco1 / Not1
pTMF9	pET28b+ Hsp26W211Y	Parent vector: pET28b+, This work	Nco1 / Not1
pTMF10	pET28b+ Hsp26W211A	Parent vector: pET28b+, This work	Nco1 / Not1
pTMF11	pET28b+ Hsp26S4C/W211Y	Parent vector: pET28b+, This work	Nco1 / Not1
pTMF12	pET28b+ Hsp26S210C	Parent vector: pET28b+, This work	Nco1 / Not1
pTMF13	pET28b+ Hsp26S4C/S210C	Parent vector: pET28b+, This work	Nco1 / Not1

Vector / Plasmid	Construct	Origin / Reference	Cloning site
pTMF14	pET28b+ Hsp26W72Y	Parent vector: pET28b+, This work	Nco1 / Not1
pTMF15	pGEX-Hsp26 Δ 192C	Parent vector: pGEX- 6p1, This work	Nco1 / Not1
pTMF16	pGEX-Hsp26 Δ 195C	Parent vector: pGEX- 6p1, This work	Nco1 / Not1
pTMF17	pET28b+ Hsp26W72Y	Parent vector: pET28b+, This work	Nco1 / Not1
pTMF18	pET28b+ Hsp26FS	Parent vector: pET28b+, This work	Nco1 / Not1
pTMF19	pET28b+ Hsp26S82C	Parent vector: pET28b+, This work	Nco1 / Not1
pTMF20	pET28b+ Hsp26 Δ 208C	Parent vector: pET28b+, This work	Nco1 / Not1
pTMF21	pET28b+ Hsp26 Δ 208/I203AC	Parent vector: pET28b+, This work	Nco1 / Not1
pTMF22	pET28b+ Hsp26 I203AC	Parent vector: pET28b+, This work	Nco1 / Not1
pTMF23	pET28b+ Hsp26 Δ 202C	Parent vector: pET28b+, This work	Nco1 / Not1
pTMF24	aB-crystallin A4C	Parent vector: pET28b+, This work	Nco1 / Not1

Vector / Plasmid	Construct	Origin / Reference	Cloning site
pTMF25	pET28b+ Hsp26S4C/I203A	Parent vector: pET28b+, This work	Nco1 / Not1
pTMF26	pET28b+ Hsp26S4C	Parent vector: pET28b+, This work	Nco1 / Not1
pTMF27	pET28b+ Hsp26FA	Parent vector: pET28b+, This work	Nco1 / Not1

3.3 Chemicals

Name	Origin
Acrylamide (38%, 2% Bisacrylamide)	Roth (Karlsruhe, Germany)
Agarose, ultra pure	Roth (Karlsruhe, Germany)
Ammoniumperoxodisulfate (APS)	Roche (Mannheim, Germany)
Ammoniumsulfate	Merck (Darmstadt, Germany)
Ampicillin	Roth (Karlsruhe, Germany)
Bacto Agar	Difco (Detroit, USA)
Bacto Tryptone	Difco (Detroit, USA)
Bacto Yeast Extract	Difco (Detroit, USA)
Bromphenolblue S	Serva (Heidelberg, Germany)
Complete Protease Inhibitor Cocktail Tablets	Roche (Mannheim, Germany)
Coomassie Brilliant-Blue R-250	Serva (Heidelberg, Germany)
Coomassie Protein Assay Reagent	Pierce (Rockford, USA)
5,5' Dithio-bis-Nitrobenzoic acid (DTNB)	Sigma (St. Louis, USA)
1,4-Dithiothreitol (DTT)	Roth (Karlsruhe, Germany)
ECL-Westernblot Detection System	GE Healthcare (Freiburg, Germany)
Ethylendiamintetraacidic acid (EDTA)	Merck (Darmstadt, Germany)
Ethidiumbromide	Sigma (St. Louis, USA)
Formaldehyde, 37% p.A.	Roth (Karlsruhe, Germany)
Glutaraldehyd, 25% in water	Serva (Heidelberg, Germany)
Glycerol, 99 %	ICN, Costa Mesa, USA
Glycine	Roth (Karlsruhe, Germany)
N-(2-Hydroxyethyl)-piperazin-N'-2-ethansulfonic acid (HEPES)	ICN (Costa Mesa, USA)
Isopropanol	Roth (Karlsruhe, Germany)
Isopropyl- β -D-thiogalaktopyranosid (IPTG)	Roth (Karlsruhe, Germany)
Kanamycin	Roth (Karlsruhe, Germany)
β -Mercaptoethanol, pure	Merck (Darmstadt, Germany)
Sodiumdodecylsulfat (SDS)	Roth (Karlsruhe, Germany)
N,N,N',N'-Tetramethylethylendiamin (TEMED)	Roth (Karlsruhe, Germany)
Polyoxyethylen-Sorbitan-monolaurat (Tween 20)	Merck (Darmstadt, Germany)

Name	Origin
Ponceau S	Sigma (St. Louis, USA)
Restriction enzymes	New England Biolabs (Beverly, USA)
T4-Ligase	Promega (Madison, USA)
Tris-(Hydroxymethyl)-aminomethan (Tris)	ICN, Costa Mesa, USA

3.4 Fluorophores

Name	$E_{X_{max}}$ (nm)	$E_{m_{max}}$ (nm)	ϵ ($M^{-1} cm^{-1}$)	Origin
4-acetamido-4'((iodoacetyl amino)stilbene-2,2' disulfonic acid (AIAS)	335	411	41,000	Invitrogen, (Karlsruhe, Germany)
Lucifer yellow iodoacetamide (LYI)	425	520	10,800	Invitrogen, (Karlsruhe, Germany)
Fluorescein isothiocyanate (FITC)	494	515	77,000	Invitrogen, (Karlsruhe, Germany)
Tetramethyl rhodamine isothiocyanate (TAMRA)	555	580	84,000	Invitrogen, (Karlsruhe, Germany)

* $E_{X_{max}}$: Spectral excitation maximum, $E_{m_{max}}$: Spectral emission maximum, ϵ : Molar extension coefficient

3.5 Size and molecular mass standard kits

Name	Origin
Low-Range Molecular Weight Standard	BioRad Laboratories (Munich, Germany)
Rainbow marker	GE Healthcare (Freiburg, Germany)
DNA-BstEII Molecular Weight Standard	New England Biolabs (Beverly, USA).
1 kb DNA Ladder Molecular Weight Standard	New England Biolabs (Beverly, USA).
QIAquick, Gel Extraction Kit	Qiagen GmbH (Hilden, Germany)
QIAprep Spin Miniprep Kit	Qiagen GmbH (Hilden, Germany)
QIAprep Spin PCR Purification Kit	Qiagen GmbH (Hilden, Germany)
Protein Standard for HPLC	GE Healthcare, (Freiburg Germany)

3.6 Proteins

Name	Origin
Citrate Synthase from pig heart	Roche (Mannheim, Germany)
Glutamate dehydrogenase from bovine	Roche (Mannheim, Germany)

3.7 Antibodies

Name	Origin
Polyclonal serum against Hsp26 (Rabbit)	Pineda Antikörper Service (Berlin, Germany)
Polyclonal serum against Hsp26 Δ N (Rabbit)	Pineda Antikörper Service (Berlin, Germany)

Name	Origin
Monoclonaler IgG-Peroxidase Conjugate against Rabbit-IgG (Goat)	Sigma (St. Louis, USA)

3.8 Chromatography

Name	Origin
Q-Sepharose (150 mL)	GE Healthcare, (Freiburg Germany)
Resource-Q (6 mL)	GE Healthcare, (Freiburg Germany)
S Sepharose (10 mL)	GE Healthcare, (Freiburg Germany)
Resource-S (6 mL)	GE Healthcare, (Freiburg Germany)
Superdex 75 Prep Grade (320 mL)	GE Healthcare, (Freiburg Germany)
Superdex 200 Prep Grade (320 mL)	GE Healthcare, (Freiburg Germany)
TSK G4000PW HPLC-Gel filtration	Tosoh Biosciences (Stuttgart, Germany)

3.9 Additional materials

Device	Origin
Amicon-Ultrafiltration Membrane YM10/30/100	Millipore (Bedford, USA)
Centricon 10/30/100- microconcentrators	Millipore (Bedford, USA)
Dialysis tubes Spectra/Por (6-8 kDa)	Spectrum (Houston, USA)
Cuvettes 1.5 mL	Zefa (Munich, Germany)
Filterpaper	Whatman (Maidstone, England)
Immobilon-P(PVDF)-Membrane	Millipore (Bedford, USA)
Cuvettes	Starna GmbH (Pfungstadt, Germany)
pH-Indicator paper	Roth (Karlsruhe, Germany)
Polyacrylamide gels (10-20 % Tricine)	Novex (Frankfurt, Germany)
Scientia EM-Film 23D56 (6,5x9 cm)	Agfa Gevaert (Belgien)
Sterile filter 0.2µm	Zefa (Munich, Germany)

3.10 Media and antibiotics

Name	Compounds	Quantities
LB ₀ :	Bacto Trypton	10 g
	Yeast extract	5 g
	NaCl	5 g
	H ₂ O	ad 1 l
	Use NaOH to adjust pH to 7.2	
	For plates: 12 g Bacto Agar	

3.11 Buffers for molecular biological methods

Name	Compounds	Quantities
TAE (50x):	2 M Tris/Acetate pH 8.0 50 mM EDTA	
BJ Buffer for DNA Analysis	50 % (v/v) Glycerol 10 mM EDTA (pH 8.0) 0.2 % (w/v) Bromphenolblue 0.2 % (w/v) Xylencyanol	
1 % Agarose-Solution:	Agarose 100 mL TAE (1x) Ethidiumbromide-Solution	1 g 1 μ l
Solution A	3 M NaAc (pH 5.5) 1 M CaCl ₂ 2.8 M MnCl ₂ H ₂ O	13 mL 100 mL 25 mL 862 mL
Solution A + Glycerol	Glycerol (87%) Solution A	69 mL 331 mL

3.12 Buffers for protein chemical methods

Buffer	Compounds	Quantities
SDS-Running Buffer (10x):	0.25 M Tris 2 M Glycine 1 % SDS	
Laemmli Sample Buffer (5x):	10 % (w/v) SDS 50 % (w/v) Glycerol 300 mM Tris 0.05 % (w/v) Bromphenolblue 5 % (w/v) b-Mercaptoethanol	

Buffer	Compounds	Quantities
Western Blotting Transfer Buffer:	Glycine	36 g
	Tris	7.6 g
	Methanol	500 mL
	H ₂ O	ad 2.5 l
PBS (-T):	NaCl	5.84 g
	Na ₂ HPO ₄	11.5 g
	NaH ₂ PO ₄	2.96 g
	H ₂ O	ad 1 l
	Tween-20	1 mL

3.12.1 Buffers for purification of Hsp26

Name	Compounds
Lysis Buffer	40 mM HEPES-KOH, pH 8.0, 5 mM EDTA
Buffer A	40 mM HEPES-KOH, pH 8.0, 5 mM EDTA
Buffer B	40 mM HEPES-KOH, pH 8.0, 1 M KCl, 5 mM EDTA
Buffer C	40 mM HEPES-KOH, pH 8.0, 150 mM KCl, 5 mM EDTA

3.13 Devices

3.13.1 Absorptions spectrophotometer

- Varian Cary 50 Bio UV-Vis-Spectrophotometer, (Varian, Palo Alto, USA)
- Varian Cary 100 Bio UV-Vis-Spectrophotometer, (Varian, Palo Alto, USA)

3.14 Circular dichroism spectropolarimeter

- Jasco J715 including PTC 343 Peltier temperature device, (Jasco, Groß-Umstadt, Germany)

3.15 Fluorescence Spectrophotometer

- Spectrofluorometer: Fluoromax I, II and III (with autopolarizers) with temperature adjustable cuvette holder (Spex: Edison, USA)

3.16 Analytical ultracentrifuge

- XL-I equipped with absorbance and interference detection systems (BeckmanCoulter, Krefeld, Germany)
- XL-A equipped with absorbance and fluorescence detection systems (BeckmanCoulter, Krefeld, Germany and AVIV Biomedical, Lakewood, USA)

3.17 Chromatography devices

- ÄKTA FPLC, (GE Healthcare, Freiburg Germany)

3.18 HPLC devices

- HPLC-Device (Jasco, Großumstadt, Germany)
Pump system: PU-1580
Fluorescence detector: FP-920
UV-detector: UV-1575

3.19 Gel electrophoresis und blotting devices

- RHU10X (Roth, Karlsruhe, Germany)
- Hoefer Mighty Small II (GE Healthcare, Freiburg, Germany)
- Fast Blot B44 Apparatus (Biometra, Göttingen, Germany)
- Peqlab Gel apparatus P8DS for Novex-Tricin-Gele (Novex, Frankfurt, Germany)

3.20 Scales

- BP 121 S (Satorius, Göttingen, Germany)
- BL 310 (Satorius, Göttingen, Germany)

3.21 Centrifuges

- Rotina 46 R Centrifuge (Hettich, Tuttlingen, Germany)
- Eppendorf-Centrifuge 5415 C (Hamburg, Germany)
- Avanti J25, JA-10 and JA-25.50-Rotor (Beckmann, Vienna, Austria)

3.22 Additional devices

- Varioklav EPZ H+P
(Oberschleißheim, Germany)
- Ice maker Ziegra
(Isernhagen, Germany)
- Electron microscope JEOL
100 CX JEOL
(Munich, Germany)
- Eppendorf-Thermomixer
Eppendorf
(Hamburg, Germany)
- Magnet stirrer
Heidolph MR2000
Heidolph
(Kehlheim, Germany)
- Metal Thermostat TB 1
Biometra
(Göttingen, Germany)
- pH-Meter WTW
(Weilheim, Germany)
- Thermo cycler MWG
(Ebersberg, Germany)
- Ultra filtration cell 8050
Amicon
(Danvers, USA)
- Incubator New Brunswick
Scientific
(Nürtingen, Germany)
- Water bath Haake F6-K
Haake
(Karlsruhe, Germany)
- Cell Disruption Apparatus
Basic Z Constant Systems
(Warwick, UK)

3.23 Computer programs

Name	Origin
Adobe Photoshop CS	Adobe Systems (San Jose, USA)
Adobe Illustrator CS	Adobe Systems (San Jose, USA)
Borwin	Jasco (Großumstadt, Germany)
CDNN	Jasco (Großumstadt, Germany)
Microsoft Office 2007	Microsoft (Unterschleißheim, Germany)
Origin 7.5	Originlab (Northhampton, USA)
UltraScan 9.3	Borries Demeler (www.ultrascan.uthscsa.edu)
SedFit/SedPhat	Peter Schuck (www.ultracentrifugation.com)
Origin 6 Beckman plug-in for analytical ultracentrifugation	Originlab (Northhampton, USA)
ProtParam Tool	Expasy (www.expasy.org)
Reference Manager 10	ISI ResearchSoft (Berkeley, USA)
Endnoteweb	ISI ResearchSoft (Berkeley, USA)

3.24 Molecular methods

3.24.1 Cultivation and storage of *E. coli*

E. coli was cultivated in a thermostated incubator at 30°C or 37°C either on LB plates or in LB liquid media. Strains were selected by addition of appropriate antibiotics to the media, hence selecting cells containing the corresponding resistance genes either on the plasmid or in the genome. Liquid cultures were inoculated 1:100 from fresh overnight cultures or by transferring single colonies from plates. Bacterial division was monitored at 600 nm (1 OD_{600nm} corresponding to approx. 8x10⁸ cells/ml) (Sambrook and maniatitis, 1989).

For long-term storage, 5 mL of a freshly inoculated culture were centrifuged at 5,000 x g and the sediment was resuspended in 1 mL medium. 300 µl 50 % glycerol were added to 700 µl of bacterial suspension resulting in a 15% glycerol culture stock. The culture was frozen using liquid nitrogen and stored at -80°C.

3.24.2 Cultivation and storage of *S. cerevisiae*

S. cerevisiae was cultivated at 30°C either on YPD plates or in YPD liquid media. Strains were selected by the lack of amino acids or nucleotides in the media, hence selecting strains containing the corresponding genes encoding for the missing amino acid or nucleotide. The complementation gene for amino acid synthesis was encoded on the plasmid. Liquid cultures were inoculated 1:100 using an overnight culture or by transferring a single colony from plates. Culture

growth was monitored at 595 nm (OD₅₉₅ nm corresponding to approx. 2x10⁷ cells/ml) (Sambrook and maniat, 1989).

For long term-storage, 5 mL of a freshly inoculated culture were sedimented at 2,000 x g and resuspended in 1 mL medium. 300 µl 50 % glycerol were added to 700 µl of suspension resulting in a 15% glycerol culture stock solution. The culture was frozen using liquid nitrogen and stored at -80°C.

3.24.3 Amplification and cloning of Hsp26 variants

3.24.3.1 Amplification and site-directed mutagenesis

Hsp26 variants were amplified by Polymerase Chain Reaction (PCR) from genomic yeast DNA using PWO polymerase (Roche). Primers (Table 1) were ordered from MWG, (Germany) and used for specific gene amplification. For mutational analysis the primer carried the corresponding modified codon.

Template	Approx. 1 ng
Forward primer	10 µM
Reverse primer	10 µM
NTBs	200 µM
MgCl ₂	1.5 mM
Polymerase buffer	1 x
Polymerase	0.25 Units
Melting	94°C, 45 s
Annealing	60°C, 45 s
Amplification	68°C, 45 s
Cycles	35 x

Table 1 List of primers used in this thesis. Shown are the individual names for the primers, the nucleotide sequence, information about the primers and available restriction sites, as well as their melting temperature.

Primer	Sequence	Comment	TM (°C)	Cleavage site
TMF1	GATCGGATCCATGTCAT TTAACAGTCCATTTTTT G	Hsp26 Forward	66	BamH1
TMF2	GATCGGATCCATGAGAG GCTACGCACCAAGAC	Hsp26 dN30 Forward	72	BamH1
TMF3	GATCGCGGCCGCTTACT TCAATTTTGGAACTGTT AATGTC	Hsp26 d192C Reverse	71	Not1
TMF4	GATCGCGGCCGCTTACT TCTGAGGCTTCAATTTT G	Hsp26 d195C Reverse	72	Not1
TMF5	GATCCCATGGGGATGTC ATTTAACAGTC	Hsp26 Forward	68	Nco1
TMF6	GATCCCATGGGGAGAGG CTACGCACCAAGAC	Hsp26 dN30 Forward	74	Nco1
TMF7	GCCTCCGCTCCGCCGT TACCCACGATTCTTGA GAAG	Hsp26 Reverse 5xGly for Linker-Fusion	75	-
TMF8	GGCGGAGGCGGAGGCGT GGTGAAGCAAGGCGAGG AG	YFP/CFP Forward 5xGly for Linker-Fusion	75	-
TMF9	GATCGCGGCCGCTTACT TGTACAGCTCGTCC	YFP/CFP Reverse	74	Not1
TMF10	GATCGCGGCCGCTTAGT TACCGTACGATTCTTGA GAAG	Hsp26 W211Y (Trp Substitution) Reverse	74	Not1
TMF11	GATCGCGGCCGCTTAGT TACCTGCCGATTCTTGA GAAG	Hsp26 W211A (Trp Substitution) Reverse	75	Not1
TMF12	GATCCCATGGGGTTCATT TAACTGTCCATTTTTTG ATTTC	Hsp26 S4C (Ser-Cys Substitution) Forward	68	Nco1

TMF13	GATCGCGGCCGCTTAGT TACCCCAACATTCTTGA GAAG	Hsp26 S210C (Ser-Cys Substitution) Reverse	74	Not1
TMF14	GTTATTAAC TTTATCGG AGTCCAAAATATCAACT GG	Hsp26 Globular Domain Reverse overlapping with SBA1 coredomain	65	-
TMF15	CCAGTTGATATTTTGGGA CTCCGATAAAGTTATTA AC	SBA1 Coredomain Forward overlapping with GD/Hsp26	65	-
TMF16	CCATCCTTCTGAGGGCT GAAATCCATTCCTTG	SBA1 Coredomain Reverse overlapping with C-term/26	70	-
TMF17	CAAGGAATGGATTTTCAG CCCTCAGAAGGATGG	Hsp26 C-terminal extension overlapping with SBA1	70	-
TMF18	CTTAGATGATTACTTCG ACAATG	Hsp26 W72Y (Trp Substitution) Forward amplification of C-terminal part		-
TMF19	CATTGTCTGAAGTAATCA TCTAAG	Hsp26 W72Y (Trp Substitution) Reverse Amplification of N-terminal par		-
TMF20	GATCGCGGCCGCTTAGT TACCTGGCGATTCTTGA GAAG	Hsp26 wt Reverse		Not1
TMF21	GATCCCATGGGGAGAAG TGTCGCAGTTCC	Hsp26 α -crystallin domain	71	Nco1
TMF22	GATCCCATGGGGACTAT GCGTAACTTCGATTTAT CC	ibpB Forward	71	Nco1
TMF23	GATCGCGGCCGCTTAGC TATTTAACGCGGGACG	ibpB Reverse	75	Not1
TMF24	GATCCCATGGGGTCATC TAACAGTCCATCTTCTG ATTCCTCT	Hsp26FS Phe-Ser Substitution	73	Nco1

TMF25	GATCCCATGGGGGATGA TTGGTTCGACAATGACT TGTG	Hsp26 dN70 Forward	73	Nco1
TMF26	CAATGACTTGTGCCTGT TCCCATC	Hsp26 S82C (Ser-Cys Substitution) Reverse Amplification of C-terminal part	63	-
TMF27	GATGGGAACAGGCACAA GTCATTG	Hsp26 S82C (Ser-Cys Substitution) Forward Amplification of N-terminal part	63	-
TMF28	GATCGCGCCGCTTATT GAGAAGAAACCTCAATC T	Hsp26 d208C	71	Not1
TMF29	CATCGCGCCGCTTATT GAGAAGAAACCTCAGCC TTCTTGAC	Hsp26 d208C I203A	75	Not1
TMF30	GATCGCGCCGCTTAGT TACCCACGATTCTTGA GAAGAAACCTCAGCCTT CTT	Hsp26 I203A	75	Not1
TMF31	GATCGCGCCGCTTACT TCTTGACGTGGTTCTTA CC	Hsp26 d202C	74	Not1
TMF32	GATCCCATGGACATCTG CATCCACCACCC	aB-crystallin A4C Forward	71	Nco1
TMF33	GATCGCGCCGCCTATT TCTTGGGGGCTGC	aB-crystallin Reverse	75	Not1
TMF34	GATCCCATGGGGTCAGC TAACAGTCCAGCTGCTG ATGCCGCT	Hsp26FA Phe-Ala Substitution	75	Nco1
TMF35	GATCCCATGGTTACTTC AATTTTGGAAGTGTAA TGTC	Hsp26 d195C reverse for 67 AFM (primer with Stopcodon)	67	Nco1

TMF36	CCCTGTTTCGCATCTGGT TTCG	Hsp26 P81A Forward	62	-
TMF37	CGAAACCAGATGCGAAC AGGG	Hsp26 P81A Reverse	62	-
TMF38	GGTTTCGGTTTCCCTAG AAGTGTC	Hsp26 P87A Forward	63	-
TMF39	GACACTTCTAGGGAAAC CGAAACC	Hsp26 P87A Reverse	63	-
TMF40	GATCCCATGGGGTCCCT GTTCCCATCTGGTTTC	Hsp26 α -crystallin domain lang dN78 forward	73	Nco1
TMF41	GATCGGTACCCTTCAAT TTTGGAAGTGTAAATGT C	Hsp26 alpha crystallin domain d195C AFM reverse	67	Kpn1
TMF42	GATCGCGGCCGCTTAGC ACTTCTGAGGCTTCAAT TTTGG	Hsp26 α -crystallin domain d195-Cys reverse	75	Not1
TMF43	CTTTGCCAGACTGGCCA GGTGTG	Hsp26 Y166W Substitution forward	66	-
TMF44	CACACCTGGCCAGTCTG GCAAAG	Hsp26 Y166W Substitution reverse	66	-
TMF45	GACTTGTCCCTGTTTCGC ATCTGGTTTCGGTTTCC	Hsp26 P81A Forward QuickXchange	72	-
TMF46	GGAAACCGAAACCAGAT GCGAACAGGGACAAGTC	Hsp26 P81A Reverse QuickXchange	72	-
TMF47	GACTTGTCCCTGTTTCGG ATCTGGTTTCGGTTTCC	Hsp26 P81G Forward QuickXchange	72	-
TMF48	GGAAACCGAAACCAGAT CCGAACAGGGACAAGTC	Hsp26 P81G Reverse QuickXchange	72	-
TMF49	GGTTTCGGTTTCGCTAG AAGTGTCGCAGTTCC	Hsp26 P87A Forward QuickXchange	71	-
TMF50	GGAAGTGCACACTTCT AGCGAAACCGAAACC	Hsp26 P87A Reverse	71	-

		QuickXchange	
TMF51	GGTTTCGGTTTCGGTAG AAGTGTCGCAGTTCC	Hsp26 P87G Forward QuickXchange	71
TMF52	GGAAGTGCACACTTCT ACCGAAACCGAAACC	Hsp26 P87G Reverse QuickXchange	71

3.24.3.2 Purification and enzymatic modification of amplified DNA

Amplified DNA was purified as described in the QiaQuick Spin Handbook (Qiagen, Germany). Purified fragments were enzymatically modified using restriction enzymes BamH1/NotI for p2 μ GPD, and NcoI/NotI for pET28b+ cloning, respectively (insert DNA: approx. 10 μ g, restriction reaction buffer: 5 μ l, restriction enzymes each: 2 Units, H₂O: add 50 μ l, incubate for 2 h at 37°C). Restriction reaction was stopped performing another purification step in accordance to the QiaQuick Spin Handbook.

3.24.3.3 Amplification and enzymatic modification of vector DNA

Vector DNA was amplified using *E. coli* XL1. p2 μ GPD and pET28b+ were isolated from transformed *E. coli* XL1 in accordance to the QiaQuick Spin Handbook. Purified vector DNA was enzymatically modified as described above to match insert DNA modification.

3.24.3.4 Ligation, transformation and selection

Insert DNA was ligated into the corresponding vector DNA resulting in the constructs listed in xx (vector DNA: 2 μ l, insert DNA: 10 μ l, ligation buffer: 2 μ l, T4-ligase: 4 Units, H₂O: add 20 μ l, incubate for 8 h at 16°C). *E. coli* XL1 was transformed and selected on selective media. Ligation constructs were isolated in accordance to the QiaQuick Spin Handbook. Isolated DNA was stored at -20°C.

3.25 Protein chemical methods

3.25.1 SDS polyacrylamid gel electrophoresis

SDS-PAGE was performed in accordance to the protocol of Laemmli (Laemmli, 1970). 15% SDS-PAGE gels were poured and contained the following compounds:

Separation gel: 3.75 mL 40% Acrylamide (40% w/v,
 Acrylamide/Bisacrylamide 38:2)
 2.5 mL 4 x SDS-Buffer (0.8% SDS, 1.5 M Tris/HCl, pH 8.8)
 3.75 mL bidest. H₂O

Stacking gel: 0.625ml 40% Acrylamide (40% w/v,
 Acrylamide/Bisacrylamide 38:2)
 2.5 mL 2 x SDS-Buffer (0.4% SDS, 0.25 M Tris/HCl, pH 6.8)
 1.875 mL bidest. H₂O

Polymerization of the solution was induced by adding TEMED and APS. Electrophoresis was carried out at constant voltages (150 V) for 1 h. Gels were stained with Coomassie in accordance to the protocol of Fairbanks et al (Fairbanks et al., 1971). When required gels were silver stained in accordance to the protocol of Heukeshoven et al (Heukeshoven and Dernick, 1988).

3.25.2 Western blotting

SDS Gels were performed as described in 3.25.1. Proteins were then blotted onto a PVDF membrane using 1.5 mA/cm² in a semi dry blotting apparatus for 50 min. Membranes were incubated with 5 % milk powder for 45 min to block free binding sites. Diluted primary antibodies (1:5000) were added, and incubated for 30 min. The membrane was washed briefly (3x5 min), and incubated with the secondary antibody (1:5000) for 30 min. Detection was carried out as described in the protocol of the ECL detection system.

3.26 Purification of Hsp26

Expression cultures of 5 l LB were inoculated 1:100 using fresh overnight culture of freshly transformed *E. coli* BL21 (DE3) codon plus containing the target gene. Growth was monitored at OD_{600 nm}. At OD_{600 nm} = 0.8 (mid exponential phase) the expression of the recombinant target gene was induced using 1 mM IPTG for 5h. Cells were harvested by centrifugation (15 min, 5,000 x g, 8°C). The sediment was resuspended in lysis buffer (20 mM HEPES, 30 mM KCl 5 mM EDTA, 1 mM DTT, pH 7.4), and lysed using a cell disruption apparatus (Basic Z Constant System) at a pressure of 2.0 kbar. 0.1 mg DNase were added to the suspension. The lysate was centrifuged (50 min, 35,000 x g, 8°C) to remove non-lysed cells, cellular debris, and insoluble cellular content from soluble compounds containing target protein

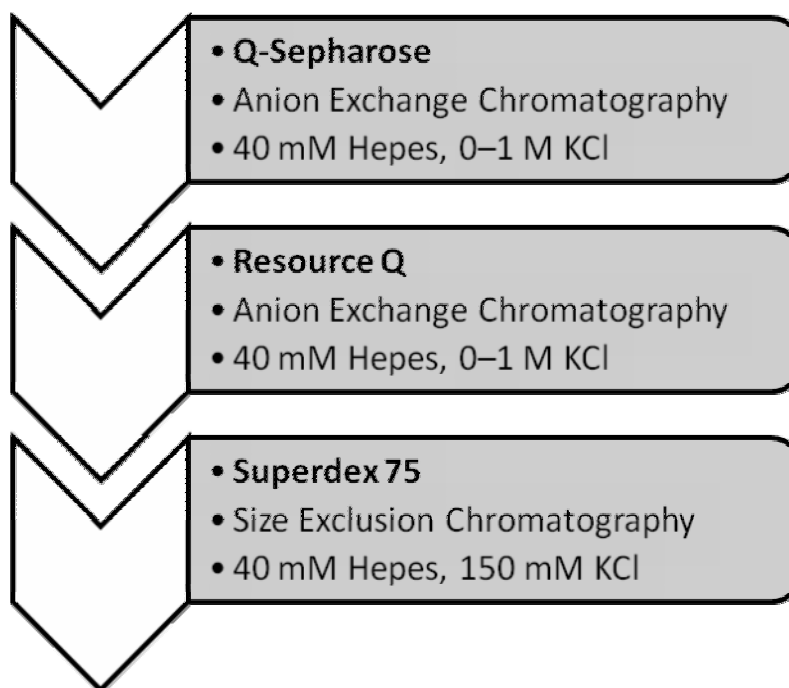


Figure 14 Schematic overview of the chromatography assisted purification of Hsp26

The supernatant was decanted and applied to an equilibrated, self-packed Q-Sepharose column (150 mL) using a super-loop (150 mL). The column was equilibrated in lysis buffer (15 column volumes) using a flow rate of 10 mL/min. The column was washed with 700 mL lysis buffer. The protein was eluted applying a 10fold linear KCl gradient (0-1 M). 10 mL fractions were collected. Fractions were analysed by SDS-PAGE and Western Blotting. Fractions containing the target protein were pooled, concentrated and diluted 1:3 with lysis buffer.

In a second purification step the solution was applied to an equilibrated, pre-packed ResourceQ column (6 mL) using the same buffer conditions. Unspecifically bound proteins were removed by washing the column with 30 mL lysis buffer. The Protein was eluted applying a linear KCl gradient (0-1 M). 2 mL fractions were collected. Fractions were analyzed and pooled as described before.

Hsp26 was then applied to a Superdex 200-pg gel filtration column, equilibrated in 150 mM potassium chloride (40 mM HEPES, 150 mM KCl, 5 mM EDTA, pH 8.0). 5 mL fractions were collected and analyzed by SDS-PAGE. Hsp26 fractions were pooled and concentrated to a final concentration of more than 6 mg/ml, dialyzed against 40 mM HEPES, 150 mM KCl, 5 mM EDTA, frozen with liquid nitrogen and stored at -80°C.

Hsp26 30-195 was purified as describes in “Structural and Functional Characterization of Carboxy-terminal Deleted Heat Shock Protein 26 (Hsp26) from *Saccharomyces cerevisiae*” (Titus M. Franzmann, Diploma Thesis, 2004, Lehrstuhl Biotechnologie, Technische Universität München)

3.27 Spectroscopy

All acquired spectra were buffer subtracted. References contained equivalent volumes of buffer instead of protein solution.

3.27.1 Absorbance spectroscopy (UV-VIS)

Absorption of electromagnetic radiation occurs when delocalized π -electrons are transferred from ground to an excited energy state. Various functional groups of proteins absorb UV light in the range from 150 to 300 nm. In the range from 180 to 240 nm the carbonyl group of the peptide bond absorbs predominantly, whereas from 250 to 300 nm mainly the aromatic ring system of phenylalanine, tyrosine and tryptophan absorb. Table 2 summarizes the absorbance properties of the aromatic amino acids and disulfide bonds (Schmid and Creighton, 1989).

Table 2 Comprehension of UV spectroscopic properties of the aromatic amino acids tryptophan, tyrosine, phenylalanine and disulfide bonds including the absorbance maxima and extinction coefficients (Schmid and Creighton, 1989).

Amino acid	λ_{\max} (nm)	ϵ_{\max} (M ⁻¹ cm ⁻¹)
Tryptophan	280	5700
Tyrosine	274	1400
Phenylalanine	257	200
Disulfide bond	250	300

* λ_{\max} : Absorbance maximum, ϵ_{\max} : Molar extension coefficient

Spectroscopic properties depend on the polarity of the solvent. Wavelength shifts and changes in intensity can be observed when solvent polarity changes. This can give rise into conformational changes and changes in solvent accessibility of

aromatic residues. Here, UV spectroscopy was used to determine the concentration of a protein solution exclusively. The law of Lambert-Beer correlates the protein concentration with the measured absorbance.

$$A = \varepsilon \times c \times d$$

Equation 1 The law of Lambert-Beer, A: Absorbance, ε : molar extinction coefficient ($M^{-1} \times cm^{-1}$), c: molar protein concentration (M), d: layer thickness (cm)

The spectroscopic properties of the proteins created for this thesis were derived from www.expasy.org and are summarized in results. In general, the intensity of stray light depends on the four power of the absorbance wavelength. Hence, stray light contributes to the absorbance of proteins. Plotting the logarithm of the absorbance intensity versus the logarithm of the absorbance wavelength allows correction for stray light from the protein absorbance spectra.

3.27.2 Fluorescence spectroscopy (FL)

Absorption of photons can lead to transition of electrons into an excited state. When returning to ground state electrons dispose of their energy. The energy is either converted completely into vibration or partially converted into electromagnetic radiation, fluorescence. Electromagnetic radiation generated from relaxation of electrons from an excited state leads to emission of photons with smaller energy and in turn emitting at longer wavelength (Lakowicz, 1999; Schmid and Creighton, 1989).

Tryptophan, tyrosine and phenylalanine show intrinsic fluorescence due to their delocalized π -electron ring systems. Tryptophan is predominantly responsible for the fluorescence properties of a protein, as its extinction coefficient is larger than those of tyrosine and phenylalanine. The relative sensitivities for these three

amino acids are: Trp : Tyr : Phe = 1100 : 200 : 8 (Lakowicz, 1999; Schmid and Creighton, 1989).

Trp fluorescence strongly depends on the solvent. The emission maximum of Trp in proteins ranges from 310 to 340 nm. The emission maximum of free tryptophan in hydrophobic environment is around 310 nm. In hydrophilic environment the maximum shifts towards longer wavelengths (> 350 nm). Thus, Trp fluorescence can be used to monitor the transition between conformational state of a protein, such as during denaturation/unfolding or folding, as buried Trp will show a wavelength shift when exposed to aqueous solvent upon unfolding. In addition, changes in fluorescence intensities may be observed. One explanation may be the loss of energy transfer from tyrosine, as the distance increases usually when proteins unfold. A second explanation may be collision quenching of exposed tryptophan by solvent molecules. Tyrosine fluorescence shows a maximum at 303 nm, which does not change with solvent polarity though changes in intensity occur. Here, fluorescence spectroscopy was used gain structural information about the chemical environment of Trp residues within Hsp26 and the variants created here. Further, structural changes within Hsp26 upon temperature treatment were monitored by changes in Trp fluorescence.

3.27.3 Circular dichroism spectroscopy (CD)

Circular dichroism is a property of optical active molecules to absorb left and right polarized light to different extent. This feature relies on the presence of asymmetric carbon atoms and/or aromatic rings. Proteins consist of optical active amino acids, hence displaying optical activity (Fasman, 1996). Two regions can be distinguished: The near (350–250 nm) and far UV (260-170 nm) regions. Near CD spectroscopy delivers information about asymmetrically arranged aromatic

rings, displaying a specific spectrum for each protein (protein finger print). The signal depends on the tertiary environment of the aromatic residues. Denatured proteins do not show a signal in this region.

In the far UV the conformation of the polypeptide displays characteristic signals, due to the differential absorption of the polypeptide backbone, placed in an asymmetric environment. α -helix e.g. shows two characteristic minima at 222 and 208 nm. β -sheet structure shows a less intense signal with a single minimum at 218 nm. Far CD spectroscopy can be used for secondary structure investigations. Nonetheless, although CD delivers detailed information about the structural elements of biomolecules, one cannot determine whether the sample adopts a “Dackel”- (unpublished data Franzmann, *et al.*) or “Tannenbaum”- (unpublished data Hainzl, *et al.*) structure. Ellipticity is used for the quantitative content of secondary structure. Conversion into mean residue ellipticity takes place after Equation 2

$$\Theta_{MRW} = \frac{\Theta \times 100 \times M}{d \times c \times N_{aa}}$$

Equation 2 Θ_{MRW} = mean residue ellipticity, Θ = obtained ellipticity, M = molecular mass (g/mol), d = layer thickness (cm), c = concentration (mg/ml), N_{aa} = number of amino acids

For secondary structure analysis, Hsp26 was dialysed against 5 l, 10 mM potassium phosphate, pH 7.5, at 4°C over night. Afterwards the protein concentration was determined by UV-spectroscopy. CD spectra were acquired using a final concentration of 0.1 mg/ml in a 1 mM cuvette. Parameters for acquisitions were set to a wavelength range of 250-185 nm, 20 nm/s, 6 accumulations. Acquisition was performed at 25°C or as stated in the figure legends. Data were buffer corrected and converted into mean residue ellipticity using Equation 2. Secondary structure prediction was carried with the CDNN and Dichroweb software (Whitmore and Wallace, 2004).

For tertiary structure analysis, spectra of 1 mg/ml Hsp26 were recorded from 320-260 nm, in potassium phosphate, pH 7.5, at 25°C or as stated in the figure legends. Data were buffer corrected and converted into mean residue ellipticity using Equation 2.

3.27.4 Thermal unfolding and refolding of Hsp26

Thermal stability of Hsp26 was analysed using CD-Spectroscopy. Protein concentration was adjusted to a final concentration of 0.1 mg/ml in 10 mM potassium phosphate, pH 7.5 using a 1 mM cuvette. Thermal transition was monitored at a constant wavelength according to maximum in signal change (220 nm). The wavelength was calculated by subtracting the spectra of native and thermally denatured protein. Transition was monitored over a temperature range from 10-95°C. Acquiring parameters were set to a thermal gradient of 10°C/h. Acquired data were converted into mean residue ellipticity (Equation 2) and plotted and analysed with Equation 3.

$$y(T) = \frac{y_N - (y_N - y_U)}{1 + \exp \frac{-\Delta G(T)}{RT}}$$

$$y_N = y_N^0 + m_N \times T$$

$$y_U = y_U^0 + m_U \times T$$

$$\Delta G(T) = \Delta H \left(1 - \frac{T}{T_M}\right) - \Delta C_p \left(T_M - T + T \ln \frac{T}{T_M}\right)$$

Equation 3 Equation for non-linear thermal transition regression; y(T): regression as the function of the temperature; y_N: signal for the natively folded protein, y_U: signal for the unfolded protein; y⁰_N and y⁰_U represent the regressed values of y_N and y_U, to T = 0 K; m determines the according slopes; T_M: midpoint of thermal transition; ΔH: van't Hoff-enthalpy in T_M; ΔC_p: change in temperature capacity correlated to the unfolding process.

3.27.5 Chemical unfolding and refolding of Hsp26

Chemical stability of Hsp26 deletion proteins was investigated using CD-Spectroscopy. Each experiment contained 0.3 mg/ml of protein. Samples were incubated overnight at 25°C with increasing concentrations of urea (0-10 M in potassium phosphate, pH 7.4). Chemical transition was monitored at a constant wavelength according to maximum in signal change (219 nm). The wavelength was calculated by subtracting the spectra of native and chemically denatured protein. Transition was monitored over 60 s for each urea concentration. Acquired data were averaged and plotted against the urea concentration. The accurate urea concentration was determined by refractometry using Equation 4. The acquired data were converted into molar ellipticity (Equation 2) and plotted and analysed using Equation 5.

$$[Urea] = 117.66(\Delta n)^1 + 29.753(\Delta n)^2 - 185.56(n)^3$$

Equation 4 The urea concentration was determined from the difference in refraction indices (Δn) of the buffer with and without urea

$$y([urea]) = \frac{y_N - (y_N - y_U)}{1 + \exp\left(\frac{-\Delta G + m \times [urea]}{RT}\right)}$$

Equation 5 Equation for non-linear chemical transition regression; $y([urea])$: regression as the function of the concentration of urea; y_N : signal for the natively folded protein, y_U : signal for the unfolded protein; y_N^0 and y_U^0 represent the regressed values of y_N and y_U , m determines the cooperativity parameter

3.27.6 Kinetic analysis of temperature-induced changes in Hsp26

To monitor structural changes within Hsp26 upon temperature activation, Hsp26 was kept at 25°C or 4°C, respectively, and then diluted into a 1.5 mL stirring cuvette pre-equilibrated at higher temperature. Fluorescence of 1 μ M Hsp26 in

40 mM HEPES, 5 mM EDTA, pH 8.0 was excited at 275 nm or 295 nm, respectively and the change in fluorescence was monitored at 340 nm. Hsp26 fluorescence traces were recorded over time and the apparent rate constant (λ) was derived from single or double exponential fitting using Equation 6 or Equation 7, respectively.

$$F = F_0 + A \cdot \exp^{-\lambda \cdot t} + m \cdot t$$

Equation 6 Single exponential function to derive the rate constant λ from kinetic experiments monitoring the time-dependent changes in Hsp26 fluorescence upon temperature shift. F: acquired fluorescence intensity, F_0 : acquired fluorescence intensity at the end of the experiment, A difference in the overall signal intensity, corresponding to the amplitude, λ : observed rate constant, t: time, m: is the slope correcting for secondary processes, such as photo bleaching.

$$F = F_0 + A_1 \cdot \exp^{-\lambda_1 \cdot t} + A_2 \cdot \exp^{-\lambda_2 \cdot t} + m \cdot t$$

Equation 7 Double exponential function to derive the rate constants λ_1 and λ_2 from kinetic experiments monitoring the time-dependent changes in Hsp26 fluorescence upon temperature shift. F: acquired fluorescence intensity, F_0 : acquired fluorescence intensity at the end of the experiment, A difference in the overall signal intensity, corresponding to the amplitude, λ_1 : first observed rate constant, λ_2 : second observed rate constant, t: time, m: is the slope correcting for secondary processes, such as photo bleaching.

3.27.7 Fluorescence quenching

In fluorescence quenching, a small molecule, such as iodide or acryl amide, absorbs energy by means of collision. Thus, a quencher molecule depopulates the excited state of a fluorophore and eliminates its fluorescence. Since the quencher must encounter the fluorophore, quenching follows a bimolecular reaction order and depends on the quencher concentration. Apparently, fluorescence quenching delivers information about the accessibility of a quencher to the fluorophore. This information can be used to determine, whether a fluorophore, such as Trp or an extrinsic fluorescence dyes is solvent exposed, or buried within the molecule.

Here, fluorescence quenching was used to determine the molar quenching coefficients of Hsp26 Cys variants in the chaperone-inactive and active state that were covalently modified with the LYI fluorophore at distinct sites. To this end, 1 μ M Hsp26 was quenched with a freshly prepared 5 M sodium iodide solution (in 40 mM HEPES; 5 mM EDTA, 100 mM sodium thiosulfate, pH 7.5). The fluorescence intensities and quencher concentration were corrected for the dilution factor. LYI was excited at 425 nm and its fluorescence was detected at 520 nm.

The fluorescence signals were plotted F_0/F in dependence of the quencher concentration [Q] and the molar quenching coefficients for dynamic and static quenching were derived from double linear fitting using the Stern-Volmer equation.

$$\frac{F_0}{F} = (1 + K_D[Q]) \cdot (1 + K_S[Q])$$

Equation 8 Stern-Volmer-Equation in which F_0/F is the quotient of the fluorescence in absence of quencher divided by the fluorescence at any given quencher concentration. K_D is the molar dynamic quenching coefficient, K_S is the molar static quenching coefficient.

3.27.8 Fluorescence resonance energy transfer (FRET)

In FRET, energy of an excited donor fluorophore is transferred to a conjugated ring system of an acceptor chromophore. This radiation less process occurs without the emission of a photon and requires that i. the fluorescence emission spectrum of the donor overlaps with the absorption spectrum of the acceptor, determining the so call overlap integral $J(\lambda)$, ii. the dipoles of the donor and acceptor have to be oriented in parallel, determining the so called orientation factor k^2 and iii. donor and acceptor must be in proximity to each other, typically within the range of 1-10 nm (Lakowicz, 1999).

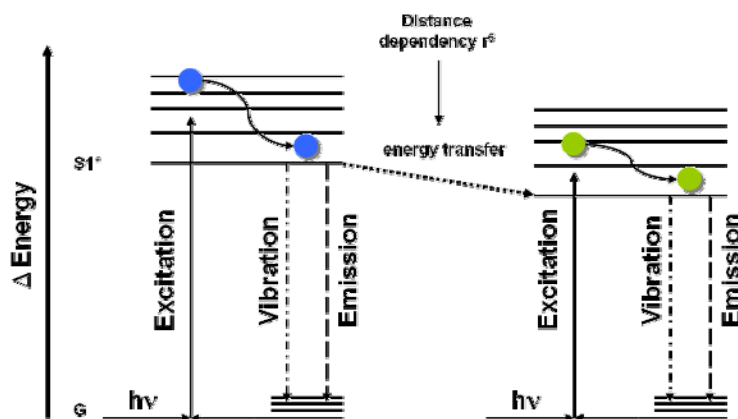


Figure 15 Jablonski diagram of FRET. When a donor (blue) fluorophore is excited it undergoes internal conversion reactions to return from the high energy excited state to its ground state. This conversion takes place mainly through vibrational relaxation and to a minor extent through fluorescence. An adjacent and correctly oriented acceptor chromophore (green) can absorb the energy from the excited donor to transfer its own electrons to the excited state. FRET is dependent on the distance (r^6) between the donor and acceptor chromophores. Adapted from (Lakowicz, 1999)

The distance dependence of the transfer efficiency is given by Equation 9, in which the Förster radius R_0 is defined as the distance that leads to 50% elimination of the donor fluorescence by the acceptor.

$$E_T = \frac{R_0^6}{R_0^6 + r^6} = 1 - \frac{F_{DA}}{F_D}$$

Equation 9 The FRET efficiency (E_T), depends on the sixth power of the distance (r) between the donor and the acceptor chromophore given by the Förster radius R_0 . R_0 is defined at the distance (r) between both chromophores that leads to 50% elimination of the donor fluorescence in the presence of the acceptor (F_{DA}) compared to the fluorescence in the absence of the acceptor (F_D).

Energy transfer depends on the sixth power of the distance between both fluorophores, making FRET sensitive to small changes in the FRET efficiency. The Förster radius (R_0) is determined by the spectral properties of the chromophore pair and can be calculated with Förster's equation

$$R_0 = 0.211 \cdot \sqrt[6]{\kappa^2 \cdot \eta \cdot Q_D \cdot J(\lambda)}$$

Equation 10 Förster equation: R_0 : Förster radius (nm), κ^2 : orientation factor, η : refractive index of the solvent, Q_D : quantum yield of the donor, $J(\lambda)$: overlap integral

Solving Equation 9 to r yields Equation 11

$$r = R_0 \cdot \sqrt[6]{\frac{1 - E_T}{E_T}}$$

Equation 11

and thus allows to determine the relative distance given in R_0 between two fluorophores from the E_T .

To determine relative distances within Hsp26, the Förster radius R_0 for the AIAS and LYI fluorophore pair was determined. The Förster equation (Equation 10) describes the Förster radius R_0 (in Å) in dependence of the orientation factor κ^2 ,

the refractive index η , the quantum yield Q_D of the donor fluorophor, and the overlap integral $J(\lambda)$ of the donor fluorescence and the acceptor absorption (Lakowicz, 1999). $J(\lambda)$ was determined experimentally using donor- and acceptor-labelled Hsp26_{S4C/W211Y}, Hsp26_{S82C} (data not shown), and Hsp26_{S210C} (data not shown) and was calculated from Equation 12

$$J(\lambda) = \frac{\int_0^{\infty} F_D(\lambda) \varepsilon_A(\lambda) \lambda^4 d\lambda}{\int_0^{\infty} F_D(\lambda) d\lambda}$$

Equation 12 The overlap integral ($J(\lambda)$ in $M^{-1} cm^{-3} nm^4$) expresses the degree of spectral overlap of the donor emission (F_D , dimensionless) and the acceptor absorbance (ε_A , in $M^{-1} cm^{-1}$).

recording absorption spectra ($\varepsilon_A(\lambda)$) of LYI-labelled Hsp26 and fluorescence spectra ($F_D(\lambda)$) of AIAS-labelled Hsp26 (Lakowicz, 1999). The spectra were integrated with the numeric integration function of the Origin software (OriginLab Corporation, Northampton, MA, USA). In all cases, the overlap integral was $2.47 M^{-1} cm^1 nm^4$.

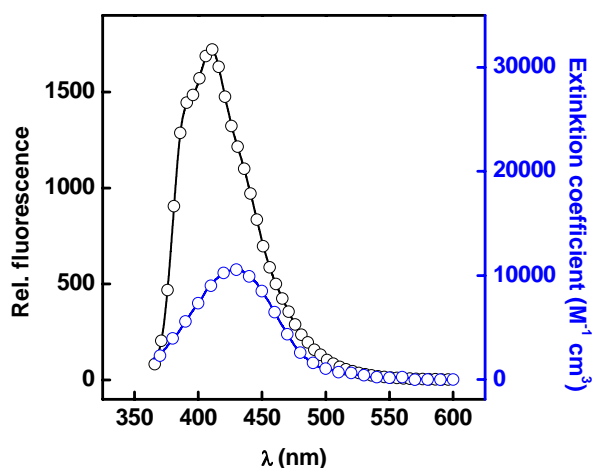


Figure 16 Fluorescence spectrum of AIAS-labelled Hsp26_{S4C/W211Y} and extension spectrum of LYI-labelled Hsp26_{S4C/W211Y}. Spectra were integrated with the Origin software and the overlap integral was calculated from Equation 12.

The relative quantum yields were determined for donor-labelled Hsp26_{S4C/W211Y}, Hsp26_{S82C} and Hsp26_{S210C} at 25°C (Figure 17), in reference to Fluorescein and LYI (Jobin Yvon, 2006; Lakowicz, 1999). Also, heat-activated samples were analyzed to detect changes in the quantum yields due to structural changes upon temperature-treatment and to correct for temperature effects (Table 3).

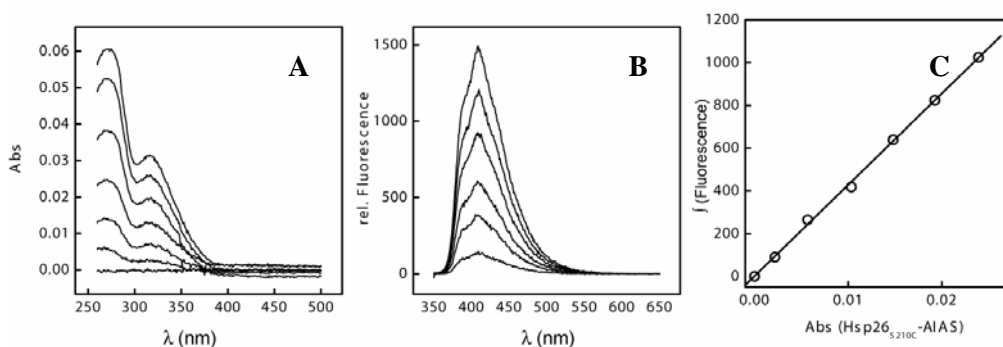


Figure 17 A: Absorbance spectra and B: Fluorescence spectra of 750 nm, 610 nm, 480 nm 315 nm, 170 nm, 47 nm AIAS-labelled Hsp26S210C in 40 mM HEPES, pH 7.5 at 25°C. C: Integrated AIAS fluorescence intensity as a function of AIAS absorbance at 330 nm to determine the relative quantum yield.

The rotational freedom of the fluorophors, when attached to Hsp26, was estimated from fluorescence anisotropy measurements (Figure 18). The qualitative analysis of the fluorescence anisotropy values obtained at 25°C and 45°C suggested that the donor and acceptor fluorophors attached to Hsp26_{S4C/W211Y} or Hsp26_{S82C} are in a dynamic environment, yet the fluorophor motion was reduced when attached to the CTE in Hsp26S210C.

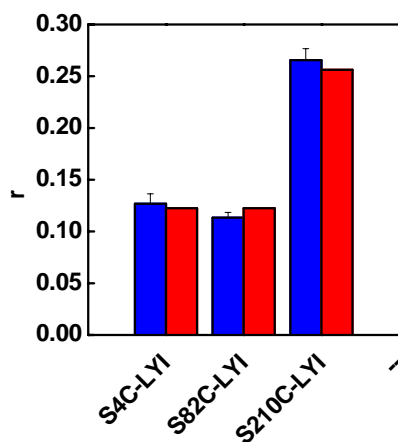


Figure 18 Fluorescence anisotropy of LYI-labelled Hsp26S4C, Hsp26S82C and Hsp26S210C at 25°C (blue) and 45°C (red). Error bars were determined from three independent experiments.

Based thereon the Förster radius R_0 was calculated for each variant, assuming a refractive index of 1.4 and the orientation factor $\kappa^2 = 2/3$ (Table 3).

Table 3 The relative quantum yields (QY) of site-specific AIAS-labelled Hsp26 cystein variants were determined in reference to the quantum yields of fluorescein and lucifer yellow, and the corresponding Förster radii (R_0) were calculated for the chaperone-inactive and the thermally activated state of Hsp26 assuming a refractive index of 1.4 and an orientation factor (κ^2) of 2/3.

	Inactive		Active	
	QY	R_0 (Å)	QY	R_0 (Å)
Hsp26S4CAIAS (NTD)	0.36	31.1	0.26	29.4
Hsp26S82CAIAS (MD)	0.58	33.7	0.39	31.5
Hsp26S210CAIAS(CTE)	0.15	26.9	0.17	27.4

To monitor FRET within Hsp26, the cystein variants Hsp26S4C, Hsp26S82C and Hsp26S210C were covalently modified with the donor fluorophors AIAS or Fluorescein and the acceptor molecules LYI or TAMRA. The labeling procedure was in accordance to the manufacturer's protocol (Invitrogen, Karlsruhe, Germany). Exploiting the phenomenon of subunit exchange (3.27.9) series of

spectroscopic heter-oligomers were generated. AIAS and LYI labelled Hsp26 were mixed in a 1:1 ratio to generate FRET active oligomers at a final concentration of 10 μ M. After mixing, the sample was diluted 1:10 into a 500 μ L cuvette at 25°C, and fluorescence spectra were recorded. The remaining sample was incubated until SX reached equilibrium. Then, another sample was diluted 1:10 and analyzed as described above. The sample was then incubated for 10 min at 45°C to allow for Hsp26 activation and thereafter quenched 1:10 into the cuvette at 25°C. To test for the reversibility of the reaction, heat-treated samples were further incubated at 25°C to allow Hsp26 inactivation and analyzed. The same procedure was also carried out without acceptor to determine the donor fluorescence intensities.

3.27.9 Subunit exchange (SX)

For subunit exchange, wt Hsp26 was covalently modified with Fluorescein-isothiocyanate and TAMRA-isothiocyanate, or Hsp26S4C with AIAS and LYI, according to the manufacture's protocol. 5 μ M fluorescein labelled wt Hsp26 were mixed with 5 μ M TAMRA labelled wt Hsp26 to allow the exchange of subunits between Hsp26 oligomers. After indicated times, samples were taken and diluted 1:10 fold into a pre-equilibrated cuvette at 20°C and fluorescence spectra were recorded. Fluorescein excitation was at 495 nm. The time-dependent changes in the donor (515 nm) and acceptor (580 nm) fluorescence were plotted as a function of the incubation time at the indicated temperatures and fitted exponentially to derive the observed exchange constant λ_{SX} .

Additionally, AIAS-labelled Hsp26S4C was mixed with LYI-labelled Hsp26S4C and the time-dependent changes in donor (410 nm) and acceptor (520 nm) fluorescence were recorded at a constant wavelength in a 1.5 mL stirring cuvette. AIAS excitation was at 336 nm. The kinetics were analyzed with the double exponential function (Equation 7) yielding the exchange rates λ_{SX-1} and λ_{SX-2} .

3.28 Analytical gel filtration (SEC-HPLC)

High performance liquid chromatography (HPLC) pumps a liquid mobile phase through a column under high pressure (up to 250 bar). An applied sample is separated at high resolution within a short running time.

As gel filtration column a Tosohaas G4000PW, separating 10-1500 kDa was used. The column can be used within a temperatures range from 10-80°C. All

experiments were performed either at 25°C or 44°C. A corresponding temperature was achieved using a temperature adjustable column oven. Tubing running from the buffer reservoir to the pumps and further to the column was kept at 25°C. Using capillary tubing, fast temperature adjustment within the column was achieved.

HPLC chromatography was applied to investigate quaternary structure and chaperone activity. All experiments were performed in 40 mM HEPES, 150 mM KCl, 5 mM EDTA pH 8.0 using a flow rate of 0.5 mL/min. Experiments were monitored by fluorescence, using an excitation wavelength of 275 nm and an emission wavelength of 307 nm. Detector sensitivity was adjusted from factor 10-1000 to enhance low signals. When required elution peaks were collected using a fraction collector, precipitated and analysed by SDS gel electrophoresis. Further experimental conditions are noted in the according figure legend.

3.29 Sedimentation equilibrium analytical ultracentrifugation (SE)

Analytical ultracentrifugation allows detection of a samples by spectroscopic techniques that is being spun at high centrifugal forces. Detection can be either by absorbance, interference, or fluorescence. Sedimentation equilibrium ultracentrifugation experiments are concerned only with the final steady-state of the experiment, when sedimentation is balanced by diffusion opposing the concentration gradient. This allows determination of molecular masses under native conditions, as the concentration distribution of the sample is independent of the shape or hydrodynamic radius of the sample.

The equilibrium concentration distribution of a sample is proportional to the angular velocity and follows a bolzman distribution. In simple cases this distribution can be described as

$$M = \frac{2RT}{(1 - v\rho)\omega^2} \cdot \frac{\delta(\ln c)}{\delta r^2}$$

Equation 13 M: molecular mass (in g/mol), R: gas constant, T: absolute temperature, ω^2 is the angular velocity of the rotor, $v\rho$: specific volume of the analyte, c is the concentration (in g/L) at a radial distance r from the axis of rotation

where M is the molecular mass (in g/mol), ω is the angular velocity of the rotor and c is the concentration (in g/L) at a radial distance r from the axis of rotation. This means that a plot of $\log(c)$ as a function of r^2 for an ideal single species sample at equilibrium sedimentation yields a slope proportional to the molecular mass.

For equilibrium sedimentation, 95 μL of the sample were mixed with 10 μL FC42 sedimentation oil and spun in a Beckman XL-A (Krefeld, Germany) equipped with absorbance and interference optics. Temperature, rotational speed and buffer conditions, were adjusted according to the experimental/sample requirements. Experimental conditions were as stated in the figure legends. Simulation of sedimentation equilibrium was carried out with the Ultrascan software. The buffer density and viscosity, as well as the specific volume (mL/g) of the polypeptide (calculated from the amino acid sequence) were calculated using the UltraScan software. Least-square fitting of the experimental data was carried out with Ultrascan, SedFit or the origin software package supplied with the instrument.

3.30 Sedimentation velocity analytical ultracentrifugation (SV)

In sedimentation velocity ultracentrifugation an initially equal distributed solute is spun at high speed, which leads to the depletion of the solute at the meniscus and its sedimentation towards the bottom of the cell. Sedimentation of a single particle cannot be followed, but the resulting sedimentation boundary allows determination of the sedimentation coefficient (s). S depends on the molecular mass and the frictional coefficient of the solute. Each solute gives a single sedimentation boundary, and thus complex mixtures can be analyzed allowing to determine homo- and heterogeneity by sedimentation velocity ultracentrifugation.

Assuming that the sedimentation of a solute delivers a sharp and symmetrical boundary, the rate of solute movement can be approximated from the midpoint or the radial position of the sedimentation boundary r (Figure 19A). The angular velocity is constant, yet the sedimentation force increases with the radial position. Thus, the velocity of the boundary increases gradually and s must thus be expressed as the differential of the time-dependent boundary movement depending on the angular velocity,

$$s = \frac{\delta r / \delta t}{\omega^2 r}$$

Equation 14 Sedimentation coefficient expressed as the differential of the radial position of the sedimentation boundary ($\delta r / \delta t$) in dependence of the angular velocity (ω^2).

A plot of $\ln(r/r_0)$, where r_0 is the radial position of the meniscus, as the function of time in seconds yields a slope of $s\omega^2$ and delivers s , where ω^2 is known from the experimental settings (Equation 15 and Figure 19B).

$$\ln(r / r_0) = s\omega^2 t$$

Equation 15

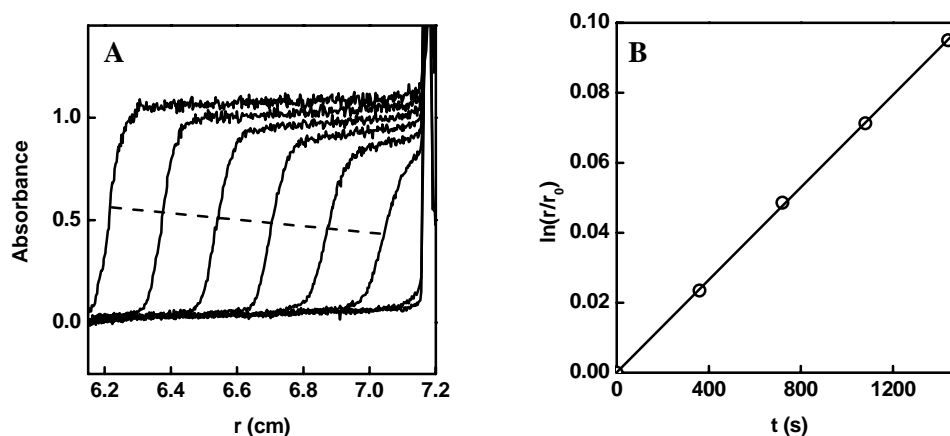


Figure 19 Example A: Sedimentation velocity profile of wt Hsp26 at 40°C indicates the movement of the sedimentation boundary of Hsp26. Sedimentation was carried out at 50,000 rpm and scans were recorded every six minute at 280 nm. B: Plot of the logarithm of the radial position of the sedimentation boundary of wt Hsp26 ($\ln(r/r_0)$) at 40°C as a function of time.

For sedimentation velocity ultracentrifugation, 350 μ L-420 μ L were spun in 2-channel centerpiece cells. The rotational speed was adjusted to the experimental conditions, in most cases 35,000 rpm-60,000 rpm. Before centrifugation, samples were temperature equilibrated at 0 rpm or max 1500 rpm for at least 2-4 hrs. Experimental conditions were as stated in the figure legends. Data analysis was carried out using the SedFit or Ultrascan software fitting the experimental data to least-square with a weight average svedberg $c(S)$ model (for details please review Lebowitz, *et al.* (Lebowitz et al., 2002)).

3.31 Dynamic light scattering (DLS)

When a beam of coherent and monochromatic light, such as from a LASER, passes through a colloidal dispersion light is scattered uniformly in all directions. In dynamic light scattering (DLS), the time-dependent changes in the scatter intensities are detected. These fluctuations arise from Brownian motion of an observed particle and apparently, DLS yields the diffusion coefficient (D) and information about a molecule's diffusion properties. The number of particles in a certain volume is given by the second Fick's law (Equation 16),

$$\frac{\delta c}{\delta t} = -D \frac{\delta^2 c}{\delta x^2}$$

Equation 16 Second Fick's law: $\delta c/\delta t$: time-dependent change of the concentration, $\delta^2 c/\delta x^2$: second derivative of the concentration in dependence of space, D: diffusion coefficient

and the time-dependent fluctuations of the scatter intensities can be detected and analyzed by autocorrelation of the signal (I) and its appearance after a defined delay time (τ) (Equation 17 and Equation 18)

$$g_2(\tau) = \frac{I(t) \cdot I(t + \tau)}{I(t)^2}$$

Equation 17 I: mean value of the signal intensity, τ : delay time

$$g_2(\tau) = e^{-\Gamma \tau}$$

Equation 18 Autocorrelation function: Γ : relaxation time, τ : delay time

Via the Stoke-Einstein equation (Equation 19), the determined diffusion coefficient at a given solvent viscosity and temperature, can be used to calculate the hydrodynamic radius (R_H). To obtain a better understanding about structural

changes that coincide with the temperature activation of Hsp26 the diffusion coefficient of Hsp26 at various temperatures was determined.

$$D = \frac{k_B T}{6\Pi\eta R_H}$$

Equation 19 Stoke-Einstein relation: D: Diffusion coefficient ($\text{m}^2 \text{s}^{-1}$), k_B : Boltzmann constant ($1,38 \cdot 10^{-23} \text{ kg m}^2 \text{ s}^{-2} \text{ K}^{-1}$), T: absolute temperature (K), η : solvent viscosity ($\text{kg m}^{-1} \text{ s}^{-1}$), R_H : hydrodynamic radius (m)

For DLS measurements, Hsp26 was diluted to $0.5\text{-}2 \text{ mg mL}^{-1}$ into 40 mM HEPES, pH 7.5, centrifuged and filtered to remove aggregates. The sample was irradiated with a 658 nm LASER and the scatter light signal was averaged over 30 s and 200 accumulations were recorded. The data were analyzed with the Quelsmon NT software (Partick Umbach, Abbott Laboratories and Yannis Georgalis, FU Berlin). Measurements were carried out at 25°C or as indicated in the figure legends.

3.32 Chaperone assays

3.32.1 Thermal-induced aggregation of citrate synthase (CS)

CS is a homodimer with a molecular mass of 2×49 kDa. Incubation of native CS at high temperatures, such as 38°C leads to its quantitative aggregation. This can be followed by monitoring increasing scatter light signal at 360 nm. Aggregation was monitored in 400 μl quartz cuvettes in a UV spectrophotometer equipped with a water bath. 0.5 μM CS were incubated at 44°C in 40 mM HEPES, 5 mM EDTA, pH 8.0 and the influence on CS aggregation of increasing Hsp26 concentrations and variants were assayed. When required, aggregation of CS in the absence of chaperones was normalized to 1.

3.32.2 Thermal-induced aggregation of glutamate dehydrogenase (GDH)

Bovine GDH (Roche, Penzberg, Germany) is a homo hexamer with a molecular mass of 6×59 kDa. Incubation of GDH at 45°C leads to unfolding, followed by aggregation. The aggregation of GDH can be monitored in a UV spectrophotometer at a wavelength of 350 nm. Here, GDH aggregation was used to test for the chaperone activity of Hsp26 and its variants. To this end, 1 μM GDH were incubated at 45°C in 40 mM HEPES, 5 mM EDTA, pH 8.0 in the absence and the presence of increasing Hsp26 concentrations.

3.32.3 Aggregation of chemically denatured CS

CS was denatured in 5 M Gdm·HCl for at least two hours at RT and then subjected to a preparative desalting column (Desalting HighPrep, GE Healthcare, Freiburg, Germany) running in 5 M Gdm·HCl. CS was then prepared at a concentration of 20 μ M. Aggregation of chemically denatured CS was induced by diluting CS 10fold into native buffer (40 mM HEPES, 5 mM EDTA, pH 8.0) at 20°C, or as indicated elsewhere. CS aggregation was monitored in a fluorescence spectrometer, recording the scatter light signal at 350 nm (Buchner et al., 1998).

3.32.4 Aggregation of chemically denatured GDH

GDH (Roche, Penzberg, Germany) was dissolved at a concentration of 10 mg/ml in 5 M Gdm·HCl and denatured for at least two hours. To separate GDH from salt and other compounds, the solution was subjected to a preparative desalting column (Desalting HighPrep, GE Healthcare, Freiburg, Germany) running in 5 M Gdm·HCl. GDH was then prepared at a concentration of 20 μ M. Aggregation of chemically denatured GDH was induced by diluting GDH 10fold into native buffer (40 mM HEPES, 5 mM EDTA, pH 8.0) at 20°C, or as indicated elsewhere. The aggregation was monitored in a fluorescence spectrometer, recording the scatter light signal at 350 nm over 400 s (Franzmann et al., 2008).

4 Results

Molecular chaperones prevent the irreversible aggregation of polypeptides and assist protein folding. To distinguish between the native and the non-native conformation of their clients, most chaperones exploit ATP binding and hydrolysis to switch between conformational states with different affinities for their polypeptide substrates (Buchner, 1996; Hartl, 1996). Hsp26 from yeast differs from these chaperones in this respect, as the shift from its low to its high affinity state for polypeptide binding is controlled by the stressor itself, temperature (Franzmann et al., 2008; Franzmann et al., 2005; Haslbeck et al., 1999). However, the underlying mechanism of this regulation principle was unknown. To obtain a mechanistic picture of this sophisticated temperature activation process, the thermodynamic and kinetic parameters of the structural rearrangements that correlate with its temperature activation were determined in a comprehensive biochemical and biophysical *in vitro* study in combination with mutational analysis.

4.1 wt Hsp26 and Hsp26 variants

The Hsp26 monomer can be dissected into four distinct parts; the N-terminal domain (NTD), the middle domain (MD), the α -crystalline domain and the C-terminal extension (CTE). Figure 20 shows a schematic overview of Hsp26 with residues indicating the domain borders. The monomers associate to form dimers, which then form the native oligomer consisting of 24 identical subunits.

In the following, the Hsp26 primary structure is presented and the rationale for mutational design is discussed.

Analysis of the Hsp26 amino acid sequence revealed that only MD and CTE possess a Trp residue. Seven Trp residues are randomly distributed throughout the MD and the α -crystallin domain. Moreover, ten of eleven Phe are located within NTD (6) and MD (4), whereas only one is in the middle of the α -crystallin domain. The fluorescence of Trp is sensitive to changes in its chemical environment. Thus, Trp can be used to monitor the transition between conformational states of a protein. Although the fluorescence of Tyr can contribute to the overall fluorescence of a protein, commonly its fluorescence does not change significantly upon conformational changes, and the fluorescence of Phe is small, and can usually be neglected.

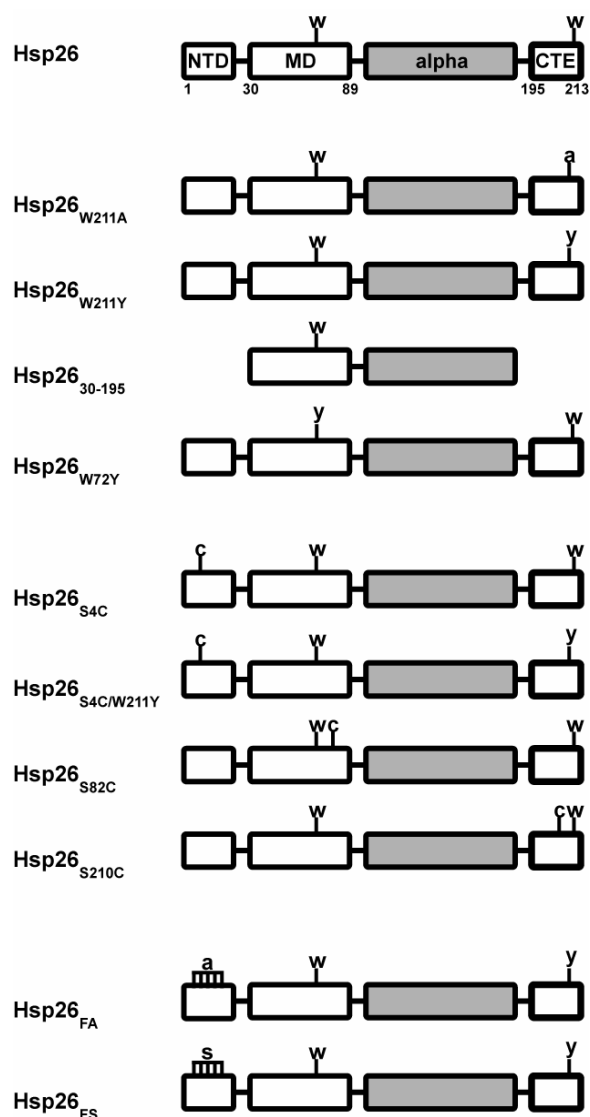


Figure 20 Schematic domain structure of wt Hsp26 and Hsp26 variants with indicated amino acids shown in single letter code. NTD: N-terminal domain, MD: Middle domain, alpha: α -crystallin domain, CTE: C-terminal extension

Cys possesses extraordinary properties. Due to the presence of a terminal thiol group (SH), it can either be in a reduced or oxidized state. This allows cysteine to form covalent bonds with either other cysteines to form disulfide bridges or with extrinsic molecules, such as activated fluorophores that carry e.g. a reactive thiol-, maleimide or iodoacetamide group. However, Hsp26 does not contain Cys residues, yet it contains Ser residues randomly distributed throughout the

polypeptide chain. The structure of Ser is very similar to that of Cys, yet it carries a terminal hydroxyl group (OH) instead. The absence of Cys residues makes Hsp26 an ideal candidate for site-specific introduction of Cys residues by a conserved substitution of Ser residues.

Based on the primary structure analysis, Hsp26 variants were generated to monitor conformational changes by fluorescence spectroscopy. In detail, both Trp residues were replaced with Try or Ala to generate the single Trp variants Hsp26W72Y, Hsp26W211Y and Hsp26W211A (Figure 20). However, Hsp26W72Y proved to be insoluble after protein biosynthesis and could not be refolded to the native state after protein purification (data not shown). Hence, this variant was not further investigated. In contrast, replacement of the C-terminal Trp W211 yielded soluble Hsp26W211Y that could be used to monitor changes in W72 fluorescence specifically.

To obtain site-specific spectroscopic probes for each domain, Cys residues were introduced by site-directed PCR mutagenesis into Hsp26, which were then subsequently modified with fluorescence dyes (Figure 20). For NTD, Ser 4 was replaced by Cys, producing the N-terminal Cys variant Hsp26S4C. In addition Ser 82 and Ser 210 were replaced, yielding the MD variant Hsp26S82C and Hsp26S210C, respectively. These variants were used to gain insight into the site-specific structural rearrangements of Hsp26 domains by fluorescence spectroscopy, fluorescence quenching and fluorescence resonance energy transfer (FRET). Besides these fluorescence applications, the Cys variants were also tested for their ability to form intramolecular disulfide bridges, covalently cross-linking neighboring Hsp26 subunits. This allowed testing for the influence of interchain disulfide bridges on oligomer stability and the chaperone activation of Hsp26.

In a different set of Hsp26 variants, the patch of N-terminal Phe residues was replaced by Ser or Ala, respectively. In addition to its spectroscopic properties, Phe belongs to the class of hydrophobic amino acids. Replacement of the

N-terminal Phe residues might thus have influence for Hsp26 oligomer stability and/or substrate binding.

All Hsp26 variants were generated by site-directed PCR mutagenesis, using primers carrying the corresponding mutant codon (Table 1). The PCR fragments were then ligated into pET28b+ via NCO1 and NOT1 restriction sites (3.2). Protein synthesis was carried out in *E.coli* BL21 DE3 cells. All proteins were purified using 150 mL Q-sepharose resin, a 6 mL Resource Q and a 26/60 Superdex 200-pg column, yielding highly purified Hsp26 with quantities of 40-120 mg L⁻¹ and OD~3 expression culture, depending on the Hsp26 variant (3.26).

4.2 Redox analysis of Hsp26

First, the Cys variants were tested for their ability to form disulfide bridges. When analyzed by SDS-PAGE, reduced Hsp26S4C and Hsp26S210C migrated as monomers like wt Hsp26. When incubated with oxidizing agents, such as GSSG, oxidized DTT or incubation with air, wt Hsp26 migrated as a monomer, whereas a significant fraction of Hsp26S4C and Hsp26S210C formed disulfide-bridged dimers (Figure 21A). In contrast to these variants, Hsp26S82C remained monomeric when incubated under oxidizing conditions (data not shown). Detection of free Cys with DTNB revealed that approx. 2/3 of the Cys in Hsp26S4C were oxidized, whereas 1/3 formed disulfides in Hsp26S210C (Figure 21B). No thiol-reactive groups were detected with wt Hsp26 and when Hsp26S82C was analyzed, almost all Cys residues were detected.

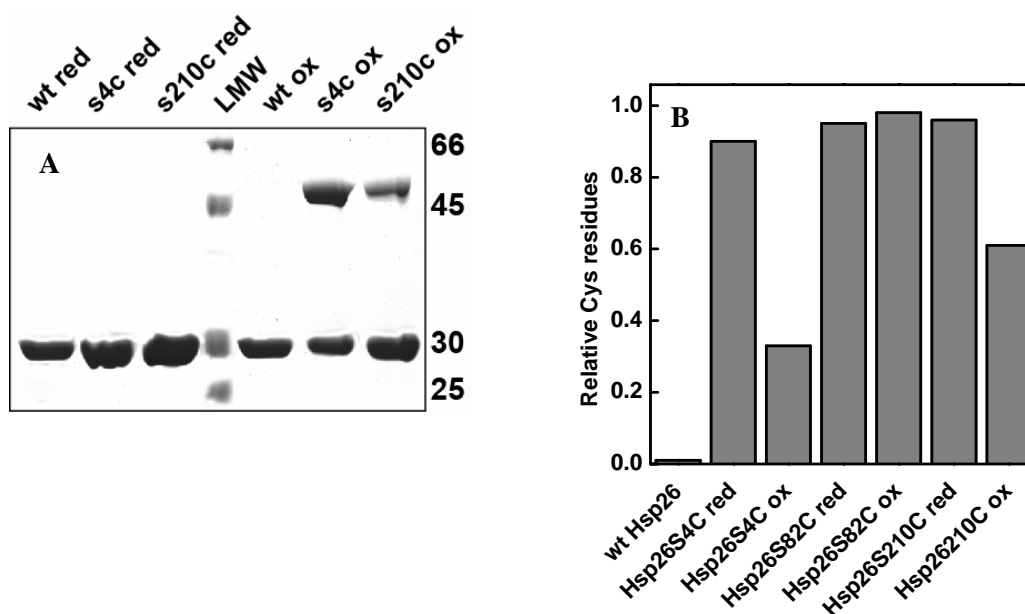


Figure 21 A: Redox-state analysis of wt Hsp26, Hsp26S4C and Hsp26S210C by SDS-PAGE. Hsp26 and Cys variants were incubated with reduced or oxidized DTT and analyzed on a 15% SDS-PAGE. B: Hsp26 and Cys variants were reduced or oxidized with DTT for 1 h at RT. Then, DTT was removed by size exclusion chromatography using a HiPrep Desalting column. The sample concentration was determined using UV-spectroscopy and the free thiols were determined with DTNB recording the absorbance at 420 nm.

These results indicate that both termini of Hsp26 are in proximity with each other, as Hsp26S4C and HspS210C can form disulfide bridges under oxidizing conditions. Furthermore, MD is unable to form disulfide bonds with other MDs. The stoichiometry allows drawing conclusions about the symmetry and the number of polypeptide chains involved. About 2/3 of the N-termini are able to form disulfide bonds. This is suggestive for a trimerization of the N-termini, in which two of the three termini become cross-linked, whereas one remains reduced and indicates that the N-termini are located in a three-fold symmetry. 1/3 of the C-termini can form disulfide bridges. One might speculate that 12 C-termini associate into four trimers, of which again two can be cross-linked under oxidizing conditions and one, as well as the remaining 12, stay reduced. This might indicate that the CTE can adopt at least two different conformations

in which 12 C-termini are located in a threefold and 12 C-termini in a twofold symmetry.

4.3 Secondary structure analysis by CD spectroscopy

Circular dichroism is the property of optically active molecules to absorb left and right polarized light to different extent. Whereas, far UV CD spectroscopy can be used to gain information about the conformation of a polypeptide backbone and thus about the secondary structure of proteins, near UV CD spectroscopy delivers information about the environment of the aromatic amino acids and hence about a proteins tertiary structure. Additionally, temperature unfolding experiments can be carried out to gain information about the structural stability and conformational changes.

4.3.1 Secondary structure analysis

Secondary structure analysis by far UV CD spectroscopy of Hsp26 and the variants revealed that all variants adopt structures with β -sheet structure (Stromer et al., 2004). This is in agreement with the structures for the α -crystallin domains determined for Hsp16.5 and Hsp16.9 by X-ray crystallography (Kim et al., 1998; van Montfort et al., 2001). At 25°C, Hsp26 exhibits a local minimum at 214 nm with mean intensities of $-9000 \text{ deg cm}^2 \text{ dmol}^{-1}$. Deconvolution of the spectrum with the CDNN software revealed a secondary structure content of $\sim 17\%$ α -helix and 55% β -sheet structure. The far UV CD spectra of the tryptophan variants Hsp26W211Y and Hsp26W211A exhibit minima at 214 nm and the spectra superimpose with the wt spectrum (Figure 22A). Deconvolution of the data with the CDNN software did not reveal significant structural differences,

indicating that the secondary structures of Hsp26W211Y and Hsp26W211A are indistinguishable from that of the wt protein (Table 4)

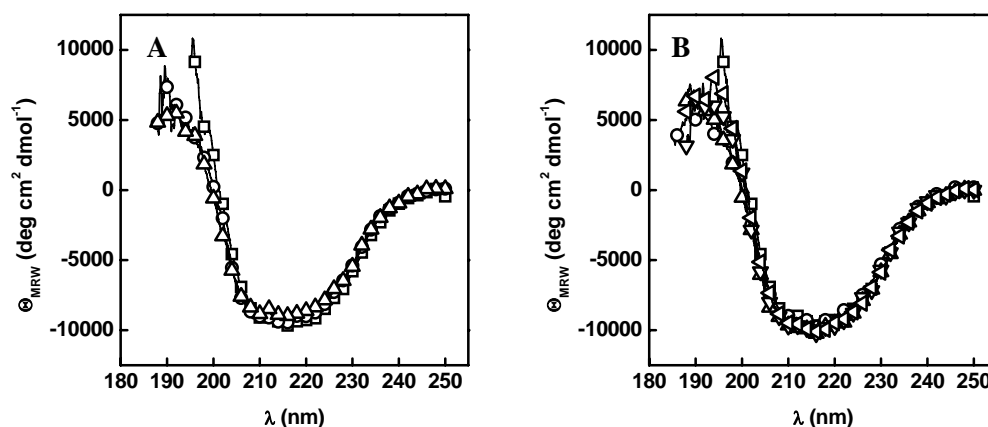


Figure 22 A: Far UV CD spectra of wt Hsp26 (\square), Hsp26W211Y (\circ) and Hsp26W211A (\triangle) and B: of wt Hsp26 (\square), Hsp26S4C (\circ), Hsp26S4C/W211Y (\triangle), Hsp26S82C (∇) and Hsp26S210C (\triangleleft) in 10 mM potassium phosphate, pH 7.5. Spectra were recorded at 25°C.

Similarly, the spectra of Hsp26S4C (data not shown), Hsp26S4C/W211Y, Hsp26S82C (data not shown) and Hsp26S210C were superimposable with the wt spectrum, indicating that the secondary structures of the cystein variants are similar to that of the wt protein (Figure 22B). Since, Hsp26S4C, Hsp26S4C/W211Y and Hsp26S210C can form intramolecular disulfide bridges, spectra of both redox states were recorded. Apparently, the secondary structures of the Cys variants are not influenced by the presence of disulfide bridges (Figure 23A and B, and data not shown).

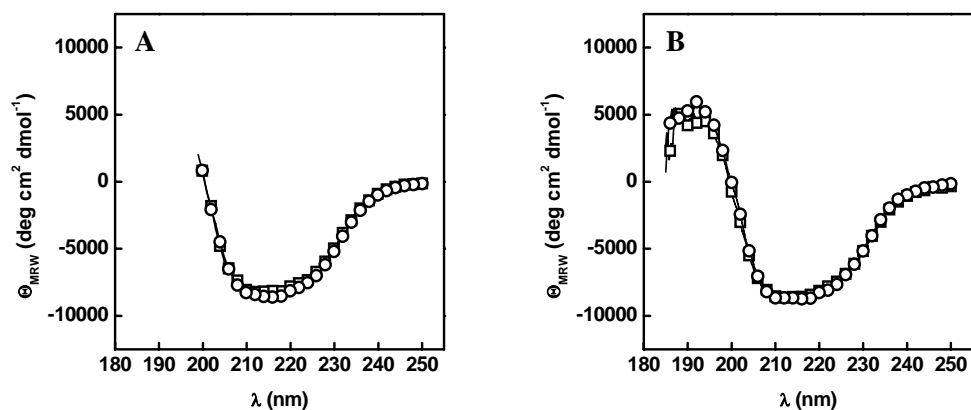


Figure 23 A: Far UV CD spectra of reduced (\square) and oxidized (\circ) Hsp26S4C/W211Y and B: Far UV CD spectra of reduced (\square) and oxidized (\circ) Hsp26S210C. Spectra were recorded at 25°C.

Substitution of the N-terminal Phe residues to Ser or Ala, respectively, altered the secondary structure of the mutants Hsp26FS and Hsp26FA (Figure 24A). The spectrum for Hsp26FS superimposes with that determined for Hsp26FA with a local minimum at 205 nm, suggestive for an increase in random coil structure compared to wt Hsp26 and indicates that the structural change is independent of the amino acid used for the replacement. The structure of the Phe variants appears to be similar to that of the truncation variant Hsp26 30-195, yet they exhibit a pronounced minimum at 205 nm, suggesting that the N-terminal and C-terminal extension can adopt random coil structure.

In contrast to the full-length variants, the truncation variant Hsp26 30-195 exhibits a local minimum at 208 nm with slightly reduced intensities, suggestive for a relative increase of random coil structure (Figure 24B). Hsp26 30-195 exhibits an increased β -sheet structure content ($\sim 70\%$), which may be due to the deletion of the N-terminal and C-terminal residues, which presumably adopt α -helical structures.

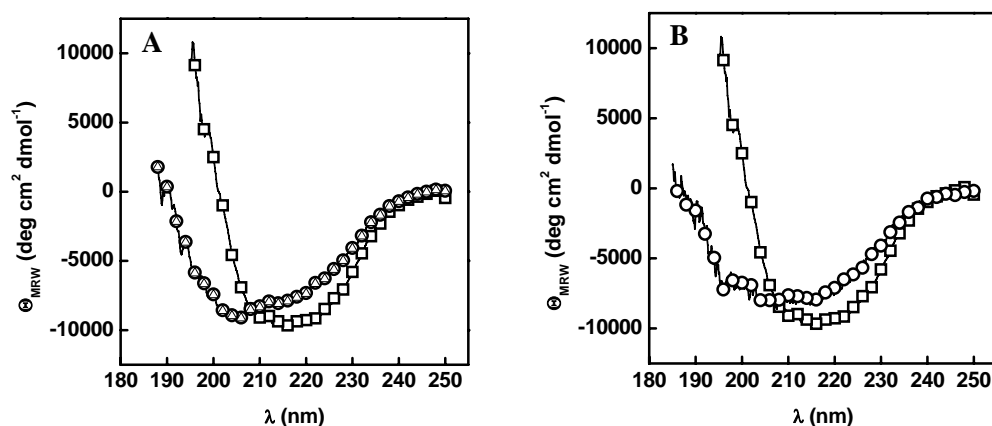


Figure 24 A: Far UV CD spectra of wt Hsp26 (\square), Hsp26FS (\circ) and Hsp26FA (\triangle), in 10 mM potassium phosphate, pH 7.5 and B: Far UV CD spectra of wt Hsp26 (\square) and Hsp26 30-195 (\circ). Spectra were recorded at 25°C.

4.3.2 Temperature-induced secondary structure changes

In order to determine the stability of the Hsp26 variants, thermal unfolding was monitored by CD spectroscopy.

In agreement with previous results, temperature unfolding of wt Hsp26 revealed two cooperative transitions (Figure 25A) (Stromer et al., 2004). The first one takes place within the physiological temperature range for yeast cells (between 30°C–45°). The second transition takes place between 60°C–80°C. Whereas the first transition was reversible and exhibits a transition midpoint of 36°C when the sample was heated to 60°C, the second transition is irreversible and exhibits a transition midpoint of 70°C. Supposedly, this reflects the thermal denaturation of Hsp26 and explains why heating Hsp26 to 60°C (to completion of the first transition) is reversible, whereas heating above 60°C induces irreversible structural changes. The high amount of secondary structure at 45°C is suggestive for a folded equilibrium intermediate. The free Gibb's energy for this transition was $\Delta G \sim 7 \text{ kJ mol}^{-1}$. A concentration-dependent analysis of the first transition

revealed a transition midpoint of 35°C at 0.1 mg mL⁻¹, whereas the midpoint was increased by only 2°C to 37°C at 1 mg mL⁻¹ (Figure 25B). The small increase in stability suggests that the conformational changes mainly result from secondary structure changes.

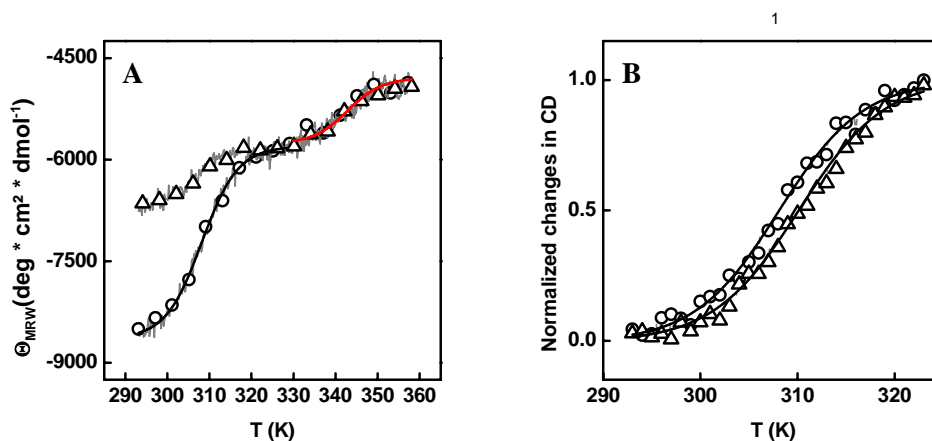


Figure 25 A: Temperature-induced unfolding (○) and refolding (△) of 50 μg mL⁻¹ wt Hsp26. Unfolding was monitored at 220 nm in a 1 mM quartz temperature cuvette in 10 mM potassium phosphate, pH 7.5. Analysis of the first transition (black line) revealed a transition midpoint of 35°C and ΔG of ~ 7 kJ mol⁻¹. Note: The first transition event was reversible when the sample was heated to temperatures below 60°C only. Analysis of the second transition (red line) revealed a transition midpoint of $\sim 70^\circ\text{C}$. B: Analysis of the first temperature transition at (○) 0.1 mg mL⁻¹ or (△) 1 mg mL⁻¹ wt Hsp26

To test whether the structural stability of Hsp26 is affected by disulfide bridges, Hsp26S4C and Hsp26S210C were subjected to thermal unfolding experiments. Like for wt Hsp26, two temperature transitions were observed with reduced (data not shown) and oxidized Hsp26S4C and Hsp26S210C, respectively (Figure 26A and B). Both variants exhibit transition midpoints at $\sim 36^\circ\text{C}$ and $\sim 73^\circ\text{C}$, respectively, similar to those observed with wt Hsp26. An increase in stability through disulfide bridges was not detected.

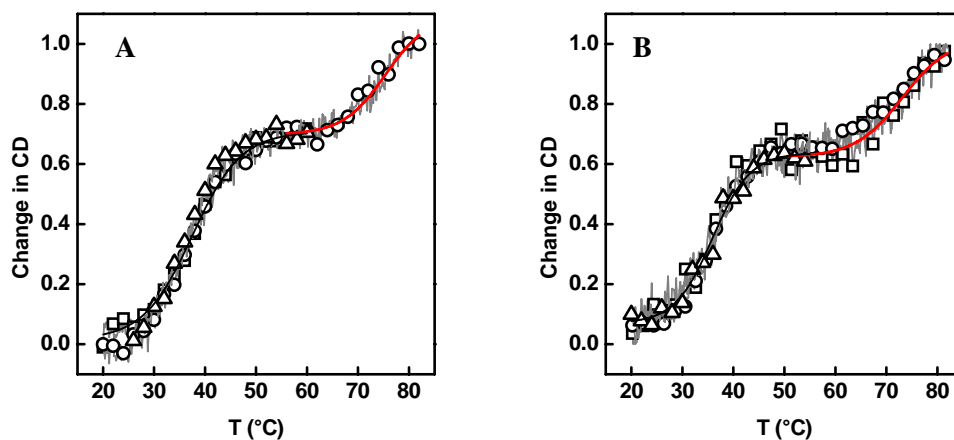


Figure 26 Thermal unfolding of (□) 0.1 mg mL⁻¹ and (○) 0.5 mg mL⁻¹ oxidized Hsp26S210C and refolding of (△) 0.1 mg mL⁻¹ reduced Hsp26S4C. B: Thermal unfolding of (□) 0.1 mg mL⁻¹ and (○) 0.5 mg mL⁻¹ oxidized Hsp26S210C and refolding of (△) 0.1 mg mL⁻¹ reduced Hsp26S210C. CD changes were monitored at 220 nm in a 1 mM quartz temperature cuvette in 10 mM potassium phosphate, pH 7.5. To maintain the redox state of the reduced and oxidized protein during the experiment, respectively, free Cys residues were covalently modified with IAA prior to the CD analysis. Analysis of the second transition (red line).

A different picture was observed with Hsp26FS and Hsp30-195. At 220 nm, for neither of the variants the signal changed between 20°C–60°C (Figure 27A and data not shown). When the signal was recorded at 205 nm, a cooperative unfolding with a transition midpoint of 34°C and a free Gibbs energy of ~6 kJ mol⁻¹ was observed with Hsp26 30-195 (Figure 27B and Suppl. Figure 1). The transition midpoint and the free Gibbs energy were similar to the stabilities determined with wt Hsp26, suggesting that they occur in the same process. Deconvolution of the CD spectrum of Hsp26 30-195 at 45°C revealed a folded β -sheet structure, very similar to the spectrum obtained with the wt protein at 45°C (data not shown).

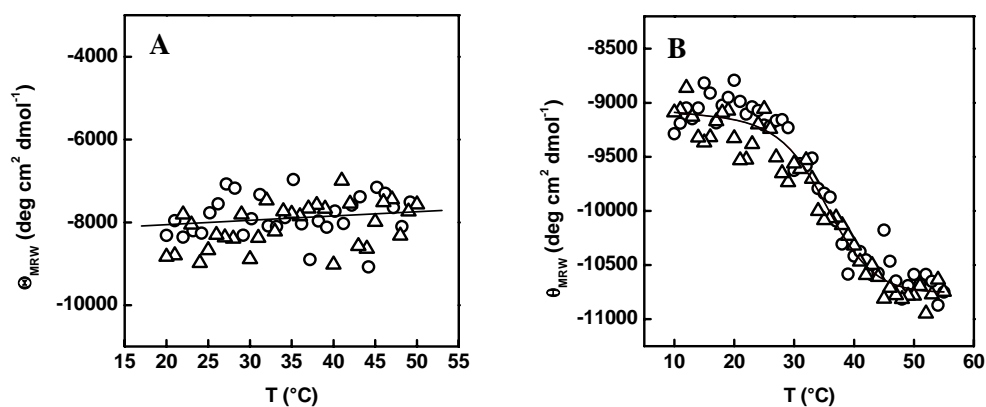


Figure 27 Thermal unfolding and refolding of Hsp26 variants monitored by CD spectroscopy. A: 0.1 mg mL⁻¹ Hsp26FS at 220 nm. B: 0.1 mg mL⁻¹ Hsp26 30-195 at 205 nm.

Table 4 Secondary structure elements and stability of Hsp26 and variants were determined by CD spectroscopy. α -helical, β -sheet and random coil structure content were predicted using the CDNN and DichroWeb software. Gibbs free energy and T_M are shown for the first and reversible transition and thermal unfolding was monitored at 220 nm. * Unfolding was determined at 205 nm.

	α -helix (%)	β -sheet (%)	Rnd coil (%)	ΔG (kJ mol ⁻¹)	T_M (°C)
Hsp26wt	17	46	37	7.3 (\pm 1.1)	36
Hsp26W211Y	16	44	38	7.4 (\pm 1.8)	35
Hsp26W211A	17	48	34	7.1 (\pm 1.9)	34
Hsp26S4C(red)	18	45	37	7.4 (\pm 1.2)	37
Hsp26S4C(ox)	17	46	37	7.6 (\pm 1.6)	36
Hsp26S210C(red)	17	46	38	7.6 (\pm 1.6)	35
Hsp26S210C(ox)	17	45	39	7.0 (\pm 1.9)	36
Hsp26FS	n.d.	n.d.	n.d.	n.d.	n.d.
Hsp26FA	n.d.	n.d.	n.d.	n.d.	n.d.
Hsp26 30195	12	46	32	5.9 (\pm 1.3)*	34*
Hsp26wt	17	46	37	7.3 (\pm 1.1)	

4.4 Tertiary structure analysis of Hsp26

4.4.1 Tertiary structure analysis by near UV CD spectroscopy

The differential absorbance of the aromatic amino acids Trp, Tyr and Phe, delivers information about their positioning in an asymmetric environment, such as in a folded polypeptide. Information about the tertiary structure of a protein can be derived from analyzing the packing of aromatic residues by near-UV CD spectroscopy.

At 25°C, wt Hsp26 exhibits absorbance maxima at 295 nm and 285 nm due to the selective absorbance of Trp 72 and 211, as well as a maximum of 278 nm due to the absorbance of Tyr residues (Figure 28A). The broad minimum below 276 nm results from the collective absorbance of Trp, Tyr and Phe residues. Similar spectra were observed for Hsp26W211Y (Figure 28B).

Heating wt Hsp26 to 45°C induced reversible spectral changes at 295 nm, 285 nm, indicating a conformational rearrangement of at least one Trp residue (Figure 28A). The absorbance at 278 nm was unaffected by temperature, suggesting that this absorbance band results mainly from Tyr residues that do not seem to alter their spectroscopic properties upon temperature shift. Similar changes were observed with the single Trp variant Hsp26W211Y, indicating that W72 is structurally rearranged upon temperature shift (Figure 28B). It is notably that temperature treatment mainly affects the absorbance signals at 268 nm. In addition to Trp and Tyr, Phe residues absorb at this wavelength as well. The molar extinction coefficient of Phe is significantly smaller compared to that of Trp, yet Hsp26 possesses 11 Phe residues and only two Trp residues. Hence, the

spectral changes observed with wt Hsp26 and Hsp26W211Y might also result from Phe residues. Interestingly, nine of the eleven Phe residues are located within the first 20 amino acids of the N-terminal region of Hsp26, supporting the conclusion that activation of Hsp26 coincides with a structural rearrangement of this region.

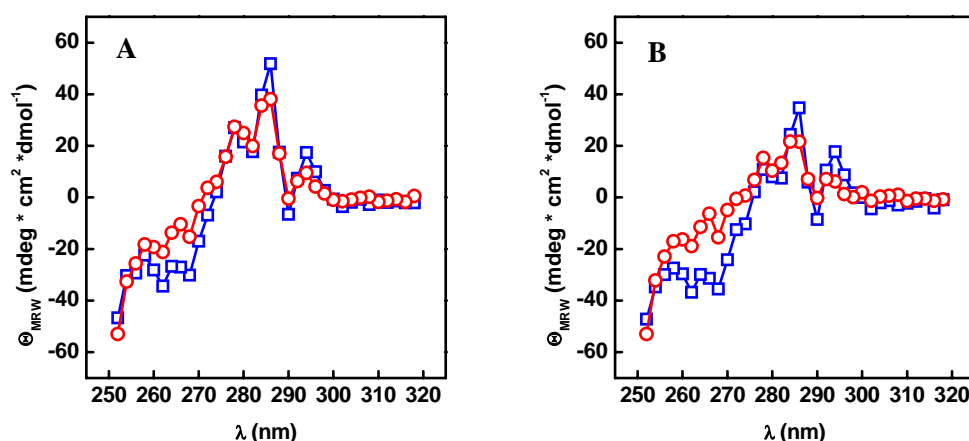


Figure 28 Near-UV CD spectra of (A) wt Hsp26 and (B) Hsp26W211Y at 25°C (\square) and 45°C (\circ), in 10 mM sodium phosphate, pH 7.5

Analysis of reduced and oxidized Hsp26S4C/W211Y at 25°C revealed similar spectra (Figure 29A and B). Like the wt protein, absorbance maxima were detected at 295 nm, 285 nm, 278 nm for both redox states, suggesting that the structure of the Cys variants is very similar to that of the wt protein and that disulfide bridges do not induce a different conformation. Analysis of the Cys variants at 45°C revealed conformational changes within Hsp26 (Figure 29A and B). Again the spectra of both redox states were very similar to that of the wt protein and apparently subunit cross linking through disulfide bridges does not abolish the structural rearrangement. The difference at 278 nm between reduced and oxidized S4C might be explained by the oxidized state of the cysteins, which can also absorb in this range.

The aromatic residues in Hsp26FS and Hsp26 30-195 appeared to be in a very similar environment compared to wt Hsp26 (Figure 29C and D). Although these variants carry substantial modifications, both exhibit maxima at 295 nm, 285 nm and 278 nm, suggesting that both adopt a conformation similar to that of the wt protein. Apparently, replacement of the N-terminal Phe residues in Hsp26FS, as well as the deletion of the N-terminal 30 amino acids and the C-terminal extension in Hsp26 30-195, did not alter the tertiary structure significantly. This in turn allows to draw the conclusion that the spectrum reflects mainly to the structure of the MD and α -crystallin domain. Structure analysis of Hsp26FS and Hsp26 30-195 at 45°C revealed spectral changes similar to those observed with wt Hsp26. Since the α -crystallin domain does not change its structure in this temperature range (Stromer et al., 2004), all spectral changes are likely to results from the conformational rearrangement of MD, which presumably is functional in Hsp26FS, as well as in Hsp26 30-195. Heating Hsp26 30-195 to 80°C resulted in a complete loss in tertiary signal, suggestive for the thermal unfolding of both, the MD and the α -crystallin domain (Figure 29D).

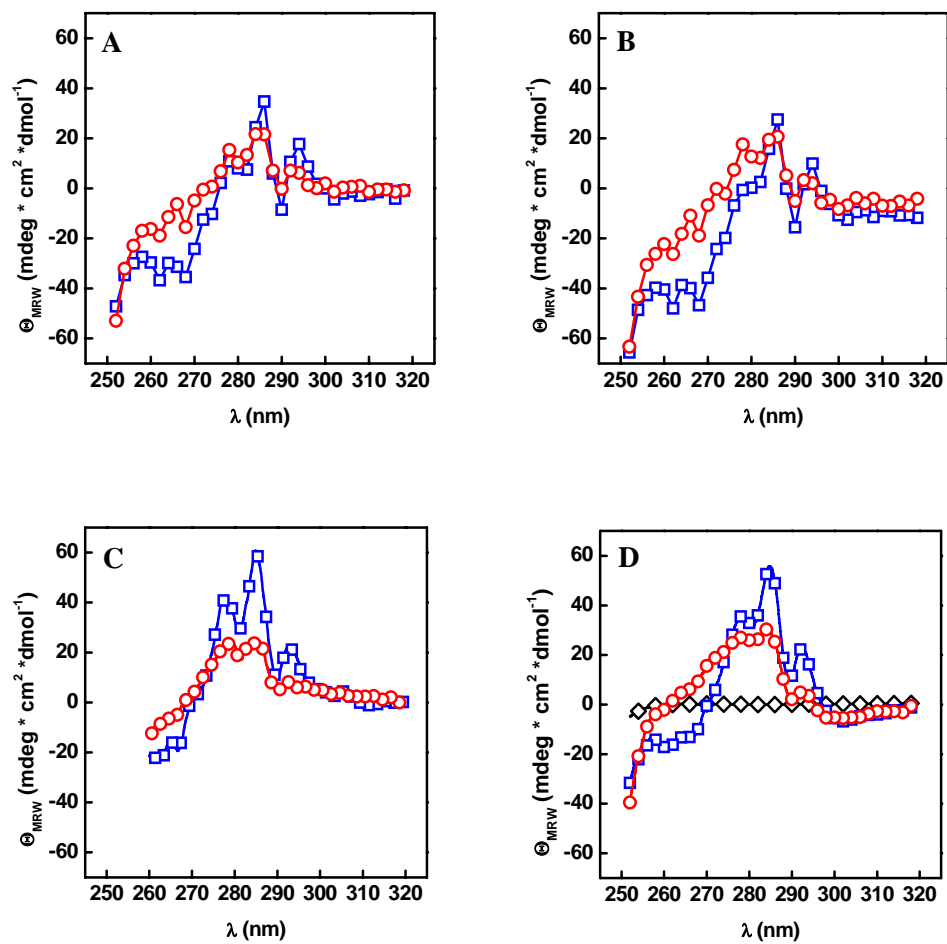


Figure 29 Near-UV CD spectra of A: reduced and B: oxidized Hsp26S4C/W211Y at 25°C (□) and 45°C (○), C: Hsp26FS and D: Hsp26 30-195 at 25°C (□), 45°C (○), and 85°C (◇) in 10 mM sodium phosphate, pH 7.5.

4.4.2 Tertiary structure analysis by fluorescence

The fluorescence of Trp is sensitive to changes in its chemical surrounding. In hydrophobic environment, such as in the core of a protein, Trp exhibits a fluorescence maximum at 310 nm, whereas the maximum shifts towards longer wavelengths (355 nm) (Schmid and Creighton, 1989). The transition between conformational states of a protein can thus be monitored by Trp fluorescence. However, the presence of multiple spectroscopic probes in a polypeptide can complicate data interpretation. Hsp26 possesses two Trp residues: W72 in the MD and W211 in the CTE. To simplify spectroscopic analysis, the single Trp variants Hsp26W211Y and Hsp26W211A were analyzed in comparison to wt Hsp26.

At 25°C, wt Hsp26 exhibits a fluorescence maximum at 326 nm, indicative for a relatively hydrophobic environment for both Trp residues (Figure 30A). In contrast to the wt protein, Hsp26W211Y and Hsp26W211A exhibit fluorescence maxima at shorter wavelength (314 nm), suggesting that W72 in MD is sequestered within the protein (Figure 30B). It can be concluded, that W211 is somehow more solvent accessible than W72. As expected, the fluorescence intensities of W211Y and W211A were reduced by half due to the replacement of the C-terminal Trp residue.

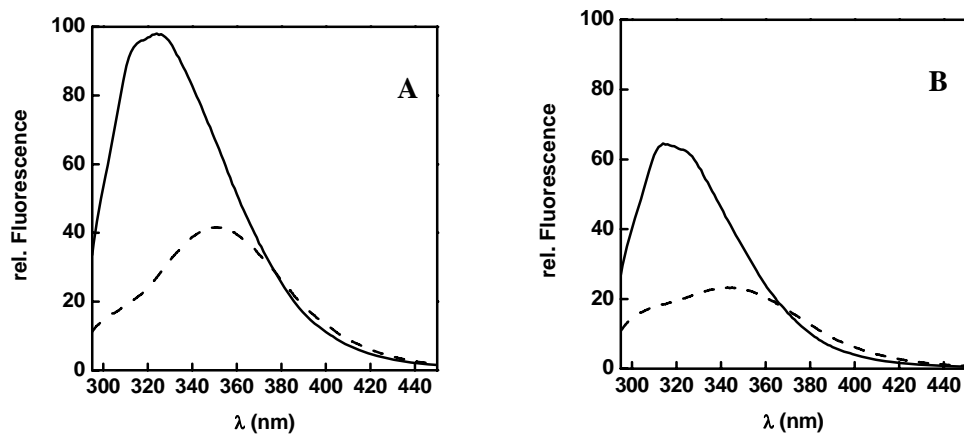


Figure 30 Fluorescence spectra of (A) 1 μ M wt Hsp26 and (B) 1 μ M Hsp26W211Y in 40 mM HEPES, 5 mM EDTA, pH 8.0 at 25°C (straight line) and 45°C (dashed line). Note: control experiments revealed that the spectral properties of Hsp26 in sodium phosphat were very similar to the results obtained using HEPES.

When analyzing the temperature-activated state of Hsp26 by fluorescence at 45°C, both Trp residues (W72 and W211) behaved differently. Whereas wt Hsp26 exhibits a maximum at 355 nm, W72 in W211Y was shifted to 343 nm only, suggesting that W72 remains at least in a partially folded structure, whereas W211 becomes more solvent accessible (Figure 30A and B). Again, the fluorescence intensity of wt Hsp26 was double that of the single Trp variants, suggesting that both Trp residues contribute by approximately 50% to the native Trp fluorescence in Hsp26 at 25°C, as at 45°C.

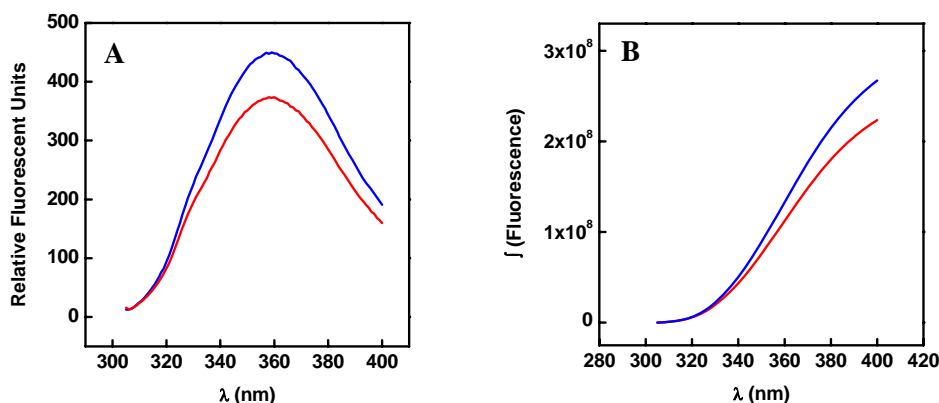


Figure 31 A: Fluorescence of 1 μM N-acetyltryptophanamide in 40 mM HEPES, pH. 7.5 at 30°C (blue) and 40°C (red). B: Integrated fluorescence intensity of N-acetyltryptophanamide at 30°C (blue) and 40°C (red).

For comparison, the effect of temperature on the spectral fluorescence properties, free N-acetyltryptophan amide was assayed at 30°C and 40°C (Figure 31A). As expected for the fluorescence of tryptophan in polar environment, the maximum of free N-acetyltryptophan amide was at 360 nm and independent of the temperature. And in agreement with the literature (Schmid and Creighton, 1989), at 40°C the integrated fluorescence signal was reduced by 16% compared to the integrated fluorescence signal at 30°C (Figure 31B). This demonstrates that the pronounced changes in fluorescence observed with Hsp26 cannot be explained by a temperature effect on Trp fluorescence but reflect conformational changes of Hsp26.

To test for the influence of cross-linked subunits upon the structure of Hsp26, oxidized Hsp26S4C/W211Y was subjected to fluorescence spectroscopy. When Hsp26S4C/W211Y was analyzed at 25°C, the fluorescence maximum was at 315 nm and intensities were similar to those observed with Hsp26W211Y (Figure 32A and B). This is suggestive for a native environment of W72, and indicates that the tertiary structure of the oxidized variant is very similar to that of Hsp26W211Y. When oxidized Hsp26S4C/W211Y was analyzed at 45°C, the emission maximum was shifted to 343 nm, indicating a conformational change that led to the structural rearrangement of W72 in MD (Figure 32B). The spectral shift is comparable to that observed with Hsp26W211Y and suggests that the disulfide bridges do not inhibit the structural rearrangement of Hsp26.

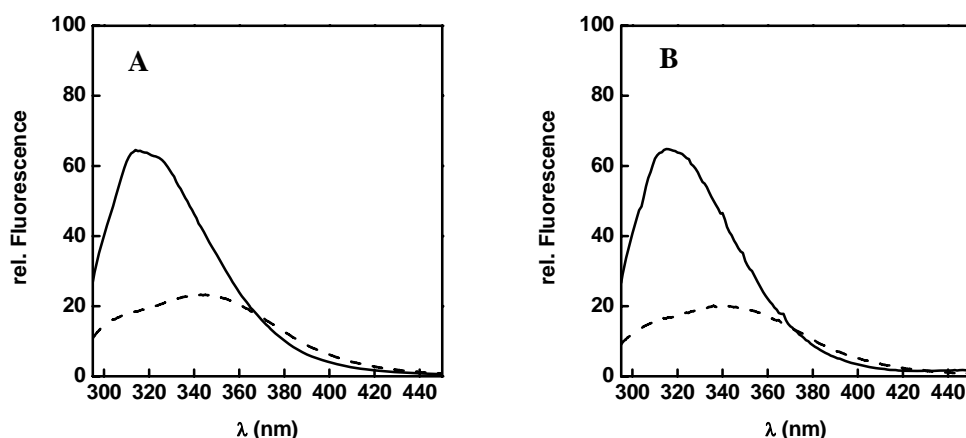


Figure 32 Fluorescence spectra of (A) 1 μM Hsp26W211Y and (B) 1 μM oxidized Hsp26S4C/W211Y in 40 mM HEPES, 5 mM EDTA, pH 8.0 at 25°C (straight line) and 45°C (dashed line).

4.5 Quaternary structure of Hsp26

4.5.1 Quaternary structure analysis by analytical gel filtration

With analytical gel filtration, information about the hydrodynamic parameters of a protein can be obtained. The molecular mass can be estimated for globular-shaped proteins under calibrated conditions. However, the observed molecular mass is strongly influenced by the shape and the hydrodynamic radius of a protein and thus analytical SEC delivers only apparent molecular weights. Here, analytical SEC was used to obtain information about the quaternary structure of Hsp26 and the variants used in this study.

Analysis of wt Hsp26 with analytical gel filtration at room temperature revealed an elution time of 16.5 min (flow rate 0.5 mL min⁻¹) (Figure 33A). The apparent molecular mass for wt Hsp26 determined from a calibration curve revealed a molecular mass of ~ 600 kDa, indicating that Hsp26 is composed of multiple subunits. When Hsp26 was analyzed with analytical gel filtration running at 45°C, the elution time was increased to 21 min, indicating a reduced Hsp26 molecular weight (Figure 33A). According to the calibration curve, this might result from oligomer dissociation into dimers. It should be noted that the amount of Hsp26 applied to the column could not be detected after the run indicating strong interactions of Hsp26 with the column matrix at high temperatures. The identical behaviour was observed with other Hsp26 variants, namely Hsp26W211Y, Hsp26W211A (Figure 33B and data not shown).

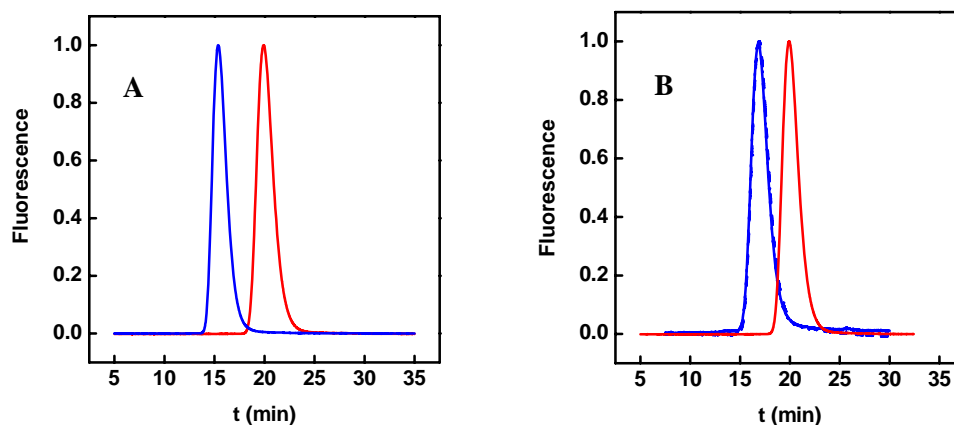


Figure 33 Analytical size exclusion chromatogram of A: wt Hsp26 at 25°C (straight line) and 45°C (dashed line) and B: of W211Y at 25°C (straight line) and 45°C (dashed line). As gel filtration column, a Tosoh TSK G4000PW equilibrated with 40 mM HEPES, 150 mM KCl pH 7.4 was used. For experiments at 45°C, the column was temperature-controlled in a column oven.

When the cystein variants Hsp26S4C and Hsp26S210C were analyzed by analytical gel filtration at 25°C and reducing conditions no difference in the elution time was observed compared to that obtained with wt Hsp26 (Figure 34A and B). Similar to the wt protein, at 45°C both variants eluted with increased elution times under reducing conditions (Figure 34A and B). However, a different behavior concerning the elution times was observed, when the proteins were analyzed at elevated temperatures under oxidizing conditions. Here, both proteins eluted with elution times identical to that obtained for samples running a 25°C, indicating that the quaternary structure of these variants was stabilized by disulfide bridges (Figure 34A and B). Similar observations were made for Hsp26S4C/W211 and the double cystein variant Hsp26S4C/S210C (data not shown). In agreement with the notion that Hsp26S82C did not form disulfide bridges, it did not maintain its oligomeric state when analyzed under oxidizing conditions at high temperature (data not shown). These results indicate that cross-linking neighboring subunits within the Hsp26 stabilizes the oligomer and

completely inhibits oligomer dissociation at elevated temperatures. Apparently, not all Cys residues need to be in an oxidized state to stabilize the oligomer, as in Hsp26S4C and Hsp26S210C only 2/3 and 1/2 of the Cys residues form disulfide bridges, respectively.

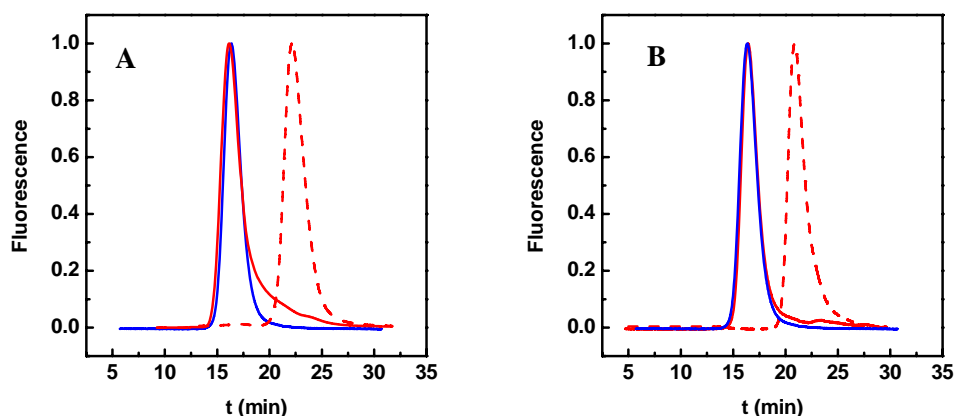


Figure 34 Analytical size exclusion chromatogram of A: reduced Hsp26S4C at 25°C (blue straight line) and 45°C (red dashed line) and oxidized Hsp26S4C (red straight line). B: Analytical SEC of reduced Hsp26S210C at 25°C (blue straight line) and 45°C (red dashed line) and oxidized Hsp26S210C (red straight line). As gel filtration column, a Tosoh TSK G4000PW was equilibrated with 40 mM HEPES, 150 mM KCl, 5 mM EDTA, pH 7.4 supplemented with either 2 mM reducing or oxidizing DTT, respectively. For experiments at 45°C, the column was temperature-controlled in a column oven.

Whereas the replacement of Ser residues did not affect the structural stability of Hsp26, replacement of the N-terminal Phe residues by Ala or Ser, respectively decreased the oligomer stability. In comparison to wt Hsp26 at 25°C, Hsp26FA and Hsp26FS eluted with significantly increased elution times, corresponding to a Hsp26 dimer (Figure 35A). Increasing the concentration applied to the column shifted the peak maximum to smaller retention times, indicating association of the Phe variants, yet the maximum value for the elution time was significantly smaller than that observed for native wt Hsp26 (Figure 35B). This suggests that

the N-terminal Phe residues stabilize the quaternary structure of Hsp26 through inter-subunit contacts. Further investigation of these variants with analytical ultracentrifugation revealed that the assembly of these variants stops at the level of a trimer or tetramer (see below).

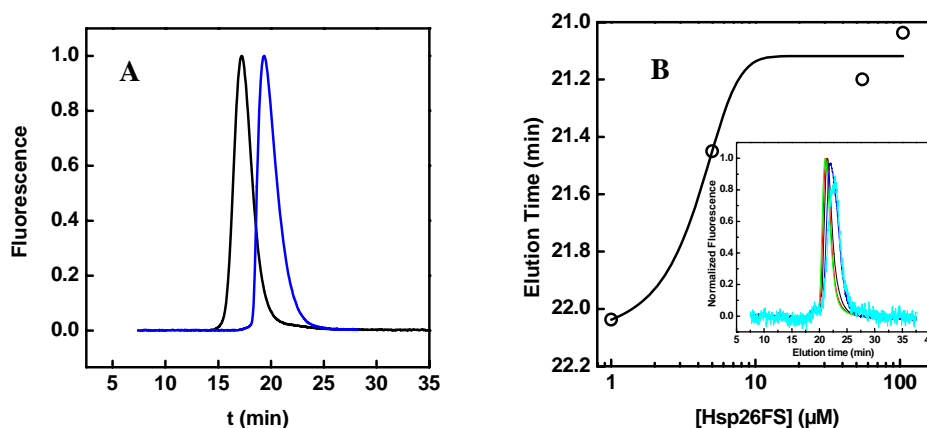


Figure 35 A: Analytical SEC of Hsp26FS (blue line) in comparison to wt Hsp26 (black line). B: Elution times of various Hsp26FS concentrations. Inset: Chromatograms of the series of Hsp26FS concentrations applied to a Tosoh G4000PW, equilibrated with 40 mM HEPES, 150 mM KCl pH 8 at 25°C. The fluorescence intensities were normalized to highlight the concentration-dependent peak shift.

4.5.2 Quaternary structure analysis by dynamic light scattering

When a beam of coherent and monochromatic light, such as from a LASER, passes through a colloidal dispersion light is scattered uniformly in all directions. In dynamic light scattering (DLS), the time-dependent changes in the scatter intensities are detected. These fluctuations arise from Brownian motion of an observed particle. Thus, DLS yields the diffusion coefficient (D) and information about a molecule's diffusion properties. Via the Stokes-Einstein equation, the diffusion coefficient at a given solvent viscosity and temperature, can be used to

calculated the hydrodynamic radius (R_H). To obtain a better understanding of the structural changes that coincide with the temperature activation of Hsp26, the diffusion coefficient of Hsp26 at various temperatures was determined.

Figure 36A shows a typical light scattering experiment with wt Hsp26. The normalized light scattering intensity (expressed as the autocorrelation function $g(\tau)$) decreases exponentially over time. The signal decay for wt Hsp26 at 25°C takes place with a frequency of $9.2 \cdot 10^3 \text{ s}^{-1}$, corresponding to $D = 2.4 \cdot 10^{-7} \text{ cm}^2/\text{s}$ (Figure 36A and Figure 37B). As expected, heating wt Hsp26 to 43°C increased D from $2.4 \cdot 10^{-7} \text{ cm}^2/\text{s}$ to $4.2 \cdot 10^{-7} \text{ cm}^2/\text{s}$, indicating faster movement at higher temperature (Figure 36A and Figure 37B). The diffusion coefficients are in agreement with the expected values for a 570 kDa proplate (spherical, but slightly football-shaped) structure. To correlate the determined diffusion coefficients with structural changes in the structure of Hsp26, R_H , that in turn gives qualitative information about the quaternary structure of Hsp26, was calculated. R_H at 25°C was 8.7 nm. At 43°C R_H was slightly reduced to 8.3 nm, suggesting that the overall structure of Hsp26 at elevated temperature is similar to that observed at 25°C (Figure 37A).

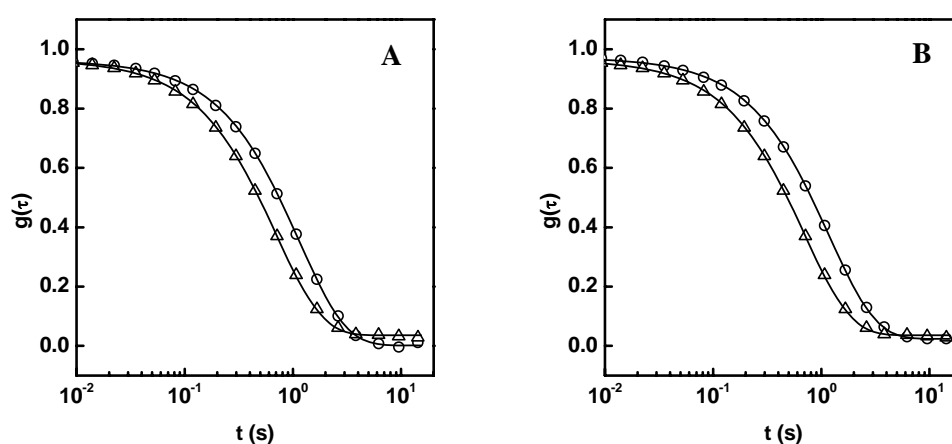


Figure 36 Autocorrelation function of (A) wt Hsp26 at 25°C (○) and 43°C (△) and (B) Hsp26S4C/W211Y at 25°C (○) and 45°C (△), respectively.

To test if the small changes in R_H observed with wt Hsp26 at elevated temperatures reflect changes of the quaternary structure of Hsp26, oxidized Hsp26S4C was investigated. This variant forms disulfide bridges between neighboring subunits and is unable to dissociate into smaller units. When this variant was analyzed at 25°C D was $2.84 \cdot 10^{-7} \text{ cm}^2/\text{s}$ and R_H was 8.6 nm, indicating that this variant possesses diffusion properties similar to that of wt Hsp26 (Figure 36B). However, when Hsp26S4C was analyzed at 45°C, D was increased to $4.64 \cdot 10^{-7} \text{ cm}^2/\text{s}$ and R_H was 8.4 nm, very similar to that observed with wt Hsp26 at 43°C (data not shown). This suggests that the observed changes in R_H do not result from dissociation of Hsp26 into small units, yet they may either result from an overall rearrangement of the Hsp26 oligomer upon temperature activation, or more likely from inaccuracy in temperature control at high temperature.

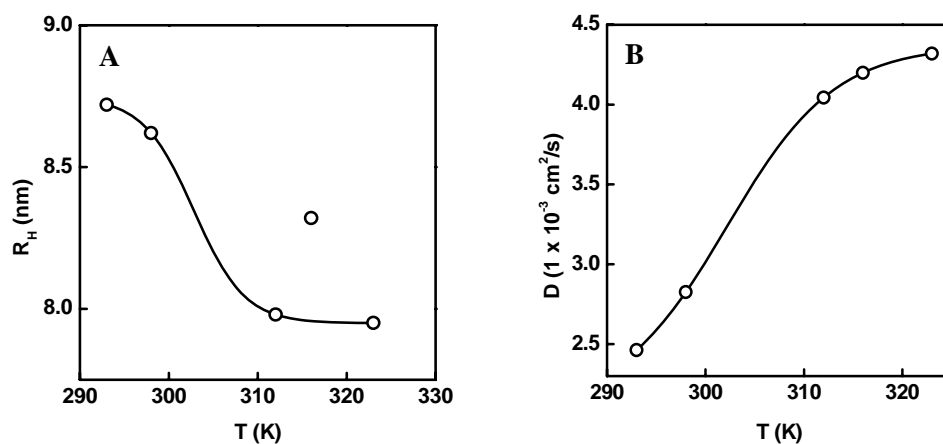


Figure 37 A: Hydrodynamic radii at were derived from Stokes-Einstein-equation determining the diffusion coefficient of wt Hsp26 by dynamic light scattering at various temperatures. B: The diffusion coefficient of wt Hsp26 was derived from dynamic light scattering experiments at various temperatures.

4.5.3 Quaternary structure analysis by analytical ultracentrifugation

Analytical SEC and DLS experiments revealed the oligomeric state of Hsp26. Its hydrodynamics, evaluated by analytical SEC and dynamic light scattering, are comparable to a prolate-shaped 600 kDa protein. However, in analytical size exclusion chromatography the retention time of a sample is determined by its hydrodynamic radius and shape. Molecular masses of biomolecules under equilibrium conditions can be determined independent of their shape and hydrodynamics by equilibrium sedimentation analytical ultracentrifugation. Here, a sample is spun until the sedimentation velocity is compensated by the diffusion- and lifting forces of the analyte. When these counteracting hydrodynamic parameters match equilibrium, then the sedimentation distribution of the analyte is determined only by its molecular mass.

When wt Hsp26 was analysed at 8,000 rpm, the molecular mass determined from equilibrium sedimentation was ~730 kDa, larger than expected for an oligomer consisting of 24 subunits (Figure 38A). However, when the rotational speed was accelerated to Yphantis conditions (10,000 rpm) (Yphantis condition: the rotational speed is selected to deplete the meniscus region by 1/3 of the total sedimentation distance), the molecular mass was determined to be 680 kDa (data not shown). Still wt Hsp26 appeared to be slightly larger than the expected 571 kDa for a 24 mer. The slope of the logarithm of the intensity ($\ln(A)$) versus the square sedimentation radius (r^2) is proportional to the molecular mass and in addition allows testing for thermodynamic non-ideality or self-association processes and thus delivers information about the homo- and heterogeneity of the solution.

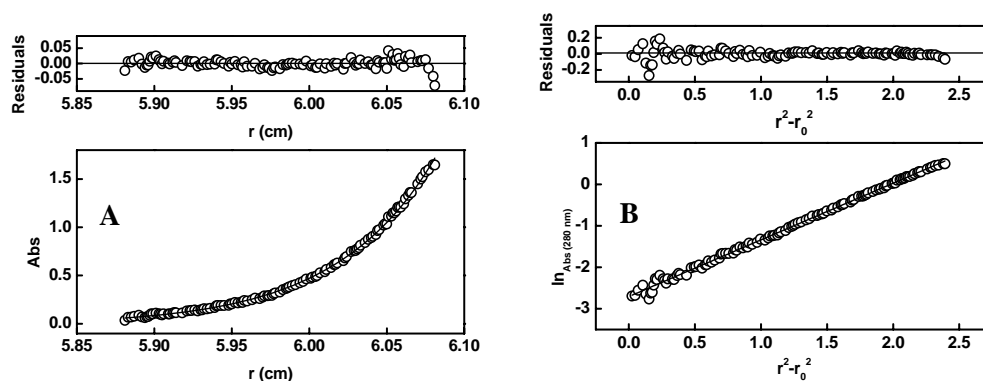


Figure 38 A: Equilibrium sedimentation ultracentrifugation concentration distribution profile of 20 μ M wt Hsp26 in 40 mM HEPES, 150 mM KCl, pH 8.0 at 20°C. Data were fitted with a single species model. Residuals are shown in upper panel. B: $\ln(a)$ - r^2 -analysis of A, testing for thermodynamic non-ideality and self-association of Hsp26. Residuals are shown in upper panel.

Linear fitting of the $\ln(A)$ vs r^2 sedimentation distribution of wt Hsp26, revealed a random distribution of the experimental data around the fit with small residuals, demonstrating that wt Hsp26 behaves as a single species (Figure 38B). The linear dependence indicates the absence of other significantly populated species and molecular mass determined was comparable to that obtained from least-square fitting. One should bare in mind that heterogeneity is detectable only when the molecular masses of the species differ by at least a factor of two and when the minor species is represented by at least 5%. Furthermore, self-association and thermodynamic non-ideality have opposite effects, which could compensate for each other.

To test, whether the replacement of the C-terminal Trp residue impaired oligomer formation, Hsp26W211Y was also subjected to sedimentation equilibrium analytical ultracentrifugation (Figure 39A). Fitting of the sedimentation distribution to least-square revealed a molecular mass of \sim 650 kDa, again slightly increased as compared to the expected mass of \sim 570 kDa. Linear fitting of the $\ln(A)$ vs r^2 for the sedimentation distribution of Hsp26W211Y

again revealed a random distribution of the experimental data with small residuals, suggesting that Hsp26W211Y behaves as a single species (Figure 39B). Although the molecular masses for wt Hsp26, as well as for Hsp26W211Y are significantly larger as expected, the results presented here demonstrate that Hsp26W211Y adopts a quaternary structure that is indistinguishable from that of the wt protein.

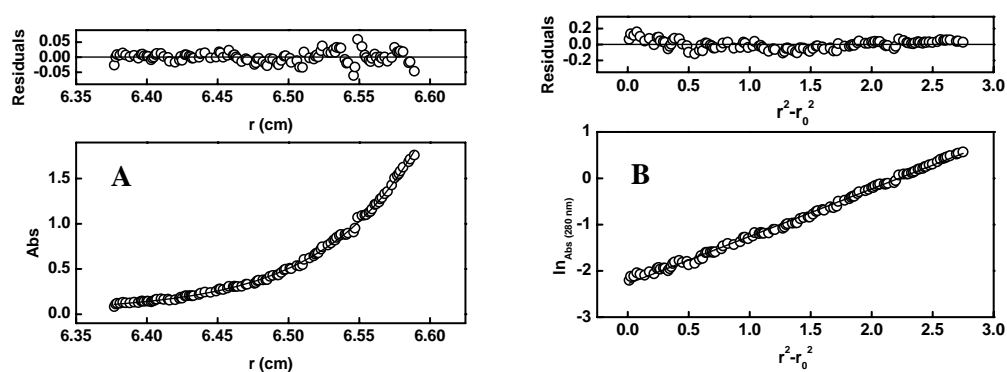


Figure 39 A: Equilibrium sedimentation ultracentrifugation concentration distribution profile of 25 μM Hsp26W211Y in 40 mM HEPES, 150 mM KCl, pH 8.0 at 20°C. Data were fitted with a single species model. Residuals are shown in upper panel. B: $\ln(a)$ - r^2 -analysis of A, testing for thermodynamic non-ideality and self-association of Hsp26W211Y. Residuals are shown in upper panel.

When Hsp26 30-195 was analyzed under equilibrium conditions, least-square fitting with a single species model revealed a molecular mass of ~ 34 kDa, slightly smaller than a theoretical dimer with a molecular mass of 36 kDa (Figure 40A). However, fitting the $\ln(a)$ vs r^2 of the sedimentation distribution of Hsp26 30-195 revealed that the experimental data do not distribute randomly around the fitted data and produced residuals with a systematic deviation (Figure 40B). This is suggestive for a self-association process and non-ideal distribution of a single Hsp26 30-195 species. The data suggest that approximately 95% of Hsp26 30-195 form dimers under these conditions.

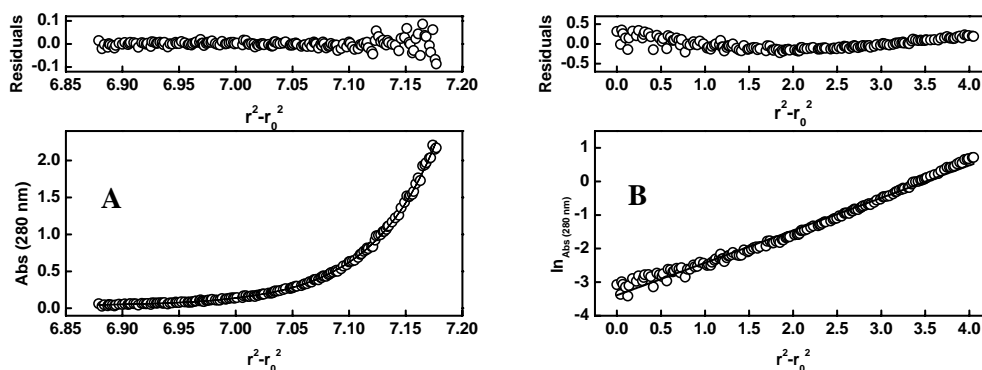


Figure 40 A: Equilibrium sedimentation ultracentrifugation concentration distribution profile of 36 μ M Hsp26 30-195 in 40 mM HEPES, 50 mM KCl, pH 7.4 at 20°C. Data were fitted with a single species model. B: ln(a)- r^2 -analysis of A, testing for thermodynamic non-ideality and self-association of Hsp26 30-195.

4.5.4 Species distribution of inactive and chaperone-active Hsp26

Sedimentation equilibrium ultracentrifugation allows mass determination under equilibrium conditions, however the question about species distribution and composition are hard to address. Information about the species composition can be derived from sedimentation velocity ultracentrifugation experiments. Here the solute is spun at high rotational forces and the time-dependent radial position of the sedimentation boundary is determined. This allows determination of the sedimentation coefficient (S) and reflects the sedimentation speed of the analyte. However, the sedimentation of a particle is shape-dependent, meaning that two particles, with identical mass, yet with different shape, may sediment at different speed. Complex mixtures can thus be separated due to their different sedimentation behavior in solution, giving a single boundary, or broadened sedimentation boundaries for each species.

When wt Hsp26 was analysed at 25°C, the major fraction (>95%) sedimented with a single boundary with an average sedimentation coefficient of $S_{20W} \sim 22$ S

(Figure 41A and data not shown). When the sedimentation experiments with wt Hsp26 were carried out at 30, 35 and 40°C, the sedimentation profile was very similar to that obtained at 25°C (data not shown, Figure 41B and Figure 41G). Again, the major fraction sedimented with an average sedimentation coefficient of $S_{20W} \sim 22$ S, even at 40°C (Figure 41B and E). Reducing the concentration fivefold did not shift the observed sedimentation coefficients towards smaller species, suggesting that the oligomer is the most abundant species (Figure 41C, F and H). A small fraction (<5%) of a ~ 2 S species was detected at all temperatures and its relative abundance was independent of the protein concentration (Figure 41E,F and H). This sedimentation coefficient is very similar to the one observed for the dimeric variant Hsp26 30-195 (Figure 41D). In contrast to the wt protein, dimeric Hsp26 30195 sedimented with a single boundary with an average $S_{20W} \sim 2$ S, confirming that this variant does not associate into large oligomers. The small S value in the wt Hsp26 samples may indicate the existence of a >5% 2 S fraction. However, control experiments, in which the concentration was reduced, did not reveal an increased abundance of this species, demonstrating that this species is not the result of mass action dissociation of Hsp26. Furthermore, simulation experiments predicted a minimum S value for the Hsp26 dimer of 46 kDa (Note: Hsp26 30-195 is a truncation variant lacking NTD and CTE. The dimer has a molecular mass of 36 kDa) would of 3.5 S, assuming an ellipsoid shaped dimer (data not shown).

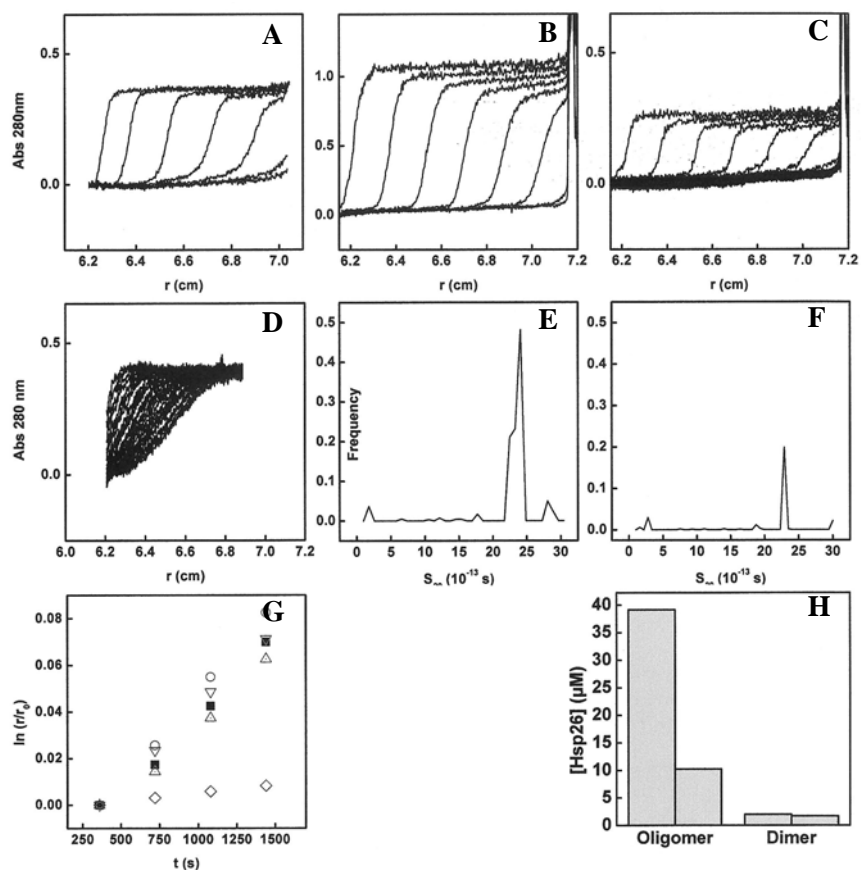


Figure 41 Movement of the sedimentation boundary of A: 15 μM wt Hsp26 at 25°C, B: 42 μM wt Hsp26 at 40°C, D: 13 μM wt Hsp26 at 40°C and 24 μM of Hsp26 30-195 at 40°C. E: Weight average Svedberg analysis $c(S)$ of B and F: $c(S)$ analysis of C. G: Logarithm of the radial position of the sedimentation boundary as a function of time of wt Hsp26 at 25°C (■), 30 (○), 35 (Δ) and 40°C (∇), as well as of Hsp26 30-195 at 40°C (\diamond). Sedimentation was at 50,000 rpm. Scans were taken every six minutes at 280 nm. H: Species analysis of the concentration-dependent $c(S)$ of wt Hsp26 at 40°C.

Next the influence of substrate binding to wt Hsp26 was analysed by analytical ultracentrifugation under heat shock conditions, e.g. 40°C. To this end wt Hsp26 was incubated at 40°C in the absence and presence of increasing concentrations of CS for two hours to allow for complex formation. Then the samples were spun at 35,000 rpm and the sedimentation was monitored at 280 nm. In agreement with previous results, wt Hsp26 sedimented with a single boundary and $c(S)$ analysis revealed a mean Svedberg of ~ 22 S (Figure 42A). $c(S)$ analysis of

Hsp26-CS complexes revealed a broad distribution of svedberg coefficients in the range of 30-150 S, indicating that CS binding to Hsp26 yields complexes under heat shock conditions (Figure 42B and C). The formation of complexes was dependent on the substrate concentration and induced a heterogeneity. $c(s)$ analysis suggests that multiple CS molecules can bind to a single Hsp26 oligomer and as the svedberg of substrate complexes increases in a substrate dependent manner, substrate complexes appear to stick together. Free CS molecules were detected at all investigated concentrations, demonstrating that not all CS molecules become incorporated into substrate complexes. Furthermore, free Hsp26 oligomers were also detected, demonstrating that the presence of unfolded substrate does not induce oligomer dissociation.

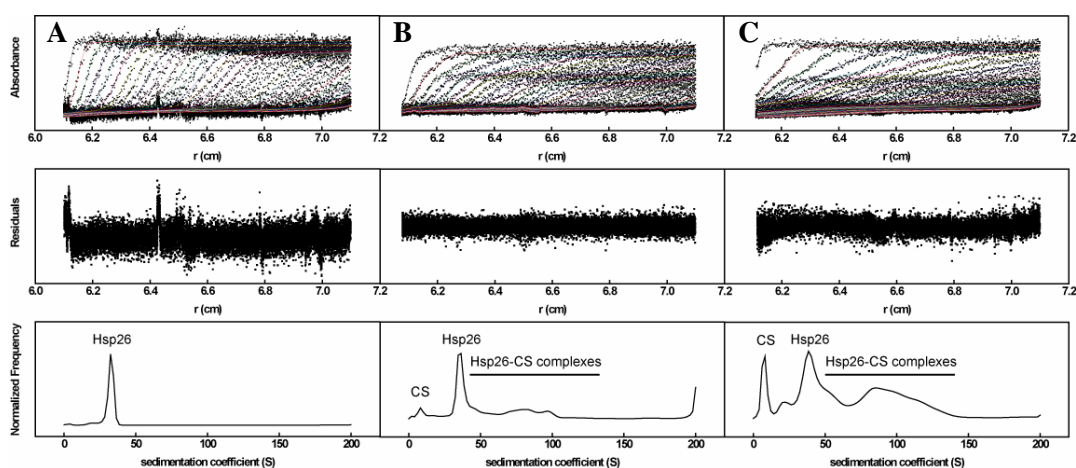


Figure 42 Sedimentation velocity ultracentrifugation analysis of Hsp26-CS substrate complexes. Sedimentation was carried out at a rotational speed of 35,000 rpm at 40°C in 20 mM HEPES, pH 7.5. The radial position of sedimentation boundary is shown in the upper panels. The middle panels show the residuals from fitting the experimental data with a weight average Svedberg concentration distribution $c(s)$ method. The average Svedberg concentration distribution of A: 15 μ M Hsp26, B: 15 μ M Hsp26 and 3.5 μ M CS, C: 15 μ M Hsp26 and 7 μ M CS.

A different sedimentation profile was observed with the Phe variants Hsp26FS and Hsp26FA (Figure 43A and data not shown). The sedimentation boundary could only be described with at least two fast interacting species with S_{20W} ~4.5 S and 5.8 S, respectively (Figure 43B). Fitting the data least square to derive molecular masses from $c(S)$ revealed that the observed species have masses of 51 kDa and 89 kDa, respectively, which is in agreement with Hsp26 dimers and tetramers. In agreement with the results obtained from analytical gel filtration experiments, these data suggest that the N-terminal Phe residues play an essential role for oligomer formation and stability. Furthermore, these data demonstrate that in addition to the C-terminal extensions that mediate oligomerization of Hsp26, a stabilizing role can be attributed to the N-terminal domain.

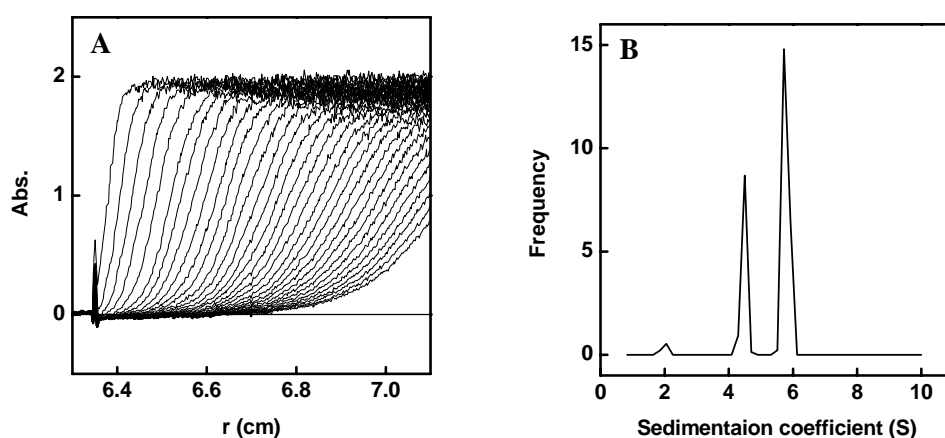


Figure 43 A: Radial position of the sedimentation boundary of Hsp26FS at 5°C. Sedimentation was in a AN60-TI rotor at 50,000 rpm. Absorbance scans were taken every six minutes at 280 nm. B: $c(S)$ of Hsp26FS.

4.6 Site-specific conformational changes upon Hsp26 temperature activation

4.6.1 Topology changes monitored by FRET

To determine how chaperone-active Hsp26 differs from the inactive state in terms of structure and conformation, the Cys variants of Hsp26 were covalently modified with the fluorescence dyes AIAS (donor) and LYI (acceptor) for subsequent FRET analysis (Franzmann et al., 2008). If the Hsp26 conformation changes upon temperature activation, this will result in changes in FRET. In general, changes in FRET efficiency can result from spectral shifts, change in the orientation of the fluorophores towards each other, changes in the quantum yield and changes in the donor-acceptor distance. Control experiments revealed, that the first two possibilities can be ruled out (3.27.8). To correct for changes in the quantum yield caused by temperature, the relative quantum yields of LYI-labelled Hsp26 was determined at 25°C and 45°C. All FRET data were then corrected for the differences in quantum yield and hence changes in FRET reflect changes in the donor-acceptor distance mainly.

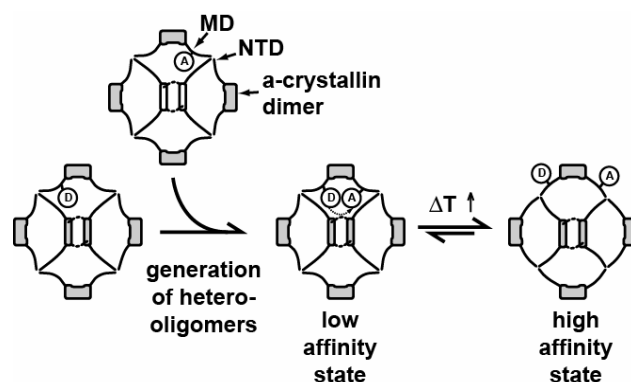


Figure 44 Schematic overview of the generation of spectroscopic heterooligomers for subsequent FRET analysis. Donor (D) and acceptor-labelled Hsp26 were mixed to form heterooligomers using the phenomenon of subunit exchange. The extent of FRET between distinct domains could be determined by mixing the appropriate Hsp26 variants. FRET efficiencies were then recorded in the inactive as well as chaperone activated state.

To monitor FRET efficiencies between domain, a series of differently labeled Hsp26 combination were generated by subunit exchange (SX) (Figure 44 and see 4.7.2) and fluorescence spectra were recorded. *In vitro*, Hsp26 oligomers continuously dissociate and reassociate, a phenomenon known as SX (Franzmann et al., 2005). This process was exploit to generate FRET-active oligomers. To this end donor- and acceptor-labelled Hsp26 were mixed in a 1:1 ration and incubated at 25°C (Figure 44). As Hsp26 oligomers are dynamic structures acceptor-labelled Hsp26 subunits will incorporate into donor-labelled oligomers. This will result in a random distribution of spectroscopic heterooligomers, suitable for FRET analysis (Figure 44).

FRET was determined at 25°C, i.e. for the inactive state of Hsp26. For all combinations of domain pairs (except for NTD-CTE), FRET could be detected, demonstrating that every dimeric subunit is in proximity to at least one NTD, MD and CTE from a neighbouring dimer. Figure 45 shows an example in which Hsp26S82C-AIAS and Hsp26S82C-LYI-labelled Hsp26 were used to determine FRET efficiencies (E_T) between MDs. In the inactive chaperone the E_T between

domains (given in either multiples of R_0 or \AA and see 3.27.8) were in the range of $1 R_0 / 30 \text{\AA}$ (Figure 46). When the chaperone-active state was tested, E_T between NTD and NTD, as well as between CTE and CTE were only barely affected (Figure 46). This is suggestive for an oligomeric state of thermally activated Hsp26. However, temperature activation of Hsp26 induced a strong decrease in E_T between the MDs (Figure 46). In addition, pronounced changes in E_T were also detectable with MD and NTD and CTE, respectively, suggesting that the MD undergoes a conformational change upon temperature activation (Suppl. Figure 2). It appears that temperature activation of Hsp26 induces a distinct conformational change in MD, whereas the terminal domains remain largely unaffected.

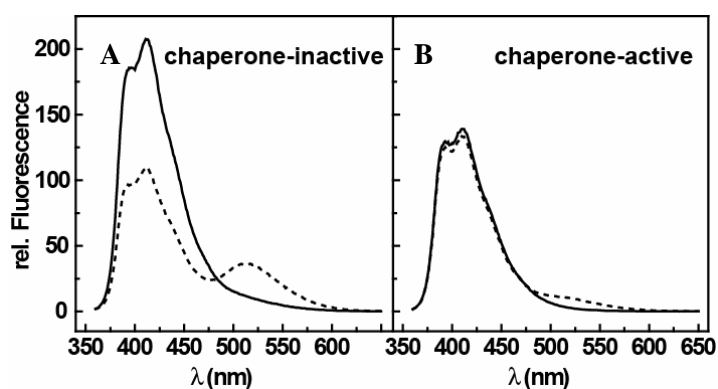


Figure 45 A: Fluorescence spectra of inactive Hsp26S82C-AIAS (donor) in the absence (straight line) and presence (dotted line) of Hsp26S82C-LYI (acceptor) and B: of thermally activated Hsp26S82C-AIAS in the absence (straight line) and presence (dotted line) of Hsp26S82C-LYI. Hsp26 was incubated at 45°C for 10 min. to allow for chaperone activation. A sample was diluted 1:10 into buffer at 25°C and fluorescence was recorded. All spectra were recorded at 25°C .

Control experiments suggest that the rotational freedom of the fluorophores attached to Hsp26 does not change with temperature and is independent of the conformational state of Hsp26 (3.27.8). This in turn allows to conclude that the FRET efficiency is mainly dependent on the distance between the fluorophores attached to Hsp26.

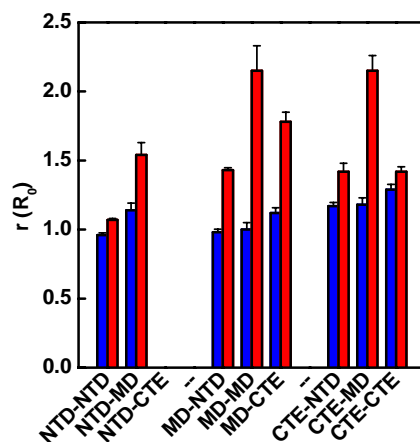


Figure 46 FRET distances given in multiples of R_0 between distinct site within inactive (blue) and active (red) Hsp26. Error bars were determined from at least three independent experiments. The combination NTD-CTE did not deliver any FRET signal and was thus not included.

Table 5 summarizes the results of the FRET analysis. It is noteworthy that the displacement of the N-terminal domains and C-terminal extensions, calculated from the differences in transfer efficiencies, corresponds to an increase in the distance between the corresponding domains within the range of a few nanometers. In contrast to the terminal domains, the displacement of the MD is within the range of 30 nm and control experiments suggest that the MDs become more solvent accessible upon temperature shift.

Table 5 Summary of FRET distance analysis. FRET-active Hsp26 heterooligomers were generated by mixing the donor (AIAS) and labelled (LYI) Hsp26. Then FRET efficiencies (E_T) were determined in the inactive (20°C) and the chaperone-active state (45°C), respectively. Control experiments revealed that the overlap integral $J(\lambda)$, and the rotational freedom (κ^2) of the fluorophors were independent of the conformational state, and thus changes in E_T mainly result from changes in the fluorophor distance (see 3.27.8). Distances were calculated to multiples of R_0 for the respective fluorophor pair, as well as for average distances in Å. The standard deviation SD was calculated from at least three independent measurement.

Donor-Acceptor	Inactive				Active			
	ET (%)	SD	Distance (R0)	Distance (Å)	ET (%)	SD	Distance (R0)	Distance (Å)
NTD - NTD	56	2.5	0.96	30	29	1.4	1.16	34
NTD - MD	31	6.6	1.14	35	5	2.8	1.63	48
NTD - CTE	n/a	n/a	>2	>62	n/a	n/a	>2	>58
MD - NTD	53	3.5	0.98	33	22	2.1	1.23	39
MD - MD	50	0.7	1.00	33	1	0.7	>2.15	>62
MD - CTE	34	4.9	1.12	38	2	0.8	>1.91	>60
CTE - NTD	28	3.0	1.17	31	13	2.8	1.37	37
CTE - MD	27	6.1	1.18	32	1	0.6	>2.15	>58
CTE - CTE	18	2.8	1.29	35	13	1.4	1.37	38

4.6.2 Conformational changes monitored by fluorescence quenching

Fluorescence quenching depopulates the excited state of a fluorophor upon encounter with a quencher molecule and thus reduces the fluorescence intensities. The molar fluorescence quenching coefficient hence expresses the degree of accessibility of the fluorophor to solvent molecules. Here, fluorescence quenching of fluorescence-labelled Hsp26 was used to determine the site-specific quenching coefficients for inactive and chaperone-active Hsp26. To this end, the fluorescence of LYI-labelled Hsp26S4C, HspS82C and Hsp26S210C was quenched with sodium iodide.

In inactive Hsp26, quenching of NTD- and CTE labelled Hsp26 was fairly efficient (Table 6 and Suppl. Figure 3). In contrast to the terminal regions, MD displayed a 3- to 5-fold lower quenching coefficient. Upon temperature activation, the quenching coefficient for MD was increased almost 3-fold, whereas the quenching coefficients for the NTD and CTE increased only slightly (Table 6 and Suppl. Figure 3). These results support the notion that temperature increase induces a specific conformational change in MD, whereas the N- or C-terminal regions remain largely unchanged in the activated oligomer.

Table 6 Molar fluorescence quenching coefficients were determined for site-specific fluorescently labelled Hsp26 in the chaperone-inactive and the thermally activated state using NaI. NTD: N-terminal domain, MD: middle domain, CTE: C-terminal extension. The stimulation factor was calculated from the ratio of the molar quenching coefficients active/inactive.

	Inactive (M ⁻¹)	Active (M ⁻¹)	Stimulation
Hsp26 _{S4C} LYI (NTD)	11.4	14.3	1.25
Hsp26 _{S82C} LYI (MD)	3.9	10.7	2.74
Hsp26 _{S210C} LYI (CTE)	19.4	25.1	1.29

4.7 Kinetic analysis of the temperature-induced structural changes in Hsp26

In contrast to other chaperones, the Hsp26 chaperone activity is temperature-controlled. At physiological temperature (30°C), Hsp26 exhibits only little chaperone activity, yet the shift to higher temperature reversibly unleashes its chaperone activity and enables the chaperone to prevent the aggregation of substrate proteins (Franzmann et al., 2008; Franzmann et al., 2005). The gain of chaperone activity correlates with structural changes of MD and the destabilization of the oligomeric state (Franzmann et al., 2008; Franzmann et al., 2005; Haslbeck et al., 1999; Stromer et al., 2004). To test which conformational changes are mechanistically linked to the gain of chaperone function, the structural conversion of Hsp26 upon temperature shift was kinetically analysed. Trp fluorescence is sensitive to its chemical environment. It can thus be used as a spectroscopic probe to monitor conformational changes in proteins by fluorescence. Hsp26 possesses two Trp residues: W72 in MD and W211 in CTE. To simplify spectroscopic analysis, the conformational changes of the single Trp variant Hsp26W211Y were compared to those observed with the wt protein. The truncation variant Hsp26 30-195 consists only of the MD and α -crystallin domain and also lacks W211. In contrast to Hsp26W211Y, its assembly stops on the level of a dimer and it does not exhibit chaperone activity. Thus, Hsp26W211Y allowed us to specifically follow changes in W72 fluorescence (and hence in the structure of MD) within the context of the 24mer, whereas Hsp26 30-195 allowed monitoring changes in MD within the simpler dimeric system. A similar analysis was carried out with wt Hsp26. It should be noted that that changes in the fluorescence observed with wt Hsp26 are mainly due to changes in W211 fluorescence.

4.7.1 Kinetic analysis of temperature-induced structural changes

When Hsp26W211Y was transferred from 25°C to higher temperature, the signal of W72 fluorescence decreased with time and the amplitude increased with rising temperature, indicating that an increased number of molecules undergo a conformational change (Figure 47).

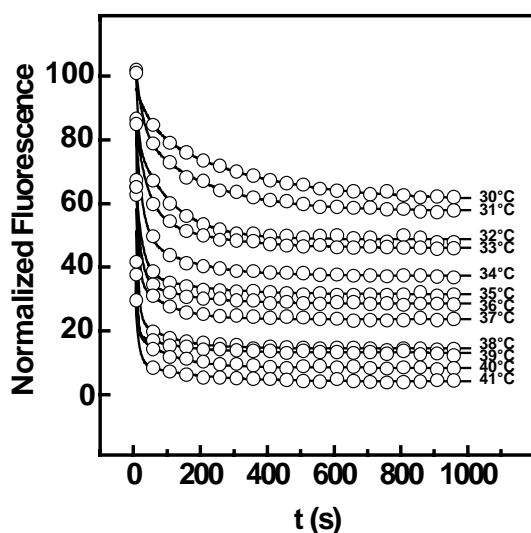


Figure 47 Fluorescence traces of Hsp26W211Y upon temperature shift from 25°C to higher temperature. Fluorescence was excited at 275 nm and detection was at 340 nm. Experimental temperature is stated at the end of the fluorescence trace. For Hsp26W211Y the fluorescence decreases double exponentially and the amplitude increases with higher temperature, indicating that an increased number of molecules undergo a conformational change upon temperature shift.

The fluorescence traces could only be described with a double exponential function, giving rise to two the rate constants λ_1 (fast) and λ_2 (slow) (Figure 48A). To test whether the conformational change was reversible, Hsp26W211Y was incubated at 36°C for 20 min and then shifted back to 25°C. As expected, the fluorescence increased over time and again the change in fluorescence could only be described with a double exponential function (Figure 48B).

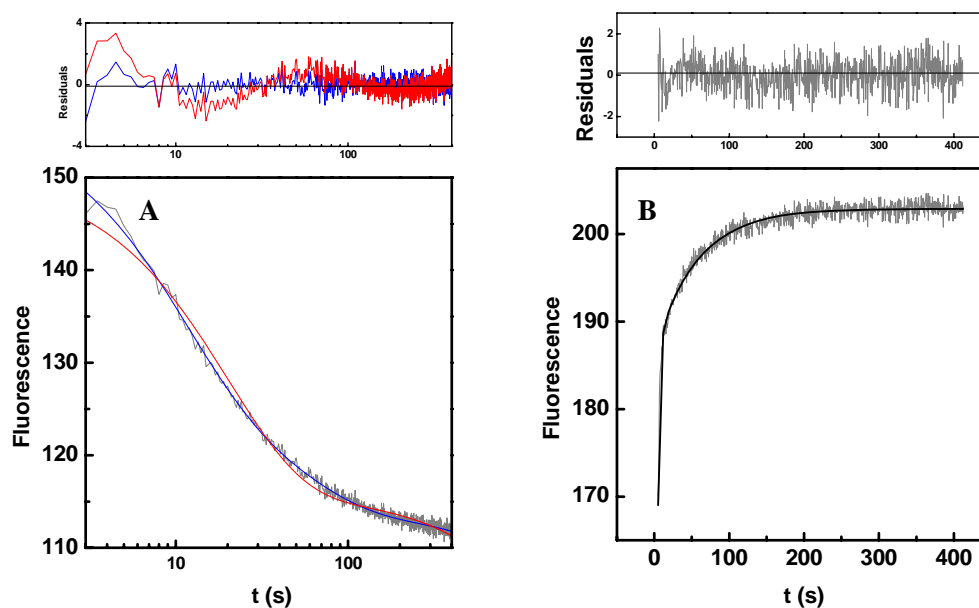


Figure 48 A: Kinetic analysis of the fluorescence decrease of Hsp26W211Y upon temperature shift from 25°C to 36°C. Lower panel: grey line: Fluorescence trace, red line: single exponential fit, blue: double exponential fit. Upper panel: Residuals for red: single exponential fit and blue: double exponential fit. B: Kinetic analysis of the fluorescence increase of Hsp26W211Y upon temperature shift from 36°C to 25°C. Lower panel: grey: Fluorescence trace, black: double exponential fit. Upper panel: Residuals for double exponential fitting.

According to transition state theory, the logarithm of a reaction rate depends linearly on the reciprocal temperature and is controlled through the energy barrier separating both states. In order to determine the energy barrier controlling the conformational rearrangement of MD, Hsp26 was shifted from 25°C to higher temperature and the conformational rearrangement of MD was monitored by fluorescence. Between 25°C and 42°C, both phases, λ_1 and λ_2 , of the kinetic MD rearrangement depend linearly on the reciprocal temperature, indicating two processes that are controlled by individual energy barriers (Figure 49). Whereas λ_1 is fast and depends strongly on changes in the temperature, λ_2 is slow and only mildly affected by the changes in the temperature, suggesting a slow intrinsic reaction rate for the λ_2 reaction. Eyring plots ($\log(k/T)$ vs $1/T$)

provide information about the energy barrier separating two states (Schellenberger, 1989). From these plots the activation enthalpy (ΔH^\ddagger), activation entropy (ΔS^\ddagger) and the free energy of activation (ΔG^\ddagger) can be calculated. Together, these values give information about the thermodynamics of the transition state, as it is in equilibrium with the ground states.

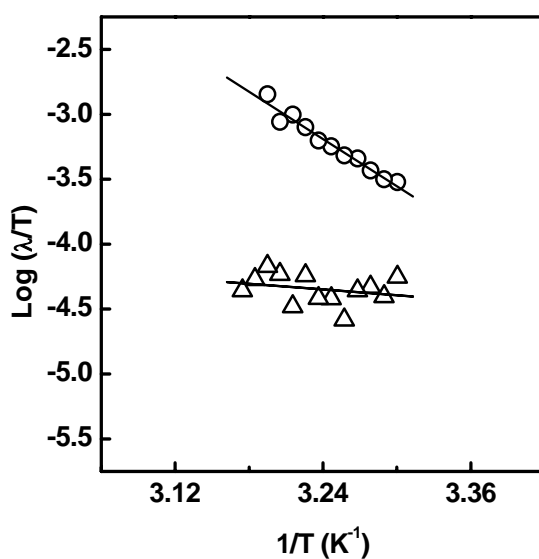


Figure 49 Eyring plot of Hsp26W211A. Temperature dependent kinetic analysis of the temperature-induced structural rearrangement of MD monitored with Hsp26W211A.

Quantitative analysis of the energetic parameters of Hsp26W211Y and Hsp26W211A revealed activation enthalpies of $\sim 120 \text{ kJ mol}^{-1}$ for λ_1 and $\sim 12 \text{ kJ mol}^{-1}$ for λ_2 , respectively. The activation entropies for λ_1 were $\sim 115 \text{ J mol}^{-1} \text{ K}^{-1}$ and $-210 \text{ kJ mol}^{-1} \text{ K}^{-1}$ for the slow λ_2 phase, respectively (Table 7). Although both phases differ significantly from each other concerning the slope, interception on the y-axis and absolute values, both reactions seem to be controlled by similarly large energy barriers of $\Delta G^\ddagger \sim 85 \text{ kJ mol}^{-1}$ (Table 7).

To test whether changes in W72 fluorescence observed with Hsp26W211A and Hsp26W211Y are specific to the rearrangement of MD, Hsp26 30-195 consisting of MD and α -crystallin domain was analysed. As in the case of Hsp26W211Y, the decrease in Hsp26 30-195 fluorescence upon temperature shift followed a double exponential function (Figure 50A) and was independent of the protein concentration (Figure 50B). Both, Hsp26W211Y and Hsp26 30-195 are described by similar Eyring plots, indicating that the MD rearrangement is independent of the N-terminal domain, the C-terminal extension and the oligomerization state (Figure 50C).

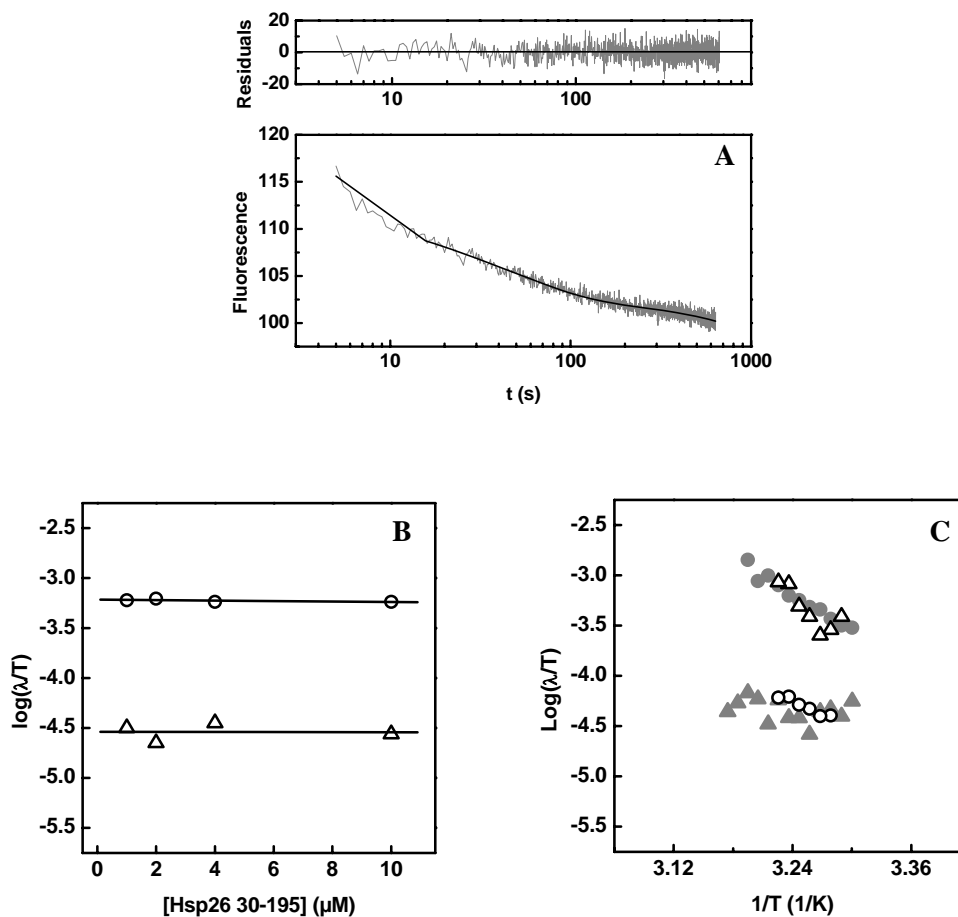


Figure 50 A: Fluorescence trace of Hsp26 30-195 upon temperature shift from 25°C to 36°C. The decrease in W72 fluorescence (grey) could only be described with a double exponential function

(black). B: The structural rearrangement of MD observed with Hsp26 30-195 is independent of the protein concentration and C: the rate constants are very similar to the rate constants determined with the full length Hsp26 variant Hsp26W211A.

As in the case of Hsp26W211Y, the temperature-induced conformational changes of the variant Hsp26S4C/W211Y followed a double exponential function (Figure 51A). However, the rate constants were reduced by one order of magnitude compared to Hsp26W211Y (Figure 51B). By introduction of a Cys residue in the Hsp26S4C/W211Y variant, neighboring subunits can be cross-linked by disulfide bridges. This illustrates that confinement of the Hsp26 flexibility through N-terminal disulfide bridges affects the MD dynamics, but does not inhibit the structural rearrangement. This demonstrates that the MD and the NTD are functionally communicating.

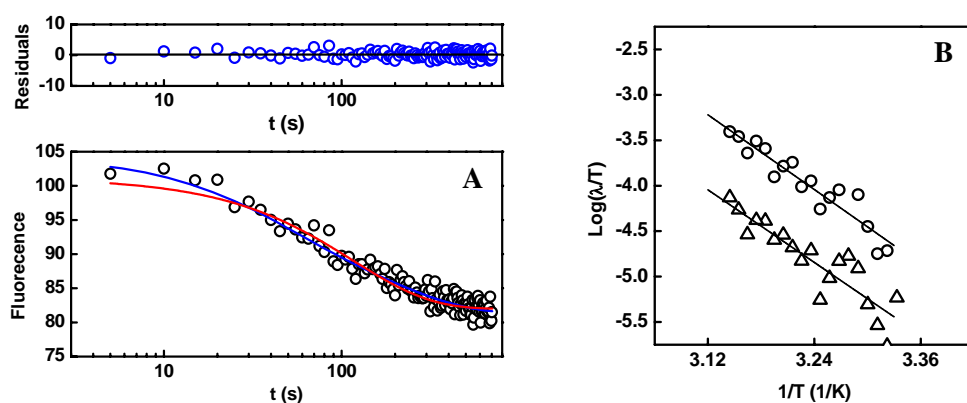


Figure 51 Eyring plot of oxidized Hsp26S4C/W211Y. The temperature dependence of the structural changes in Hsp26S4C/W211Y upon temperature shift could only be analyzed with a double exponential function, yielding the two rate constants λ_1 and λ_2 . Both rate constants are slowed down by one order of magnitude, compared to Hsp26W211Y, which resembles the reduced state.

In wt Hsp26, the fluorescence also decreased upon temperature shift. However, wt Hsp26 fluorescence decreased about 40 units, whereas the fluorescence in Hsp26W211Y decreased only 20 units (Figure 30 and Figure 32). This indicates

that the C-terminal Trp W211 also changes its conformation upon temperature shift. Yet, in contrast to the Hsp26 tryptophane variants, the decrease in wt Hsp26 fluorescence follows a single exponential function and changes in the temperature strongly affect the rate constants (Figure 52A). A quantitative analysis of the energetic profile revealed a large energy barrier of $\Delta G^\ddagger \sim 93 \text{ kJ mol}^{-1}$ (Table 7 and Figure 52B).

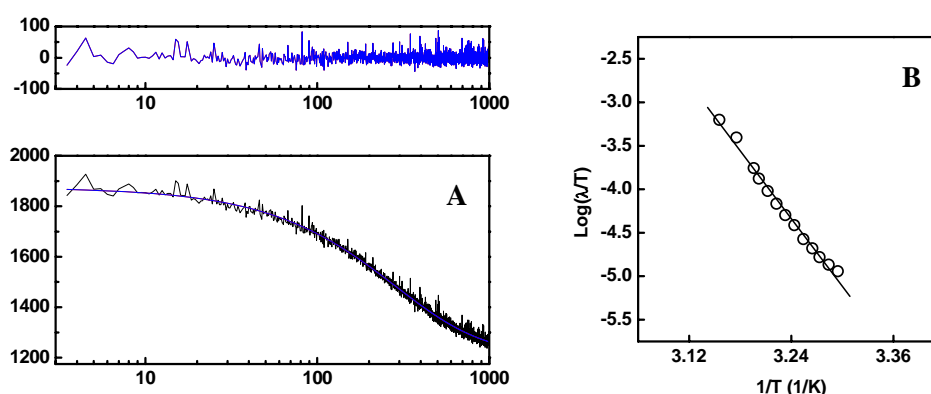


Figure 52 A: Lower panel: Fluorescence trace of wt Hsp26 upon temperature shift from 25°C to 36°C (black). blue: single exponential fit. Upper panel: Residuals analysis: single exponential fit. B: Eyring plot of wt Hsp26. The temperature dependence of the structural rearrangement upon temperature shift observed with wt Hsp26 revealed a large energy barrier of $\sim 92 \text{ kJ mol}^{-1}$.

Upon temperature shift, the environment of both Trp residues, W72 and W211, changes and leads to a decrease in fluorescence. This is in agreement with a conformational rearrangement of Hsp26 upon temperature activation, in which both Trp residues become more solvent-exposed. But, the kinetics of both Trp residues differ substantially. Comparison of the energetic profiles determined with wt Hsp26 and Hsp26W211Y suggests, that both Trp residues, W72 in MD and W211 in the C-terminal extension, report on different structural processes that are mechanistically distinct from each other (Table 7).

Table 7 Summary of the energetic profiles determined for wt Hsp26, Hsp26W211Y, oxidized Hsp26S4C/W211Y and for the Hsp26 subunit exchange.

	λ_{wt}/λ_1			λ_2		
	ΔH^\ddagger (kJ mol ⁻¹)	ΔS^\ddagger (J mol ⁻¹ K ⁻¹)	ΔG^\ddagger (kJ mol ⁻¹)	ΔH^\ddagger (kJ mol ⁻¹)	ΔS^\ddagger (J mol ⁻¹ K ⁻¹)	ΔG^\ddagger (kJ mol ⁻¹)
Hsp26	248.2	520	93.3	n/a	n/a	n/a
Hsp26W211Y	118.3	116	83.7	12.4	-209	86.0
Hsp26S4C(ox)	130.9	145	87.5	127.3	118	92.0
SX Hsp26	207.1	390	90.7	186.3	311	93.6

4.7.2 Kinetic analysis of the Hsp26 subunit exchange (SX)

In vitro, Hsp26 exchange subunits (dimers) between oligomers (Franzmann et al., 2005). To monitor subunit exchange (SX) between Hsp26 oligomers, Hsp26 was covalently modified with fluorescent dyes and SX was monitored by FRET.

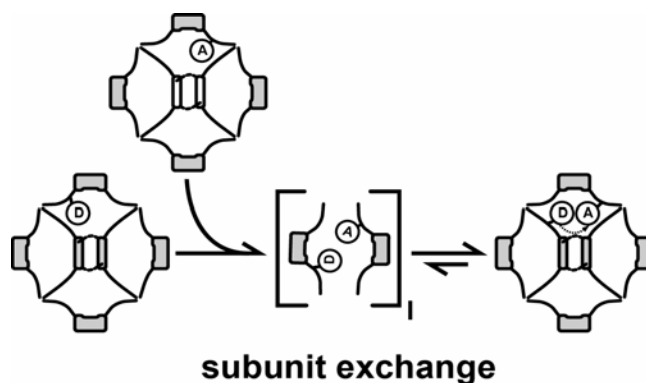


Figure 53 Schematic overview SX monitored by FRET. Donor-labelled Hsp26 (D) was mixed in a 1:1 ratio with acceptor-labelled (A) Hsp26. The mixture was then incubated to allow for SX. As a consequence of SX, FRET-active heterooligomers are generated, as donor- and acceptor-labelled Hsp26 become incorporated and positioned adjacent to each other within the same oligomer. Thus, changes in FRET correlates with SX, allowing to derive its kinetic parameters.

When a donor-labelled Hsp26 was mixed with acceptor-labelled Hsp26, the exchange of subunits could be observed monitoring the changes in donor- and acceptor fluorescence (Figure 53). This is due to the incorporation and generation FRET-active Hsp26 heterooligomers, in which a donor is close to an acceptor. Due to energy transfer from the donor to the acceptor molecule, the donor fluorescence is eliminated and acceptor fluorescence can be detected. When a mixture of fluorescein- and tetramethylrhodamine-labelled Hsp26 was monitored by fluorescence over time, the fluorescence of fluorescein at 515 nm decreased and the fluorescence of tetramethylrhodamine at 580 nm increased, by means of FRET (Figure 54A). At 25°C, SX is rather slow with a half life of $t_{1/2} \sim 2000$ s and a rate of $k = 0.0003 \text{ s}^{-1}$ (Figure 54C). At 40°C, SX is accelerated about 10fold with a half life of $t_{1/2} \sim 250$ s and rate of $k = 0.004 \text{ s}^{-1}$ (Figure 54B and C). Apparently, SX at 40°C results in significantly larger amplitudes, indicating that the exchange of subunits is not only faster, but also more efficient. It is noteworthy, that FRET is detected at elevated temperature at all, demonstrating that Hsp26 must be in an oligomeric state, as all FRET signal would be lost, if Hsp26 was dissociated.

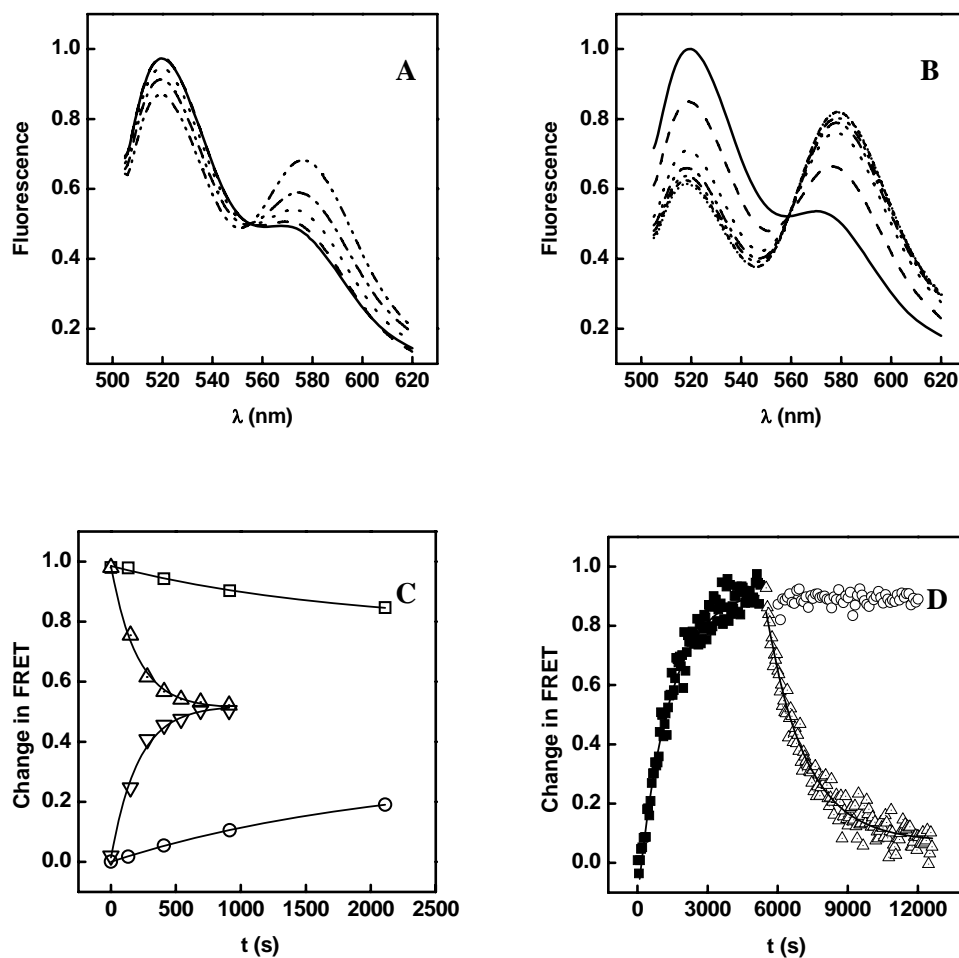


Figure 54 A: Changes in the fluorescence of FITC and TAMRA labelled Hsp26 at 25°C and B: at 40°C. C: Time-dependent changes in FRET at 25°C and 40°C monitored with FITC- and TAMRA-labelled wt Hsp26. D: Time-dependent changes in FRET monitored with AIAS- and LYI-labelled Hsp26S4C. To test for the reversibility, an 40fold excess of unlabelled wt Hsp26 or oxidized Hsp26S4C was added after 6000 s.

To test whether SX is a reversible and continuous process, a FRET complex formed between AIAS-donor and LYI-acceptor labelled Hsp26S4C was reverted with an excess of unlabelled wt Hsp26 (Figure 54D). At 30°C, the formation of the FRET-active hetero-complex was followed at 520 nm, monitoring the increase in LYI-acceptor fluorescence. As expected, SX was slightly faster at 30°C ($k =$

0.0007 s⁻¹) than at 25°C. Addition of a 10fold excess of unlabelled wt Hsp26 to the FRET-active complex, reverted the LYI-acceptor fluorescence with the same rate of $k = 0.0007 \text{ s}^{-1}$, indicating incorporation of unlabelled wt subunits into the oligomer (Figure 54D). This demonstrates that SX of Hsp26 is a continuous process and that Hsp26S4C behaves very similar compared to wt Hsp26, in terms of SX. When the competition experiment was carried out with oxidized Hsp26S4C, the FRET signal was not reverted, demonstrating that oxidized Hsp26S4C is not able to incorporate into the FRET-active oligomer. Apparently, oxidized Hsp26S4C exhibits decreased oligomer dynamics, due to the presence of disulfide bridges, which covalently cross-link neighboring subunits. This prevents oligomer dissociation in the case of oxidized Hsp26S4C.

To gain a better understanding for SX and its functional importance for the chaperone mechanism, the temperature-dependence of SX was analyzed by FRET. In agreement with previous experiments, the SX rate increased with rising temperature. A more careful analysis of the kinetics revealed that changes in FRET could only be analyzed with a double exponential function, giving rise to the two exchange rates λ_{sx-1} and λ_{sx-2} . Both phases exhibit a similar temperature dependence, yet λ_{sx-2} is smaller by one order of magnitude (Figure 55). The parallel behavior of λ_{sx-1} and λ_{sx-2} might result from two individual Hsp26 species, which exchange subunits with different rates. This explanation takes into account that two distinct populations have been observed by CryoEM (White et al., 2006). The quantitative analysis of the energetic SX profile revealed an energy barrier of $\sim 93 \text{ kJ mol}^{-1}$ and $\sim 90 \text{ kJ mol}^{-1}$ for λ_{sx-1} and λ_{sx-2} , respectively. Apparently, SX and changes in wt Hsp26 fluorescence can be described by remarkably similar Eyring plots, although only one phase was detected in the latter. A prerequisite for subunit exchange is that the Hsp26 oligomer must disassemble. The C-terminal extensions were shown to be involved in inter-subunit interactions stabilizing the Hsp26 oligomer. This in turn

suggests that changes in W211 fluorescence (in the C-terminal extension) reports on SX and that a conformational change in this domain precedes SX.

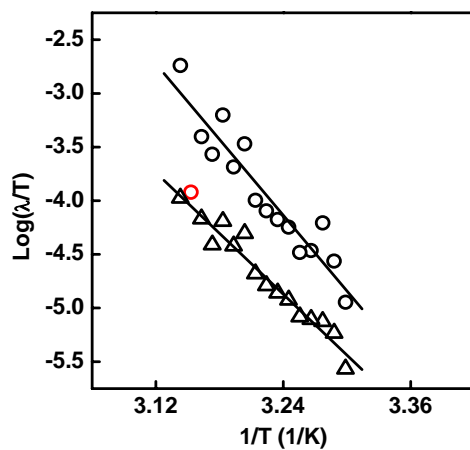


Figure 55 Eyring plot of the Hsp26 subunit exchange. The temperature-dependent analysis of the Hsp26 subunit exchange revealed two rate constants. The parallel behavior of both rate constants might give rise to two independent oligomer species. The assumption takes into account that two distinct Hsp26 populations have been observed with CryEM.

4.7.3 Influences of salt on the kinetics of structural changes and subunit exchange

Reactions are sensitive to the chemical environment. In proteins, charged residues, such as lysine or aspartic acid are often involved in salt bridges and contribute to protein stability. Here the influence of ions upon Hsp26 stability was tested.

Upon temperature shift from 25°C to 36°C, wt Hsp26 fluorescence decreases exponentially with time (Figure 56A). The rate of conversion appeared to be dependent on ions. Whereas the fluorescence signal decreased with a half life of 100 s in the absence of ions, the half life increased by a factor of 2-3 when the temperature shift is carried out in the presence of 150 mM sodium or potassium chloride, respectively (Figure 56A). This effect becomes even more pronounced in the presence of high salt concentrations, or double ions, such as calcium, or magnesium (data not shown).

To test whether the conformational rearrangement of MD is also effected by ions the identical experiment was carried out with Hsp26W211Y. The decrease in W72 fluorescence followed a double exponential function over time with a half life of 20 s and did not change when 150 mM sodium or potassium chloride were added (Figure 56B). This demonstrates that the C-terminal W211 and the MD W72 report on distinct, yet different conformational changes, as their behavior towards ionic strength differs substantially.

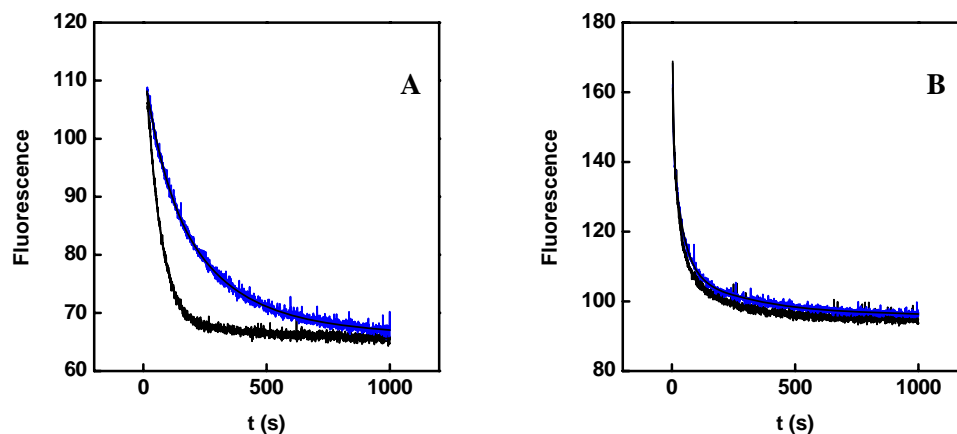


Figure 56 Fluorescence traces of wt Hsp26 (black line) and Hsp26W211Y (blue line) upon temperature shift from 25°C to 36°C in A: 40 mM HEPES, pH 8 and B: in the additional presence of 150 mM KCl.

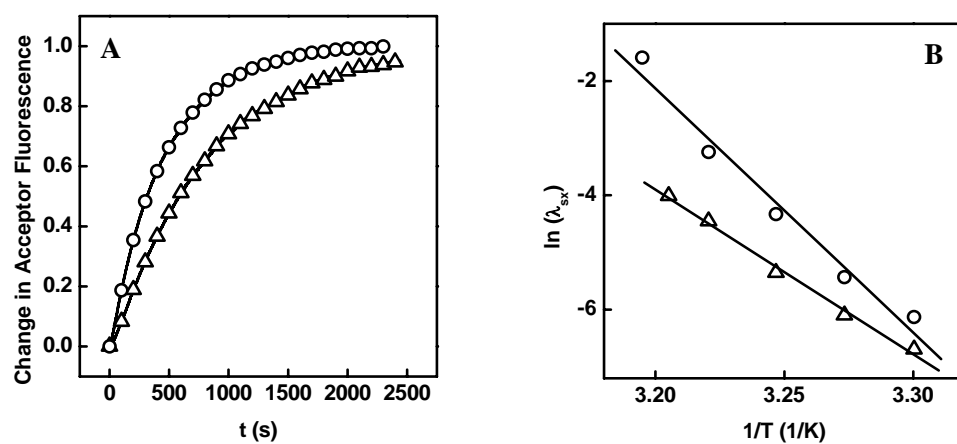


Figure 57 A: Subunit exchange of FRET-labelled Hsp26S4C in 40 mM HEPES, pH 7.5 (○) and in the additional presence of 150 mM KCl (△). B: Analysis of the temperature dependence of Hsp26 subunit exchange monitored by FRET in the absence (○) and in the additional presence of 150 mM KCl (△).

Previous experiments revealed that the change in W211 fluorescence correlates with a conformational change in CTE and suggest that this conformational rearrangement precedes SX. As the conformational rearrangement of CTE is influenced by ionic strength, salt may also have impact on the mechanism of SX. This can be tested by monitoring SX in the absence and presence of ions by means of FRET. In agreement with previous experiments, SX between Hsp26 oligomers revealed a half life of ~500 s at 36°C, in the absence of ions. As expected, the exchange rate was slowed down by a factor of 2 when 150 mM KCl were added. This indicates that a conformational change in CTE is directly related to SX (Figure 57A and B).

4.8 Chaperone activity of Hsp26

Hsp26 belongs to the family of sHsps (Susek and Lindquist, 1989). These molecular chaperones prevent the irreversible aggregation of non-native polypeptides (Haslbeck et al., 1999; Horwitz, 1992; Jakob et al., 1993). This function can be analyzed by aggregation assays, in which the unfolding of a model substrate leads to the formation of light scattering particles by means of aggregation (Horwitz, 1992; Jakob et al., 1993; Kiefhaber et al., 1991). Here, citrate synthase (CS) was used to test for the chaperone function of wt Hsp26 and the variants used for this study. When incubated at high temperature, e.g. 45°C, CS unfolds and aggregates (Figure 58A). The aggregation can be followed by monitoring the absorbance signal at 340 nm. In the presence of increasing concentrations of wt Hsp26, the light scattering signal was reduced, indicating the suppression of CS aggregation by forming Hsp26-CS complexes (Figure 58A). Testing Hsp26W211Y and Hsp26W211A revealed no functional differences, demonstrating that both variants exhibit chaperone activities indistinguishable from that of the wt protein (Figure 58B). A similar behaviour was observed for the Cys variants Hsp26S4C (Figure 59A) and Hsp26S210C, Hsp26S82C and Hsp26S4C/S210C (data not shown). Interestingly, the chaperone function of Hsp26S4C, Hsp26S210C and Hsp26S4C/S210C was independent of their redox states, indicating that the presence of disulfide bridges does not influence the chaperone function (Figure 59A and B and Figure 60A and B).

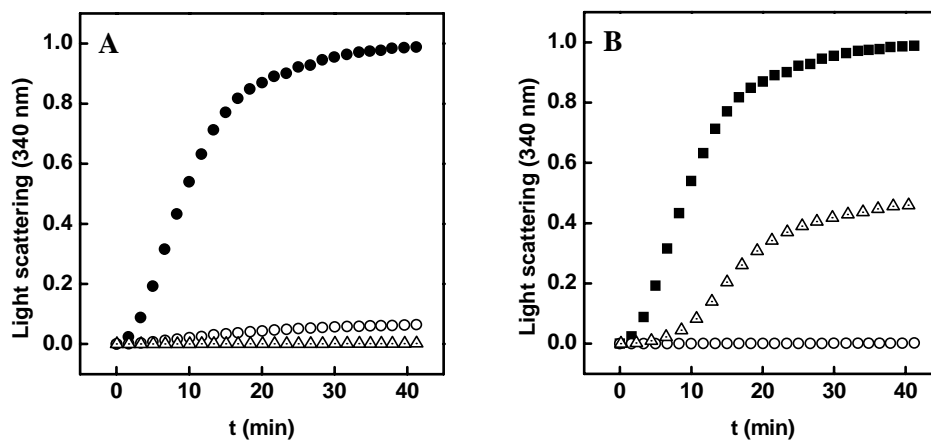


Figure 58 Chaperone activity of wt Hsp26 and Hsp26W211Y on temperature-induced CS aggregation. CS aggregation was monitored in a UV spectrophotometer at 350 nm at 45°C in 40 mM HEPES, 5 mM EDTA, pH 7.5. A: 0.5 μM CS in the absence and the presence of 1 μM and 2 μM wt Hsp26 and B: 0.5 μM CS in the absence and the presence of 1 μM and 2 μM Hsp26W211Y.

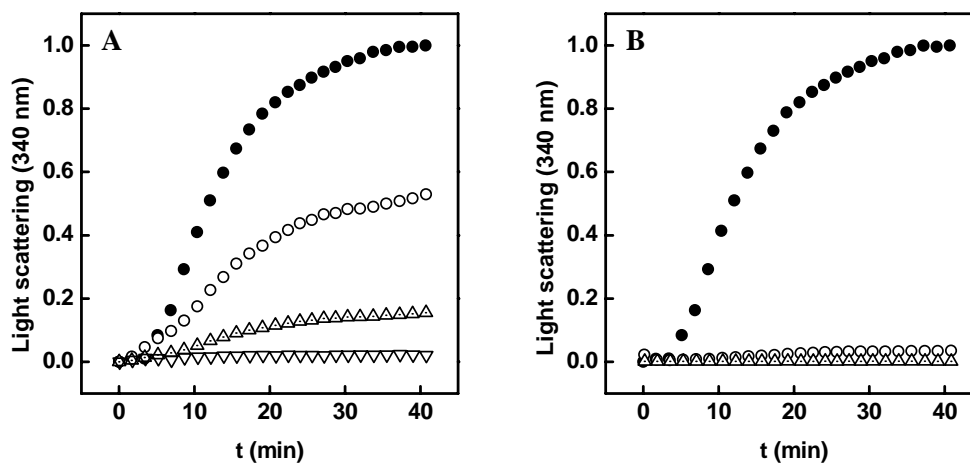


Figure 59 Chaperone activity of reduced and oxidized Hsp26S4C/W211Y on temperature-induced CS aggregation. CS aggregation was monitored in a UV spectrophotometer at 350 nm at 45°C in 40 mM HEPES, 5 mM EDTA, pH 7.5. A: 0.5 μM CS in the absence and the presence of 1 μM and 2 μM reduced Hsp26S4C/W211Y and B: 0.5 μM CS in the absence and the presence of 1 μM and 2 μM oxidized Hsp26S4C/W211Y.

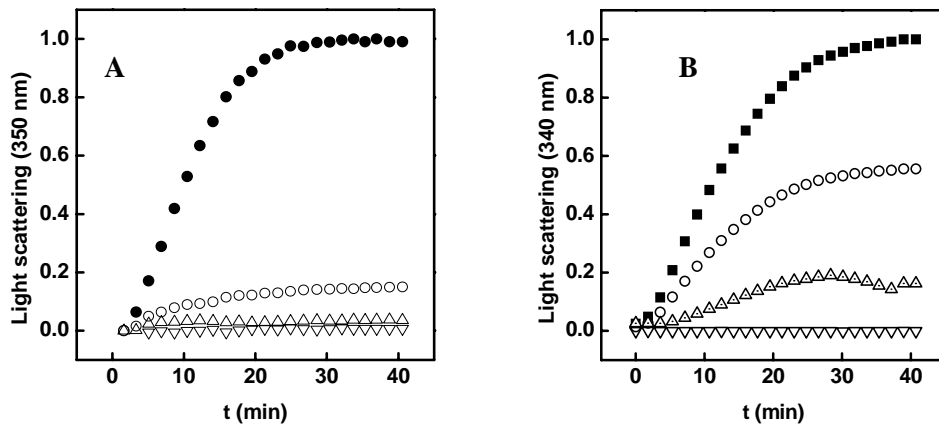


Figure 60 Chaperone activity of oxidized Hsp26S210C and Hsp26S4C/S210C on temperature-induced CS aggregation. CS aggregation was monitored in a UV spectrophotometer at 350 nm at 45°C in 40 mM HEPES, 5 mM EDTA, pH 7.5. A: 0.5 μ M CS in the absence and the presence of 1 μ M and 2 μ M oxidized Hsp26S210C and B: 0.5 μ M CS in the absence and the presence of 1 μ M and 2 μ M oxidized Hsp26S4C/S210C.

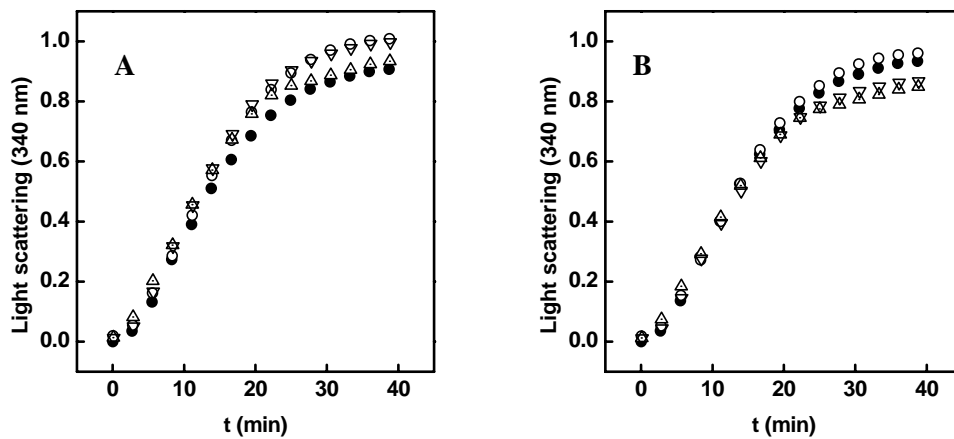


Figure 61 Chaperone activity of Hsp26 30-195 and Hsp26FS on temperature induced CS aggregation. CS aggregation was monitored in a UV spectrophotometer at 350 nm at 45°C in 40 mM HEPES, 5 mM EDTA, pH 7.5. A: 0.5 μ M CS in the absence and the presence of 1 μ M, 2 μ M and 5 μ M Hsp26 30-195 and B: 0.5 μ M CS in the absence and the presence of 1 μ M, 2 μ M and 5 μ M Hsp26FS.

In contrast to these variants, the truncation variant Hsp26 30-195 did not inhibit CS aggregation at any tested concentration, suggesting that the variant lacks important regions for substrate interaction (Figure 61A). Also Hsp26FS and Hsp26FA did not suppress CS aggregation, suggesting that N-terminal modification already impairs chaperone function (Figure 61B).

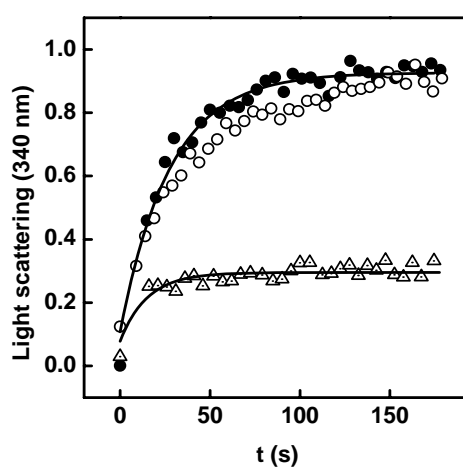


Figure 62 Chaperone activity of wt Hsp26 on the aggregation of chemically denatured CS. The aggregation of 200 nm denatured CS was monitored in a fluorescence spectrometer, detecting light scattering at 340 nm. CS aggregation was induced by diluting chemically denatured CS (5 M GdmHCl, 40 mM HEPES, 5 mM EDTA, pH 7.5) 100fold into 40 mM HEPES, 5 mM EDTA, pH 7.5 at 20°C. CS aggregation in the absence and in the presence of 600 nm chaperone inactive and temperature-treated wt Hsp26.

A key feature of Hsp26 is that its chaperone activity is temperature-controlled. Whereas Hsp26 does not interact with unfolded polypeptides at physiological conditions, heat shock conditions, e.g. 45°C unleash its chaperone activity (Franzmann et al., 2005; Haslbeck et al., 1999). To demonstrate this, the effect of inactive and temperature-activated Hsp26 on the aggregation of chemically denatured CS was investigated. When chemically denatured CS is diluted into

native buffer, CS fails to refold and subsequently aggregates (Figure 62). At 25°C, a twofold excess of Hsp26 did not inhibit CS aggregation, demonstrating that Hsp26 adopts a binding-incompetent conformation at low temperatures (Figure 62). However, when Hsp26 was pre-incubated for ten minutes at 45°C to allow for chaperone-activation, and was then shifted back to 25°C, CS aggregation was significantly reduced, demonstrating that Hsp26 was converted to its chaperone-active form and that chaperone-active species persist for some time at low temperature (Figure 62).

For Hsp26, elevated temperatures are essential to display chaperone activity. The question remained, whether Hsp26S4C also requires elevated temperatures for its activation. Testing reduced and oxidized Hsp26S4C at room temperature with chemically unfolded CS, revealed that neither of the proteins exhibits chaperone activity (Figure 63A and B). This shows that the oxidized variant is not trapped in a permanently active state. Next temperature-activated reduced and oxidized Hsp26S4C were tested. Interestingly, heat activated Hsp26S4C suppressed substrate aggregation at room temperature, demonstrating that both, the reduced and oxidized variant require heat treatment to gain chaperone activity (Figure 63A and B). In agreement with the results for heat-induced aggregation of CS, aggregation of chemically denatured CS was largely suppressed with a 2fold excess of chaperone (Figure 63A and B).

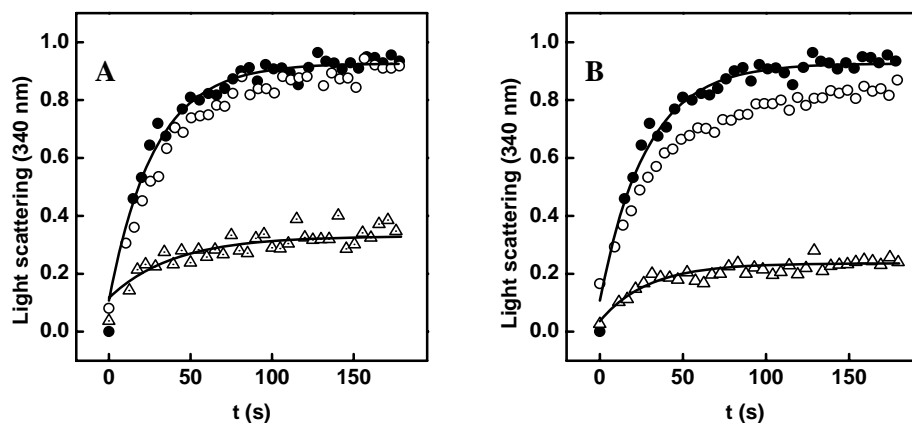


Figure 63 Chaperone activity of reduced and oxidized Hsp26S4C/W211Y on the aggregation of chemically denatured CS. The aggregation of 200 nm denatured CS was monitored in a fluorescence spectrometer, detecting light scattering at 340 nm. CS aggregation was induced by diluting chemically denatured CS (5 M GdmHCl, 40 mM HEPES, 5 mM EDTA, pH 7.5) 100fold into 40 mM HEPES, 5 mM EDTA, pH 7.5 at 20°C. A: CS aggregation in the absence and in the presence of 600 nm chaperone inactive and temperature-treated reduced and B oxidized Hsp26S4C/W211Y.

4.9 Kinetic analysis of Hsp26 chaperone activation

Increase in ambient temperature unleashes Hsp26 chaperone activity. To gain more information about the structural rearrangements of Hsp26, the kinetics of chaperone activation were analyzed. By varying the temperature in the kinetic experiments, the energy barriers governing this activation process could be estimated and comparison of these data to those obtained for the structural rearrangements derived from fluorescence spectroscopy allow to draw conclusions about the mechanistic contribution of each process to the chaperone function.

Like CS, chemically denatured Glutamate dehydrogenase (GDH) fails to refold and subsequently aggregates when diluted into native buffer conditions (Figure

64A). This can be monitored in a fluorescence spectrophotometer monitoring the increase in scatter light (Figure 64A). GDH aggregation was not affected, when inactive Hsp26 was present (Figure 64A). Only after exposure to higher temperature, Hsp26 was able to prevent GDH aggregation. When Hsp26 was incubated at 36°C for 10 s, GDH aggregation was reduced by approx. 50% and after a preincubation time at 36°C of five minutes, GDH aggregation was suppressed entirely (Figure 64A). This demonstrated that Hsp26 activation is a time-dependent process that requires elevated temperature. Detailed analysis of the reaction kinetics revealed that Hsp26 temperature activation follows a double exponential function with half lives of ~10 s and 100 s for the first and second phase, respectively (Figure 64B). The relative amplitudes were ~55% and 45% for the fast and slow phase, respectively. When the activation of Hsp26 chaperone function was analyzed at 33°C, the half life was reduced to 100 s and when analyzed at 45°C it was increased to approx. 4 s (Figure 64C). It should be noted that due to the poor signal-to-noise ratio of the assay at 33°C (only few active Hsp26 species exist) and the fast activation reaction at 45°C, only the fast phase of the kinetics was analyzed. It appears that Hsp26 chaperone activation is a biphasic process. This can be explained by a sequential mechanism, in which a chaperone active intermediate is generated during the fast phase. This intermediate state undergoes further conformational rearrangements during the slow phase and yields Hsp26 molecules with increased chaperone activity. In a parallel pathway model, two distinct species activate through two distinct pathways. An inactive intermediate can be excluded, as chaperone-active species are generated during the fast phase.

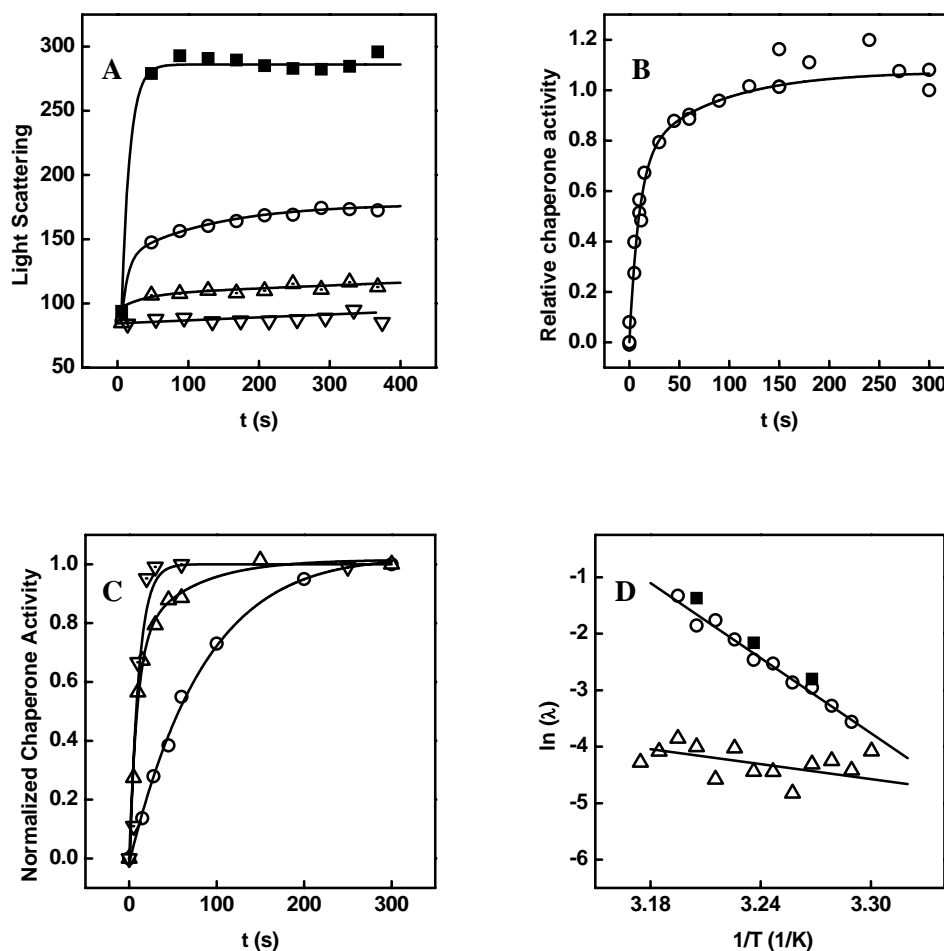


Figure 64 A: Aggregation of chemically denatured GDH in the absence of presence of Hsp26 pre-incubated at 36°C for 0 (■), 10 (○), 30 (△) or 5 min (▽). B: Kinetic analysis of Hsp26 chaperone activation at 36°C. The relative chaperone activity of Hsp26 was determined from its ability to suppress the aggregation amplitude of chemically denatured GDH. t refers to the pre-incubation time of Hsp26 at 36°C to allow for chaperone activation. C: Kinetic analysis of chaperone activation of Hsp26 at (○) 33°C, (△) 36°C or (▽) 43°C. D: Eyring plot of the (■) chaperone activation of Hsp26 at various temperatures in comparison to the kinetic analysis of the (○ and △) structural rearrangement of the Hsp26 MD monitored by W72 fluorescence with Hsp26W211Y.

Although previous results showed that the MD undergoes a structural rearrangement when Hsp26 is thermally activated, this does not necessarily mean that both processes are mechanistically connected. If two processes show

superimposing Arrhenius plots ($\ln(\lambda)$ vs $1/T$), i.e. their rates match over the tested temperature range, it is likely that they are controlled by the same rate-limiting step. Comparison of the temperature-dependencies of the gain of chaperone activation and the MD rearrangement determined by fluorescence spectroscopy revealed that both processes are described by remarkably similar Eyring plots, suggesting that they occur in the same process (Figure 64D).

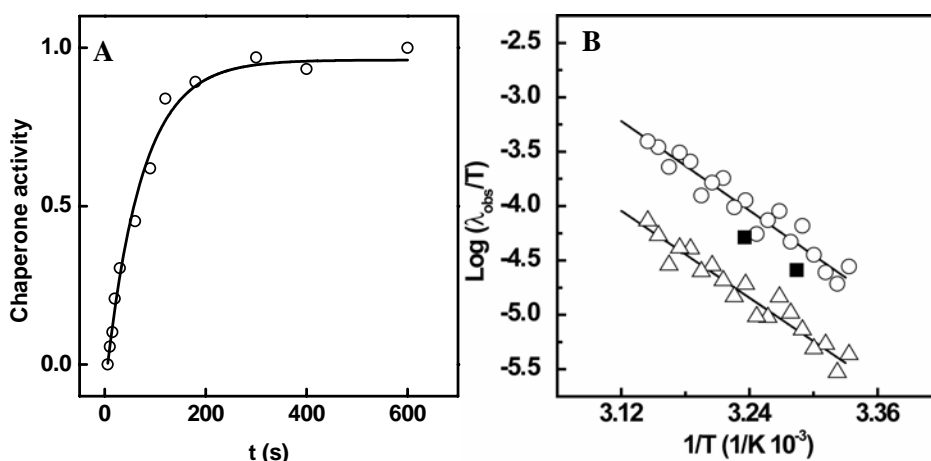


Figure 65 A: Kinetic analysis of oxidized Hsp26S4C/W211Y chaperone activation at 36°C. The relative chaperone activity of Hsp26 was determined from its ability to suppress the aggregation of chemically denatured GDH. t refers to the pre-incubation time of the chaperone at 36°C to allow for chaperone activation. B: Eyring plot of the (■) chaperone activation of oxidized Hsp26S4C at 33°C and 36°C in comparison to the kinetic analysis of the (○ and △) structural rearrangement of the MD monitored by W72 fluorescence with oxidized Hsp26S4C/W211Y.

If the chaperone activity of Hsp26 is controlled by a conformational change in MD, one expects that mutations that alter the dynamics of this conformational change directly affect the kinetics of activation. As shown above, in oxidized Hsp26S4C/W211Y N-terminal cross-linking by disulfide bridges slows down the MD rearrangement by one order of magnitude (Figure 51A and B) To prove that the gain of chaperone function is strictly coupled to the MD rearrangement, the kinetic activation for the oxidized Hsp26S4C/W211Y was tested. In agreement with the reduced dynamics of the MD rearrangement in oxidized

Hsp26S4C/W211Y, the kinetics for chaperone activation were also slowed down by one order of magnitude as well (Figure 65A and B). This demonstrates that the conformational change in MD occurs with the same rate as the gain in chaperone activity.

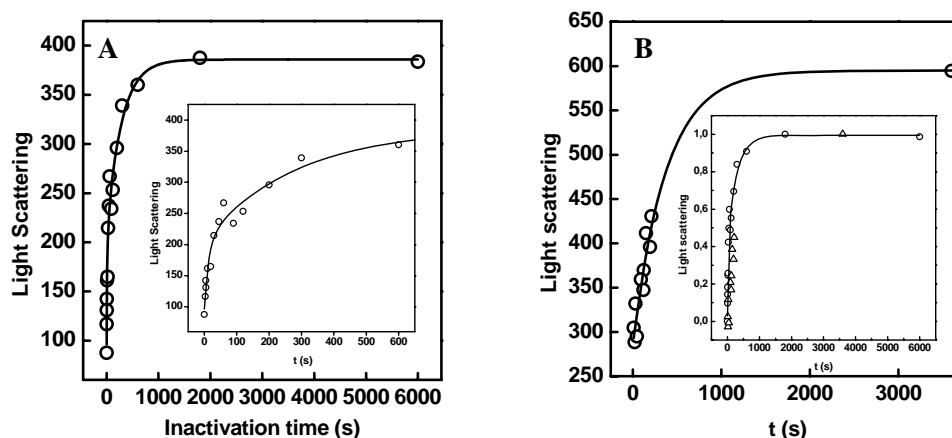


Figure 66 Hsp26 chaperone inactivation was monitored by the GDH aggregation assay. Hsp26 was incubated at 45°C to allow for full chaperone activation. Then Hsp26 was shifted back to 25°C and the residual chaperone activity was assayed. A: Inactivation kinetics of Hsp26 that was activated for 10 min at 45°C and B: in activation kinetics of Hsp26 that was activated for 30 min. Inactivation follows a double exponential function (inset A) and is independent of the incubation time at 45°C (inset B).

Hsp26 temperature activation is reversible. When the chaperone was incubated at 45°C for 10 min to allow for full chaperone activation, and was then shifted back to 25°C to test the residual chaperone activity, the chaperone activity decreased with time. The inactivation followed a double exponential function (Figure 66A). However, chaperone inactivation was significantly slower compared to the activation process. This may simply be a consequence of the differences in reaction temperature, as in general reactions are slower at lower temperatures. Extending the incubation time at 45°C from 10 min to 30 min did not alter the inactivation kinetics, suggesting that Hsp26 reaches the full

chaperone active state through the observed fast and slow phase and that no additional conformational rearrangements, such as proline-isomerization, occur after chaperone activation (Figure 66B).

4.10 Hsp26 in the Cell – Simulating molecular crowding

In vitro, the experimental conditions differ significantly from those defined by the cellular environment. An important aspect of the cytosol is its crowdedness and high dynamic viscosity caused by high protein concentrations, as well as by large amounts of other cellular constituents, such as carbon hydrates, lipids and nucleotides. The crowded environment effects the equilibrium rates and protein stability (Cheung et al., 2005; Despa et al., 2005; Zhou, 2004). The common strategy to address mechanistic issues under aqueous buffer conditions *in vitro* neglects this important issue and might thus not reflect the actual cellular situation.

In vitro, Hsp26 oligomers exchange subunits continuously (Franzmann et al., 2005). Whether SX is also a continuum in the cell remains enigmatic. Simulating the cellular environment using molecular crowding agents, such as polymeric ethylene glycole (PEG), Ficoll 70 or high concentrations of bovine serum albumin (BSA), allows analysis of the Hsp26 oligomer stability at high viscosity and crowding (Despa et al., 2005; Venturoli and Rippe, 2005).

When SX between Hsp26 oligomers was analysed in aqueous buffer systems by FRET, the donor fluorescence decreased upon addition of acceptor-labelled Hsp26 (Figure 67A). This is because Hsp26 oligomers are dynamic and form heterooligomers consisting of donor and acceptor labelled Hsp26 molecules. Thus, energy can be transferred from the donor to the acceptor dye through FRET. When the experiment was carried out in the presence of PEG 3000,

PEG 6000 and Ficoll 70, no change in the donor fluorescence/FRET was detected upon addition of acceptor-labelled Hsp26 (Figure 67A). This is suggestive for a stabilization of the Hsp26 oligomers under molecular crowding conditions, which in turn inhibits oligomer dissociation and mixing of Hsp26 subunits. One might argue that molecular crowding causes dissociation of the oligomer and thereby prevents oligomer assembly.

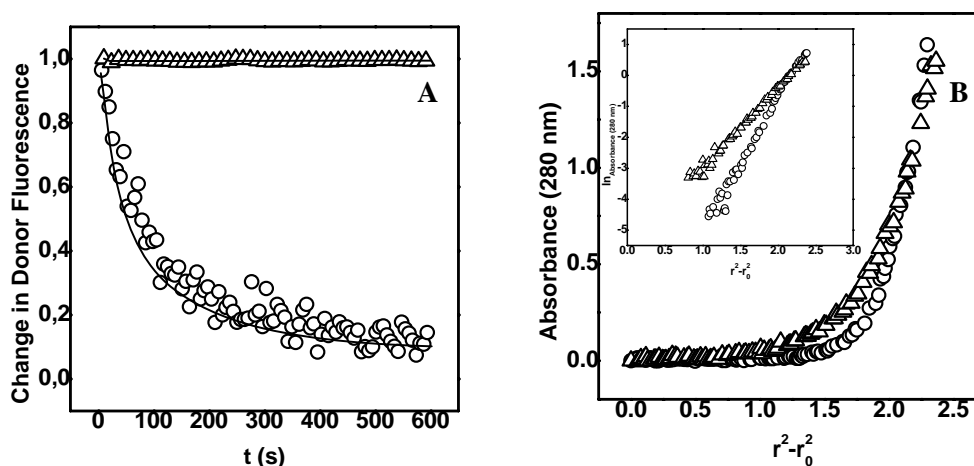


Figure 67 A: Subunit exchange monitored by FRET with CPM and LYI-labelled Hsp26S4C/W211Y in 40 mM HEPES, pH 7.5 and in 40 mM HEPES, 150 mg mL⁻¹ Ficoll 70, pH 7.5. B: Equilibrium sedimentation ultracentrifugation distribution profile of wt Hsp26 in 40 mM HEPES, pH 7.5 and in 40 mM HEPES, 150 mg mL⁻¹ Ficoll 70 at 20°C. Inlay: ln- r^2 Plot to test for self-association or thermodynamic non-ideality of wt Hsp26 under molecular crowding conditions.

Analysis of Hsp26 by analytical ultracentrifugation in the presence of Ficoll70, revealed an apparent molecular of 500 kDa (Figure 67B). It should be noted that mass determination by analytical ultracentrifugation under molecular crowding is affected, as the crowding agents form a shallow density gradient. Although the molecular mass determined under molecular crowding is smaller than in aqueous solution (800 kDa), the result demonstrates that Hsp26 that the concentration distribution of Hsp26 under molecular crowding is similar to that observed in

aqueous solution, suggesting that Hsp26 is a stable oligomer under molecular crowding conditions (Figure 67B). This demonstrates that Hsp26 SX is significantly slowed down in the presence of molecular crowding agents. It is tempting to speculate that Hsp26 exists mainly in an oligomeric state *in vivo*.

Next, Hsp26 chaperone activity was analyzed under molecular crowding conditions. When CS was incubated at 45°C in the presence of Ficoll 70, the light scattering increased over time. Although the absolute signal for CS aggregation was slightly reduced compared to the aggregation signal observed in aqueous buffer, the aggregation kinetics were unaffected. Apparently, molecular crowding does not prevent substrate aggregation. Whether the differences in aggregation signal observed for CS under various condition correlates with the a reduced extend of aggregation, remains to be elucidated. However, CS appears to be well suited to investigate the chaperone function of molecular chaperones under molecular crowding conditions.

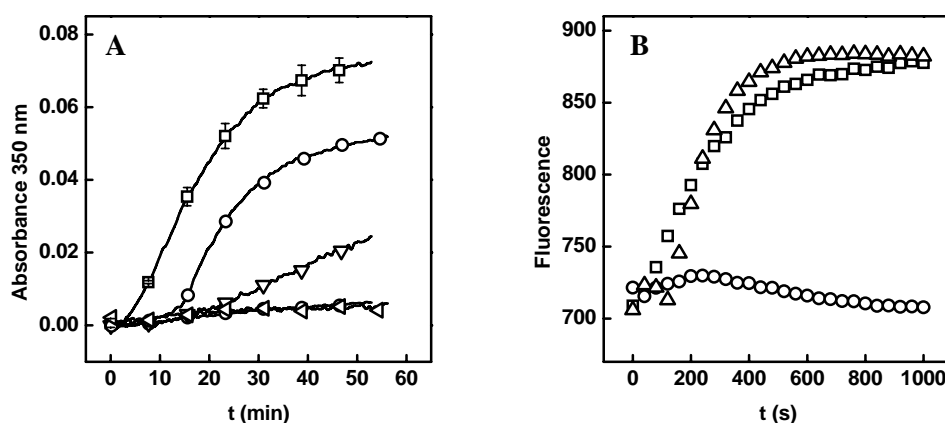


Figure 68 A: Temperature-induced aggregation of CS in PBS, 150 mg mL⁻¹ Ficoll70 at 45°C. 0.5 μM CS in the absence (□) and in the presence of 0.5 μM (○), 1.0 μM (▽), 1.5 μM (△) and 2.0 μM (◁) wt Hsp26. B: Aggregation of 200 nm chemically denatured GDH in the absence (□) and presence of inactive (△) and temperature-activated (○) wt Hsp26 in 40 mM HEPES, 150 mg mL⁻¹ PEG6000, pH 7.5.

Equimolar Hsp26 concentrations suppressed CS aggregation by ~30% and a twofold excess had even greater effect on the CS aggregation. A threefold excess of chaperone over substrate was sufficient to suppress CS aggregation entirely, demonstrating that the chaperone efficiency of Hsp26 is very similar to the chaperone activity observed in aqueous solution. One might argue that molecular crowding induces a permanently chaperone active state of Hsp26. To test this, the aggregation of chemically denatured GDH was monitored in the absence and the presence of Hsp26. When denatured GDH was diluted into buffer containing PEG6000, the light scattering signal increased exponentially over time, suggesting that GDH fails to refold and subsequently aggregates. In the presence of Hsp26 that was not heat-treated, the aggregation profile was barely affected. This demonstrates that Hsp26 adopts a conformation that is unable to interact with the substrate. When Hsp26 was temperature-activated prior to the experiment and then tested with GDH, the aggregation of GDH was suppressed. This demonstrates on the one hand that molecular crowding conditions do not induce a permanently chaperone-active conformation of Hsp26, and on the other hand that the chaperone activation mechanism appears to compare very well to the situation in aqueous solution.

The Hsp26 chaperone activity is barely affected in the presence of molecular crowding agents, such as PEG6000 or Ficoll70, yet both compounds prevent oligomer dissociation. It appears as if subunit exchange might rather be an *in vitro* phenomenon that likely reflects the requirements for oligomer flexibility to undergo intra-molecular conformational changes to allow for the chaperone activation in the cellular environment. Two explanations can account for this: First, the Hsp26 dissociation rate is significantly slowed down, or second its association rate is accelerated by molecular crowding. Both explanations would lead to a kinetic stabilization of the oligomeric structure.

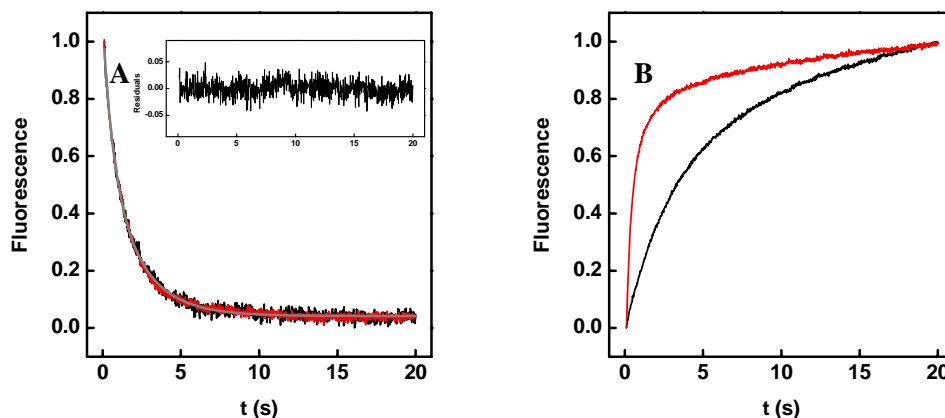


Figure 69 A: Unfolding of 5 μM wt Hsp26 with 5 M GdmCl in 40 mM HEPES, pH 7.5 (black line) and 5 M GdmCl in 40 mM HEPES, 150 mg mL^{-1} Ficoll70, pH 7.5. Inset: Residuals from double exponential fitting of the Hsp26 unfolding trace. B: Refolding of 5 μM wt Hsp26 with 5 M GdmCl in 40 mM HEPES, pH 7.5 (black line) and 5 M GdmCl in 40 mM HEPES, 150 mg mL^{-1} Ficoll70, pH 7.5. All experiments were carried out 25°C.

To test this, Hsp26 was subjected to folding experiments, monitoring the time-dependent changes in Hsp26 fluorescence upon unfolding or refolding, respectively. Unfolding of Hsp26 with GdmCl leads to a decrease in fluorescence that follows a double exponential function and is independent of the concentration. When Hsp26, that was prior to the experiment equilibrated with Ficoll 70 and was then unfolded with GdmCl in the presence of Ficoll 70, the unfolding rates were similar to those observed upon Hsp26 unfolding in aqueous solution. However, Ficoll 70 had great effect on the Hsp26 refolding rates. When Hsp26 was refolded under molecular crowding conditions, refolding was accelerated by a factor of six. This demonstrates that crowding stabilizes the native conformation by accelerating the folding rates, whereas the unfolding rates appear to be unaffected. This might also explain the effect of crowding agents upon SX. One might speculate that more likely the association rate is accelerated, rather than the dissociation rate slowed down, which leads to the kinetic stabilization of the Hsp26 oligomer.

5 Discussion

sHsps bind non-native proteins in a cooperative and efficient manner. It appears as if this class of molecular chaperones can be subdivided into two kinds of sHsps: I. constitutively active and II. temperature-controlled sHsps. Hsp26 resembles an ideal class II sHsp, for which elevated temperatures are obligatory to gain chaperone activity. Apparently, this class of sHsps can sense changes in the temperature autonomously. Previous results showed that coinciding with increased activity, the complex of 24 subunits becomes destabilized, resulting in the appearance of dimers in analytical gel experiments (Haslbeck et al., 1999). In addition, electron microscopy analysis of Hsp26 and the Hsp26-substrate complexes indicated large rearrangements of the quaternary structure (Haslbeck et al., 1999). Both observations led to the generally accepted notion that sHsp oligomers dissociate into dimers and reassociate with the substrate into the larger complexes (Haslbeck et al., 1999; Stromer et al., 2003). sHsps appear to exist as dynamic molecules which can exchange subunits (Aquilina et al., 2005; Bova et al., 1997; Bova et al., 2002; Bova et al., 2000; Franzmann et al., 2005; Ghahghaei et al., 2007; Haley et al., 1998; Sobott et al., 2002). It was unclear whether this common feature is linked to their chaperone mechanism. Hsp26, together with few other sHsps, including Hsp16.6 from *Synechocystis spec.* and Hsp16 from *S. pombe*, seem to possess dynamic properties allowing them to exchange subunits rapidly, leading to the temperature-sensitive destabilization of the oligomers and the subsequent dissociation under specific conditions (Franzmann et al., 2005; Giese and Vierling, 2002; Haslbeck et al., 1999; Lentze et al., 2004). For others, including Hsp25, α -crystallin and IbpA, complete oligomer dissociation under

the same conditions was never observed (Aquilina et al., 2005; Ehrnsperger et al., 1999; Horwitz, 2003; Narberhaus, 2002; Stromer et al., 2003). The question remained whether the dissociation or the exchange of subunits is an essential incidence in the chaperone mechanism of sHsps. To obtain a detailed understanding of the underlying regulatory mechanism, the structural features of inactive and active Hsp26 and the kinetic barrier that separates these functionally distinct states were analyzed in a comprehensive *in vitro* study.

5.1 Structural changes

sHsps share an identical domain organization in which the variable N-terminal region is followed by the α -crystallin domain and the C-terminal extension (De Jong et al., 1998). Structure analysis of various sHsps including the crystal structures available for Hsp16.5 from *M. jannaschii* and wheat Hsp16.9 suggest that the N-terminal regions are located at close quarters within the hollow complexes (Kim et al., 1998; van Montfort et al., 2001). The structure-function relationship remains unclear, but for Hsp26 it was shown that residues of the N-terminal regions are required for substrate interaction and oligomer stability (Haslbeck et al., 2004). The C-terminal extensions of Hsp16.5 and Hsp16.9 were found to mediate the self-association into the oligomeric complex via inter-subunit interactions (Kim et al., 1998; van Montfort et al., 2001). This was confirmed for various sHsps in which the C-terminal extensions were either removed or mutated (Fernando et al., 2002; Giese et al., 2005; Pasta et al., 2004; Studer et al., 2002). In agreement with this observation, C-terminally truncated Hsp26 fails to associate into oligomers (Franzmann et al., 2008). Both, the N-terminal region and the C-terminal extension emerge to have overlapping functions. On the one hand, both parts stabilize the oligomers, yet to different extent, on the other hand both regions are required for efficient chaperone

activity (Franzmann et al., 2008; Haslbeck et al., 2004; Stromer et al., 2004). Introducing Cys residues into these regions allowed covalent cross-linking of subunits within the Hsp26 oligomer and analysis of stabilized Hsp26 oligomers with respect to their dynamics and chaperone function.

Using the N-terminal Cys variant Hsp26S4C, $\sim 2/3$ of the subunits were cross-linked within the Hsp26 oligomer. Since every subunit contains a single Cys, only inter-molecular disulfide bonds can be formed. It is tempting to speculate that the N-termini form trimers. This could be explained easiest when two of three N-termini become oxidized and form a disulfide bond, while the third remains reduced. Similarly, $1/2$ of the subunits were cross-linked using the C-terminal Cys variant. This is indicative for at least two different conformations of the C-termini. If all C-termini were in similar environment one would expect all termini to cross-link under oxidizing conditions. This demonstrates that the N-termini are in close proximity with the N-terminus of an adjacent subunit and that at least 50% of all C-termini are located in close distance to C-termini from another subunits. In contrast to the terminal regions, introduction of a cystein residue in the middle domain did not result in cross-linked subunits. This suggests that the MDs are somehow isolated from each other. One might argue that the cystein residues in MD are not able to form disulfide bonds as they might point towards opposing directions. But even at elevated temperatures and under extensive oxidizing condition, no MD-cross-linked Hsp26 molecules were detected.

Although high resolution structure information about Hsp26 is missing, two distinct populations, termed compact and extended, were observed by CryoEM (White et al., 2006). The overall appearance of both structures is similar, but the two assemblies differ with respect to their inner compaction. Four distinct mass densities were observed in the interior of the large extended structure, and a single mass density was detected inside of the compact form (Figure 70). These

densities could be assigned to the C-terminal extensions. Based on mass assignment, only twelve of the entire 24 C-terminal extensions contribute to this particular assembly, whereas the remaining once were identified to be involved in intersubunit contacts between the C-terminal extension of one subunit with the MD of an adjacent one. This is in agreement with the observation of two distinct cross-linking ratios upon oxidation, in which either 50% or 33% are involved in the formation of disulfide bridges. Both oxidizing ratios exhibit indistinguishable chaperone activity, suggesting that the degree of C-terminal packing is not directly related to the chaperone mechanism.

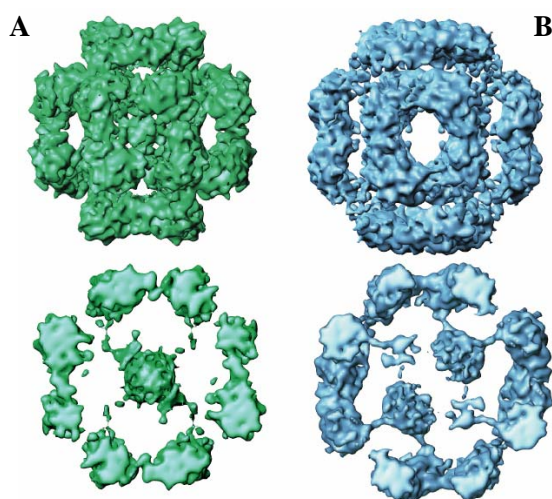


Figure 70 CryoEM structure of wt Hsp26 (White et al., 2006). Two distinct assemblies were observed that differ in the degree of packing insight of the shell. A: compact structure revealed a single mass density in the center of the sphere. B: extended structure with four distinct mass densities. Lower panel shows a sectional cut through the center of the structures.

Structural investigations with CD and analytical SEC revealed that the oxidized variants adopt secondary and quaternary structures indistinguishable from the wt protein. However, the N- and C-terminal Cys variants maintained their oligomeric state under oxidizing conditions at elevated temperatures and did not dissociate into dimers in gel filtration experiments. Thus inter-molecular cross-linking of subunits stabilized the oligomer and reduced the dynamics.

Temperature unfolding experiments with wt Hsp26 revealed two thermal transition midpoints. The first one takes place between 20 and 50°C and is fully reversible when Hsp26 is heated to 60°C only. This structural change takes place within the physiological temperature range for yeast cells. The second thermal transition midpoint is at ~75°C and resembles the irreversible unfolding of Hsp26. Although the first thermal transition midpoint (36°C) of wt Hsp26 is slightly concentration dependent and shifts towards higher temperatures when the experiment is carried out at a 10fold higher protein concentration, the transition midpoints and the ΔG values of the oxidized forms were indifferent from those obtained for the wt protein. Since these variants maintain their oligomeric state at elevated temperatures, the first transition rather represents structural rearrangements inside the oligomer than cooperative dissociation into dimers. In agreement with this, investigating Hsp26 at elevated temperatures with sedimentation velocity ultracentrifugation showed that the oligomerization equilibrium is not shifted towards smaller species. Even at low concentrations the oligomer was the most abundant species.

Temperature activation is obligatory for Hsp26. Activation appears to correlate with changes of its secondary and tertiary structure, as the oxidized variants Cys variants do not dissociate at elevated temperatures, but exhibit unrestricted chaperone activity. These data suggest that the Hsp26 oligomer binds substrate molecules. Furthermore, like the wt protein, the Cys variants require elevated temperature to display chaperone activity. This demonstrates that the oligomer exists in at least two distinct conformations with different affinities for substrate molecules: A low affinity state, in which Hsp26 adopts a conformation that is unable to interact with unfolded polypeptides, and a high affinity state, which allows Hsp26 to bind substrate molecules. These functional distinct states are correlated to conformational changes of the Hsp26 oligomer, and these rearrangements can occur without the necessity of oligomer dissociation. A

correlation between changes in structure and chaperone activity has also been reported for α -crystallin (Raman et al., 1995; Raman and Rao, 1997). Using the two Hsp26 variants Hsp26 Δ N30, lacking residues 1 to 30, and Hsp26 Δ N, lacking the residues 1-95, it was shown that the N-terminal region of Hsp26 is bi-functional; residues 1-30 appear to be essential for substrate interaction, whereas amino acids 30-95 were proposed to be required for the correct assembly of the oligomer (Haslbeck et al., 2004; Stromer et al., 2004). While Hsp26dN30 exhibits a thermal transition similar to that of the wild type protein, this is no longer observed in Hsp26dN, indicating that the transition may reflect rearrangements of residues 30-95 (Franzmann et al., 2005). This region of the protein might represent a temperature-regulated relay, switching the oligomer between a low and high affinity state (Franzmann et al., 2005). This is in agreement with the result that temperature activation coincides with tertiary structure changes of Phe residues (Franzmann et al., 2005). Since nine of the eleven Phe residues of Hsp26 are located within the N-terminal region, this can be seen as further evidence that the N-terminal region changes its structure at elevated temperatures (Franzmann et al., 2005).

5.2 The middle domain changes its conformation upon temperature shift

Based on the results presented here, the Hsp26 MD changes its conformation specifically upon temperature activation. The FRET efficiency between MD-attached fluorophores decreases upon temperature shift, and the accessibility of quencher molecules to MD increases, indicating a major conformational rearrangement of this domain, whereas other parts of Hsp26 remain mostly unaffected. FRET experiments suggest that the distance between MDs increases by almost 3 nm and the increased quenching coefficient of MD-labelled fluorophores in activated Hsp26 suggests that this domain becomes solvent-

exposed upon activation. FRET efficiencies can be influenced by the donor quantum yield, restriction of the rotational freedom and spectral shifts. Control experiments suggest that the latter two can be ruled out and corrections for changes in quantum yields could be carried out. However, in Hsp26 the situation is even more complex, as multiple donor and acceptor fluorophors are present in one oligomer. Here, a single donor fluorophor might transfer its energy to multiple acceptors resulting in kinetic partitioning of the energy transfer rates. Hence, the observed changes in the FRET efficiencies reflect major conformational rearrangements, yet the distances measured with FRET carry an uncertainty, which must be reviewed with other techniques, such as structure determination by NMR. In agreement with this, the tryptophan fluorescence of W72 that is located in MD decreases upon temperature shift. However, neither the fluorescence quenching coefficient, nor the fluorescence maximum of activated Hsp26, correlate with the expected values for a fully unfolded or solvent exposed domain, suggesting that MD remains at least partially folded. Structure analysis of MD using the truncation variant Hsp26 30-195 by CD spectroscopy revealed that MD consists of 55% β -sheet structure and this secondary structure composition does not change upon activation (Suppl. Figure 1). It was shown previously that tryptophan residues also contribute to the CD of proteins in the far-UV region (Andersson et al., 2001). Therefore, it is likely that the differences in the far-UV spectra do not reflect changes in the secondary structure of Hsp26 30-195 but rather changes in the local environment of W72. Fluorescence and near UV CD spectroscopy indicated that temperature activation induces tertiary structure changes in MD without perturbation of its secondary structure (Suppl. Figure 1). These changes appear to be only local and do not affect the overall structure, as no differences in the hydrodynamic radius were detected when Hsp26 was analyzed at elevated temperature by dynamic light scattering. It should be noted that MD is not able to interact with unfolded

polypeptides, demonstrating that substrate binding involves other parts of Hsp26. Supposedly, MD controls the accessibility of unfolded polypeptide substrates to the substrate binding site on Hsp26. This can either be achieved by breaking an inhibitory binding between MD and the substrate binding site (supposedly located in NTD), or by uncovering the substrate binding site through a conformational displacement of MD. Thus, the intramolecular rearrangement of MD establishes the mechanistic link between thermal stress and Hsp26 chaperone activity (Figure 71B).

5.3 A large energy barrier controls the chaperone activity of Hsp26

Although the structure of MD rearranges upon temperature activation, this does not necessarily mean that the structural rearrangement of MD is correlated with the chaperone mechanism of Hsp26 *per se*. To test for this, the time dependent structural changes were analyzed at various temperatures, allowing determination of the energy barrier that separates the two conformational states. In addition, the gain of chaperone function upon temperature shift was also determined at various temperatures, allowing to determine the energy barrier separating the functional inactive from the function active state. According to transition state theory, the logarithm of a rate constant depends linearly on the reciprocal temperature. Eyring plots ($\ln(k)$ vs $1/T$) provide information about the transition state and hence about the coupling of processes (Schellenberger, 1989). If two processes have superimposing Eyring plots over a wide temperature range, then they are most likely controlled by the same energy barrier.

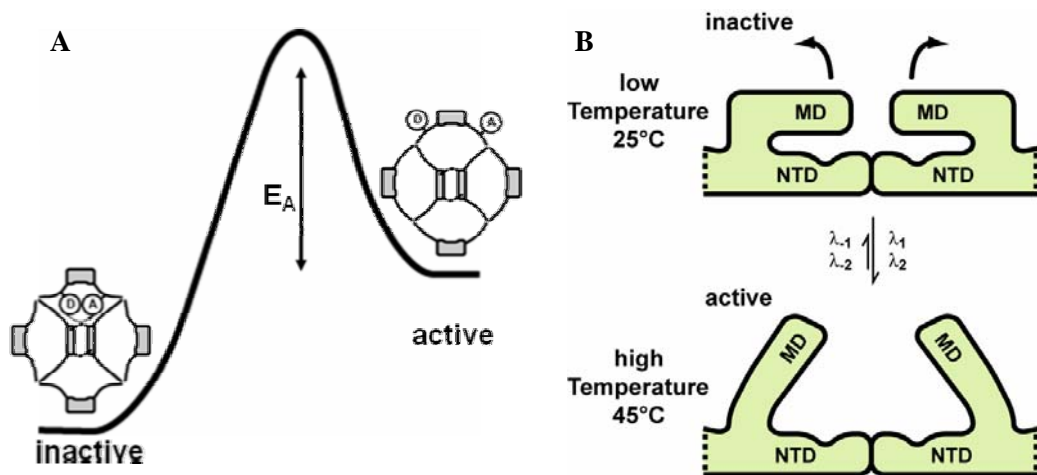


Figure 71 Model for the regulation of the Hsp26 chaperone activity. A: A large energy barrier separates structurally distinct Hsp26 oligomers. Both states represent distinct functional states. At low temperatures, Hsp26 adopts a conformation that is unable to interact with unfolded polypeptides. An increase in ambient temperature induces a conformational rearrangement of the Hsp26 oligomer which renders Hsp26 binding competent. The interconversion rate is controlled by the energy barrier. Without this energy barrier, both functional states would be kinetically indistinguishable and Hsp26 could not be stored in an inactive state at low temperatures. B: According to the data presented here, MD changes its conformation upon temperature activation. This in turn renders Hsp26 binding competent. This could be achieved by breaking either an inhibitory binding between MD and the substrate binding sites (supposedly located in NTD), or by uncovering the substrate binding site.

Temperature activation of Hsp26 is a fast and biphasic process. Two models can account for this behavior: (i) On a sequential pathway, partially active Hsp26 are generated in during the fast phase. These intermediate molecules undergo further conformational rearrangements, which increase their chaperone activity during the second, slower phase. An inactive intermediate can be excluded, as binding competent molecules are generated during the first phase. (ii) On a parallel pathway, two conformationally distinct Hsp26 populations activate through either of the pathways. The latter explanation takes into account that structurally distinct assembly forms of Hsp26 have been observed by CryoEM (White et al., 2006). Also chaperone inactivation follows a double exponential function, yet the inactivation is 10times slower compared to the activation. This

may simply be a consequence of the reaction temperature, as in general reactions are faster at higher temperatures.

Analysis of the time-dependent changes of MD upon temperature shift, revealed two rate constants. Whereas λ_1 is fast and depends strongly on changes in the temperature, λ_2 is slow and barely affected by changes in the temperature. Importantly, the gain of chaperone function followed the same temperature-dependence as determined for the conformational rearrangement of MD, suggesting that both processes are linked to each other. Moreover, confinement of the N-terminal flexibility through disulfide bridges slowed down the MD rearrangement upon temperature activation, demonstrating that NTD and MD are functionally communicating. One would expect that if MD controls the activation process of Hsp26, then mutations altering the dynamics of the MD rearrangement would also affect the chaperone activation. This is indeed the case. The gain of chaperone function of N-terminally oxidized Hsp26S4C was also slowed down, demonstrating that MD is a molecular switch controlling the activity of Hsp26. The energy barrier controls the position of the switch and the rate of interconversion. Without this energy barrier, both states would be kinetically indistinguishable and a cooperative activation of Hsp26 could not be achieved.

Quantitative analysis of the reaction kinetics revealed similar large energy barriers for both reactions with $\Delta G^* \sim 85 \text{ kJ mol}^{-1}$, a value also found in the range for isomerization reactions of proline peptide bond (Fanghänel and Fischer, 2004). In the case of antibody molecules, the folding of immunoglobulin domains (IG) is strictly coupled to the isomerization of a single proline residue that has to adopt a cis-conformation in the native domain structure (Feige et al., 2004). Also, the association of antibody subunits can depend on proline isomerization (Thies et al., 1999). Proline isomerization is not only of importance in protein folding, but is also of biological relevance. The infection mechanism of the bacteriophage fd,

as well as the allosteric communication between the ATPase and substrate binding domains of Hsp70 dependent on the conformational rearrangement of prolines (Eckert et al., 2005; Vogel et al., 2006). Whether the Hsp26 temperature activation is controlled by this principle remains to be elucidated. First evidence comes from experiments carried out with Hsp26 variants, in which P81 and P87 were replaced by alanine and glycine, respectively (Master's thesis Petra Menhorn). The absence of proline in the thermo switch slows down its conformational rearrangement by a factor of 40 and alters the fractional ratio of species passing through this pathway to the active state.

Such a distinct regulation mechanism puts Hsp26 in an exceptional position. The activity of most chaperones is regulated on the level of transcription. In addition to this, Hsp26 activity is also subjected to an intrinsic conformational regulation. The high energy barrier allows Hsp26 to reside inside of the yeast cytosol in an inactive state and restricts Hsp26 activity to temperatures when required. This allows the precise autoregulation of Hsp26 without the necessity of additional regulatory factors.

5.4 Subunit exchange of Hsp26

In vitro, sHsps exchange subunit continuously. Previously it was shown that an increase in temperature accelerates subunit exchange (SX) and unleashes chaperone activity of several sHsps. Whereas increased dynamics destabilize the oligomeric state of some sHsps (Hsp26 from *S. cerevisiae*, Hsp16.6 from *Synechocystis spec*, Hsp16 from *S. pombe*), dissociation for other sHsps has not been observed (human and bovine α -crystallin, mouse Hsp25, Hsp16.5 from *M. jannaschii*, Hsp16.9 from wheat). Aware of this discrepancy, differences in chaperone efficiency had been attributed to the differences in dynamics (Bova et

al., 1997; Giese and Vierling, 2002; Haslbeck et al., 1999). A model summarizing these observations, postulates a dimeric intermediate that becomes substrate binding competent, which then reassociates to form sHsps-substrate complexes (Giese and Vierling, 2002; Haslbeck et al., 1999).

Neither oxidized Hsp26S4C, nor Hsp26S210C exchanges subunits or dissociates into dimers at elevated temperature, but both variants exhibit unrestricted chaperone activity (Franzmann et al., 2005). This demonstrates that oligomer dissociation, as well as SX are not essential for the chaperone activation of Hsp26. Furthermore, it could be shown that CS aggregation is ten times faster than Hsp26 SX and that the Hsp26 chaperone activation is significantly faster than the exchange of subunits between wt Hsp26 oligomers (Franzmann et al., 2008; Franzmann et al., 2005). This becomes most prominent at 36°C, where the gain of Hsp26 chaperone function is ten times faster than subunit exchange. Detailed analysis of Hsp26 SX revealed two phases. Both have similar large energy barriers ($\sim 95 \text{ kJ mol}^{-1}$) and a parallel behavior of the temperature dependence, suggesting that they originate from two distinct Hsp26 populations. This is in good agreement with the observation of two distinct oligomer assemblies of Hsp26 by CryoEM that differ in the degree of the C-terminal packing (White et al., 2006). The rates and temperature dependence of subunit exchange superimpose with the structural rearrangement of the C-terminal extension monitored by Trp W211. The C-terminal involvement in SX would explain why the two Eyring plots show superimposing phases. Hsp26 SX appears to be independent of the protein concentration (data not shown). This can only be explained when the dissociation of Hsp26 or a structural change is limiting the overall reaction. The latter could be a structural rearrangement of the C-terminal extension that precedes oligomer dissociation or when dissociated Hsp26 subunits can only assemble in a certain conformation.

The phenomenon of SX remains enigmatic and whether it is of biological relevance remains to be carefully elucidated. Simulating the cellular environment with molecular crowding agents allowed addressing this question *in vitro*. Under molecular crowding SX of Hsp26 was not detected by FRET, while its oligomeric state and chaperone activity were maintained. Apparently, crowding stabilizes the oligomer. Folding experiments suggest that the association process is kinetically accelerated, whereas the dissociation rates are independent of the solvent composition. This can be taken as first evidence that subunit exchange *in vitro* rather reflects the requirement of a highly flexible structure to allow for conformational rearrangements in the cell. Oligomer dissociation is not required for substrate binding (Franzmann et al., 2008; Franzmann et al., 2005). Dissociation of the Hsp26 oligomer might be of importance for the release of sHsp-trapped polypeptides by other chaperone systems. However, currently this aspect has yet not been addressed.

5.5 Hypothesis about substrate binding by Hsp26

sHsps bind unfolded polypeptides in a stable manner. sHsps-substrate complexes have been studied by electron microscopy and other biochemical tools (Friedrich et al., 2004; Haslbeck et al., 1999; Stromer et al., 2003). However, a high resolution structure of a sHsps-substrate complex is yet missing. Complexes formed with Hsp26 and Hsp25 using the model substrates rhodanese, insulin and α -glucosidase had been reported to be irregular complexes with diameters of 50-100 nm (Stromer et al., 2003). Complexes formed with Hsp16.9 and Hsp17.8 using the substrates luciferase and MDH, respectively, differ in shape and size (Basha et al., 2004b; Friedrich et al., 2004). The data suggest that the substrate, as well as the sHsp contribute to the process of complex formation and dictate the extent of heterogeneity. In contrast to these observations, complexes formed between Hsp26 and CS appeared as regular, round-shaped particles with diameters of 30-50 nm (Haslbeck et al., 1999; Stromer et al., 2003). Surprisingly, analysis of Hsp26-CS complexes by analytical ultracentrifugation revealed an enormous heterogeneity (Figure 42). The heterogeneity becomes even more pronounced at higher substrate concentrations. The average Svedberg size distribution of substrate complexes increases in a substrate concentration dependent manner, indicating that multiple substrates can be bound to a single Hsp26 oligomer and that substrate complexes “grow” (Figure 42). Supposedly, unfolded substrate molecules “stick” Hsp26-substrate complexes together. This observation argues against a simple coordinated cooperative binding mode, but rather suggests that unfolded substrate molecules selectively bind to active Hsp26 molecules.

Recent data suggest that the N-terminal region plays an important role in substrate recognition and binding, yet details about the substrate binding sites on sHsps remain enigmatic. N-terminally truncated Hsp26, lacking the first 30 amino acids is able to interact with some substrate molecules, but exhibits reduced chaperone activity, whereas the deletion of the entire N-terminal region (residues 1-95) results in a complete loss of activity (Haslbeck et al., 2004; Stromer et al., 2004). In *Synechocytis spec* Hsp16.6, random mutagenesis produced single point mutants that were unable to mediate thermotolerance *in vivo* (Giese et al., 2005). This illustrates the fragile nature of the N-terminal region with respect to substrate binding properties of sHsps.

In a set of Hsp26 variants, the N-terminal Phe residues were replaced. Neither Hsp26FS nor Hsp26FA exhibit chaperone activity. Both proteins were unable to suppress the thermal aggregation of CS, as well as the aggregation of chemically unfolded GDH. Structure analysis by CD revealed spectra resembling wt Hsp26 at 45°C, but both variants were unable to associate into oligomers. The assembly of both variants stopped on the level of tetramers, even at very high concentrations (125 µM). A single amino acid exchange in Hsp26, in which the Trp W72 was replaced by Tyr, resulted in insoluble protein after biosynthesis which could not be refolded to the native state. Nonetheless, Hsp26W72Y could be resolubilized, but its the assembly stopped on the level of a dimer (and weak tetramer) (data not shown). Structure analysis by CD at 25°C gave spectra resembling wt Hsp26 at 45°C, but this variant was unable to suppress the thermally-induced aggregation of CS or GDH. Loss of chaperone function was correlated with destabilization of the quaternary structure. It is tempting to speculate that the substrate binding site *per se* is not present in a single Hsp26 polypeptide chain and that it is only formed upon oligomerization of Hsp26. Thus, oligomerization is a prerequisite for chaperone function. Using 300 nm N-terminally fluorescence-labelled Hsp26 to test for the binding of Hsp26 to CS,

revealed that in contrast to the literature, approximately three Hsp26 molecules bind to one CS molecule (data not shown) (Haslbeck et al., 1999; Stromer et al., 2003).

Taking into account that the Hsp26 oligomer consists of 24 subunits, this would allow eight CS molecules to be bound. The N-terminal regions form disulfide bridges with stoichiometries suggesting that they form trimers (Franzmann et al., 2005). In agreement with this notion, the CryoEM structure of Hsp26 revealed a threefold symmetry which was postulated to be formed by the N-termini (White et al., 2006). In the hypothesis presented here, three N-termini come together to form the substrate binding site within the Hsp26 oligomer and the position of the binding site is controlled by the thermo switch.

5.6 Hsp26 in the cell

Precise regulation of protein function plays a key role for the integrity of the cell in response to changing environmental conditions. Cellular stress, such as heat shock, can render polypeptides prone to aggregation. This in turn interferes with protein homeostasis. Molecular chaperones assist in protein folding and prevent unspecific protein aggregation (Buchner, 1996). Commonly, molecular chaperones utilize ATP binding and hydrolysis to switch between conformational states with different affinities for polypeptides to allow for protein refolding (Hartl, 1996). However, as long as the stress persists, the ATP dependent cycling may not be productive, as the polypeptide substrate is released into environmental conditions, detrimental for refolding. sHsps could help the cell to manage this problem, since they form stable substrate complexes and act independent from ATP (Ehrnsperger et al., 1997b; Jakob et al., 1993). Thus, they play a buffering role in the context of the cellular multi-chaperone network and separate the binding of unfolded polypeptides from their refolding process. With ~19,300 molecules/cell (corresponding to ~0.5-1 μ M) under physiological conditions, Hsp26 is the principal sHsp in the yeast cytosol (Hsp42 1,470 molecules/cell, Hsp104 32,800 molecules/cell, Hsp82 445,000 molecules/cell) (Ghaemmaghami et al., 2003). Hsp26 activation by temperature is fast and independent of other regulatory factors, such as transcription. Thus, Hsp26 is the first chaperone to encounter unfolded polypeptides generated by stress. Analysis of the Hsp26 structure and function under molecular crowding revealed that the native oligomer is stabilized, while its chaperone efficiency was unaffected. This is in agreement with the observation that, in general, molecular crowding conditions facilitate protein folding and stabilize the native conformation (Eggers

and Valentine, 2001; Guo et al., 2005; Zhou, 2004). It is tempting to speculate, that the activation of Hsp26 chaperone function in the cell is even more cooperative, since cellular conditions would presumably stabilize its inactive state. Why should Hsp26 be inactive under physiological conditions? It has been shown previously that RheA, a bacterial transcription factor, undergoes a temperature-induced conformational change upon heat shock that leads to the transcription activation of heat shock genes (Servant et al., 2000; Servant et al., 1999). Similarly, in response to an increased amount of unfolded proteins in the cytosol, the DnaJ- σ 32 complex dissociates and activates the transcription of heat shock genes (Bukau, 1993). Additionally, a distinct domain of the Hsp70 nucleotide exchange factor, GrpE, unfolds under heat shock conditions and provides a resting signal and traps the Hsp70 chaperone in its high affinity state for unfolded polypeptides (Groemping and Reinstein, 2001). These systems can be seen as intracellular thermometers that control the heat shock response. Hsp26 may also be involved in the regulation of the heat shock response in yeast, as its thermo sensor makes it a perfect candidate to function as the intracellular thermometer. However, Hsp26 itself is not a key regulator of the yeast heat shock response. Hsp26 may rather play an auxiliary function. One might speculate that Hsp26 binds or facilitates proteolytic degradation of a certain regulatory factor under heat shock conditions, and thus fine tunes the heat shock response and/or provides a feedback signal for how long the heat shock condition persists.

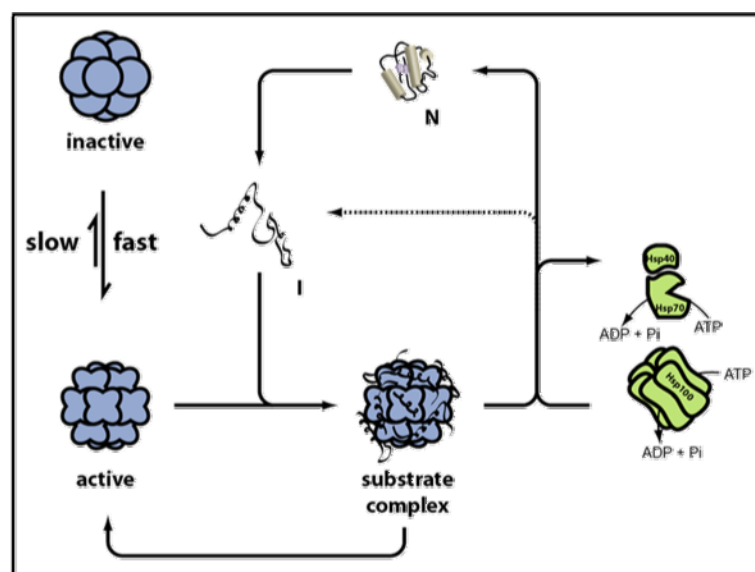


Figure 72 Schematic illustration of Hsp26 in the yeast chaperone network. Under physiological conditions inactive Hsp26 resides in the cytosol. Upon heat shock cytosolic proteins unfold. Concomitantly Hsp26 becomes activated and binds to unfolded polypeptides and forms substrate complexes. When yeast cells reenter physiological conditions, its functional partners Hsp104 and Hsp70 release polypeptides from the complex and mediate proper refolding.

sHsps bind polypeptides in a stable manner and substrate complexes persist for a long period of time (Ehrnsperger et al., 1997b). Its high affinity for unfolded polypeptides makes Hsp26 a very potent chaperone in suppressing protein aggregation. Uncontrolled binding of Hsp26 to newly synthesized proteins might interfere with fundamental processes and folding pathways and might unnecessarily route polypeptides through a chaperone-dependent folding pathway.

Compared to its temperature activation, Hsp26 inactivation is slow (Franzmann et al., 2008). This leaves Hsp26 binding competent for a certain period of time after the cell has reentered physiological conditions. Hsp26 functionally interacts with the molecular chaperone and disaggregase Hsp104 (Cashikar et al., 2005). This ATP-driven machine resolves protein aggregates after heat shock (Glover and Lindquist, 1998). It is noteworthy, that Hsp104 gene expression is enhanced only after heat shock. However, Hsp104 is the crucial factor that mediates

thermotolerance in yeast (Sanchez and Lindquist, 1990). Apparently, yeast cannot withstand the severe accumulation of protein aggregates. Deletion of both, Hsp26 and Hsp104 from yeast cells reduces the survival rate after severe heat shock fivefold (Cashikar et al., 2005). It appears that polypeptides can be recovered more efficiently from Hsp26-complexes than from pure aggregates (Cashikar et al., 2005; Haslbeck et al., 2005b). Deletion of Hsp26 did neither affect thermotolerance, nor revealed a phenotype under a broad variety of stress conditions (budding, sporulation, starvation), yet trapping unfolded polypeptides on sHsps appears to simplify refolding and might be beneficial to cells on an evolutionary scale (Cashikar et al., 2005; Haslbeck et al., 2005b; Petko and Lindquist, 1986). And its regulation through its thermo switch restricts Hsp26 chaperone activity to heat shock conditions and ensures its instantaneous availability when required.

6 References

Ali, M.M., Roe, S.M., Vaughan, C.K., Meyer, P., Panaretou, B., Piper, P.W., Prodromou, C., and Pearl, L.H. (2006). Crystal structure of an Hsp90-nucleotide-p23/Sba1 closed chaperone complex. *Nature* *440*, 1013-1017.

Allen, S.P., Polazzi, J.O., Gierse, J.K., and Easton, A.M. (1992). Two novel heat shock genes encoding proteins produced in response to heterologous protein expression in *Escherichia coli* 1. *J.Bacteriol.* *174*, 6938-6947.

Andersson, D., Carlsson, U., and Freskgard, P.O. (2001). Contribution of tryptophan residues to the CD spectrum of the extracellular domain of human tissue factor: application in folding studies and prediction of secondary structure. *Eur.J.Biochem.* *268*, 1118-1128.

Anfinsen, C.B. (1973). *Science* *181*, 223-230.

Anfinsen, C.B., Haber, E., Sele, M., and White, F.H. (1961). *Proc.Natl.Acad.Sci.U.S.A* *47*, 1309-1314.

Aquilina, J.A., Benesch, J.L., Ding, L.L., Yaron, O., Horwitz, J., and Robinson, C.V. (2005). Subunit exchange of polydisperse proteins: mass spectrometry reveals consequences of alphaA-crystallin truncation. *Journal of Biological Chemistry* *280*, 14485-14491.

Basha, E., Friedrich, K.L., and Vierling, E. (2006). The N-terminal arm of small heat shock proteins is important for both chaperone activity and substrate specificity. *J Biol Chem* *281*, 39943-39952.

Basha, E., Lee, G.J., Breci, L.A., Hausrath, A.C., Buan, N.R., Giese, K.C., and Vierling, E. (2004a). The identity of proteins associated with a small heat shock protein during heat stress in vivo indicates that these chaperones protect a wide range of cellular functions. *Journal of Biological Chemistry* 279, 7566-7575.

Basha, E., Lee, G.J., Demeler, B., and Vierling, E. (2004b). Chaperone activity of cytosolic small heat shock proteins from wheat. *Eur.J.Biochem.* 271, 1426-1436.

Beissinger, M., and Buchner, J. (1998). How chaperones fold proteins. *Biol.Chem.* 379, 245-259.

Benndorf, R., Hayess, K., Ryazantsev, S., Wieske, M., Behlke, J., and Lutsch, G. (1994). Phosphorylation and supramolecular organization of murine small heat shock protein HSP25 abolish its actin polymerization-inhibiting activity. *Journal of Biological Chemistry* 269, 20780-20784.

Bhattacharyya, J., Padmanabha Udupa, E.G., Wang, J., and Sharma, K.K. (2006). Mini-alphaB-crystallin: a functional element of alphaB-crystallin with chaperone-like activity. *Biochemistry* 45, 3069-3076.

Bose, S., Weikl, T., Bugl, H., and Buchner, J. (1996). Chaperone function of Hsp90-associated proteins. *Science* 274, 1715-1717.

Bosl, B., Grimminger, V., and Walter, S. (2005). Substrate binding to the molecular chaperone Hsp104 and its regulation by nucleotides. *J Biol Chem* 280, 38170-38176.

Bosl, B., Grimminger, V., and Walter, S. (2006). The molecular chaperone Hsp104 - a molecular machine for protein disaggregation. *J.Struct.Biol.* 156, 139-148.

Bova, M.P., Ding, L.L., Horwitz, J., and Fung, B.K. (1997). Subunit exchange of alphaA-crystallin. *J.Biol Chem.* 272, 29511-29517.

Bova, M.P., Huang, Q., Ding, L., and Horwitz, J. (2002). Subunit exchange, conformational stability, and chaperone-like function of the small heat shock

protein 16.5 from *Methanococcus jannaschii*. *Journal of Biological Chemistry* 277, 38468-38475.

Bova, M.P., McHaourab, H.S., Han, Y., and Fung, B.K. (2000). Subunit exchange of small heat shock proteins. Analysis of oligomer formation of alphaA-crystallin and Hsp27 by fluorescence resonance energy transfer and site-directed truncations. *Journal of Biological Chemistry* 275, 1035-1042.

Bova, M.P., Yaron, O., Huang, Q., Ding, L., Haley, D.A., Stewart, P.L., and Horwitz, J. (1999). Mutation R120G in alphaB-crystallin, which is linked to a desmin-related myopathy, results in an irregular structure and defective chaperone-like function 2. *Proc.Natl.Acad.Sci.U.S.A* 96, 6137-6142.

Braig, K., Otwinowski, Z., Hegde, R., Boisvert, D.C., Joachimiak, A., Horwich, A.L., and Sigler, P.B. (1994). The crystal structure of the bacterial chaperonin GroEL at 2.8 Å. *Nature* 371, 578-586.

Buchberger, A., Theyssen, H., Schröder, H., McCarty, J., Virgallita, G., Milkereit, P., Reinstein, J., and Bukau, B. (1995). Nucleotide-induced conformational changes in the ATPase and substrate binding domains of the DnaK chaperone provide evidence for interdomain communication. *J Biol Chem* 270, 16903-16910.

Buchner, J. (1996). Supervising the fold: functional principles of molecular chaperones. *FASEB J.* 10, 10-19.

Buchner, J. (1999). Hsp90 & Co. - a holding for folding. *Trends Biochem.Sci.* 24, 136-141.

Buchner, J., Grallert, H., and Jakob, U. (1998). Analysis of chaperone function using citrate synthase as nonnative substrate protein. *Methods Enzymol.* 290, 323-338.

Bukau, B. (1993). Regulation of the *Escherichia coli* heat-shock response. *Mol Microbiol* 9, 671-680.

Bukau, B., Deuerling, E., Pfund, C., and Craig, E.A. (2000). Getting newly synthesized proteins into shape. *Cell* 101, 119-122.

Bukau, B., and Horwich, A.L. (1998). The Hsp70 and Hsp60 chaperone machines. *Cell* 92, 351-366.

Carver, J.A., and Lindner, R.A. (1998). NMR spectroscopy of alpha-crystallin. Insights into the structure, interactions and chaperone action of small heat-shock proteins. *Int.J.Biol.Macromol.* 22, 197-209.

Cashikar, A.G., Duennwald, M., and Lindquist, S.L. (2005). A chaperone pathway in protein disaggregation. Hsp26 alters the nature of protein aggregates to facilitate reactivation by Hsp104. *Journal of Biological Chemistry* 280, 23869-23875.

Chen, J., Walter, S., Horwich, A., and Smith, D. (2001). Folding of malate dehydrogenase inside the GroEL-GroES cavity. *Nat Struct Biol* 8, 721-728.

Cheung, M.S., Klimov, D., and Thirumalai, D. (2005). Molecular crowding enhances native state stability and refolding rates of globular proteins. *Proc Natl Acad Sci U S A* 102, 4753-4758.

Creighton, T.E. (1990). Protein folding. *Biochem J* 270, 1-16.

Datta, S.A., and Rao, C.M. (1999). Differential temperature-dependent chaperone-like activity of alphaA- and alphaB-crystallin homoaggregates 4. *Journal of Biological Chemistry* 274, 34773-34778.

De Jong, W.W., Caspers, G.J., and Leunissen, J.A. (1998). Genealogy of the alpha-crystallin--small heat-shock protein superfamily. *Int.J.Biol.Macromol.* 22, 151-162.

Despa, F., Orgill, D.P., and Lee, R.C. (2005). Molecular crowding effects on protein stability. *Ann N Y Acad Sci* 1066, 54-66.

Dittmar, K.D., and Pratt, W.B. (1997). Folding of the glucocorticoid receptor by the reconstituted Hsp90-based chaperone machinery. The initial

hsp90.p60.hsp70-dependent step is sufficient for creating the steroid binding conformation. *J Biol Chem* 272, 13047-13054.

Dollins, D.E., Warren, J.J., Immormino, R.M., and Gewirth, D.T. (2007). Structures of GRP94-nucleotide complexes reveal mechanistic differences between the hsp90 chaperones. *Mol Cell* 28, 41-56.

Doyle, S.M., Shorter, J., Zolkiewski, M., Hoskins, J.R., Lindquist, S., and Wickner, S. (2007). Asymmetric deceleration of ClpB or Hsp104 ATPase activity unleashes protein-remodeling activity. *Nat Struct Mol Biol* 14, 114-122.

Eckert, B., Martin, A., Balbach, J., and Schmid, F.X. (2005). Prolyl isomerization as a molecular timer in phage infection. *Nat.Struct.Mol.Biol.* 12, 619-623.

Eggers, D.K., and Valentine, J.S. (2001). Molecular confinement influences protein structure and enhances thermal protein stability. *Protein Sci* 10, 250-261.

Ehrnsperger, M., Buchner, J., and Gaestel, M. (1997a). Structure and Function of Small Heat-Shock Proteins. (Marcel Dekker, New York: A.L. Fink and Y.Goto, eds), pp. 533-575.

Ehrnsperger, M., Graber, S., Gaestel, M., and Buchner, J. (1997b). Binding of non-native protein to Hsp25 during heat shock creates a reservoir of folding intermediates for reactivation. *EMBO J.* 16, 221-229.

Ehrnsperger, M., Hergersberg, C., Wienhues, U., Nichtl, A., and Buchner, J. (1998). Stabilization of proteins and peptides in diagnostic immunological assays by the molecular chaperone Hsp25. *Anal.Biochem.* 259, 218-225.

Ehrnsperger, M., Lilie, H., Gaestel, M., and Buchner, J. (1999). The dynamics of Hsp25 quaternary structure. Structure and function of different oligomeric species. *Journal of Biological Chemistry* 274, 14867-14874.

- Elad, N., Farr, G.W., Clare, D.K., Orlova, E.V., Horwich, A.L., and Saibil, H.R. (2007). Topologies of a substrate protein bound to the chaperonin GroEL. *Mol Cell* 26, 415-426.
- Engel, K., Ahlers, A., Brach, M.A., Herrmann, F., and Gaestel, M. (1995). MAPKAP kinase 2 is activated by heat shock and TNF-alpha: in vivo phosphorylation of small heat shock protein results from stimulation of the MAP kinase cascade. *J.Cell Biochem.* 57, 321-330.
- Fairbanks, G., Steck, T.L., and Wallach, D.F. (1971). Electrophoretic analysis of the major polypeptides of the human erythrocyte membrane. *Biochemistry* 10, 2606-2617.
- Fanghänel, J., and Fischer, G. (2004). Insights into the catalytic mechanism of peptidyl prolyl cis/trans isomerases. *Front Biosci* 9, 3453-3478.
- Fasman, G.D. (1996). *Circular Dichroism and the Conformational Analysis of Biomolecules* (New York: Plenum Press).
- Feige, M.J., Walter, S., and Buchner, J. (2004). Folding mechanism of the CH2 antibody domain. *J.Mol.Biol.* 344, 107-118.
- Feil, I.K., Malfois, M., Hendle, J., van Der, Z.H., and Svergun, D.I. (2001). A novel quaternary structure of the dimeric alpha-crystallin domain with chaperone-like activity. *J Biol Chem.* 276, 12024-12029.
- Fenton, W., Kashi, Y., Furtak, K., and Horwich, A. (1994). Residues in chaperonin GroEL required for polypeptide binding and release. *Nature* 371, 614-619.
- Fenton, W.A., and Horwich, A.L. (1997). GroEL-mediated protein folding. *Protein Sci* 6, 743-760.
- Fernando, P., Abdulle, R., Mohindra, A., Guillemette, J.G., and Heikkila, J.J. (2002). Mutation or deletion of the C-terminal tail affects the function and

structure of *Xenopus laevis* small heat shock protein, hsp30. *Comp Biochem. Physiol B Biochem. Mol. Biol.* 133, 95-103.

Foss, J.G. (1961). Hydrophobic bonding and conformational transitions in lysozyme, ribonuclease and chymotrypsin. *Biochim Biophys Acta* 47, 569-579.

Franzmann, T.M., Menhorn, P., Walter, S., and Buchner, J. (2008). Activation of the chaperone Hsp26 is controlled by the rearrangement of its thermosensor domain. *Mol. Cell* 29, 207-216.

Franzmann, T.M., Wuhr, M., Richter, K., Walter, S., and Buchner, J. (2005). The Activation Mechanism of Hsp26 does not Require Dissociation of the Oligomer. *J. Mol. Biol.* 350, 1083-1093.

Friedrich, K.L., Giese, K.C., Buan, N.R., and Vierling, E. (2004). Interactions between small heat shock protein subunits and substrate in small heat shock protein-substrate complexes. *Journal of Biological Chemistry* 279, 1080-1089.

Gaestel, M., Benndorf, R., Hayess, K., Priemer, E., and Engel, K. (1992). Dephosphorylation of the small heat shock protein hsp25 by calcium/calmodulin-dependent (type 2B) protein phosphatase. *Journal of Biological Chemistry* 267, 21607-21611.

Gamer, J., Multhaup, G., Tomoyasu, T., McCarty, J.S., Rüdiger, S., Schönfeld, H.J., Schirra, C., Bujard, H., and Bukau, B. (1996). A cycle of binding and release of the DnaK, DnaJ and GrpE chaperones regulates activity of the *Escherichia coli* heat shock transcription factor sigma32. *EMBO J* 15, 607-617.

Gething, M.J., and Sambrook, J. (1992). Protein folding in the cell. *Nature* 355, 33-45.

Ghaemmaghami, S., Huh, W.K., Bower, K., Howson, R.W., Belle, A., Dephoure, N., O'Shea, E.K., and Weissman, J.S. (2003). Global analysis of protein expression in yeast. *Nature* 425, 737-741.

Ghahghaei, A., Rekas, A., Price, W.E., and Carver, J.A. (2007). The effect of dextran on subunit exchange of the molecular chaperone alphaA-crystallin. *Biochim Biophys Acta* 1774, 102-111.

Giese, K.C., Basha, E., Catague, B.Y., and Vierling, E. (2005). Evidence for an essential function of the N terminus of a small heat shock protein in vivo, independent of in vitro chaperone activity. *Proc.Natl.Acad.Sci.U.S.A* 102, 18896-18901.

Giese, K.C., and Vierling, E. (2002). Changes in oligomerization are essential for the chaperone activity of a small heat shock protein in vivo and in vitro. *Journal of Biological Chemistry* 277, 46310-46318.

Giese, K.C., and Vierling, E. (2004). Mutants in a small heat shock protein that affect the oligomeric state. Analysis and allele-specific suppression. *Journal of Biological Chemistry* 279, 32674-32683.

Glover, J.R., and Lindquist, S. (1998). Hsp104, Hsp70, and Hsp40: a novel chaperone system that rescues previously aggregated proteins. *Cell* 94, 73-82.

Groemping, Y., Klostermeier, D., Herrmann, C., Veit, T., Seidel, R., and Reinstein, J. (2001). Regulation of ATPase and chaperone cycle of DnaK from *Thermus thermophilus* by the nucleotide exchange factor GrpE. *J Mol Biol* 305, 1173-1183.

Groemping, Y., and Reinstein, J. (2001). Folding properties of the nucleotide exchange factor GrpE from *Thermus thermophilus*: GrpE is a thermosensor that mediates heat shock response. *J.Mol.Biol.* 314, 167-178.

Gu, L., Abulimiti, A., Li, W., and Chang, Z. (2002). Monodisperse Hsp16.3 nonamer exhibits dynamic dissociation and reassociation, with the nonamer dissociation prerequisite for chaperone-like activity. *J.Mol.Biol.* 319, 517-526.

Guo, W., Shea, J.E., and Berry, R.S. (2005). The physics of the interactions governing folding and association of proteins. *Ann N Y Acad Sci* 1066, 34-53.

- Haley, D.A., Bova, M.P., Huang, Q.L., McHaourab, H.S., and Stewart, P.L. (2000). Small heat-shock protein structures reveal a continuum from symmetric to variable assemblies. *J.Mol.Biol.* 298, 261-272.
- Haley, D.A., Horwitz, J., and Stewart, P.L. (1998). The small heat-shock protein, alphaB-crystallin, has a variable quaternary structure. *J.Mol Biol* 277, 27-35.
- Harrison, C.J., Hayer-Hartl, M., Di Liberto, M., Hartl, F., and Kuriyan, J. (1997). Crystal structure of the nucleotide exchange factor GrpE bound to the ATPase domain of the molecular chaperone DnaK. *Science* 276, 431-435.
- Hartl, F.U. (1996). Molecular chaperones in cellular protein folding. *Nature* 381, 571-579.
- Haslbeck, M., Franzmann, T., Weinfurter, D., and Buchner, J. (2005a). Some like it hot: the structure and function of small heat-shock proteins. *Nat.Struct.Mol.Biol.* 12, 842-846.
- Haslbeck, M., Ignatiou, A., Saibil, H., Helmich, S., Frenzl, E., Stromer, T., and Buchner, J. (2004). A domain in the N-terminal part of Hsp26 is essential for chaperone function and oligomerization. *J.Mol.Biol.* 343, 445-455.
- Haslbeck, M., Miess, A., Stromer, T., Walter, S., and Buchner, J. (2005b). Disassembling protein aggregates in the yeast cytosol. The cooperation of Hsp26 with Ssa1 and Hsp104. *Journal of Biological Chemistry* 280, 23861-23868.
- Haslbeck, M., Walke, S., Stromer, T., Ehrnsperger, M., White, H.E., Chen, S., Saibil, H.R., and Buchner, J. (1999). Hsp26: a temperature-regulated chaperone. *EMBO J.* 18, 6744-6751.
- Haslberger, T., Weibezahn, J., Zahn, R., Lee, S., Tsai, F.T., Bukau, B., and Mogk, A. (2007). M domains couple the ClpB threading motor with the DnaK chaperone activity. *Mol Cell* 25, 247-260.

- Hendrick, J.P., and Hartl, F.U. (1993). Molecular chaperone functions of heat-shock proteins. *Annu.Rev Biochem.* 62, 349-384.
- Hendrick, J.P., and Hartl, F.U. (1995). The role of molecular chaperones in protein folding. *FASEB J.* 9, 1559-1569.
- Heukeshoven, J., and Dernick, R. (1988). Increased sensitivity for Coomassie staining of sodium dodecyl sulfate-polyacrylamide gels using PhastSystem Development Unit. *Electrophoresis* 9, 60-61.
- Horwich, A., Fenton, W., Chapman, E., and Farr, G. (2007). Two families of chaperonin: physiology and mechanism. *Annu Rev Cell Dev Biol* 23, 115-145.
- Horwich, A.L., Farr, G.W., and Fenton, W.A. (2006). GroEL-GroES-mediated protein folding. *Chem Rev* 106, 1917-1930.
- Horwitz, J. (1992). Alpha-crystallin can function as a molecular chaperone. *Proc.Natl.Acad.Sci.U.S.A* 89, 10449-10453.
- Horwitz, J. (2003). Alpha-crystallin. *Exp.Eye Res.* 76, 145-153.
- Hunt, J.F., Weaver, A.J., Landry, S.J., Gierasch, L., and Deisenhofer, J. (1996). The crystal structure of the GroES co-chaperonin at 2.8 Å resolution. *Nature* 379, 37-45.
- Ishihama, A. (1993). Protein-protein communication within the transcription apparatus. *J Bacteriol* 175, 2483-2489.
- Ito, H., Kamei, K., Iwamoto, I., Inaguma, Y., Nohara, D., and Kato, K. (2001). Phosphorylation-induced change of the oligomerization state of alpha B-crystallin. *Journal of Biological Chemistry* 276, 5346-5352.
- Jaenicke, R. (1991). Protein stability and protein folding. *Ciba Found.Symp.* 161, 206-216.

- Jakob, U., Gaestel, M., Engel, K., and Buchner, J. (1993). Small heat shock proteins are molecular chaperones. *Journal of Biological Chemistry* 268, 1517-1520.
- Jakob, U., Lilie, H., Meyer, I., and Buchner, J. (1995). Transient interaction of Hsp90 with early unfolding intermediates of citrate synthase. Implications for heat shock in vivo. *Journal of Biological Chemistry* 270, 7288-7294.
- Jakob, U., Muse, W., Eser, M., and Bardwell, J.C. (1999). Chaperone activity with a redox switch. *Cell* 96, 341-352.
- Jobin Yvon, L. (2006). A guide to recording fluorescence quantum yields. <http://www.jobinyvon.com/us/divisions/fluorescence/applications/quantumyieldstrad.pdf>.
- Joseph, M., and Nagaraj, R. (1992). Unfolding of lysozyme by breaking its disulphide bridges results in exposure of hydrophobic sites. *Biochem Int* 26, 973-978.
- Kato, K., Inaguma, Y., Ito, H., Iida, K., Iwamoto, I., Kamei, K., Ochi, N., Ohta, H., and Kishikawa, M. (2001). Ser-59 is the major phosphorylation site in alphaB-crystallin accumulated in the brains of patients with Alexander's disease. *J.Neurochem.* 76, 730-736.
- Kauzmann, W. (1959). Some factors in the interpretation of protein denaturation. *Adv Protein Chem* 14, 1-63.
- Kennaway, C.K., Benesch, J.L., Gohlke, U., Wang, L., Robinson, C.V., Orlova, E.V., Saibil, H.R., and Keep, N.H. (2005). Dodecameric structure of the small heat shock protein Acr1 from *Mycobacterium tuberculosis*. *Journal of Biological Chemistry* 280, 33419-33425.
- Kiefhaber, T., Rudolph, R., Kohler, H.H., and Buchner, J. (1991). Protein aggregation in vitro and in vivo: a quantitative model of the kinetic competition between folding and aggregation. *Nature Biotechnology* 9, 825-829.

Kim, K.K., Kim, R., and Kim, S.H. (1998). Crystal structure of a small heat-shock protein. *Nature* 394, 595-599.

Kirschner, M., Winkelhaus, S., Thierfelder, J.M., and Nover, L. (2000). Transient expression and heat-stress-induced co-aggregation of endogenous and heterologous small heat-stress proteins in tobacco protoplasts 1. *Plant J.* 24, 397-411.

Klaus Richter, B.M.J.B. (2008). Hsp90: From Dispensable Heat Shock Protein to Global Player. In *Protein Folding Handbook*, P.D.T.K. Prof. Dr. Johannes Buchner, ed., pp. 768-829.

Koteiche, H.A., and McHaourab, H.S. (2006). Mechanism of a hereditary cataract phenotype. Mutations in alphaA-crystallin activate substrate binding. *J Biol Chem* 281, 14273-14279.

Laemmli, U.K. (1970). *Nature* 227, 680-686.

Lakowicz, J. (1999). *Principles of fluorescence spectroscopy*. Kluwer Academic / Plenum Publisher *Second Edition*.

Lambert, H., Charette, S.J., Bernier, A.F., Guimond, A., and Landry, J. (1999). HSP27 multimerization mediated by phosphorylation-sensitive intermolecular interactions at the amino terminus. *J.Biol Chem.* 274, 9378-9385.

Landry, S., Zeilstra-Ryalls, J., Fayet, O., Georgopoulos, C., and Gierasch, L. (1993). Characterization of a functionally important mobile domain of GroES. *Nature* 364, 255-258.

Langer, T., Lu, C., Echols, H., Flanagan, J., Hayer, M.K., and Hartl, F.U. (1992). Successive action of DnaK, DnaJ and GroEL along the pathway of chaperone-mediated protein folding. *Nature* 356, 683-689.

Lebowitz, J., Lewis, M.S., and Schuck, P. (2002). Modern analytical ultracentrifugation in protein science: a tutorial review. *Protein Sci* 11, 2067-2079.

- Lee, G.J., Roseman, A.M., Saibil, H.R., and Vierling, E. (1997). A small heat shock protein stably binds heat-denatured model substrates and can maintain a substrate in a folding-competent state. *EMBO J.* *16*, 659-671.
- Lee, G.J., and Vierling, E. (2000). A small heat shock protein cooperates with heat shock protein 70 systems to reactivate a heat-denatured protein. *Plant Physiol* *122*, 189-198.
- Lee, S., Owen, H.A., Prochaska, D.J., and Barnum, S.R. (2000). HSP16.6 is involved in the development of thermotolerance and thylakoid stability in the unicellular cyanobacterium, *Synechocystis* sp. PCC 6803. *Curr.Microbiol.* *40*, 283-287.
- Lentze, N., Aquilina, J.A., Lindbauer, M., Robinson, C.V., and Narberhaus, F. (2004). Temperature and concentration-controlled dynamics of rhizobial small heat shock proteins. *Eur.J.Biochem.* *271*, 2494-2503.
- Leroux, M.R., Melki, R., Gordon, B., Batelier, G., and Candido, E.P. (1997). Structure-function studies on small heat shock protein oligomeric assembly and interaction with unfolded polypeptides. *Journal of Biological Chemistry* *272*, 24646-24656.
- Liberek, K., Marszalek, J., Ang, D., Georgopoulos, C., and Zylicz, M. (1991a). *Escherichia coli* DnaJ and GrpE heat shock proteins jointly stimulate ATPase activity of DnaK. *Proc Natl Acad Sci U S A* *88*, 2874-2878.
- Liberek, K., Skowyra, D., Zylicz, M., Johnson, C., and Georgopoulos, C. (1991b). The *Escherichia coli* DnaK chaperone, the 70-kDa heat shock protein eukaryotic equivalent, changes conformation upon ATP hydrolysis, thus triggering its dissociation from a bound target protein. *J Biol Chem* *266*, 14491-14496.
- Lin, Z., Madan, D., and Rye, H.S. (2008). GroEL stimulates protein folding through forced unfolding. *Nat Struct Mol Biol* *15*, 303-311.

- Lindner, R.A., Carver, J.A., Ehrnsperger, M., Buchner, J., Esposito, G., Behlke, J., Lutsch, G., Kotlyarov, A., and Gaestel, M. (2000). Mouse Hsp25, a small shock protein. The role of its C-terminal extension in oligomerization and chaperone action. *Eur.J.Biochem.* 267, 1923-1932.
- Lindner, R.A., Kapur, A., Mariani, M., Titmuss, S.J., and Carver, J.A. (1998). Structural alterations of alpha-crystallin during its chaperone action 1. *Eur.J.Biochem.* 258, 170-183.
- Lindquist, S. (1981). Regulation of protein synthesis during heat shock. *Nature* 293, 311-314.
- Lindquist, S. (1986). The heat-shock response. *Annu.Rev Biochem.* 55, 1151-1191.
- Lindquist, S., and Craig, E.A. (1988). The heat-shock proteins. *Annu.Rev Genet.* 22, 631-677.
- Lum, R., Tkach, J.M., Vierling, E., and Glover, J.R. (2004). Evidence for an unfolding/threading mechanism for protein disaggregation by *Saccharomyces cerevisiae* Hsp104. *Journal of Biological Chemistry* 279, 29139-29146.
- MacRae, T.H. (2000). Structure and function of small heat shock/alpha-crystallin proteins: established concepts and emerging ideas. *Cell Mol Life Sci.* 57, 899-913.
- Massey, T.H., Mercogliano, C.P., Yates, J., Sherratt, D.J., and Lowe, J. (2006). Double-stranded DNA translocation: structure and mechanism of hexameric FtsK. *Mol Cell* 23, 457-469.
- Mayer, M., Rüdiger, S., and Bukau, B. (2000). Molecular basis for interactions of the DnaK chaperone with substrates. *Biol Chem* 381, 877-885.
- McCarty, J., Buchberger, A., Reinstein, J., and Bukau, B. (1995). The role of ATP in the functional cycle of the DnaK chaperone system. *J Mol Biol* 249, 126-137.

McQuillen, K., Roberts, R.B., and Britten, R.J. (1959). SYNTHESIS OF NASCENT PROTEIN BY RIBOSOMES IN ESCHERICHIA COLI. *Proc.Natl.Acad.Sci.U.S.A* 45, 1437-1447.

Mogk, A., and Bukau, B. (2004). Molecular chaperones: structure of a protein disaggregase. *Curr Biol* 14, R78-80.

Mogk, A., Deuerling, E., Vorderwulbecke, S., Vierling, E., and Bukau, B. (2003a). Small heat shock proteins, ClpB and the DnaK system form a functional triade in reversing protein aggregation. *Mol.Microbiol.* 50, 585-595.

Mogk, A., Haslberger, T., Tessarz, P., and Bukau, B. (2008). Common and specific mechanisms of AAA+ proteins involved in protein quality control. *Biochem Soc Trans* 36, 120-125.

Mogk, A., Schlieker, C., Friedrich, K.L., Schonfeld, H.J., Vierling, E., and Bukau, B. (2003b). Refolding of substrates bound to small Hsps relies on a disaggregation reaction mediated most efficiently by ClpB/DnaK. *J Biol Chem* 278, 31033-31042.

Morimoto, R.I. (1998). Regulation of the heat shock transcriptional response: cross talk between a family of heat shock factors, molecular chaperones, and negative regulators. *Genes Dev* 12, 3788-3796.

Motohashi, K., Watanabe, Y., Yohda, M., and Yoshida, M. (1999). Heat-inactivated proteins are rescued by the DnaK.J-GrpE set and ClpB chaperones. *Proc Natl Acad Sci U S A* 96, 7184-7189.

Narberhaus, F. (2002). Alpha-crystallin-type heat shock proteins: socializing minichaperones in the context of a multichaperone network. *Microbiol.Mol.Biol.Rev.* 66, 64-93.

Obermann, W.M., Sonderrmann, H., Russo, A.A., Pavletich, N.P., and Hartl, F.U. (1998). In vivo function of Hsp90 is dependent on ATP binding and ATP hydrolysis. *J Cell Biol* 143, 901-910.

Packschies, L., Theyssen, H., Buchberger, A., Bukau, B., Goody, R.S., and Reinstein, J. (1997). GrpE accelerates nucleotide exchange of the molecular chaperone DnaK with an associative displacement mechanism. *Biochemistry* 36, 3417-3422.

Panaretou, B., Prodromou, C., Roe, S.M., O'Brien, R., Ladbury, J.E., Piper, P.W., and Pearl, L.H. (1998). ATP binding and hydrolysis are essential to the function of the Hsp90 molecular chaperone in vivo. *EMBO J* 17, 4829-4836.

Parsell, D.A., Kowal, A.S., Singer, M.A., and Lindquist, S. (1994). Protein disaggregation mediated by heat-shock protein Hsp104. *Nature* 372, 475-478.

Pasta, S.Y., Raman, B., Ramakrishna, T., and Rao, C. (2004). The IXI/V motif in the C-terminal extension of alpha-crystallins: alternative interactions and oligomeric assemblies. *Mol.Vis.* 10, 655-662.

Petko, L., and Lindquist, S. (1986). Hsp26 is not required for growth at high temperatures, nor for thermotolerance, spore development, or germination. *Cell* 45, 885-894.

Phillips, J.J., Yao, Z.P., Zhang, W., McLaughlin, S., Laue, E.D., Robinson, C.V., and Jackson, S.E. (2007). Conformational dynamics of the molecular chaperone Hsp90 in complexes with a co-chaperone and anticancer drugs. *J Mol Biol* 372, 1189-1203.

Pirkel, F., and Buchner, J. (2001). Functional analysis of the Hsp90-associated human peptidyl prolyl cis/trans isomerases FKBP51, FKBP52 and Cyp40. *J Mol Biol* 308, 795-806.

Plater, M.L., Goode, D., and Crabbe, M.J. (1996). Effects of site-directed mutations on the chaperone-like activity of alphaB-crystallin. *J Biol Chem* 271, 28558-28566.

- Popp, S., Packschies, L., Radzwill, N., Vogel, K.P., Steinhoff, H.J., and Reinstein, J. (2005). Structural dynamics of the DnaK-peptide complex. *J Mol Biol* 347, 1039-1052.
- Pratt, W.B., Galigniana, M.D., Morishima, Y., and Murphy, P.J. (2004). Role of molecular chaperones in steroid receptor action. *Essays Biochem* 40, 41-58.
- Pratt, W.B., Gehring, U., and Toft, D.O. (1996). Molecular chaperoning of steroid hormone receptors. *EXS* 77, 79-95.
- Pratt, W.B., and Toft, D.O. (1997). Steroid receptor interactions with heat shock protein and immunophilin chaperones. *Endocr Rev* 18, 306-360.
- Privalov, P.L., Tiktopulo, E.I., Venyaminov, S.Y., Griko, Y., Makhatadze, G.I., and Khechinashvili, N.N. (1989). Heat capacity and conformation of proteins in the denatured state. *J.Mol Biol* 205, 737-750.
- Prodromou, C., Panaretou, B., Chohan, S., Siligardi, G., O'Brien, R., Ladbury, J.E., Roe, S.M., Piper, P.W., and Pearl, L.H. (2000). The ATPase cycle of Hsp90 drives a molecular 'clamp' via transient dimerization of the N-terminal domains. *EMBO J* 19, 4383-4392.
- Raman, B., Ramakrishna, T., and Rao, C.M. (1995). Temperature dependent chaperone-like activity of alpha-crystallin. *FEBS Lett.* 365, 133-136.
- Raman, B., and Rao, C.M. (1997). Chaperone-like activity and temperature-induced structural changes of alpha-crystallin. *J.Biol Chem.* 272, 23559-23564.
- Richter, K., Moser, S., Hagn, F., Friedrich, R., Hainzl, O., Heller, M., Schlee, S., Kessler, H., Reinstein, J., and Buchner, J. (2006). Intrinsic inhibition of the Hsp90 ATPase activity. *J Biol Chem* 281, 11301-11311.
- Richter, K., Soroka, J., Skalniak, L., Leskovar, A., Hessling, M., Reinstein, J., and Buchner, J. (2008). Conserved conformational changes in the ATPase cycle of human Hsp90. *J Biol Chem.*

- Riggs, D.L., Cox, M.B., Cheung-Flynn, J., Prapapanich, V., Carrigan, P.E., and Smith, D.F. (2004). Functional specificity of co-chaperone interactions with Hsp90 client proteins. *Crit Rev Biochem Mol Biol* 39, 279-295.
- Rogalla, T., Ehrnsperger, M., Preville, X., Kotlyarov, A., Lutsch, G., Ducasse, C., Paul, C., Wieske, M., Arrigo, A.P., Buchner, J., and Gaestel, M. (1999). Regulation of Hsp27 oligomerization, chaperone function, and protective activity against oxidative stress/tumor necrosis factor alpha by phosphorylation. *Journal of Biological Chemistry* 274, 18947-18956.
- Ruddock, L.W., and Klappa, P. (1999). Oxidative stress: Protein folding with a novel redox switch. *Curr.Biol* 9, R400-R402.
- Rüdiger, S., Buchberger, A., and Bukau, B. (1997a). Interaction of Hsp70 chaperones with substrates. *Nat Struct Biol* 4, 342-349.
- Rüdiger, S., Germeroth, L., Schneider-Mergener, J., and Bukau, B. (1997b). Substrate specificity of the DnaK chaperone determined by screening cellulose-bound peptide libraries. *EMBO J* 16, 1501-1507.
- Rye, H.S., Roseman, A.M., Chen, S., Furtak, K., Fenton, W.A., Saibil, H.R., and Horwich, A.L. (1999). GroEL-GroES cycling: ATP and nonnative polypeptide direct alternation of folding-active rings. *Cell* 97, 325-338.
- Saibil, H. (2000). Molecular chaperones: containers and surfaces for folding, stabilising or unfolding proteins. *Curr.Opin.Struct.Biol.* 10, 251-258.
- Saibil, H., Dong, Z., Wood, S., and auf der Mauer, A. (1991). Binding of chaperonins. *Nature* 353, 25-26.
- Saibil, H.R., Horwich, A.L., and Fenton, W.A. (2001). Allostery and protein substrate conformational change during GroEL/GroES-mediated protein folding. *Adv.Protein Chem.* 59, 45-72.

- Sambrook, J.F.E.F., and maniatitis, T. (1989). *Molecular Cloning* (Cold Spring Harbor Press, New York).
- Sanchez, Y., and Lindquist, S.L. (1990). HSP104 required for induced thermotolerance. *Science* 248, 1112-1115.
- Sanchez, Y., Parsell, D.A., Taulien, J., Vogel, J.L., Craig, E.A., and Lindquist, S. (1993). Genetic evidence for a functional relationship between Hsp104 and Hsp70. *J Bacteriol* 175, 6484-6491.
- Schaupp, A., Marcinowski, M., Grimminger, V., Bosl, B., and Walter, S. (2007). Processing of proteins by the molecular chaperone Hsp104. *J Mol Biol* 370, 674-686.
- Schellenberger, A. (1989). *Enzymkatalyse. Einführung in die Chemie, Biochemie und Technologie der Enzyme*. Gustav Fischer Verlag.
- Schmid, D., Baici, A., Gehring, H., and Christen, P. (1994). Kinetics of molecular chaperone action. *Science* 263, 971-973.
- Schmid, F.X., and Creighton, T.E. (1989). In *Protein Structure: A Practical Approach* (Oxford, New York, Tokyo: IRL Press), pp. 251-285.
- Schröder, H., Langer, T., Hartl, F.U., and Bukau, B. (1993). DnaK, DnaJ and GrpE form a cellular chaperone machinery capable of repairing heat-induced protein damage. *EMBO J* 12, 4137-4144.
- Servant, P., Grandvalet, C., and Mazodier, P. (2000). The RheA repressor is the thermosensor of the HSP18 heat shock response in *Streptomyces albus*. *Proc Natl Acad Sci U S A* 97, 3538-3543.
- Servant, P., Rapoport, G., and Mazodier, P. (1999). RheA, the repressor of hsp18 in *Streptomyces albus* G. *Microbiology* 145 (Pt 9), 2385-2391.

Sharma, K.K., Kaur, H., and Kester, K. (1997). Functional elements in molecular chaperone alpha-crystallin: identification of binding sites in alpha B-crystallin. *Biochem.Biophys.Res.Commun.* 239, 217-222.

Sharma, K.K., Kumar, R.S., Kumar, G.S., and Quinn, P.T. (2000). Synthesis and characterization of a peptide identified as a functional element in alphaA-crystallin. *Journal of Biological Chemistry* 275, 3767-3771.

Shiau, A.K., Harris, S.F., Southworth, D.R., and Agard, D.A. (2006). Structural Analysis of *E. coli* hsp90 reveals dramatic nucleotide-dependent conformational rearrangements. *Cell* 127, 329-340.

Sigler, P., and Horwich, A. (1995). Unliganded GroEL at 2.8 Å: structure and functional implications. *Philos Trans R Soc Lond B Biol Sci* 348, 113-119.

Smulders, R.H.P.H., Carver, J.A., Lindner, R.A., Van Boekel, M.A., Bloemendal, H., and De Jong, W.W. (1996). Immobilization of the C-terminal extension of bovine alphaA-crystallin reduces chaperone-like activity. *Journal of Biological Chemistry* 271, 29060-29066.

Sobott, F., Benesch, J.L., Vierling, E., and Robinson, C.V. (2002). Subunit exchange of multimeric protein complexes. Real-time monitoring of subunit exchange between small heat shock proteins by using electrospray mass spectrometry. *Journal of Biological Chemistry* 277, 38921-38929.

Stover, C.K., Pham, X.Q., Erwin, A.L., Mizoguchi, S.D., Warrener, P., Hickey, M.J., Brinkman, F.S., Hufnagle, W.O., Kowalik, D.J., Lagrou, M., *et al.* (2000). Complete genome sequence of *Pseudomonas aeruginosa* PA01, an opportunistic pathogen. *Nature* 406, 959-964.

Stromer, T., Ehrnsperger, M., Gaestel, M., and Buchner, J. (2003). Analysis of the interaction of small heat shock proteins with unfolding proteins. *J Biol Chem.* 278, 18015-18021.

- Stromer, T., Fischer, E., Richter, K., Haslbeck, M., and Buchner, J. (2004). Analysis of the regulation of the molecular chaperone Hsp26 by temperature-induced dissociation: the N-terminal domain is important for oligomer assembly and the binding of unfolding proteins. *Journal of Biological Chemistry* 279, 11222-11228.
- Studer, S., Obrist, M., Lentze, N., and Narberhaus, F. (2002). A critical motif for oligomerization and chaperone activity of bacterial alpha-heat shock proteins. *Eur.J.Biochem.* 269, 3578-3586.
- Suh, W.C., Burkholder, W.F., Lu, C.Z., Zhao, X., Gottesman, M.E., and Gross, C.A. (1998). Interaction of the Hsp70 molecular chaperone, DnaK, with its cochaperone DnaJ. *Proc Natl Acad Sci U S A* 95, 15223-15228.
- Sun, T.X., Das, B.K., and Liang, J.J. (1997). Conformational and functional differences between recombinant human lens alphaA- and alphaB-crystallin 2. *Journal of Biological Chemistry* 272, 6220-6225.
- Susek, R.E., and Lindquist, S.L. (1989). hsp26 of *Saccharomyces cerevisiae* is related to the superfamily of small heat shock proteins but is without a demonstrable function. *Mol.Cell Biol.* 9, 5265-5271.
- Thies, M.J., Mayer, J., Augustine, J.G., Frederick, C.A., Lilie, H., and Buchner, J. (1999). Folding and association of the antibody domain CH3: prolyl isomerization precedes dimerization. *J.Mol.Biol.* 293, 67-79.
- Thirumalai, D., and Lorimer, G.H. (2001). Chaperonin-mediated protein folding. *Annu Rev Biophys Biomol Struct* 30, 245-269.
- Van Montfort, R., Slingsby, C., and Vierling, E. (2002). Structure and function of the small heat shock protein/alpha-crystallin family of molecular chaperones. *Adv.Protein Chem.* 59, 105-156.

van Montfort, R.L., Basha, E., Friedrich, K.L., Slingsby, C., and Vierling, E. (2001). Crystal structure and assembly of a eukaryotic small heat shock protein. *Nat.Struct.Biol.* 8, 1025-1030.

Vaughan, C.K., Gohlke, U., Sobott, F., Good, V.M., Ali, M.M., Prodromou, C., Robinson, C.V., Saibil, H.R., and Pearl, L.H. (2006). Structure of an Hsp90-Cdc37-Cdk4 complex. *Mol Cell* 23, 697-707.

Velazquez, J.M., DiDomenico, B.J., and Lindquist, S. (1980). Intracellular localization of heat shock proteins in *Drosophila*. *Cell* 20, 679-689.

Venturoli, D., and Rippe, B. (2005). Ficoll and dextran vs. globular proteins as probes for testing glomerular permselectivity: effects of molecular size, shape, charge, and deformability. *Am J Physiol Renal Physiol* 288, F605-613.

Vogel, M., Bukau, B., and Mayer, M.P. (2006). Allosteric regulation of Hsp70 chaperones by a proline switch. *Mol.Cell* 21, 359-367.

Walter, S., and Buchner, J. (2002). Molecular chaperones-cellular machines for protein folding. *Angew.Chem.Int.Ed Engl.* 41, 1098-1113.

Walter, S., Lorimer, G.H., and Schmid, F.X. (1996). A thermodynamic coupling mechanism for GroEL-mediated unfolding. *Proc.Natl.Acad.Sci.U.S.A* 93, 9425-9430.

Wegele, H., Muller, L., and Buchner, J. (2004). Hsp70 and Hsp90--a relay team for protein folding. *Rev.Physiol Biochem.Pharmacol.* 151, 1-44.

Weibezahn, J., Tessarz, P., Schlieker, C., Zahn, R., Maglica, Z., Lee, S., Zentgraf, H., Weber-Ban, E.U., Dougan, D.A., Tsai, F.T., *et al.* (2004). Thermotolerance requires refolding of aggregated proteins by substrate translocation through the central pore of ClpB. *Cell* 119, 653-665.

- Weickl, T., Muschler, P., Richter, K., Veit, T., Reinstein, J., and Buchner, J. (2000). C-terminal regions of Hsp90 are important for trapping the nucleotide during the ATPase cycle. *J Mol Biol* 303, 583-592.
- Weissman, J.S., Kashi, Y., Fenton, W.A., and Horwich, A.L. (1994). GroEL-mediated protein folding proceeds by multiple rounds of binding and release of nonnative forms. *Cell* 78, 693-702.
- Wendler, P., Shorter, J., Plisson, C., Cashikar, A.G., Lindquist, S., and Saibil, H.R. (2007). Atypical AAA+ subunit packing creates an expanded cavity for disaggregation by the protein-remodeling factor Hsp104. *Cell* 131, 1366-1377.
- White, H.E., Orlova, E.V., Chen, S., Wang, L., Ignatiou, A., Gowen, B., Stromer, T., Franzmann, T.M., Haslbeck, M., Buchner, J., and Saibil, H.R. (2006). Multiple distinct assemblies reveal conformational flexibility in the small heat shock protein hsp26. *Structure*. 14, 1197-1204.
- Whitmore, L., and Wallace, B.A. (2004). DICHROWEB, an online server for protein secondary structure analyses from circular dichroism spectroscopic data. *Nucleic Acids Res.* 32, W668-W673.
- Xu, Z., Horwich, A.L., and Sigler, P.B. (1997). The crystal structure of the asymmetric GroEL-GroES-(ADP) 7 chaperonin complex. *Nature* 388, 741-750.
- Yura, T., Kawasaki, Y., Kusukawa, N., Nagai, H., Wada, C., and Yano, R. (1990). Roles and regulation of the heat shock sigma factor sigma 32 in *Escherichia coli*. *Antonie Van Leeuwenhoek* 58, 187-190.
- Zeilstra-Ryalls, J., Fayet, O., and Georgopoulos, C. (1991). The universally conserved GroE (Hsp60) chaperonins. *Annu.Rev.Microbiol.* 45, 301-325.
- Zhou, H.X. (2004). Protein folding and binding in confined spaces and in crowded solutions. *J Mol Recognit* 17, 368-375.

References

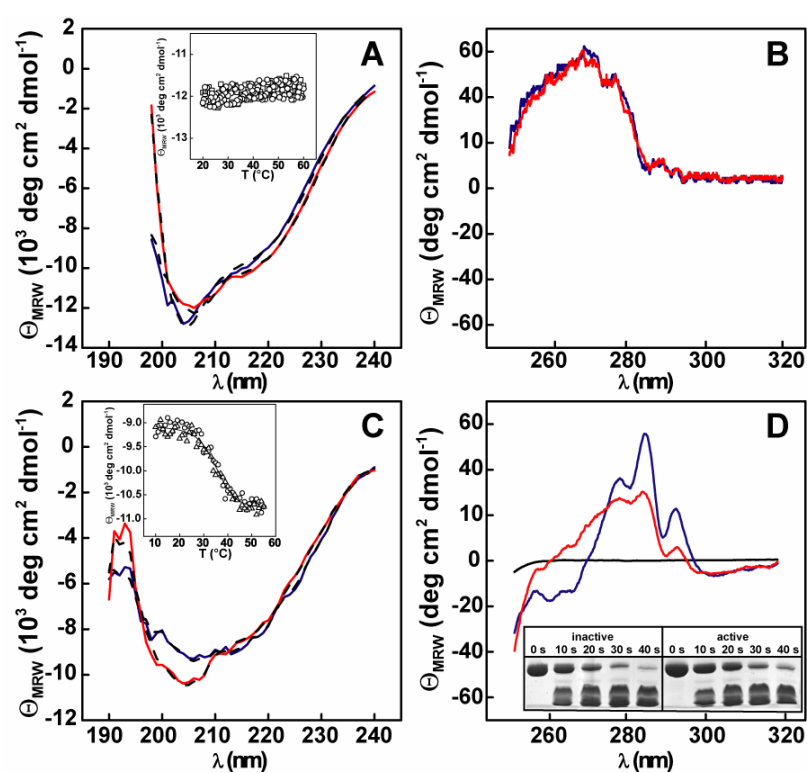
Zhu, X., Zhao, X., Burkholder, W.F., Gragerov, A., Ogata, C.M., Gottesman, M.E., and Hendrickson, W.A. (1996). Structural analysis of substrate binding by the molecular chaperone DnaK. *Science* 272, 1606-1614.

7 Acknowledgments

This thesis was prepared at the Technische Universität München, Department Chemie, Lehrstuhl für Biotechnologie. I would like to thank Prof. Johannes Buchner for offering me the scientific tasks and encouraged my enthusiasm. I want to emphasize special thanks to Stephan G. Walter. I am grateful to his advises. Jirka Peschek I thank for the great collaboration and Sebastian Leptihn, Fabio Falsone, Stephan Frey, Birgit Meinschmidt, Daniel Weinfurtner and all the others are acknowledged for the good work environment. I am thankful to Frau Susanne Hilber, our secretary, who took care of the important things I try to avoid: bureaucracy! I thank my mother Martha, my father Heinz W. and my brother Arnim for their support throughout my studies. And last but not least, I thank Petra for her support and our first son, Feodor Fidelis, who was born at the end of my thesis.

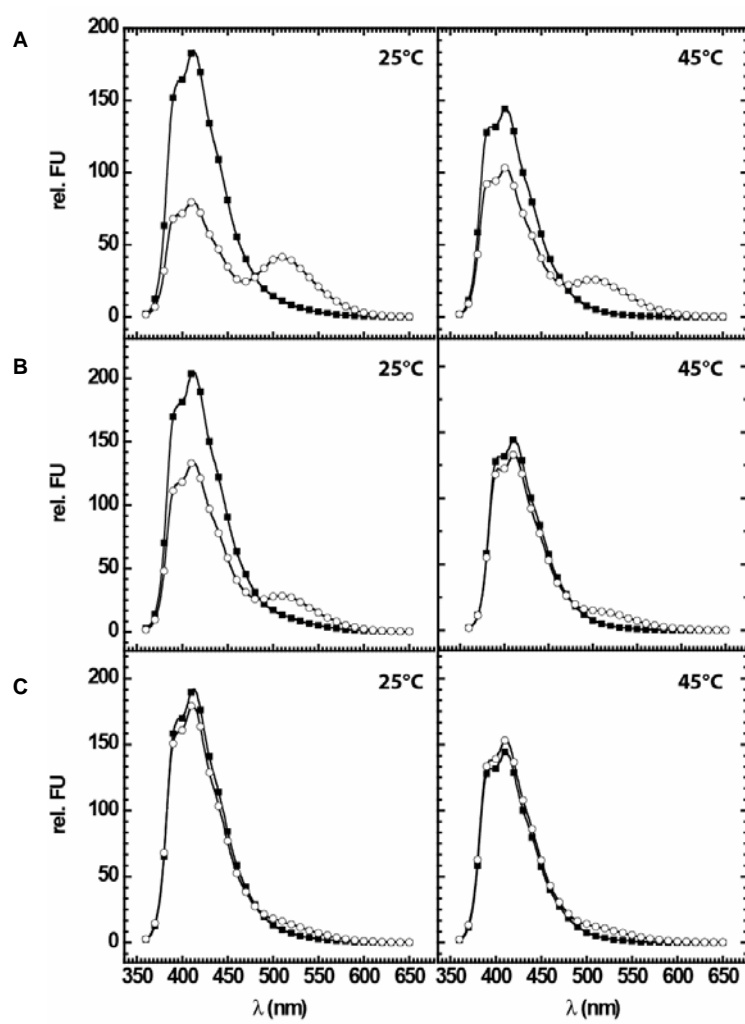
8 Appendix

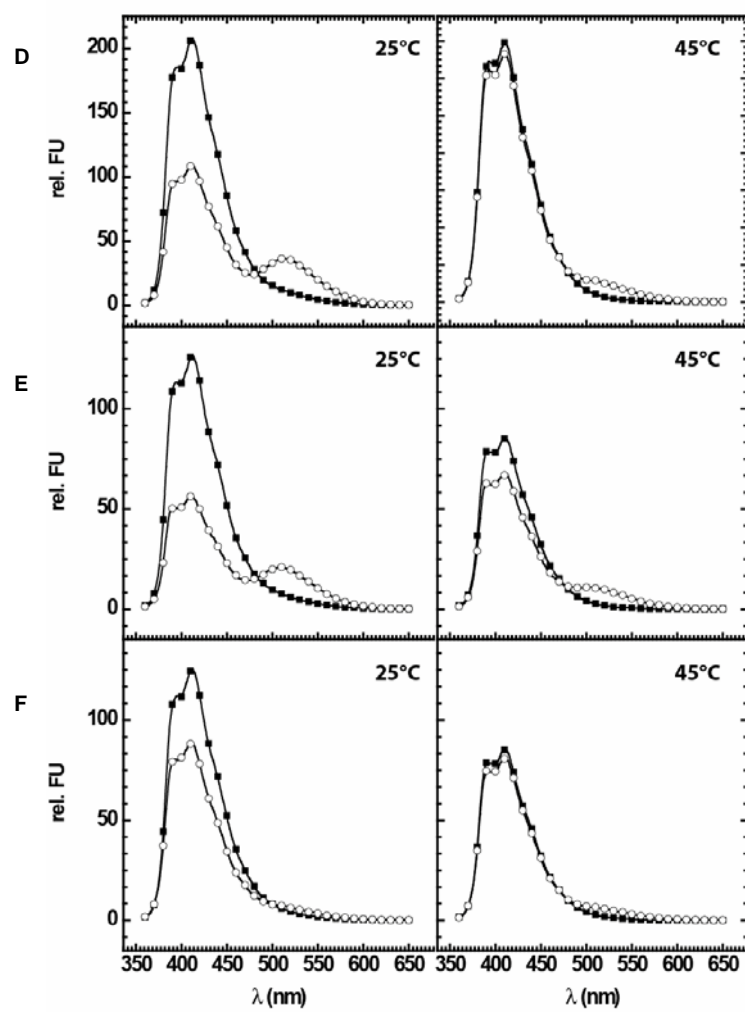
8.1 Supplemental data: Structure analysis of the Hsp26 thermosensor domain

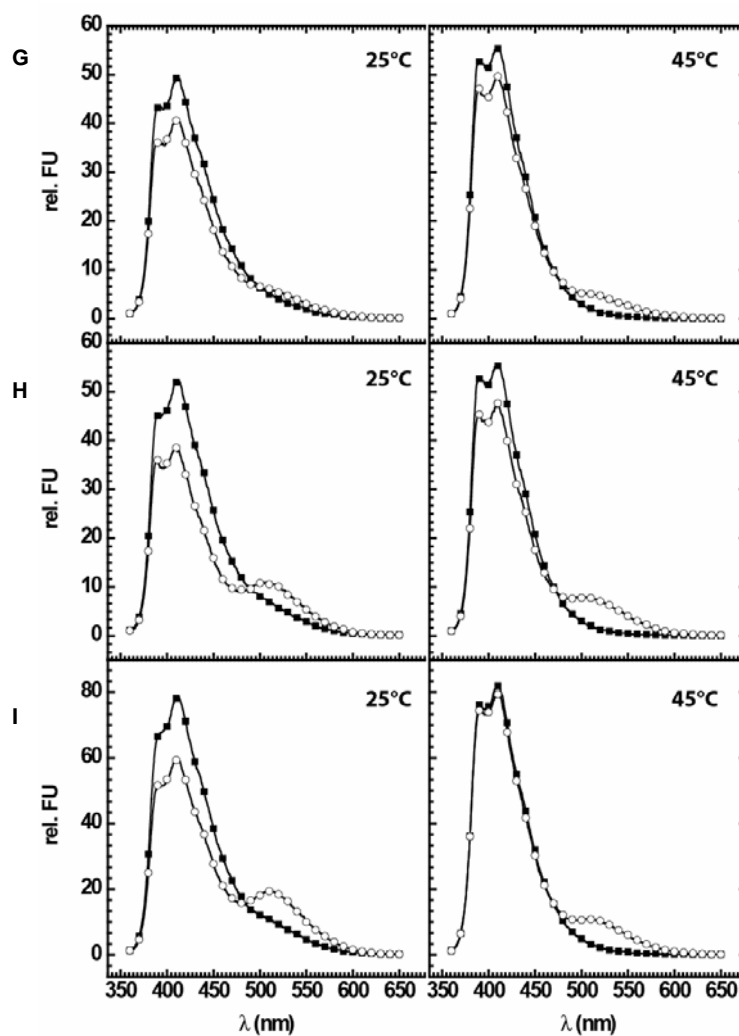


Suppl. Figure 1 Structure analysis of the Hsp26 α -crystallin domain (Hsp26dN) and Hsp26 30-195 by CD spectroscopy. A: Far UV CD spectra of the Hsp26 α -crystallin domain at 25°C (blue) and 45°C (red). Fit of the CD spectra is shown in dashed lines. Inset: Thermal unfolding (\circ) and refolding (\square) monitored by CD at 205 nm B: Near UV CD spectra of the Hsp26 α -crystallin domain at 25°C (blue) and 45°C (red). C: Far UV CD spectra of Hsp26₃₀₋₁₉₅ at 25°C (blue) and 45°C (red). Fit of the CD spectra is shown in dashed lines. Inset: Thermal unfolding (\circ) and refolding (\triangle) monitored by CD at 205 nm. D: Far UV CD spectra of Hsp26₃₀₋₁₉₅ at 25°C (blue), 45°C (red) and 85°C (black). Inset: Proteolytic stability of inactive and thermally activated Hsp26₃₀₋₁₉₅ against Chymotrypsin.

8.2 Supplemental data for FRET distance analysis

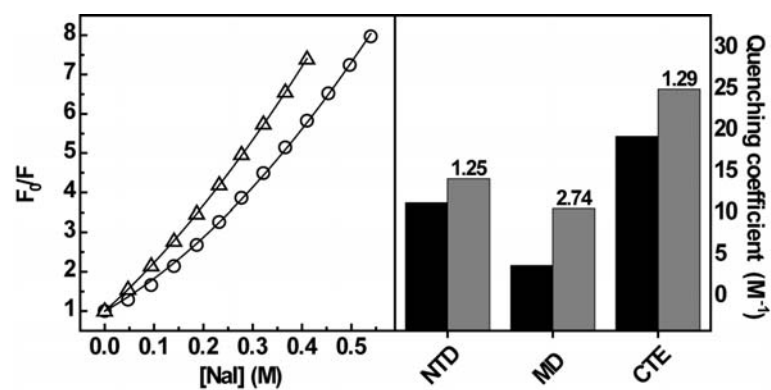






Suppl. Figure 2 Average distances between the donor and acceptor fluorophor attached to Hsp26 were determined by FRET. Fluorescence spectra of inactive (25°C) and temperature-activated (45°C) Hsp26 in the absence (■) and presence (○) of acceptor were recorded at 25°C. Hsp26^{S4C/W211Y} was used to label the N-terminal domain (NTD), Hsp26^{S82C} to label the middle domain (MD), and Hsp26^{S210C} to label the C-terminal extension (CTE) with the AIAS donor and LYI acceptor fluorophor. The distances were determined for the following combinations of donor-acceptor "spectroscopic hetero oligomers". A: NTD-NTD, B: NTD-MD, C: NTD-CTE, D: MD-MD, E: MD-NTD, F: MD-CTE, G: CTE-CTE, H: CTE-NTD, and I: CTE-MD.

8.3 Supplemental data for fluorescence quenching



Suppl. Figure 3 Fluorescence quenching of LYI-labelled Hsp26 A: F_0/F as a function of the molar NaI quencher concentration for MD-labelled Hsp26S82C in the inactive (○) and chaperone-active state (Δ). B: Solvent accessibility of NTD, MD and CTE determined by NaI-quenching of inactive (black bars) and active Hsp26 (grey bars).

9 Declaration

I, Titus Marcellus Franzmann, hereby declare that this thesis was prepared by me independently and using only the references and resources stated here. The work has so far not been submitted to any audit commission. Parts of this work have been published in scientific journals.

Hiermit erkläre ich, Titus Marcellus Franzmann, dass ich die vorliegende Arbeit selbständig verfasst und keine anderen als die angegebenen Quellen und Hilfsmittel verwendet habe. Die Arbeit wurde bisher keiner Prüfungskommission vorgelegt. Teile dieser Arbeit wurde in wissenschaftlichen Journalen veröffentlicht.

Titus M. Franzmann

München, 21. Januar 2004

10 Publications

- **Franzmann TM**, Menhorn P, Walter S, Buchner J. Activation of the chaperone Hsp26 is controlled by the rearrangement of its thermosensor domain. **Mol Cell. 2008**
- White HE, Orlova EV, Chen S, Wang L, Ignatiou A, Gowen B, Stromer T, **Franzmann TM**, Haslbeck M, Buchner J, Saibil HR. Multiple distinct assemblies reveal conformational flexibility in the small heat shock protein Hsp26. **Structure. 2006**
- **Franzmann TM**. Matrix-assisted refolding of oligomeric small heat-shock protein Hsp26. **Int J Biol Macromol. 2006**
- Haslbeck M, **Franzmann T**, Weinfurtner D, Buchner J. Some like it hot: the structure and function of small heat-shock proteins. **Nat Struct Mol Biol. 2005**
- **Franzmann TM**, Wühr M, Richter K, Walter S, Buchner J. The activation mechanism of Hsp26 does not require dissociation of the oligomer. **J Mol Biol. 2005**

The Activation Mechanism of Hsp26 does not Require Dissociation of the Oligomer

Titus M. Franzmann, Martin Wühr, Klaus Richter, Stefan Walter and Johannes Buchner*

Department Chemie, Technische Universität München, 85747 Garching, Germany

Small heat shock proteins (sHsps) are molecular chaperones that specifically bind non-native proteins and prevent them from irreversible aggregation. A key trait of sHsps is their existence as dynamic oligomers. Hsp26 from *Saccharomyces cerevisiae* assembles into a 24mer, which becomes activated under heat shock conditions and forms large, stable substrate complexes. This activation coincides with the destabilization of the oligomer and the appearance of dimers. This and results from other groups led to the generally accepted notion that dissociation might be a requirement for the chaperone mechanism of sHsps.

To understand the chaperone mechanism of sHsps it is crucial to analyze the relationship between chaperone activity and stability of the oligomer. We generated an Hsp26 variant, in which a serine residue of the N-terminal domain was replaced by cysteine. This allowed us to covalently crosslink neighboring subunits by disulfide bonds. We show that under reducing conditions the structure and function of this variant are indistinguishable from that of the wild-type protein. However, when the cysteine residues are oxidized, the dissociation into dimers at higher temperatures is no longer observed, yet the chaperone activity remains unaffected. Furthermore, we show that the exchange of subunits between Hsp26 oligomers is significantly slower than substrate aggregation and even inhibited in the presence of disulfide bonds. This demonstrates that the rearrangements necessary for shifting Hsp26 from a low to a high affinity state for binding non-native proteins occur without dissolving the oligomer.

© 2005 Elsevier Ltd. All rights reserved.

Keywords: small heat shock protein; molecular chaperone; alpha crystallin; aggregation; disulfide bond

*Corresponding author

Introduction

Small heat shock proteins (sHsps) belong to the functionally related class of molecular chaperones that specifically recognize non-native proteins.^{1–3}

Abbreviations used: sHsps, small heat shock proteins; AIAS, 4-acetamido-4'-((iodoacetyl)amino)stilbene-2,2'-disulfonic acid; CD, circular dichroism; CS, citrate synthase; DTNB, 5,5'-dithiobis(2-nitrobenzoic acid); DTT_(red), reduced form of dithiothreitol; DTT_(ox), oxidized form of dithiothreitol; FITC, fluorescein isothiocyanate; GdmCl, guanidinium hydrochloride; GSSG, oxidized glutathione; IAA, iodoacetamide; LYI, lucifer yellow iodoacetamide; SEC, size exclusion chromatography; TAMRA, tetramethylrhodamine; TEM, transmission electron microscopy.

E-mail address of the corresponding author: johannes.buchner@ch.tum.de

As part of the cellular multi-chaperone network, sHsps possess a substantial binding capacity for protein folding intermediates, which allows them to prevent their irreversible aggregation.^{4–8} sHsps are characterized by several structural and functional features. The most significant is the presence of the highly conserved α -crystallin domain in the C-terminal part of the proteins.^{9,10} In α A and α B-crystallin, the two major eye lens proteins in vertebrates, these domains are composed of about 80 residues with 60% sequence identity.^{11,12} Besides this, sHsps share monomeric masses between 12 kDa and 43 kDa. These monomers associate into oligomeric structures with mostly 12 or 24 subunits. Even larger complexes with up to 50 subunits were observed for α -crystallin.^{13,14} The large variability in the length of the N-terminal regions appears to be responsible for the significant variations of the sizes of the oligomers.¹² So far, two

X-ray structures of sHsps have been resolved. Hsp16.5 from *Methanocaldococcus jannaschii* assembles into a 24mer and forms a hollow sphere with octahedral symmetry.¹⁵ Hsp16.9 from wheat forms a 12mer arranged into two hexameric rings.¹⁶ Both structures revealed the α -crystallin domain as the dimeric building block. In addition to the α -crystallin domain, sHsps comprise a flexible, disordered N-terminal region and a C-terminal extension. From structural investigations carried out for various sHsps, including Hsp16.5, α -crystallin and Hsp16.2 from *Caenorhabditis elegans*, it was proposed that the N-terminal regions are sequestered inside the oligomers.^{15,17,18} Recently it was shown that the N-terminal regions are required for substrate interactions¹⁹ and that they play a role in stabilizing the oligomeric state.^{20,21} The C-terminal extensions appear to be moderately conserved throughout the sHsps family. In Hsp16.5, these were found to mediate the self-association into the oligomeric complex *via* inter-subunit interactions.¹⁵ This was confirmed for various sHsps in which the C-terminal extensions were either removed or mutated.^{21–24} Mostly these variants fail to associate into their native quaternary structure. The N-terminal region and the C-terminal extension seem to have partially overlapping functions with respect to the association of the oligomer. Furthermore, both regions are required for efficient chaperone activity^{20,24} and recent investigations suggest that oligomerization of sHsps is a prerequisite for their chaperone mechanism.^{17,21,25–28} sHsps are dynamic structures, which permanently exchange subunits between oligomers.^{29–33} Although this dynamic behavior seems to be a common feature, no functional importance could be assigned to it so far and it was speculated that the exchange of subunits is linked to the chaperone mechanism.

Hsp26 is one of the two cytosolic sHsps from *Saccharomyces cerevisiae*.³⁴ Under physiological conditions, it exists as a hollow sphere of 24 subunits assembled from 12 dimers.^{35–37} We have shown previously that Hsp26 efficiently suppresses heat-induced aggregation of substrates *in vivo* and *in vitro* and associates into defined, stable complexes with model substrates including citrate synthase (CS) and insulin, indicating promiscuous binding properties.^{6,7,38} The first 30 amino acid residues of the N-terminal domain of Hsp26 are required for substrate interaction and stabilize the oligomeric state.²⁰ Residues 30–95 play a role in the association of the native oligomer.¹⁹ An important functional characteristic is that Hsp26 requires elevated temperatures for activation, as it fails to efficiently suppress the reduction-induced aggregation of insulin at room temperature.³⁸ Coinciding with the temperature-dependent activation, the Hsp26 oligomer was shown to become destabilized and dissociate into dimers.

To gain further insight into the chaperone mechanism of sHsps, we generated a point mutant of Hsp26, in which the residue serine 4 of the

N-terminal domain (Hsp26_{S4C}) was replaced by cysteine. The introduction of this reactive residue allowed covalent cross-linking of neighboring subunits by oxidation. Analysis of the structure and function under reducing conditions showed that Hsp26_{S4C} behaved indistinguishably from the Hsp26 wild-type protein. Interestingly, when the cysteine residues were oxidized, the Hsp26 oligomer was stabilized and subunit exchange and dissociation into dimers was completely inhibited, yet the chaperone activity remained unaffected. These results show that the rearrangements necessary for activation of Hsp26 can occur without dissolving the oligomer and indicate that the Hsp26 oligomer can interact with substrate proteins.

Results

Structural analysis of reduced and oxidized Hsp26_{S4C}

sHsps consist of a predominantly β -structured α -crystallin domain,^{9,10} an unstructured N-terminal region and a moderately conserved C-terminal extension. Since truncations in the N-terminal regions affect the stability of the oligomeric structure, it was tempting to speculate that the N-terminal regions are involved in inter-subunit interactions. The introduction of artificial disulfide bridges in proteins had been used successfully to analyze the importance of conformational rearrangements in chaperone mechanisms.³⁹ Thus, we generated a variant of Hsp26 in which the residue S4 of the N-terminal region was replaced by cysteine (Hsp26_{S4C}). It should be noted that the Hsp26 wild-type protein does not contain cysteine residues.

First, we analyzed the cysteine variant with respect to its ability of disulfide bond formation. Quantification of the reduced samples with the DTNB reaction revealed one free cysteine per subunit, indicating that all cysteine residues were accessible and reduced (data not shown). In agreement with this, we determined a specific labelling efficiency of one fluorescence probe per subunit by UV spectroscopy (data not shown). No free thiol groups were present after IAA treatment, showing that all cysteine residues were blocked covalently (data not shown). Testing the oxidized form revealed 0.3 free cysteine residue in Hsp26_{S4C} (data not shown). In agreement, we found that $\sim 2/3$ of the subunits were cross-linked by disulfide bond formation with SDS-PAGE under non-reducing conditions (Figure 1). The cross-linking efficiency was not increased using other oxidative agents such as oxidized glutathione or air.

To test whether the mutation affected the structural integrity of the protein, we analyzed the secondary structure by circular dichroism (CD) spectroscopy. Hsp26 exhibits a minimum at ~ 214 nm with intensities of $-8500 \text{ deg} \cdot \text{cm}^2 \cdot \text{dmol}^{-1}$ (Figure 2(a)). Deconvolution of the data

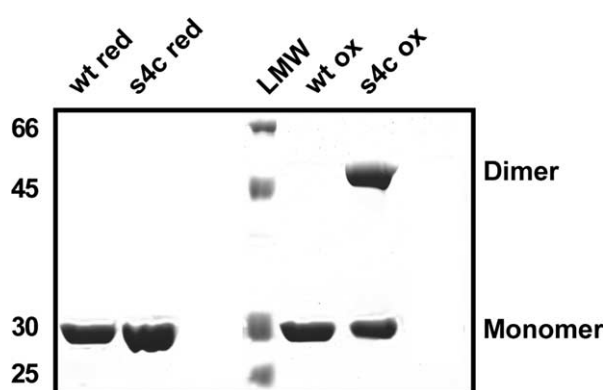


Figure 1. Non-reducing SDS-PAGE of Hsp26 and Hsp26_{S4C}. Samples were prepared as described in Materials and Methods with reducing or oxidizing DTT, respectively.

revealed 17% α -helical and 45% β -sheet content.¹⁹ CD spectra of reduced and oxidized Hsp26_{S4C} were indistinguishable from that of the wild-type protein (Figure 2(b)), indicating that the cysteine variant is natively folded under both reducing and oxidizing conditions.

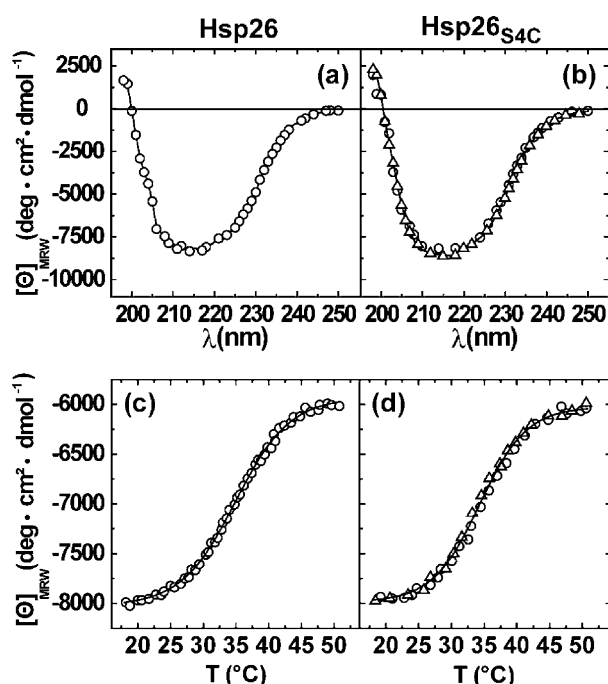


Figure 2. Far UV CD spectra and thermal transitions of Hsp26 and Hsp26_{S4C}. Spectra were recorded at 20 °C in 10 mM potassium phosphate (pH 7.5). (a) Far UV CD spectrum of 0.1 mg/ml Hsp26 (O). (b) Far UV CD spectra of 0.1 mg/ml of reduced (O) and oxidized (Δ) Hsp26_{S4C}. Temperature-induced changes in the far UV signal of the proteins were monitored at a constant wavelength of 220 nm. Transitions of 0.1 mg/ml were recorded in 10 mM potassium phosphate (pH 7.5) with a heating rate of 10 deg. C/hour. (c) Thermal unfolding of Hsp26 (O). (d) Thermal unfolding of reduced (O) and oxidized (Δ) Hsp26_{S4C}.

Hsp26 exhibits two thermal transition midpoints,¹⁹ the first at ~ 36 °C (Figure 2(c)) and a second at ~ 74 °C (not shown). The first transition represents defined structure changes while the second transition leads to global unfolding. Here we analyzed the first transition, which occurs at physiologically relevant conditions. It should be noted that Hsp26 exhibits chaperone activity at these temperatures. These temperature-induced structural changes in Hsp26 thus do not refer to thermal-induced denaturation, but coincide with the activation of the chaperone. The midpoint of the thermal transition of the wild-type protein was at 36 °C and the structural transition was reversible when the sample was heated to 55 °C only. The ΔG value calculated for this transition was 7.3 (± 1.1) kJ/mol. The oxidized and reduced cysteine variant exhibits reversible transitions with identical transition midpoints and ΔG values (Figure 2(d)), demonstrating that the transitions are unaffected by the redox state of the cysteine residues.

Further, we analyzed the tertiary structure of Hsp26 and the reduced and oxidized cysteine variants by near UV spectroscopy. Analysis of Hsp26 at 25 °C revealed maxima at 294 nm and 285 nm due to the absorbance of tryptophan residues, a maximum at 278 nm due to tyrosine absorbance and a broad minimum around 265 nm due to phenylalanine absorbance⁴⁰ (Figure 3(a)). Similar spectra were obtained for the reduced and oxidized cysteine variant at 25 °C, indicating that the tertiary structure is highly similar under reducing and oxidizing conditions (Figure 3(b) and (c)). Analysis of Hsp26 at 45 °C revealed intensity changes at 294 nm, 285 nm and 265 nm (Figure 3(a)). The tyrosine absorbance signal at 278 nm remained unchanged. Analysis of the reduced cysteine variant also revealed changes at 294 nm, 285 nm and 268 nm, demonstrating that the reduced form undergoes identical temperature-induced changes (Figure 3(b)). Interestingly, analysis of the oxidized variant at elevated temperatures revealed comparable changes in the tertiary structure (Figure 3(c)). However, additionally the signal intensities at 278 nm were altered, due to the presence of disulfide bonds. This demonstrates that cross-linking subunits by oxidation did not prevent Hsp26 tertiary structure changes. It is notable that temperature-induced changes of the tertiary structure in Hsp26 mainly affect the absorbance signals at 268 nm corresponding to rearrangements of phenylalanine residues. Interestingly, nine of a total of 11 phenylalanine residues are located within the N-terminal region of Hsp26.

Hsp26 is a temperature-regulated sHsp.³⁸ The activation coincides with the destabilization of the oligomer and the appearance of dimers. To determine whether the redox state of the cysteine variant affected the dynamics and stability of the oligomer, we performed gel filtration experiments under oxidizing and reducing conditions. At room temperature (25 °C), Hsp26 eluted as a 24mer (Figure 4(a), straight line). Identical profiles were

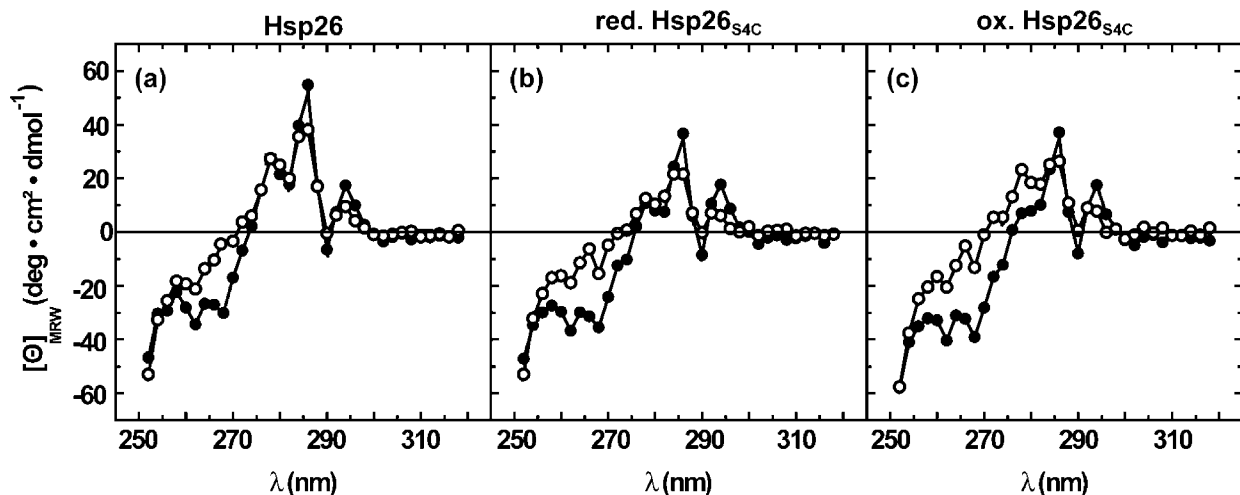


Figure 3. Temperature-induced tertiary structure changes of Hsp26 and Hsp26_{S4C}. Near UV CD spectra of 1 mg/ml Hsp26 and Hsp26_{S4C} were recorded at 25 °C and 45 °C, respectively, in 10 mM potassium phosphate (pH 7.5). (a) Hsp26 at 25 °C (●) and 45 °C (○); (b) reduced Hsp26_{S4C} at 25 °C (●) and 45 °C (○); (c) oxidized Hsp26_{S4C} at 25 °C (●) and 45 °C (○).

obtained for the cysteine variant of Hsp26 under reducing (Figure 4(b), straight line) and oxidizing conditions (data not shown). In agreement with previous results,^{19,38} Hsp26 eluted as a dimer at elevated temperature (Figure 4(a), dotted line). Prolonged incubation of Hsp26 at elevated temperatures and subsequent analysis by analytical SEC at 44 °C over a period of six hours did not shift the elution profiles towards larger species, showing that the dimer is a stable exchangeable unit (data not shown). Analysis of Hsp26_{S4C} at 44 °C and reducing conditions (Figure 4(b), dotted lines) revealed that the protein was also destabilized and eluted as dimers. However, under oxidizing conditions, the oligomeric complex was significantly stabilized and Hsp26_{S4C} eluted as an oligomer of 24 subunits, with elution times equal to that at 25 °C (Figure 4(b), broken lines). This shows that the dissociation of the oligomer into dimers is inhibited in the presence of disulfide bonds. The question remained, whether the oxidized variant exhibits dynamic subunit exchange. To analyze this, we labelled Hsp26 and the reduced and oxidized proteins with fluorescent dyes and monitored the exchange of subunits by fluorescence resonance energy transfer (FRET). At 25 °C, we measured a subunit exchange rate of $k_{\text{transfer}} = 4.9 \times 10^{-4} \text{ s}^{-1}$ with a half-life of $t_{1/2} \sim 1400 \text{ s}$ for Hsp26 (Figure 4(a) and (c)) and reduced Hsp26_{S4C} (Figure 5(d), squares). At 40 °C, the rate of subunit exchange was increased by one order of magnitude, giving a rate $k_{\text{transfer}} = 4.4 \times 10^{-3} \text{ s}^{-1}$ and a half-life of $\sim 158 \text{ seconds}$ for both, Hsp26 (Figure 5(b) and (c)) and reduced Hsp26_{S4C} (data not shown). The subsequent addition of a 40-fold excess of unlabelled Hsp26 to the mixed oligomers led to the complete reversion of the FRET signals, showing that subunit exchange of Hsp26 is a dynamic and reversible process (Figure 5(d), triangles). However, subunit exchange was not detected for oxidized

Hsp26_{S4C}. This was not due to the low labelling efficiency of the oxidized species, as unlabelled, oxidized Hsp26_{S4C} was unable to disrupt the FRET signal of mixed Hsp26 oligomers (Figure 5(d), circles). This demonstrates that in the presence of disulfide bonds the dynamics and stability of the oligomeric complex are strongly affected and that subunit exchange and dissociation of Hsp26 are completely inhibited.

Chaperone activity of Hsp26_{S4C}

The oxidized cysteine variant allowed us to investigate whether the destabilization of the Hsp26 oligomer at higher temperatures and the subsequent dissociation into dimers are essential for the chaperone function of Hsp26. As shown previously, thermally induced aggregation of CS was efficiently prevented in the presence of a twofold excess of Hsp26 (Figure 6(a)).³⁸ Analysis of reduced Hsp26_{S4C} revealed that the protein exhibits chaperone activity indistinguishable from that of the wild-type protein (Figure 6(b)). Surprisingly, the chaperone activity of oxidized Hsp26_{S4C} was identical to that of the reduced protein (Figure 6(c)). Previously we reported that incubation of Hsp26 with CS at elevated temperatures leads to the formation of high molecular mass substrate complexes with diameters of $\sim 50 \text{ nm}$.^{6,38} Analysis by analytical SEC showed that the substrate complexes between CS and Hsp26 were formed efficiently (Figure 6(d)) and that the substrate complexes of CS and the reduced or oxidized form of the cysteine variant did not reveal any significant differences (Figure 6(e) and (f)). This was confirmed by electron microscopy of the substrate complexes (Figure 6(g)–(i)). In all cases, round-shaped substrate complexes with diameters of 40–60 nm were observed. Taken together, these

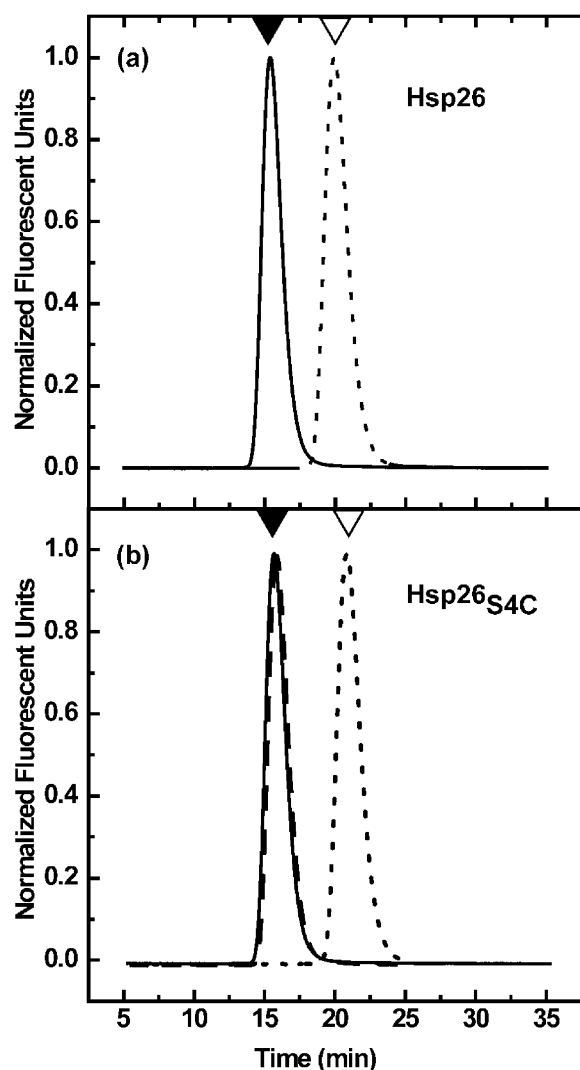


Figure 4. Temperature-dependent quaternary structure analysis of Hsp26 and reduced and oxidized Hsp26_{S4C}. SEC was carried out using a TosoHaas TSK G4000PW equilibrated at either 25 °C or 44 °C in 40 mM Hepes (pH 7.5), 150 mM KCl, 5 mM EDTA. (▼) Indicates the elution peak of the Hsp26 oligomer, (▽) the elution peak of the Hsp26 dimer. (a) Hsp26 at 25 °C (continuous line) and at 44 °C (dotted line); (b) Hsp26_{S4C} at 25 °C (continuous line), at 44 °C under reducing (dotted line) and oxidizing (broken line) conditions.

results demonstrate that dissociation of Hsp26 is not required for chaperone activity.

For Hsp26, elevated temperatures are essential to display chaperone activity. The question remained, whether the mutant also requires elevated temperatures for its activation. Testing the proteins at room temperature with chemically unfolded CS, we found that neither the wild-type protein, nor the reduced or oxidized Hsp26 variant exhibit chaperone activity (Figure 7(a)–(c), circles). This shows that the oxidized variant is not trapped within a permanently active state. Next, we tested whether the heat-activated state persists after shifting Hsp26 back from elevated temperatures to room tempera-

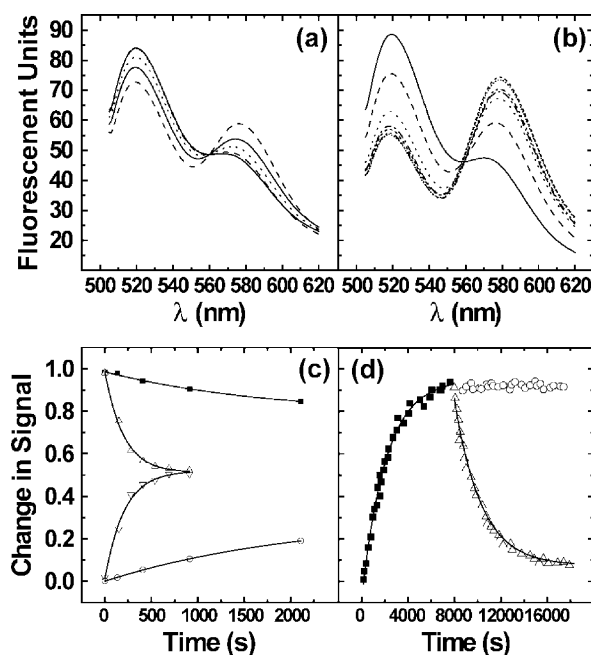


Figure 5. Subunit exchange of Hsp26 and Hsp26_{S4C}. Subunit exchange between Hsp26 oligomers was measured by fluorescence resonance energy transfer in 40 mM Hepes (pH 7.5). Time-dependent changes in emission spectra of 5 μ M FITC and 5 μ M TAMRA labelled Hsp26 at (a) 25 °C and (b) 40 °C. (c) Time-dependent changes in donor (■) and acceptor emission intensities (○) at 25 °C and, changes in donor (△) and acceptor emission (▽) intensities at 40 °C. (d) Subunit exchange of AIAS and LYI labelled Hsp26_{S4C}. (■) Subunit exchange of 1 μ M Hsp26_{S4C}. (△) FRET displacement by the subsequent addition of a 40-fold excess of unlabeled Hsp26 and (○) of oxidized, unlabelled Hsp26_{S4C}.

ture. Interestingly, after incubation of Hsp26 at elevated temperatures, reduced and oxidized Hsp26_{S4C} suppressed substrate aggregation at room temperature, demonstrating that Hsp26, the reduced and oxidized variant require heat-treatment to gain chaperone activity. In agreement with our results for heat-induced aggregation of CS, aggregation of chemically denatured CS was predominantly suppressed with a twofold excess of chaperone (Figure 7(a)–(c), triangles). When heat-treated Hsp26 was incubated for 45 minutes at room temperature it was completely inactive again, demonstrating that this activation is a reversible process (data not shown). Comparison of the half-life of subunit exchange at 25 °C ($t_{1/2} \sim 1400$ s) to that of the aggregation of unfolded CS at 25 °C ($t_{1/2} \sim 17$ s) illustrates that subunit exchange between Hsp26 oligomers is significantly slower than substrate aggregation (Figure 7(d)).

Quaternary structure analysis of Hsp26 under equilibrium conditions

Our results on the cysteine variant required

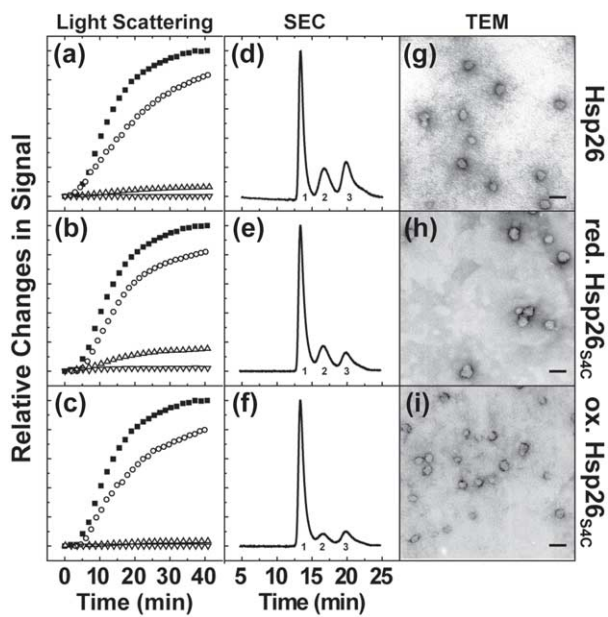


Figure 6. Chaperone activity of reduced and oxidized Hsp26_{S4C}. Chaperone activity and complex formation was determined by light scattering ((a)–(c)), SEC ((d)–(f)) and TEM ((g)–(i)), respectively. Heat-induced aggregation of 1 μ M CS at 44 $^{\circ}$ C in 40 mM Hepes (pH 7.5) in the presence of 0 μ M (■), 1 μ M (○) and 2 μ M (Δ) and 4 μ M (∇) molecular chaperone. (a) Hsp26; (b) reduced Hsp26_{S4C}; (c) oxidized Hsp26_{S4C}. SEC analysis of substrate complex formation with 2 μ M chaperone and 1 μ M CS. Numbers in the graphs refer to the substrate complex (1), free Hsp26 (2) and free CS (3), respectively. (d) Hsp26; (e) reduced Hsp26_{S4C}; (f) oxidized Hsp26_{S4C}. TEM analysis of CS substrate complexes with (g) Hsp26, (h) reduced Hsp26_{S4C}; (i) oxidized Hsp26_{S4C}. Bars represent 100 nm.

further analysis of Hsp26 with respect to the stability of the oligomeric complex. With subunit exchange experiments we had analyzed the dynamic behavior of Hsp26 at various temperatures. However, these results do not fully describe the oligomerization equilibrium of Hsp26, though they indicate that the Hsp26 oligomer is also present at elevated temperatures, since FRET was detectable at 40 $^{\circ}$ C. We therefore wanted to know whether the quaternary structure of Hsp26 is shifted in a temperature-dependent way from its oligomeric state towards the dimer under equilibrium conditions. In ultracentrifugation sedimentation experiments with Hsp26 at 25 $^{\circ}$ C, we obtained a single apparent sedimentation coefficient of 22 S, demonstrating that Hsp26 sediments as an oligomeric species (Figure 8(a) and (d)). Sedimentation experiments at 30 $^{\circ}$ C, 35 $^{\circ}$ C (data not shown) and 40 $^{\circ}$ C also revealed sedimentation coefficients of \sim 22 S (Figure 8(b) and (d)). A fivefold reduction in the concentration of Hsp26 did not shift the oligomerization equilibrium towards smaller species (data not shown). For Hsp26 Δ N, a variant of Hsp26 lacking the N-terminal region, which assembles into dimers only,¹⁹ we determined a sedimentation coefficient of 1.9 S at 25 $^{\circ}$ C (data not shown) and at 40 $^{\circ}$ C (Figure 8(c) and (d)), respectively. Taken together these results show that the rate for the exchange of subunits between oligomers increases temperature-dependently, nevertheless the oligomerization equilibrium remains unaffected. Thus Hsp26 becomes destabilized at elevated temperatures but this does not necessarily lead to the complete dissociation into dimers.

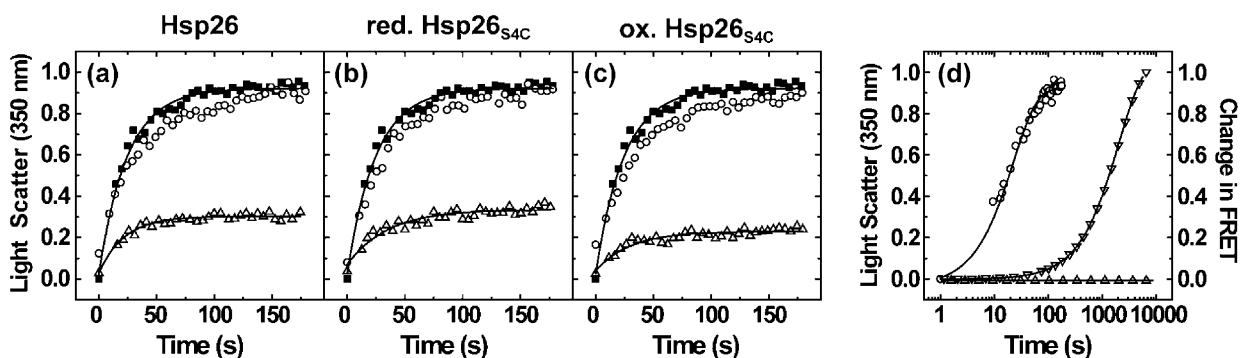


Figure 7. Chaperone activity of Hsp26 with chemically unfolded CS. CS was prepared as described in Materials and Methods. CS aggregation was induced by diluting the substrate 100-fold into 40 mM Hepes (pH 7.5), 2 mM GSH or 1 mM GSSG, respectively, at 25 $^{\circ}$ C. (a) Aggregation of 150 nM CS in the absence of chaperone (■), in the presence of 300 nM Hsp26 (○) and in the presence of heat-treated Hsp26 (Δ). (b) Aggregation of 150 nM CS in the absence of chaperone (■), in the presence of 300 nM reduced Hsp26_{S4C} (○) and in the presence of reduced and heat-treated Hsp26_{S4C} (Δ). (c) Aggregation of 150 nM CS in the absence of chaperone (■), in the presence of 300 nM oxidized Hsp26_{S4C} (○) and in the presence of oxidized and heat-treated Hsp26_{S4C} (Δ). Aggregation of chemically unfolded CS in the absence of sHsps was normalized to 1. ((d) Comparison between the velocities of the aggregation of chemically denatured CS (○) and the subunit exchange of reduced (∇) and oxidized Hsp26_{S4C} (Δ) at 25 $^{\circ}$ C.

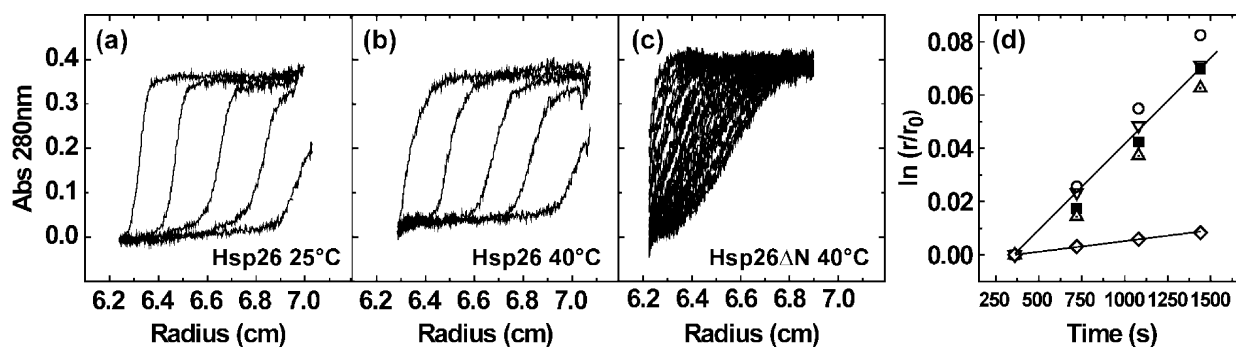


Figure 8. Analytical sedimentation ultracentrifugation analysis of Hsp26 and Hsp26 Δ N. Analytical sedimentation ultracentrifugation was carried at various temperatures of Hsp26 and Hsp26 Δ N. (a) Sedimentation profile of 0.3 mg/ml Hsp26 at 25 °C. (b) Sedimentation profile of 0.3 mg/ml Hsp26 at 40 °C. (c) Sedimentation profile of 0.5 mg/ml Hsp26 Δ N. (d) Evaluation of sedimentation coefficients for Hsp26 protein at 25 °C (■), 30 °C (○), 35 °C (△) 40 °C (▽) and Hsp26 Δ N at 40 °C (◇).

Discussion

sHsps form oligomeric structures, which bind non-native proteins in a cooperative and efficient manner.³ It appears that this class of molecular chaperones can be divided into constitutively active and temperature-controlled sHsps. Hsp26 is a prototypic temperature-regulated sHsp, as it requires elevated temperatures to display chaperone activity. Previously, we reported that the complex of 24 subunits becomes destabilized upon heat-activation, resulting in the appearance of dimers in analytical gel filtration experiments.³⁸ At the same time, electron microscopy revealed that Hsp26 substrate-complexes were oligomeric structures. Both observations led to the notion that the heat-activation requires oligomer dissociation into dimers, which re-associate with substrate proteins to form large complexes.^{6,38} Such a cooperative dissociation has not been observed for all sHsps, yet all of the so far investigated sHsps were reported to be dynamic oligomers exchanging subunits.^{29–31,41} It is generally accepted that sHsps continuously dissociate into smaller units and re-associate. These observations led to the notion, that dissociation is a requirement for the chaperone activity of sHsps.^{31,41} This raised the question whether the formation of dimers is an essential part in the chaperone mechanism of sHsps. We addressed this question by investigating an Hsp26 mutant that did not dissociate into dimers at elevated temperatures.

Previous structure analysis of sHsps suggested that the N-terminal regions are sequestered inside the oligomers.^{15,42,43} Using the N-terminal cysteine variant, Hsp26_{S4C}, we were able to cross-link ~65% of the subunits. The cross-linking ratio suggests that the N termini form trimers. Under oxidizing conditions, two of three subunits form a disulfide bond, while the third remains reduced. This stoichiometry suggests an octahedral symmetry with eight trimerization sites of the N-terminal regions. Given that two Hsp26 subunits associate into antiparallel dimers, mediated by the α -crystallin domain,^{15,43} the trimerization links six

Hsp26 monomers. Such a hexameric arrangement of three dimers has been observed in the crystal structure of Hsp16.5.¹⁵

Our structural investigations revealed that reduced and oxidized Hsp26_{S4C} adopts secondary and quaternary structures indistinguishable from that of the wild-type protein. However, under oxidizing conditions and in the presence of disulfide bonds the cysteine variant maintained its oligomeric state at elevated temperatures and did not dissociate into dimers. Further, oxidized Hsp26_{S4C} did not exchange subunits, indicating a complete loss of the dynamics. According to our data, the oxidized cysteine variant exhibits chaperone activity identical to that measured for the wild-type protein. This implies that the rate of subunit exchange cannot be a major determinant for chaperone activity of sHsps. This conclusion is further supported by the observation that subunit exchange in Hsp26 at 25 °C occurs with a similar rate ($k_{\text{transfer}} = 4.9 \times 10^{-4} \text{ s}^{-1}$ at 25 °C) compared to that of α A-crystallin ($k_{\text{transfer}} = 6.36 \times 10^{-4} \text{ s}^{-1}$ at 37 °C).⁴¹ Yet, while α A-crystallin, similar to Hsp25 or Hsp42,^{6,7,29} displays chaperone activity at room temperature, Hsp26 does not. The half-life of $t_{1/2} > 1000$ s, illustrates that the rate of the subunit exchange is significantly slower than the aggregation of chemically unfolded CS ($t_{1/2} = 17$ s). At elevated temperatures the dynamics increase as determined by subunit exchange experiments. Due to the principle of separation by SEC and the increased dynamics at elevated temperatures, the Hsp26 dimer is separated from the 24mer, disturbing the oligomerization equilibrium between the Hsp26 oligomer and association intermediates. This leads to the cooperative dissociation into stable dimers. However, under equilibrium conditions the Hsp26 oligomer is the most abundant species, also at elevated temperatures.

As a consequence, the activation of Hsp26 at elevated temperatures does not require dissociation into dimers nor increased dynamics of subunit exchange. Rather the essential steps are temperature-induced, structural rearrangements within the

oligomer. These rearrangements can occur without the necessity of oligomer dissociation. A correlation between changes in structure and chaperone activity has also been observed for α -crystallin.^{44,45} Using the two Hsp26 variants Hsp26 Δ N30, lacking residues 1–30, and Hsp26 Δ N, lacking the residues 1–95, we had previously shown that the N-terminal region of Hsp26 is bi-functional;^{19,20} Residues 1–30 are essential for substrate interaction, and amino acid residues 30–95 are required for the correct assembly of the oligomer. While Hsp26 Δ N30 exhibits a thermal transition similar to that of the wild-type protein,²⁰ this is no longer observed in Hsp26 Δ N,¹⁹ indicating that the transition may reflect rearrangements of residues 30–95. This region of the protein might represent a temperature-regulated relay, switching the oligomer between a low and high affinity state. This is in agreement with our result that temperature-activation coincides with tertiary structure changes to phenylalanine residues. Since nine of the 11 phenylalanine residues of Hsp26 are located within the N-terminal region, this can be seen as further evidence that the N-terminal region changes its structure at elevated temperatures.

In summary, we propose two alternative conformations for the Hsp26 oligomer with differing affinities for unfolded proteins of 24 subunits (Figure 9). At physiological temperatures, Hsp26 is in an inactive, low affinity state, which is unable to bind unfolded proteins. Presumably, the substrate binding sites are largely buried inside the oligomer. It is tempting to speculate that the N-terminal regions associate into trimers and stabilize the inactive state by inter-molecular “self-

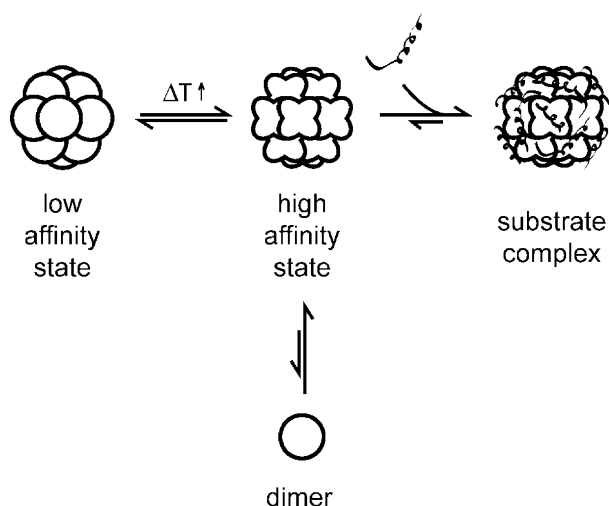


Figure 9. Model for the chaperone mechanism of a temperature-controlled sHsp. Hsp26 reversibly assembles from 12 dimers into the complex of 24 subunits. In the low affinity state Hsp26 does not interact with unfolded proteins. Elevated temperatures lead to conformational changes within the oligomer, thus switching the molecule from the low to the high affinity state. The Hsp26 oligomer becomes activated and associates with non-native proteins into the substrate complex.

recognition”. Upon temperature increase, the Hsp26 oligomer undergoes structural rearrangements, involving the N-terminal domain, which converts it into an active chaperone. In this high affinity conformation, the substrate binding sites become exposed and the Hsp26 oligomer is able to bind non-native proteins. This active state persists for some time after shifting to lower temperatures, until the inactive state is restored.

Materials and Methods

Cloning and purification of Hsp26 and Hsp26_{S4C}

Structural genes of Hsp26 and the Hsp26 cysteine variants were amplified from genomic yeast DNA using PWO polymerase (Roche, Germany) with the following primers (Forward Hsp26: GAT CCC ATG GGG ATG TCA TTT AAC AGT C, Reverse Hsp26: GAT CGC GGC CGC TTA GTT ACC GTA CGA TTC TTG AGA AG, Forward Hsp26_{S4C}: GAT CCC ATG GGG TCA TTT AAC TGT CCA TTT TTT GAT TTC). The DNA fragments were ligated into pET28b+ (Novagene) and expressed in *Escherichia coli* BL21 (DE3) (Stratagene) at 30 °C for four hours. Expression was induced with 1 mM IPTG. The proteins were purified to homogeneity using a Q-Sepharose anion exchange matrix, a Resource Q and a Superdex 200-pg size exclusion column.³⁸ All chromatographic materials were from Amersham Bioscience, Freiburg, Germany. Identity of the proteins was confirmed by matrix-assisted laser desorption ionisation (MALDI) mass spectrometry and Western blotting. The proteins were stored in 40 mM Hepes (pH 7.5), 150 mM KCl at –80 °C.

Reduction and oxidation of the Hsp26 cysteine variant

Hsp26_{S4C} was reduced with a tenfold molar excess of DTT_(red) or GSH in 40 mM Hepes (pH 7.5) for 120 minutes at room temperature, or overnight at 4 °C, respectively. Free reducing agents were removed using a 5 ml Desalting SEC (Amersham Bioscience, Freiburg, Germany). Re-oxidation of the cysteine residues was blocked by covalent modification with a 100-fold excess of IAA for 60 minutes at room temperature. Free IAA was removed as described for DTT. Oxidation of the protein was carried out with a tenfold molar excess of DTT_(ox) or GSSG. The samples were purified using a 5 ml desalting SEC. The efficiency of reduction and oxidation was determined with DTNB.⁴⁶

Circular dichroism spectroscopy for secondary and tertiary structure analysis

Far and near UV CD measurements were carried out in a Jasco J-715 spectropolarimeter (Jasco, Gross-Umstadt, Germany) equipped with a PTC343 peltier unit. The proteins were dialyzed against 10 mM potassium phosphate (pH 7.5) overnight at 4 °C. CD signals were accumulated ten times from 250 nm to 195 nm and 320 nm to 260 nm, respectively, using a scanning rate of 20 nm/minute. Far UV measurements were carried out at 20 °C. Near UV spectra were recorded at 25 °C and 45 °C, respectively. The molecular ellipticities were calculated for the mean residue weight (MRW) using the equation: $[\Theta]_{MRW} = \Theta \times 100 \times M_R / d \times c \times N_{aa}$, where Θ represents the measured ellipticities in degree, M_R the molecular

mass of the protein in g/mol, d the layer thickness in cm, c the sample concentration in mg/ml and N_{aa} the number of residues. Deconvolution of far UV spectra for secondary structure prediction was carried out using the CDNN software.⁴⁷

Thermodynamic stability measurements

To monitor differences in thermal stability Hsp26, oxidized and reduced Hsp26_{S4C} were equilibrated in 10 mM potassium phosphate (pH 7.5) overnight at 4 °C. The thermal unfolding and refolding was monitored in a Jasco J-715 spectropolarimeter equipped with a PTC343 peltier unit (Jasco, Gross-Umstadt, Germany). Signals of 0.1 mg/ml were recorded at $\lambda=220$ nm. The samples were heated from 20 °C to 55 °C and cooled *vice versa* using a heating and cooling rate of 10 deg. C/hour. The thermal stabilities were calculated from reversible experiments assuming a simple two-state model for the high and low affinity states of Hsp26 as described by Pace & Scholtz.⁴⁸ We assumed a theoretical ΔC_p of 10,650 J mol⁻¹ K⁻¹.⁴⁸

Analytical size exclusion chromatography

A TosohHaas TSK G4000PW (30 cm×0.75 cm) gel filtration column with a separating range from 10 to 1500 kDa was used (Tosoh Bioscience, Stuttgart, Germany). All experiments were performed at either 25 °C or 44 °C. Temperature was maintained using a temperature adjustable column oven (Jasco, Gross-Umstadt, Germany). All experiments were performed in 40 mM Hepes (pH 7.5), 150 mM KCl, 5 mM EDTA with 1 mM DTT_(red) or 1 mM DTT_(ox), respectively, using a flow rate of 0.5 ml/minute. Detection was with a Jasco FP 920 fluorescence detector, using an excitation wavelength of 275 nm and an emission wavelength of 307 nm.

Analytical ultracentrifugation

To determine the sedimentation coefficients of Hsp26 and Hsp26 Δ N, analytical sedimentation ultracentrifugation was carried out using a Beckman XL-A ultracentrifuge equipped with a UV/VIS and interference detection unit (Beckman Coulter, Krefeld, Germany). The sample concentration was varied from 2 mg/ml to 0.1 mg/ml in 40 mM Hepes (pH 7.5). The samples were equilibrated at the corresponding temperature for four hours at 3000 rpm. Sedimentation was carried out in a TI-60 rotor, using a final rotation speed of 50,000 rpm. Detection was at 280 nm recording UV scans every six minutes. Evaluation of the data was carried out with the UltraScan software using the van Holde–Weischet velocity analysis.[†]

Thermal aggregation of CS

CS aggregation assays were carried out as described by Buchner *et al.*^{49,50} In short, CS aggregates quantitatively at temperatures above 40 °C. The aggregation was followed at 340 nm recording the changes in absorbance signal in an Amersham Bioscience 4060 UV/VIS spectrophotometer equipped with a temperature-adjustable cuvette holder (Amersham Bioscience, Freiburg, Germany). To determine the chaperone activity increasing concen-

trations of Hsp26 were pre-incubated at 44 °C in 40 mM Hepes (pH 7.5). Substrate aggregation was induced by diluting the substrate to a final concentration of 1 μ M into the pre-heated cuvette. The heat-induced aggregation of CS was normalized to 1.

Chemically induced aggregation of CS

CS was unfolded in 40 mM Hepes (pH 7.5), 6 M GdmCl following the protocol described by Buchner *et al.*⁵¹ Aggregation of CS was induced by diluting the substrate 100-fold to a final concentration of 150 nM into 40 mM Hepes (pH 7.5) with 2 mM GSH or 1 mM GSSG, respectively. Aggregation was monitored at 25 °C in a SPEX Fluoromax-1 fluorescence spectrometer (Jobin Yvon, Munich, Germany) at an excitation and emission wavelength of $\lambda=350$ nm. To monitor the temperature activation and inactivation of Hsp26, the proteins were incubated in the sample buffers at 50 °C for 20 minutes. The samples were then diluted tenfold into the cuvette and equilibrated for ten seconds at 25 °C. Subsequently, the aggregation of CS was induced as described above. The half-life of CS aggregation was derived from the half maximal light scatter signal.

Complex formation of Hsp26 and the cysteine variant with substrate proteins

To test if the reduced and oxidized form of Hsp26_{S4C} differ in activity, 2 μ M of each variant were co-incubated with 1 μ M CS at 44 °C for 30 minutes in 40 mM Hepes (pH 7.5). Samples were then incubated on ice for ten minutes, centrifuged at 15,000g for one minute, and analyzed by analytical SEC and TEM.

Electron microscopy of Hsp26–substrate complexes

Complex formation of Hsp26 and the cysteine variants with CS was performed following the protocol used for the substrate complex formation experiments. The samples were directly applied to glow-discharged carbon-coated copper grids and negatively stained with 3% uranyl acetate. Electron micrographs were recorded at a nominal magnification of 33,000 \times using a Jeol 100CX electron microscope (Jeol, Eching, Germany) operating at 100 kV.

Subunit exchange measurements

Subunit exchange between Hsp26 complexes was monitored by fluorescence resonance energy transfer (FRET) in 40 mM Hepes (pH 7.5). Hsp26_{S4C} was labelled with LYI or AIAS and Hsp26 with FITC or TAMRA. The labelling procedure was in accordance to the manufacturer's protocol (Molecular Probes, Karlsruhe, Germany). Subunit exchange was measured at a final concentration of 10 μ M Hsp26 or 1 μ M Hsp26_{S4C}, respectively, in 40 mM Hepes (pH 7.5) in a SPEX Fluoromax-1 fluorescence spectrophotometer (Jobin Yvon, Munich, Germany), monitoring the time-dependent changes in emission spectra or changes in the donor and acceptor signals, respectively. Excitation of AIAS labelled Hsp26_{S4C} was at 336 nm and of FITC labelled Hsp26 at 495 nm. The reversibility of the process was controlled by the subsequent addition of a 40-fold excess of unlabelled protein to the mixed oligomers. The rate of subunits exchange was determined as described by Bova *et al.*²⁹ The half-life was calculated from $t_{1/2} = \ln 2/k_{\text{transfer}}$.

[†] <http://www.ultrascan.uthscsa.edu>

Acknowledgements

Hsp26 Δ N was a kind gift from Thusnelda Stromer. We are indebted to Martin Heßling and Lin Müller for discussions. Bettina Richter is acknowledged for TEM assistance. We thank Helmut Krause and Anja Osterauer for support with mass spectrometry and protein purification. We also thank Birgit Meinschmidt, Martin Haslbeck and Daniel Weinfurter for reading the manuscript. This work was funded by the grants of the Deutsche Forschungsgesellschaft to J.B. and S.W.

References

- Lindquist, S. & Craig, E. A. (1988). The heat-shock proteins. *Annu. Rev. Genet.* **22**, 631–677.
- Walter, S. & Buchner, J. (2002). Molecular chaperones—cellular machines for protein folding. *Angew. Chem., Int. Ed Engl.* **41**, 1098–1113.
- Jakob, U., Gaestel, M., Engel, K. & Buchner, J. (1993). Small heat shock proteins are molecular chaperones. *J. Biol. Chem.* **268**, 1517–1520.
- Ehrnsperger, M., Graber, S., Gaestel, M. & Buchner, J. (1997). Binding of non-native protein to Hsp25 during heat shock creates a reservoir of folding intermediates for reactivation. *EMBO J.* **16**, 221–229.
- Haslbeck, M. (2002). sHsps and their role in the chaperone network. *Cell Mol. Life Sci.* **59**, 1649–1657.
- Stromer, T., Ehrnsperger, M., Gaestel, M. & Buchner, J. (2003). Analysis of the interaction of small heat shock proteins with unfolding proteins. *J. Biol. Chem.* **278**, 18015–18021.
- Haslbeck, M., Braun, N., Stromer, T., Richter, B., Model, N., Weinkauff, S. & Buchner, J. (2004). Hsp42 is the general small heat shock protein in the cytosol of *Saccharomyces cerevisiae*. *EMBO J.* **23**, 638–649.
- Basha, E., Lee, G. J., Demeler, B. & Vierling, E. (2004). Chaperone activity of cytosolic small heat shock proteins from wheat. *Eur. J. Biochem.* **271**, 1426–1436.
- De Jong, W. W., Caspers, G. J. & Leunissen, J. A. (1998). Genealogy of the alpha-crystallin–small heat-shock protein superfamily. *Int. J. Biol. Macromol.* **22**, 151–162.
- Mornon, J. P., Halaby, D., Malfois, M., Durand, P., Callebaut, I. & Tardieu, A. (1998). alpha-Crystallin C-terminal domain: on the track of an Ig fold. *Int. J. Biol. Macromol.* **22**, 219–227.
- Sun, T. X., Das, B. K. & Liang, J. J. (1997). Conformational and functional differences between recombinant human lens alphaA- and alphaB-crystallin 2. *J. Biol. Chem.* **272**, 6220–6225.
- Narberhaus, F. (2002). Alpha-crystallin-type heat shock proteins: socializing minichaperones in the context of a multichaperone network. *Microbiol. Mol. Biol. Rev.* **66**, 64–93.
- Horwitz, J. (1992). Alpha-crystallin can function as a molecular chaperone. *Proc. Natl Acad. Sci. USA*, **89**, 10449–10453.
- Horwitz, J. (2003). Alpha-crystallin. *Expt. Eye Res.* **76**, 145–153.
- Kim, K. K., Kim, R. & Kim, S. H. (1998). Crystal structure of a small heat-shock protein. *Nature*, **394**, 595–599.
- van Montfort, R. L., Basha, E., Friedrich, K. L., Slingsby, C. & Vierling, E. (2001). Crystal structure and assembly of a eukaryotic small heat shock protein. *Nature Struct. Biol.* **8**, 1025–1030.
- Leroux, M. R., Melki, R., Gordon, B., Batelier, G. & Candido, E. P. (1997). Structure–function studies on small heat shock protein oligomeric assembly and interaction with unfolded polypeptides. *J. Biol. Chem.* **272**, 24646–24656.
- Haley, D. A., Bova, M. P., Huang, Q. L., Mchaourab, H. S. & Stewart, P. L. (2000). Small heat-shock protein structures reveal a continuum from symmetric to variable assemblies. *J. Mol. Biol.* **298**, 261–272.
- Stromer, T., Fischer, E., Richter, K., Haslbeck, M. & Buchner, J. (2004). Analysis of the regulation of the molecular chaperone Hsp26 by temperature-induced dissociation: the N-terminal domain is important for oligomer assembly and the binding of unfolding proteins. *J. Biol. Chem.* **279**, 11222–11228.
- Haslbeck, M., Ignatiou, A., Saibil, H., Helmich, S., Frenzl, E., Stromer, T. & Buchner, J. (2004). A domain in the N-terminal part of Hsp26 is essential for chaperone function and oligomerization. *J. Mol. Biol.* **343**, 445–455.
- Giese, K. C. & Vierling, E. (2004). Mutants in a small heat shock protein that affect the oligomeric state. Analysis and allele-specific suppression. *J. Biol. Chem.* **279**, 32674–32683.
- Carver, J. A., Esposito, G., Schwedersky, G. & Gaestel, M. (1995). ¹H NMR spectroscopy reveals that mouse Hsp25 has a flexible C-terminal extension of 18 amino acids. *FEBS Letters*, **369**, 305–310.
- Fernando, P., Abdulle, R., Mohindra, A., Guillemette, J. G. & Heikkila, J. J. (2002). Mutation or deletion of the C-terminal tail affects the function and structure of *Xenopus laevis* small heat shock protein, hsp30. *Comput. Biochem. Physiol. B Biochem. Mol. Biol.* **133**, 95–103.
- Lindner, R. A., Carver, J. A., Ehrnsperger, M., Buchner, J., Esposito, G., Behlke, J. *et al.* (2000). Mouse Hsp25, a small shock protein. The role of its C-terminal extension in oligomerization and chaperone action. *Eur. J. Biochem.* **267**, 1923–1932.
- Raman, B. & Rao, C. M. (1997). Chaperone-like activity and temperature-induced structural changes of alpha-crystallin. *J. Biol. Chem.* **272**, 23559–23564.
- Kokke, B. P., Leroux, M. R., Candido, E. P., Boelens, W. C. & De Jong, W. W. (1998). *Caenorhabditis elegans* small heat-shock proteins Hsp12.2 and Hsp12.3 form tetramers and have no chaperone-like activity. *FEBS Letters*, **433**, 228–232.
- Guo, Z. & Cooper, L. F. (2000). An N-terminal 33-amino-acid-deletion variant of hsp25 retains oligomerization and functional properties. *Biochem. Biophys. Res. Commun.* **270**, 183–189.
- Studer, S., Obrist, M., Lentze, N. & Narberhaus, F. (2002). A critical motif for oligomerization and chaperone activity of bacterial alpha-heat shock proteins. *Eur. J. Biochem.* **269**, 3578–3586.
- Bova, M. P., Huang, Q., Ding, L. & Horwitz, J. (2002). Subunit exchange, conformational stability, and chaperone-like function of the small heat shock protein 16.5 from *Methanococcus jannaschii*. *J. Biol. Chem.* **277**, 38468–38475.
- Bova, M. P., Ding, L. L., Horwitz, J. & Fung, B. K. (1997). Subunit exchange of alphaA-crystallin. *J. Biol. Chem.* **272**, 29511–29517.
- Sobott, F., Benesch, J. L., Vierling, E. & Robinson, C. V. (2002). Subunit exchange of multimeric protein complexes. Real-time monitoring of subunit exchange

- between small heat shock proteins by using electrospray mass spectrometry. *J. Biol. Chem.* **277**, 38921–38929.
32. Wintrode, P. L., Friedrich, K. L., Vierling, E., Smith, J. B. & Smith, D. L. (2003). Solution structure and dynamics of a heat shock protein assembly probed by hydrogen exchange and mass spectrometry. *Biochemistry*, **42**, 10667–10673.
 33. Lentze, N., Aquilina, J. A., Lindbauer, M., Robinson, C. V. & Narberhaus, F. (2004). Temperature and concentration-controlled dynamics of rhizobial small heat shock proteins. *Eur. J. Biochem.* **271**, 2494–2503.
 34. Susek, R. E. & Lindquist, S. L. (1989). hsp26 of *Saccharomyces cerevisiae* is related to the superfamily of small heat shock proteins but is without a demonstrable function. *Mol. Cell Biol.* **9**, 5265–5271.
 35. Bossier, P., Fitch, I. T., Boucherie, H. & Tuite, M. F. (1989). Structure and expression of a yeast gene encoding the small heat-shock protein Hsp26. *Gene*, **78**, 323–330.
 36. Tuite, M. F., Bentley, N. J., Bossier, P. & Fitch, I. T. (1990). The structure and function of small heat shock proteins: analysis of the *Saccharomyces cerevisiae* Hsp26 protein. *Antonie Van Leeuwenhoek*, **58**, 147–154.
 37. Bentley, N. J., Fitch, I. T. & Tuite, M. F. (1992). The small heat-shock protein Hsp26 of *Saccharomyces cerevisiae* assembles into a high molecular weight aggregate. *Yeast*, **8**, 95–106.
 38. Haslbeck, M., Walke, S., Stromer, T., Ehrnsperger, M., White, H. E., Chen, S. *et al.* (1999). Hsp26: a temperature-regulated chaperone. *EMBO J.* **18**, 6744–6751.
 39. Murai, N., Makino, Y. & Yoshida, M. (1996). GroEL locked in a closed conformation by an interdomain cross-link can bind ATP and polypeptide but cannot process further reaction steps. *J. Biol. Chem.* **271**, 28229–28234.
 40. Fasman, G. D. (1996). *Circular Dichroism and the Conformational Analysis of Biomolecules*, Plenum Press, New York.
 41. Bova, M. P., Mchaourab, H. S., Han, Y. & Fung, B. K. (2000). Subunit exchange of small heat shock proteins. Analysis of oligomer formation of alphaA-crystallin and Hsp27 by fluorescence resonance energy transfer and site-directed truncations. *J. Biol. Chem.* **275**, 1035–1042.
 42. Haley, D. A., Horwitz, J. & Stewart, P. L. (1999). Image restrained modeling of alphaB-crystallin. *Expt. Eye Res.* **68**, 133–136.
 43. van Montfort, R. L., Basha, E., Friedrich, K. L., Slingsby, C. & Vierling, E. (2001). Crystal structure and assembly of a eukaryotic small heat shock protein. *Nature Struct. Biol.* **8**, 1025–1030.
 44. Raman, B., Ramakrishna, T. & Rao, C. M. (1995). Temperature dependent chaperone-like activity of alpha-crystallin. *FEBS Letters*, **365**, 133–136.
 45. Raman, B. & Rao, C. M. (1994). Chaperone-like activity and quaternary structure of alpha-crystallin. *J. Biol. Chem.* **269**, 27264–27268.
 46. Evans, J. C. & Ellman, G. L. (1959). The ionization of cysteine. *Biochim. Biophys. Acta*, **33**, 574–576.
 47. Bohm, G., Muhr, R. & Jaenicke, R. (1992). Quantitative analysis of protein far UV circular dichroism spectra by neural networks. *Protein Eng.* **5**, 191–195.
 48. Myers, J. K., Pace, C. N. & Scholtz, J. M. (1995). Denaturant m values and heat capacity changes: relation to changes in accessible surface areas of protein unfolding. *Protein Sci.* **4**, 2138–2148.
 49. Kiefhaber, T., Rudolph, R., Kohler, H. H. & Buchner, J. (1991). Protein aggregation *in vitro* and *in vivo*: a quantitative model of the kinetic competition between folding and aggregation. *Nature Biotechnol.* **9**, 825–829.
 50. Buchner, J., Grallert, H. & Jakob, U. (1998). Analysis of chaperone function using citrate synthase as non-native substrate protein. *Methods Enzymol.* **290**, 323–338.
 51. Buchner, J., Schmidt, M., Fuchs, M., Jaenicke, R., Rudolph, R., Schmid, F. X. & Kiefhaber, T. (1991). GroE facilitates refolding of citrate synthase by suppressing aggregation. *Biochemistry*, **30**, 1586–1591.

Edited by K. Kuwajima

(Received 16 March 2005; received in revised form 28 April 2005; accepted 18 May 2005)

Some like it hot: the structure and function of small heat-shock proteins

Martin Haslbeck, Titus Franzmann, Daniel Weinfurter & Johannes Buchner

Small heat-shock proteins (sHsps) are a widespread and diverse class of molecular chaperones. Recent evidence suggests that they maintain protein homeostasis by binding proteins in non-native conformations, thereby preventing substrate aggregation. Some members of the sHsp family are inactive or only partially active under physiological conditions, and transition toward the active state is induced by specific triggers, such as elevated temperature. Release of substrate proteins bound to sHsps requires cooperation with ATP-dependent chaperones, suggesting that sHsps create a reservoir of non-native proteins for subsequent refolding.

sHsps comprise the most widespread but also the most poorly conserved family of molecular chaperones. Phylogenetic analyses suggest that sHsps diverged very early in evolution^{1,2}. Members of the sHsp family have been found throughout all kingdoms (Fig. 1) except in some pathogenic bacteria such as *Mycoplasma genitalium* and *Helicobacter pylori*^{1,3}. Bacteria (with the exception of Rhizobia), archaea and single-celled eukaryotes usually contain one or two sHsps^{1,4–7}. However, in most higher, multi-cellular eukaryotes, the number of genes encoding sHsps is higher, often considerably so: 4 in *Drosophila melanogaster*, 16 in *Caenorhabditis elegans*, 10 in humans and 19 in *Arabidopsis thaliana*. The reason for this expansion is not clear, but specific functional roles for sHsps in certain cell types and organelles and during differentiation may have driven diversification.

Although proteins belonging to the sHsp superfamily are diverse in sequence and size, most share characteristic features, including (i) a conserved α -crystallin domain of ~90 residues, (ii) a small molecular mass of 12–43 kDa, (iii) formation of large oligomers, (iv) a dynamic quaternary structure and (v) induction by stress conditions and chaperone activity in suppressing protein aggregation.

The most widely studied family member, α -crystallin⁶, is a major constituent of the human eye lens. In the center of the lens, the protein concentration reaches up to 450 mg ml⁻¹ (ref. 7). In this crowded environment, α A- and α B-crystallins seem to prevent proteins from forming light-scattering aggregates⁶. The two isoforms, which have close to 60% amino acid sequence identity, make up one-third of the eye lens. α A-crystallin is mainly confined to the lenticular compartment, whereas

its close relative α B-crystallin is also a heat-inducible protein present in many other tissues⁷. The most compelling evidence that α -crystallin is essential for lens transparency and prevents protein aggregation *in vivo* comes from α A-crystallin-knockout mice, which develop severe cataracts at an early age^{7,8}. The clinical importance of sHsps is further highlighted by a growing number of fundamental cellular processes in which they have been found to be involved, among them protection against oxidative stress and aging, interference with apoptosis, neurological disorders and neuroprotective effects^{9–12}. It is tempting to speculate that protein misfolding is the common theme in all these events and that sHsps carry out a protective function by preventing deleterious protein aggregation.

Structure of sHsps

One of the most notable features of sHsps is their organization as large oligomeric structures. The structures of five family members have been determined by X-ray crystallography or electron microscopy (Fig. 2). The outside diameters range from 100 Å to 180 Å (Fig. 2a). Hsp16.5 from *Methanocaldococcus jannaschii* (Fig. 2b)¹³, Hsp16.3 (also called Acr1) from *Mycobacterium tuberculosis*¹⁴ and Hsp26 from *Saccharomyces cerevisiae*¹⁵ all form hollow, ball-like structures, but the number of subunits in the oligomers vary: *M. jannaschii* Hsp16.5 and yeast Hsp26 complexes have 24 subunits, whereas *M. tuberculosis* Hsp16.3 has 12. Hsp16.9 from wheat¹⁶, meanwhile, is a barrel-shaped structure assembled from two hexameric double disks with a total of 12 subunits (Fig. 2c). In contrast to these two defined oligomeric structures, the quaternary structure of α -crystallin is variable¹⁷: it forms polydisperse oligomeric assemblies with up to 50 subunits per complex. Despite their sequence diversity and differences in oligomeric assemblies, the sHsp proteins have a conserved structural organization^{1,3,18}: an N-terminal region followed by the conserved α -crystallin domain and a C-terminal region (Fig. 2d,e).

The α -crystallin domain represents the signature motif of sHsps. Except for a few positions, the amino acid sequence is variable. However, the structure, a compact β -sheet sandwich similar to the immunoglobulin-like fold (Fig. 2d,f), is conserved throughout the sHsp family^{13,16,19}. The sheet is composed of two layers of three and five antiparallel strands, respectively, connected by a short interdomain loop. α -crystallin domains can dimerize through the formation of an intersubunit composite β -sheet; this dimerization is a conserved feature of sHsps^{13,16}.

The N-terminal region is highly variable in both sequence and length. It varies from 24 residues in *C. elegans* Hsp12.2 (ref. 20) to 247 residues in *S. cerevisiae* Hsp42 (ref. 21,22). The N-terminal regions are only partially resolved in the available crystal structures, suggesting increased flexibility^{16,19}. For wheat Hsp16.9, the N-terminal region seems to be important

Technische Universität München, Department Chemie, Lichtenbergstr. 4, 85747 Garching, Germany. Correspondence should be addressed to J.B. (johannes.buchner@ch.tum.de).

Published online 4 October 2005; doi:10.1038/nsmb993

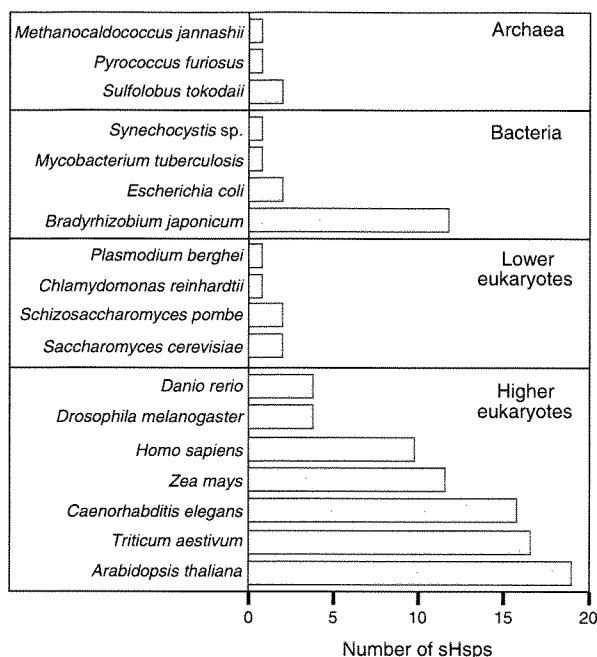


Figure 1 Schematic overview of the number of representatives of the sHsp family in different organisms. In general, from bacteria to higher eukaryotes, a substantial increase in the number of sHsps per organism is observed. Rhizobia are a notable exception to this trend.

for stabilizing the oligomer: the N-terminal arms of the subunits from the two disks intertwine to form pairs of knot-like structure, and the hydrophobic contacts in these knots are buried inside the oligomer^{16,19}.

In the two sHsp crystal structures, the C-terminal region after the α -crystallin domain is also involved in stabilizing the oligomer. Comparison of the assemblies shows that there is a binding site for the C-terminal region on a neighboring α -crystallin domain. However, the orientation of the C-terminal region is flexible. Recently, it was shown that contacts between a conserved motif (with the sequence Ile-Xxx-Ile/Val²³) in the C-terminal region and a hydrophobic patch in the α -crystallin domain of a neighboring subunit are critical for oligomer formation^{3,13,16,19}.

The picture emerging from these structural analyses shows that residues in all three regions of sHsps are required for oligomerization. Although the α -crystallin domain is necessary for dimer formation and thus assembles the basic building block, both flanking regions promote the formation of higher-order structures.

Chaperone function of sHsps

Although α -crystallin and a number of sHsps had been identified decades ago^{24,25}, their function remained elusive until *in vitro* studies in the early 1990s showed that sHsps bind denatured proteins and prevent their irreversible aggregation. Bovine α -crystallin and murine Hsp25 were the first sHsps reported to have chaperone activity^{6,26}. Since then, sHsps from other species have been shown to bind a variety of non-native proteins *in vitro*^{15,21,27–29}. Notably, and in contrast to other classes of molecular chaperones, several non-native polypeptide chains are bound by each oligomeric sHsp complex. Ratios of up to one non-native model substrate protein per dimeric subunit have been reported^{15,29}. Concerning substrate specificity, the first proteomic studies in *S. cerevisiae* and *Synechocystis* sp. showed that approximately one-third of the cytosolic protein is maintained in a soluble state by sHsps under heat-shock conditions^{21,30}. The

fact that a wide range of proteins are protected from precipitation suggests that sHsps may act rather promiscuously, similarly to the molecular chaperones GroEL and Hsp70. The question of substrate specificity is of special interest when multiple sHsps are found in one cellular compartment. In *S. cerevisiae*, there are two different cytosolic sHsps, Hsp26 and Hsp42. Their substrate protein profiles seem to be overlapping but not identical²¹, indicating some degree of selectivity. However, the substrate specificities of sHsps are still largely unknown.

Once formed, complexes between substrates and sHsps are very stable at physiological temperatures. EM images have revealed large complexes of defined size and shape whose morphology depends on the identities of the substrate proteins and to some extent also of the respective sHsp^{31,32}. In addition to these defined complexes, larger assemblies of substrate proteins and sHsps have been observed when an excess of non-native proteins is present. These are reminiscent of the 'heat-shock granules,' which are large, ordered structures found upon heat shock in plants³³. In this context, it should be noted that prokaryotic sHsps are specifically associated with inclusion bodies, intracellular aggregates of overexpressed proteins⁵.

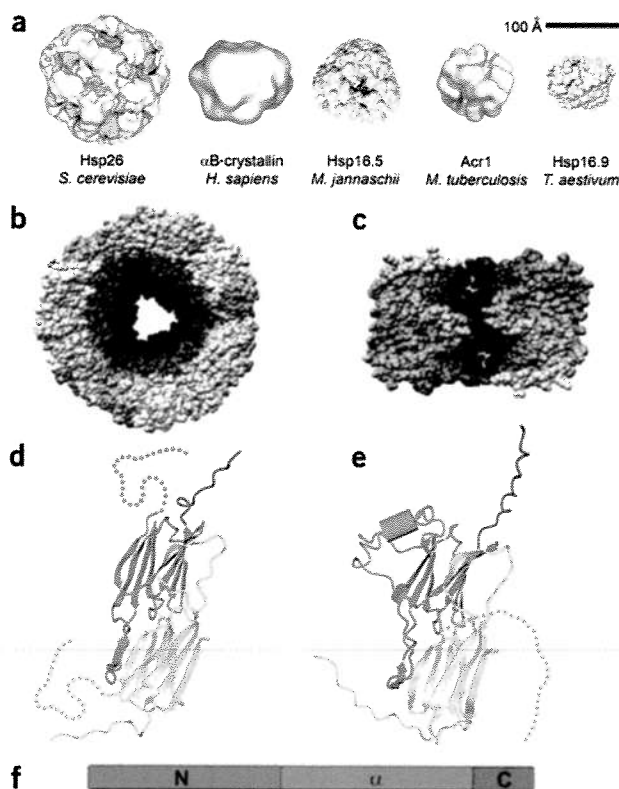
Several sites have been postulated to be involved in the chaperone function and complex formation of sHsps, including the N-terminal and C-terminal regions^{32,34–38}. The proposed sites are hydrophobic in character. In the crystal structure of wheat Hsp16.9, the hydrophobic N-terminal regions are integrated into the oligomeric assembly¹⁶. Deletion of the corresponding N-terminal region of yeast Hsp26 results in a dimer without chaperone activity³⁵. This observation is in agreement with results for the isolated α -crystallin domains of several sHsps, all of which lacked chaperone activity^{34,39,40}. A truncated Hsp26 in which the first 30 N-terminal residues are removed is still a large oligomer able to suppress the aggregation of substrate proteins³⁵. However, complexes of non-native proteins with this variant are less stable than complexes with full-length Hsp26, suggesting that the hydrophobic N-terminal segment may contribute to substrate binding³⁵. Because of low conservation of the various motifs in sHsps, sequence comparisons do not provide sufficient information to predict potential binding sites. The idea that substrate binding involves variable sequences outside the α -crystallin domain supports the hypothesis that substrate profiles vary among different sHsps. At present, it is not possible to distinguish clearly the parts of sHsps that are necessary for chaperone function and those involved in oligomer interactions or to determine whether there is substantial crosstalk between these two functions.

Release of substrate

The interactions between unfolded proteins and sHsps lead to stable and defined substrate-chaperone complexes. The non-native proteins are neither transferred between different sHsp complexes nor spontaneously released^{29,41}. For α -crystallin, it has been suggested that irreversible binding of other lens crystallins, which occurs in the aging lens, prevents aggregation and light scattering⁷. Although trapping of aggregation-prone polypeptides may be sufficient in the static protein environment of the eye lens, in the living cell it seems detrimental to have a chaperone system that binds non-native proteins without allowing reactivation once a stress period is over. *In vitro* experiments have shown that the non-native proteins trapped in sHsp complexes are folding competent⁴¹. Additional chaperones could potentially facilitate the release of these substrates.

A clue about the contributions of additional chaperones to this reaction came from heat-shock experiments in mammalian cells. Here, Hsp70 is required for the refolding of protein from insoluble aggregates consisting of sHsps and model substrate proteins⁴². *In vitro* experiments showed that Hsp70 allowed reactivation of the sHsp-bound proteins in the presence of ATP^{29,41,43,44}. For the *Escherichia coli* sHsp IbpB it was

Figure 2 Features of sHsp structures. (a) Quaternary structures of sHsps, determined either by cryo-EM or X-ray crystallography. Hsp26 from *S. cerevisiae* (24 subunits, cryo-EM; H. Saibil and H. White (Birkbeck College, London), personal communication), α B-crystallin from *Homo sapiens* (16 subunits, cryo-EM)¹⁷, Hsp16.5 from *M. jannaschii* (24 subunits, crystal)¹³, Hsp16.3/Acr1 from *M. tuberculosis* (12 subunits, cryo-EM)¹⁴ and Hsp16.9 from *T. aestivum* (12 subunits, crystal)¹⁶. (b,c) *M. jannaschii* Hsp16.5 (b), whose quaternary structure consists of 24 identical subunits arranged into a tetrahedral hollow sphere, and *T. aestivum* Hsp16.9 (c), a barrel-like assembly of 12 subunits; cross-sections show inner surfaces of both proteins; colors distinguish neighboring dimers. (d,e) Crystal structures of two sHsp dimers, from *M. jannaschii* Hsp16.5 (d; PDB code 1SHS) and *T. aestivum* Hsp16.9 (e; PDB code 1GME), highlighting three functionally important regions. Green, N-terminal region; blue, α -crystallin domain; magenta, C-terminal extension; gray, the other sHsp in the dimer; dotted line, N-terminal residues not resolved in the structures. (f) Domain organization of sHsps.



shown that bound non-native proteins were specifically transferred to the DnaK-DnaJ-GrpE chaperone system and reactivated⁴⁵.

Recent studies expanded the picture of the chaperone network connected to the sHsp-substrate protein complexes (Fig. 3). Studies in *E. coli* and *S. cerevisiae* revealed a conserved mechanism that involves Hsp70-Hsp40 and members of the Hsp100 family, including ClpB in *E. coli* and Hsp104 in *S. cerevisiae*^{46–49}. The types of sHsp-substrate interactions—either defined complexes or aggregate-like structures with incorporated sHsps—seem to dictate a requirement for a specific ATP-dependent chaperone or combinations of them. Together, these results suggest that sHsps give the organism the opportunity to separate the prevention of aggregation from the ATP-dependent processing steps. In light of this, the incorporation of sHsps into protein aggregates is beneficial for reactivation of substrates compared to situations where sHsps are absent from the aggregates.

Regulation of activity

A conserved trait of molecular chaperones is the existence of states of low and high affinity for non-native proteins. In the case of ATP-dependent chaperones, the shift between the two functional states is governed by ATP binding and hydrolysis⁵⁰. Although there have been reports of ATP binding by α -crystallin^{51,52}, the general view is that ATP does not have a direct role in the regulation of sHsp chaperone activity^{3,7,18,19}. For sHsps, shifting between active and inactive states involves a different mechanism. In light of this, it should be noted that many sHsps are not constitutively active; they are specifically activated upon the introduction of stress conditions such as elevated temperatures.

sHsp complexes are dynamic structures and exchange subunits (presumably dimers) constantly^{27,53–55}. One consequence of this reaction is the possibility to form hetero-oligomeric assemblies with other sHsp species present in the same compartment, such as the two α -crystallins⁵⁵. One could imagine that these hetero-oligomeric complexes would have binding specificities different from the homo-oligomeric complexes.

The dynamic behavior of sHsps could allow the substrate-binding sites, which seem to be buried in the oligomeric complex, to become exposed by dissociation^{37,56–59}. This is consistent with the observation that the hydrophobicity of several sHsps increases under stress conditions^{38,57,58}. The spontaneous dissociation-reassociation process may thus be a 'sensing' mechanism to monitor the presence of non-native proteins in the cellular environment. Studies on human Hsp27 support the hypothesis that dissociation of the oligomer is required for recognition of the substrate⁵⁶.

However, other recent experiments challenge aspects of this view. For example, yeast Hsp26 is known to be regulated by elevated

temperatures^{15,34}. Coincidentally with the appearance of a dimeric species, it is transformed from a largely inactive form to an active chaperone. Notably, when an Hsp26 variant is used in which subunits are cross-linked via disulfide bonds, dissociation at elevated temperatures is no longer observed but the activation of the chaperone is not affected⁶⁰. Similar results have been obtained for α -crystallin whereby dissociation and subunit exchange do not correlate with chaperone activity⁶¹. This suggests that the activation process in these cases involves rearrangements within the oligomeric structure. Whether there is a universal mechanism for activation remains to be determined.

Perspectives

Progress in recent years has defined the basic structural features of sHsps. Furthermore, their role in assisting the folding of proteins in the cytosol is becoming evident. The current evidence suggests that sHsps effectively trap aggregation-prone folding intermediates and maintain them in a conformation suitable for refolding. Interestingly, despite great variation in sequence and size, the basic mechanisms and the cooperation of some sHsps with ATP-dependent chaperones seem to be conserved between bacteria and humans (Fig. 3).

Another key question still to be resolved is the contribution of the dynamic subunit exchange between oligomers and the dissociation into smaller oligomers to the chaperone mechanism. At present, evidence exists, on the one hand, for conformational changes within the large oligomer, which shift sHsps to a binding mode for non-native proteins, and, on the other hand, for the requirement to dissociate the complex into subunits before non-native proteins can be efficiently bound. The exchange of subunits could occur on the level of dimers, but at present, the involvement of other oligomeric substates such as tetramers⁶² cannot be excluded. It is reasonable to assume that temperature is just one trigger for activation. Post-translational modifications, in particular

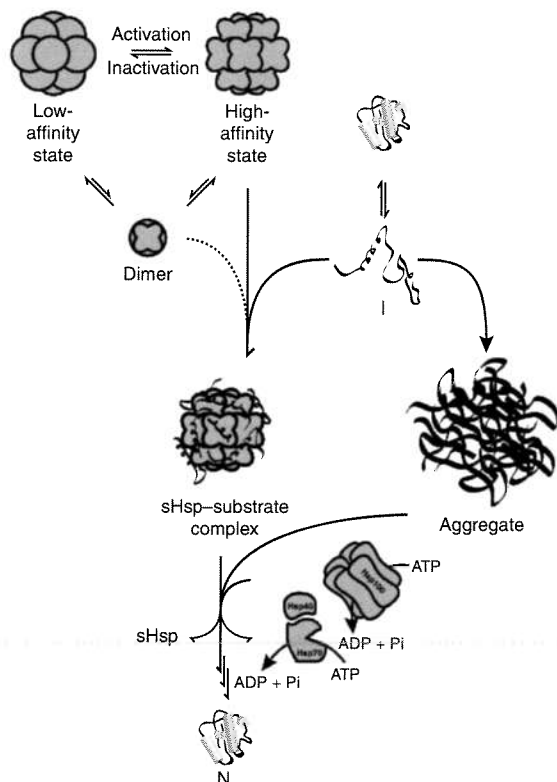


Figure 3 Model for the chaperone function of sHsps. sHsps are dynamic oligomeric structures, permanently exchanging subunits. Concerning interaction with non-native proteins, they exist in two states: an inactive, low-affinity state and an active, high-affinity state. The equilibrium between these two modes is controlled in a temperature-dependent manner. Upon heat shock, the equilibrium is shifted toward the high-affinity state. The active oligomer thus becomes competent to associate with substrate proteins to form a stable sHsp-substrate complex. This allows efficient prevention of irreversible substrate aggregation. Release of active substrate proteins from these complexes requires cooperation with proteins of ATP-dependent chaperone families such as Hsp70-Hsp40 or Hsp100. Although Hsp70-Hsp40 and Hsp100 can act directly on protein aggregates, the presence of sHsps increases the efficiency of the process. Hsp100 proteins have so far been identified only in bacteria, fungi and plants.

one complex and in a coordinated manner, at least when studied with one or two different model substrates during conditions of thermal unfolding *in vitro*. But what happens *in vivo* with a large variety of unfolded proteins present? Isolation of these complexes, composed of an sHsp and a presumably heterogeneous mixture of substrate proteins, and their subsequent analysis by mass spectrometry and EM is a daunting task. Together with a rigorous biophysical analysis of the conformations of bound substrate proteins, these data will guide experiments aimed at defining the reactions that lead to functional refolding of sHsp-bound substrate proteins in the presence of ATP-dependent chaperones.

sHsps are not essential folding factors, but, depending on the extent of protein aggregation, they can contribute substantially to the folding capacity of the cell^{8,21,24,69}. This scenario does not exclude the possibility that some sHsps may have evolved to perform specific functions with a limited number of target proteins or maybe even independent of protein folding. Whether the expansion of the number of sHsps in metazoans goes along with functional diversification is a key unresolved question. The comparative analysis of a complete set of sHsps in a higher eukaryote is clearly needed to address this issue.

ACKNOWLEDGMENTS

We would like to apologize to all researchers in the field to whose work we could not refer because of a limit on the number of citations. We thank C. Slingsby (Birkbeck College, London) and P. Stewart (Vanderbilt University Medical Center, Nashville, Tennessee, USA) for data on the oligomeric complexes of wheat Hsp16.9 and α -crystallin, respectively. Work in the authors' laboratory was supported by grants from the Deutsche Forschungsgemeinschaft and the Fonds der Chemischen Industrie to J.B. and M.H.

COMPETING INTERESTS STATEMENT

The authors declare that they have no competing financial interests.

Published online at <http://www.nature.com/nsmb/>

Reprints and permissions information is available online at

<http://npg.nature.com/reprintsandpermissions/>

phosphorylation, observed for mammalian sHsps seem to be another mechanism to change the activity profiles of sHsps according to cellular demands^{63,64}. The presence of non-native proteins may also be important in creating a high-affinity conformation.

Structural information for sHsps is just beginning to emerge. So far, the available structures suggest a plasticity of quaternary structure not previously observed for any other chaperone family. Clearly, structural analysis of additional family members is needed to further define the variable and invariant features. This will also help to identify the binding sites for non-native proteins. Several sites distributed over the three structural regions of sHsps have been postulated to be involved in the binding of non-native proteins^{37,65,66}. All of the proposed sites are of hydrophobic character and, in addition to chaperone function, influence oligomerization of sHsps. Thus, it is still unclear which of the proposed sites are necessary for chaperone function and which are involved in oligomer interactions. Comparisons between different sHsps are limited by the low sequence conservation of the motifs, making differences in the substrate binding sites of various sHsps very likely.

One of the large gaps in our current understanding of sHsps as molecular chaperones concerns the mechanism governing the formation of defined complexes with non-native substrate proteins and the structural organization of these complexes. So far, studies on this topic have been performed almost exclusively with model substrates *in vitro*. Some of them indicate that the substrate is accessible and thus might be on the surface of the complex^{67,68}. However, there is also evidence for protection of sHsp-bound proteins from proteolysis⁶⁸. In electron micrographs, it is not possible to locate the sHsp oligomer in the structure of the sHsp-substrate complex. This points to a substantial rearrangement of the sHsp oligomer and a partial incorporation of the substrate into the structure^{15,31,32}.

In addition, one should bear in mind that, in contrast to all other known chaperones, sHsps bind a large number of non-native proteins in

1. Kappe, G., Leunissen, J.A. & De Jong, W.W. Evolution and diversity of prokaryotic small heat shock proteins. *Prog. Mol. Subcell. Biol.* **28**, 1–17 (2002).
2. Waters, E.R., Lee, G.J. & Vierling, E. Evolution, structure and function of the small heat shock proteins in plants. *J. Exp. Bot.* **47**, 325–338 (1996).
3. Narberhaus, F. Alpha-crystallin-type heat shock proteins: socializing minichaperones in the context of a multichaperone network. *Microbiol. Mol. Biol. Rev.* **66**, 64–93 (2002).
4. Laksanalamai, P. & Robb, F.T. Small heat shock proteins from extremophiles: a review. *Extremophiles* **8**, 1–11 (2004).
5. Allen, S.P., Polazzi, J.O., Gierse, J.K. & Easton, A.M. Two novel heat shock genes encoding proteins produced in response to heterologous protein expression in *Escherichia coli*. *J. Bacteriol.* **174**, 6938–6947 (1992).
6. Horwitz, J. Alpha-crystallin can function as a molecular chaperone. *Proc. Natl. Acad. Sci. USA* **89**, 10449–10453 (1992).
7. Horwitz, J. Alpha-crystallin. *Exp. Eye Res.* **76**, 145–153 (2003).
8. Brady, J.P. *et al.* Targeted disruption of the mouse alpha A-crystallin gene induces cataract and cytoplasmic inclusion bodies containing the small heat shock protein alpha B-crystallin. *Proc. Natl. Acad. Sci. USA* **94**, 884–889 (1997).
9. Stege, G.J. *et al.* The molecular chaperone alphaB-crystallin enhances amyloid beta

PERSPECTIVE

- neurotoxicity. *Biochem. Biophys. Res. Commun.* **262**, 152–156 (1999).
10. Hsu, A.L., Murphy, C.T. & Kenyon, C. Regulation of aging and age-related disease by DAF-16 and heat-shock factor. *Science* **300**, 1142–1145 (2003).
 11. Clark, J.I. & Muchowski, P.J. Small heat-shock proteins and their potential role in human disease. *Curr. Opin. Struct. Biol.* **10**, 52–59 (2000).
 12. Latchman, D.S. Protection of neuronal and cardiac cells by HSP27. *Prog. Mol. Subcell. Biol.* **28**, 253–265 (2002).
 13. Kim, K.K., Kim, R. & Kim, S.H. Crystal structure of a small heat-shock protein. *Nature* **394**, 595–599 (1998).
 14. Kennaway, C.K. *et al.* Dodecameric structure of the small heat shock protein ACR1 from mycobacterium tuberculosis. *J. Biol. Chem.*, published online 26 July 2005 (doi:10.1074/jbc.M504263200).
 15. Haslbeck, M. *et al.* Hsp26: a temperature-regulated chaperone. *EMBO J.* **18**, 6744–6751 (1999).
 16. van Montfort, R.L., Basha, E., Friedrich, K.L., Slingsby, C. & Vierling, E. Crystal structure and assembly of a eukaryotic small heat shock protein. *Nat. Struct. Biol.* **8**, 1025–1030 (2001).
 17. Haley, D.A., Horwitz, J. & Stewart, P.L. The small heat-shock protein, alphaB-crystallin, has a variable quaternary structure. *J. Mol. Biol.* **277**, 27–35 (1998).
 18. Haslbeck, M. & Buchner, J. Chaperone function of sHsps. *Prog. Mol. Subcell. Biol.* **28**, 37–59 (2002).
 19. Van Montfort, R., Slingsby, C. & Vierling, E. Structure and function of the small heat shock protein/alpha-crystallin family of molecular chaperones. *Adv. Protein Chem.* **59**, 105–156 (2001).
 20. Candido, E.P. The small heat shock proteins of the nematode *Caenorhabditis elegans*: structure, regulation and biology. *Prog. Mol. Subcell. Biol.* **28**, 61–78 (2002).
 21. Haslbeck, M. *et al.* Hsp42 is the general small heat shock protein in the cytosol of *Saccharomyces cerevisiae*. *EMBO J.* **23**, 638–649 (2004).
 22. Narberhaus, F. & Haslbeck, M. Small heat shock proteins: dynamic players in the folding game. in *Protein Folding Handbook* (eds. Buchner, J. & Kiefhaber, T.) 830–857 (Wiley-VCH, Weinheim, Germany, 2005).
 23. Pasta, S.Y., Raman, B., Ramakrishna, T. & Rao, C. The IXI/V motif in the C-terminal extension of alpha-crystallins: alternative interactions and oligomeric assemblies. *Mol. Vis.* **10**, 655–662 (2004).
 24. Petko, L. & Lindquist, S. Hsp26 is not required for growth at high temperatures, nor for thermotolerance, spore development, or germination. *Cell* **45**, 885–894 (1986).
 25. Ingolia, T.D. & Craig, E.A. Four small *Drosophila* heat shock proteins are related to each other and to mammalian alpha-crystallin. *Proc. Natl. Acad. Sci. USA* **79**, 2360–2364 (1982).
 26. Jakob, U., Gaestel, M., Engel, K. & Buchner, J. Small heat shock proteins are molecular chaperones. *J. Biol. Chem.* **268**, 1517–1520 (1993).
 27. Studer, S. & Narberhaus, F. Chaperone activity and homo- and hetero-oligomer formation of bacterial small heat shock proteins. *J. Biol. Chem.* **275**, 37212–37218 (2000).
 28. Roy, S.K., Hiyaama, T. & Nakamoto, H. Purification and characterization of the 16-kDa heat-shock-responsive protein from the thermophilic cyanobacterium *Synechococcus vulcanus*, which is an alpha-crystallin-related, small heat shock protein. *Eur. J. Biochem.* **262**, 406–416 (1999).
 29. Lee, G.J., Roseman, A.M., Saibil, H.R. & Vierling, E. A small heat shock protein stably binds heat-denatured model substrates and can maintain a substrate in a folding-competent state. *EMBO J.* **16**, 659–671 (1997).
 30. Basha, E. *et al.* The identity of proteins associated with a small heat shock protein during heat stress *in vivo* indicates that these chaperones protect a wide range of cellular functions. *J. Biol. Chem.* **279**, 7566–7575 (2004).
 31. Stromer, T., Ehrnsperger, M., Gaestel, M. & Buchner, J. Analysis of the interaction of small heat shock proteins with unfolding proteins. *J. Biol. Chem.* **278**, 18015–18021 (2003).
 32. Basha, E., Lee, G.J., Demeler, B. & Vierling, E. Chaperone activity of cytosolic small heat shock proteins from wheat. *Eur. J. Biochem.* **271**, 1426–1436 (2004).
 33. Nover, L., Scharf, K.D. & Neumann, D. Formation of cytoplasmic heat shock granules in tomato cell cultures and leaves. *Mol. Cell. Biol.* **3**, 1648–1655 (1983).
 34. Stromer, T., Fischer, E., Richter, K., Haslbeck, M. & Buchner, J. Analysis of the regulation of the molecular chaperone Hsp26 by temperature-induced dissociation - The N-terminal domain is important for oligomer assembly and the binding of unfolding proteins. *J. Biol. Chem.* **279**, 11222–11228 (2004).
 35. Haslbeck, M. *et al.* A domain in the N-terminal part of Hsp26 is essential for chaperone function and oligomerization. *J. Mol. Biol.* **343**, 445–455 (2004).
 36. Friedrich, K.L., Giese, K.C., Buan, N.R. & Vierling, E. Interactions between small heat shock protein subunits and substrate in small heat shock protein-substrate complexes. *J. Biol. Chem.* **279**, 1080–1089 (2004).
 37. Giese, K.C. & Vierling, E. Changes in oligomerization are essential for the chaperone activity of a small heat shock protein *in vivo* and *in vitro*. *J. Biol. Chem.* **277**, 46310–46318 (2002).
 38. Lindner, R.A. *et al.* Mouse Hsp25, a small shock protein. The role of its C-terminal extension in oligomerization and chaperone action. *Eur. J. Biochem.* **267**, 1923–1932 (2000).
 39. Kokke, B.P., Leroux, M.R., Candido, E.P., Boelens, W.C. & De Jong, W.W. *Caenorhabditis elegans* small heat-shock proteins Hsp12.2 and Hsp12.3 form tetramers and have no chaperone-like activity. *FEBS Lett.* **433**, 228–232 (1998).
 40. van de Klundert, F.A. *et al.* The mammalian small heat-shock protein Hsp20 forms dimers and is a poor chaperone. *Eur. J. Biochem.* **258**, 1014–1021 (1998).
 41. Ehrnsperger, M., Graber, S., Gaestel, M. & Buchner, J. Binding of non-native protein to Hsp25 during heat shock creates a reservoir of folding intermediates for reactivation. *EMBO J.* **16**, 221–229 (1997).
 42. Stege, G.J., Li, G.C., Li, L., Kampinga, H.H. & Konings, A.W. On the role of hsp72 in heat-induced intranuclear protein aggregation. *Int. J. Hyperthermia* **10**, 659–674 (1994).
 43. Lee, G.J. & Vierling, E. A small heat shock protein cooperates with heat shock protein 70 systems to reactivate a heat-denatured protein. *Plant Physiol.* **122**, 189–198 (2000).
 44. Wang, K. & Spector, A. alpha-crystallin prevents irreversible protein denaturation and acts cooperatively with other heat-shock proteins to renature the stabilized partially denatured protein in an ATP-dependent manner. *Eur. J. Biochem.* **267**, 4705–4712 (2000).
 45. Veinger, L., Diamant, S., Buchner, J. & Goloubinoff, P. The small heat-shock protein IbpB from *Escherichia coli* stabilizes stress-denatured proteins for subsequent refolding by a multichaperone network. *J. Biol. Chem.* **273**, 11032–11037 (1998).
 46. Matuszewska, M., Kuczynska-Wisnik, D., Laskowska, E. & Liberek, K. The small heat shock protein IbpA of *Escherichia coli* cooperates with IbpB in stabilization of thermally aggregated proteins in a disaggregation competent state. *J. Biol. Chem.* **280**, 12292–12298 (2005).
 47. Mogk, A., Deuring, E., Vorderwulbecke, S., Vierling, E. & Bukau, B. Small heat shock proteins, ClpB and the DnaK system form a functional triade in reversing protein aggregation. *Mol. Microbiol.* **50**, 585–595 (2003).
 48. Haslbeck, M., Miess, A., Stromer, T., Walter, S. & Buchner, J. Disassembling protein aggregates in the yeast cytosol: The cooperation of Hsp26 with Ssa1 and Hsp104. *J. Biol. Chem.* **280**, 23861–23868 (2005).
 49. Cashikar, A.G., Duennwald, M.L. & Lindquist, S.L. A chaperone pathway in protein disaggregation: Hsp26 alters the nature of protein aggregates to facilitate reactivation by Hsp104. *J. Biol. Chem.* **280**, 23869–23875 (2005).
 50. Buchner, J. & Walter, S. Analysis of chaperone function *in vitro*. in *Protein Folding Handbook* (eds. Buchner, J. & Kiefhaber, T.) 162–196 (Wiley-VCH, Weinheim, Germany, 2005).
 51. Muchowski, P.J. & Clark, J.I. ATP-enhanced molecular chaperone functions of the small heat shock protein human alphaB crystallin. *Proc. Natl. Acad. Sci. USA* **95**, 1004–1009 (1998).
 52. Biswas, A. & Das, K.P. Role of ATP on the interaction of alpha-crystallin with its substrates and its implications for the molecular chaperone function. *J. Biol. Chem.* **279**, 42648–42657 (2004).
 53. Sobott, F., Benesch, J.L., Vierling, E. & Robinson, C.V. Subunit exchange of multimeric protein complexes. Real-time monitoring of subunit exchange between small heat shock proteins by using electrospray mass spectrometry. *J. Biol. Chem.* **277**, 38921–38929 (2002).
 54. Lentze, N., Aquilina, J.A., Lindbauer, M., Robinson, C.V. & Narberhaus, F. Temperature and concentration-controlled dynamics of rhizobial small heat shock proteins. *Eur. J. Biochem.* **271**, 2494–2503 (2004).
 55. Bova, M.P., Mchaourab, H.S., Han, Y. & Fung, B.K.K. Subunit exchange of small heat shock proteins - Analysis of oligomer formation of alpha A-crystallin and Hsp27 by fluorescence resonance energy transfer and site-directed truncations. *J. Biol. Chem.* **275**, 1035–1042 (2000).
 56. Shashidharamurthy, R., Koteiche, H.A., Dong, J. & Mchaourab, H.S. Mechanism of chaperone function in small heat shock proteins: dissociation of the HSP27 oligomer is required for recognition and binding of destabilized T4 lysozyme. *J. Biol. Chem.* **280**, 5281–5289 (2005).
 57. Yang, H. *et al.* The *Mycobacterium tuberculosis* small heat shock protein Hsp16.3 exposes hydrophobic surfaces at mild conditions: conformational flexibility and molecular chaperone activity. *Protein Sci.* **8**, 174–179 (1999).
 58. Lindner, R.A., Kapur, A., Mariani, M., Titmuss, S.J. & Carver, J.A. Structural alterations of alpha-crystallin during its chaperone action. *Eur. J. Biochem.* **258**, 170–183 (1998).
 59. Mchaourab, H.S., Dodson, E.K. & Koteiche, H.A. Mechanism of chaperone function in small heat shock proteins. Two-mode binding of the excited states of T4 lysozyme mutants by alphaA-crystallin. *J. Biol. Chem.* **277**, 40557–40566 (2002).
 60. Franzmann, T.M., Wühr, M., Richter, K., Walter, S. & Buchner, J. The activation mechanism of Hsp26 does not require dissociation of the oligomer. Dissociation is not required. *J. Mol. Biol.* **350**, 1083–1093 (2005).
 61. Aquilina, J.A. *et al.* Subunit exchange of polydisperse proteins: mass spectrometry reveals consequences of alphaA-crystallin truncation. *J. Biol. Chem.* **280**, 14485–14491 (2005).
 62. Ehrnsperger, M., Lillie, H., Gaestel, M. & Buchner, J. The dynamics of Hsp25 quaternary structure. Structure and function of different oligomeric species. *J. Biol. Chem.* **274**, 14867–14874 (1999).
 63. Koteiche, H.A. & Mchaourab, H.S. Mechanism of chaperone function in small heat-shock proteins. Phosphorylation-induced activation of two-mode binding in alpha B-crystallin. *J. Biol. Chem.* **278**, 10361–10367 (2003).
 64. Gaestel, M. sHsp-phosphorylation: enzymes, signaling pathways and functional implications. *Prog. Mol. Subcell. Biol.* **28**, 151–169 (2002).
 65. Smulders, R.H. *et al.* The mutation Asp69→Ser affects the chaperone-like activity of alpha A-crystallin. *Eur. J. Biochem.* **232**, 834–838 (1995).
 66. Lentze, N. & Narberhaus, F. Detection of oligomerisation and substrate recognition sites of small heat shock proteins by peptide arrays. *Biochem. Biophys. Res. Commun.* **325**, 401–407 (2004).
 67. Ehrnsperger, M., Hergersberg, C., Wienhues, U., Nichtl, A. & Buchner, J. Stabilization of proteins and peptides in diagnostic immunological assays by the molecular chaperone Hsp25. *Anal. Biochem.* **259**, 218–225 (1998).
 68. Kim, R. *et al.* On the mechanism of chaperone activity of the small heat-shock protein of *Methanococcus jannaschii*. *Proc. Natl. Acad. Sci. USA* **100**, 8151–8155 (2003).
 69. Lee, S., Owen, H.A., Prochaska, D.J. & Barnum, S.R. HSP16.6 is involved in the development of thermotolerance and thylakoid stability in the unicellular cyanobacterium, *Synechocystis sp. PCC 6803*. *Curr. Microbiol.* **40**, 283–287 (2000).





ELSEVIER

International Journal of Biological Macromolecules 39 (2006) 104–110

INTERNATIONAL JOURNAL OF

**Biological
Macromolecules**

STRUCTURE, FUNCTION AND INTERACTIONS

www.elsevier.com/locate/ijbiomac

Matrix-assisted refolding of oligomeric small heat-shock protein Hsp26[☆]

Titus M. Franzmann^{*}

Department Chemie, Technische Universität München, 85747 Garching, Germany

Received 30 November 2005; received in revised form 27 February 2006; accepted 27 February 2006

Available online 19 April 2006

Abstract

Recombinant gene expression in the prokaryotic host *Escherichia coli* is of general interest for both biotechnology and basic research. Use of *E. coli* is inexpensive and advantageous due to the fully developed genetic accessibility. However, often insoluble target protein (inclusion body) accumulates in the cell. Especially when producing eukaryotic or disulfide bridged proteins in *E. coli*, inclusion body formation is observed. Nonetheless, insoluble protein can be regained and refolded in vitro. Commonly, renaturation of proteins is accomplished by methods involving dilution and/or dialysis. An interesting alternative is matrix-assisted refolding in which the denatured protein is refolded in the immobilized state. Here, matrix-assisted refolding was applied to refold a double cysteine variant of Hsp26, a small heat-shock protein from *Saccharomyces cerevisiae* which was insoluble after biosynthesis in *E. coli* BL21 (DE3) cells. This oligomeric protein was efficiently recovered from the insoluble fraction and refolded to its native oligomeric and chaperone-active state using ion exchange and size exclusion chromatography.
© 2006 Elsevier B.V. All rights reserved.

Keywords: Matrix-assisted; Protein refolding; Oligomer; Disulfide bond small heat-shock protein; sHsp; Alpha crystallin; Aggregation

1. Introduction

Protein folding is the reversible transformation of a linear amino acid sequence into its unique three-dimensional structure [1]. During the folding process, proteins expose hydrophobic surface and can therefore easily undergo unwanted intermolecular interactions that lead to protein aggregation [2]. In vivo, the protein concentration is high and many polypeptide chains emerging the ribosome channel are prone to aggregation [3]. Especially when proteins are produced at high concentrations protein folding competes with this unwanted side reaction [4–6]. However, recombinant gene expression is of general interest for both, biotechnology and basic research and because of its advantages over other expression systems, such as yeast or eukaryotic cells lines, most commonly the bacterial host *Escherichia coli* is used. Its short generation time, inexpensive cultivation and most importantly, the excellent genetic accessibility make it an efficient tool for recombinant protein production. Nonetheless, producing proteins at non-physiologically high levels frequently leads to accumulation of insoluble and inactive deposits (in-

clusion bodies) of the target protein in the cell [7]. Especially, for eukaryotic proteins and proteins containing disulfide bridges in their native structure inclusion body formation is observed [8]. The reducing milieu of the bacterial cytosol prevents disulfide bond formation. Consequently, these proteins cannot reach their native state and purification is usually carried out under denaturing conditions followed by in vitro refolding.

Non-native proteins can be recovered and solubilized from the insoluble fraction using strong denaturants such as urea or guanidine [9]. In general, protein refolding requires a decrease in protein concentration and the removal of denaturant [8,10]. Commonly this is achieved by dilution or dialysis. An interesting and promising alternative is so called matrix-assisted refolding [11]. In this approach, protein refolding is carried out while the protein is immobilized on a chromatographic matrix. Binding occurs under denaturing conditions and refolding is induced by buffer exchange from denaturing to native conditions. This technique offers several advantages, e.g. intermolecular interactions are restrained, as the protein remains immobilized during the folding process and secondly the protein undergoes a first purification step. Third, the refolded protein is eluted at rather high concentrations and can easily be processed. Typically, this method is used for proteins fused to affinity-tags such as the HIS-tag, the cellulose binding domain from *Clostridium thermocellum* or a glutamic acid tag [12–15]. Here, matrix-assisted

[☆] This paper was presented at the Challenging Proteins Workshop in Paris, October 17–18, 2005.

^{*} Tel.: +49 89 289 13349; fax: +49 89 289 13345.

E-mail address: titus.franzmann@ch.tum.de.

refolding was used to refold a cysteine variant of Hsp26, an oligomeric small heat-shock protein from *Saccharomyces cerevisiae*. In contrast to the Hsp26 wild type protein, this cysteine variant was detected in the insoluble fraction after protein synthesis in *E. coli* BL21 (DE3) cells and in vitro refolding involving anion-exchange (IEX) and size exclusion chromatography (SEC) was required.

2. Materials and methods

2.1. Cloning, expression and purification of Hsp26_{S4C/S210C}

The Hsp26_{S4C/S210C} structure gene was amplified from genomic yeast DNA using PWO polymerase (Roche Applied Sciences, Mannheim, Germany). Serine replacement was carried out using oligonucleotides ordered from MWG Biotech AG (Ebersberg, Germany) carrying the mismatching nucleotide sequences (forward primer: GAT CCC ATG GGG TCA TTT AAC TGT CCA TTT TTT GAT TTC, reverse primer: GAT CGC GGC CGC TTA GTT ACC CCA ACA TTC TTG AGA AG). Amplified Hsp26_{S4C/S210C} was ligated into pET28b+ (Novagen, Heidelberg, Germany) using the restriction sites *NcoI* and *NotI*. Recombinant gene expression of Hsp26_{S4C/S210C} was carried out in *E. coli* BL21 (DE3) cells (Stratagene, Heidelberg, Germany). Gene expression was induced in the mid-exponential growth phase with 1 mM IPTG for 4 h at 30 °C. Cells were harvested at 5000 × g, washed with 40 mM HEPES, 5 mM EDTA, 1 mM DTT pH 7.5 and cracked using a basic Z cell disrupter (Constant Systems, Warwick, UK). The lysate was centrifuged at 35,000 × g for 50 min at 8 °C. The sediment was then washed with 40 mM HEPES, 5 mM EDTA, 1 mM DTT, pH 7.5 and again centrifuged at 35,000 × g for 30 min at 8 °C. Hsp26_{S4C/S210C} was resolubilized with 40 mM HEPES, 5 M Urea, 5 mM EDTA, 1 mM DTT, pH 7.5 stirring at room temperature for 2 h. Insoluble compounds were removed by centrifugation at 35,000 × g for 50 min at room temperature. The denatured, resolubilized protein was applied to a Q-Sepharose FastFlow anion-exchange matrix equilibrated in 40 mM HEPES, 5 M Urea, 5 mM EDTA, 1 mM DTT, pH 7.5. Partial refolding of Hsp26_{S4C/S210C} was induced by quick buffer exchange to 40 mM HEPES, 3 M Urea, 5 mM EDTA, 1 mM DTT, pH 7.5. Hsp26_{S4C/S210C} was eluted using a 15-fold linear gradient from 0 to 1 M KCl. Fractions containing Hsp26_{S4C/S210C} were pooled and dialysed against 40 mM HEPES, 3 M Urea, 150 mM KCl, 5 mM EDTA, 1 mM DTT, pH 7.5. The sample was then concentrated by ultra filtration (Milipore 30,000) and applied to a Superdex 200-pg column running in 40 mM HEPES, 150 mM KCl, 5 mM EDTA, 1 mM DTT, pH 7.5. Fractions containing Hsp26_{S4C/S210C} were pooled and diluted five-fold with 40 mM HEPES, 5 mM EDTA, 1 mM DTT, pH 7.5 and applied to a 6 ml ResourceQ column. The protein was eluted with a 15-fold linear gradient from 30 mM to 1 M KCl, dialysed against 40 mM HEPES, 150 mM KCl, 5 mM EDTA, 1 mM DTT, pH 7.5, concentrated to a final concentration of 4 mg/ml and stored at –80 °C. Identity of the protein was confirmed by mass spectrometry. All chromatographic material was from GE Healthcare Life Sciences, Freiburg, Germany.

2.2. Circular dichroism spectroscopy

Far-UV circular dichroism (CD) measurements were carried out in a Jasco J-715 spectropolarimeter (Jasco, Gross-Umstadt, Germany) equipped with a PTC343 peltier unit. The proteins were dialyzed against 10 mM potassium phosphate, pH 7.5 overnight at 4 °C. CD signals were accumulated 10 times from 250 to 198 nm using a scanning rate of 20 nm/min. Measurements were carried out at 20 °C. The molecular ellipticities were calculated for the mean residue weight (MRW) using the equation $[\Theta]_{MRW} = \Theta \times 100M_R/dcN_{aa}$, where Θ represents the measured ellipticities in degree, M_R the molecular mass of the protein in g mol⁻¹, d the layer thickness in cm, c the sample concentration in mg/ml and N_{aa} is the number of residues. Deconvolution was carried out using the CDNN software [16].

2.3. Analytical size exclusion chromatography

For quaternary structure analysis a TSK G-4000PW (30 cm × 0.75 cm) gel filtration column was used (Tosoh Bioscience, Stuttgart, Germany). All experiments were performed in 40 mM HEPES, 150 mM KCl, 5 mM EDTA, pH 7.5 at 25 °C, using a flow rate of 0.5 ml/min. Detection was with a Jasco FP 920 fluorescence detector (Jasco, Gross-Umstadt, Germany), using an excitation wavelength of 275 nm and an emission wavelength of 307 nm.

2.4. Analytical ultracentrifugation

To monitor the chemically induced dissociation of Hsp26 under semi-equilibrium conditions analytical sedimentation velocity ultracentrifugation was carried out using a Beckman XL-A ultracentrifuge equipped with an UV-vis and interference detection unit (Beckman Coulter, Krefeld, Germany). The protein concentration was 0.5 mg/ml in 40 mM HEPES, pH 7.5 with increasing concentrations of urea. The samples were equilibrated at 20 °C for 4 h at 3000 rpm. Sedimentation was carried in a TI-60 rotor, using a final rotation speed of 50,000 rpm. Evaluation of the sedimentation profiles was carried out with the UltraScan software using the enhanced van Holde-Weischet analysis (<http://www.ultrascan.uthscsa.edu>).

2.5. Thermal aggregation of CS

Citrate synthase (CS) aggregation assays were carried out as described by Buchner et al. [17,18]. Temperature-induced CS aggregation was followed at 340 nm recording the changes in absorbance signal in a Cary 50 UV-vis spectrophotometer equipped with a temperature-adjustable cuvette holder (Varian, Freiburg, Germany) operating at 44 °C. To determine the chaperone activity of Hsp26_{S4C/S210C}, increasing concentrations were pre-incubated at 44 °C in 40 mM HEPES, pH 7.5 and CS aggregation was induced by diluting the substrate to a final concentration of 1 μM into the heated cuvette. The aggregation signal of CS without chaperone was normalized to one.

3. Results

3.1. Chemical stability of the Hsp26 oligomer against urea-induced dissociation into dimers

Hsp26 is a sHsps from *S. cerevisiae*. Its quaternary structure is assembled from 24 monomers associating to form an oligomer with a molecular mass of ~ 570 kDa. We investigated the chemical stability of the Hsp26 oligomer against urea-induced dissociation using analytical sedimentation velocity ultracentrifugation to find conditions for stepwise refolding of the dimeric building block followed by oligomer reassembly. In agreement with previous results, Hsp26 sedimented with an apparent sedimentation coefficient of ~ 24 S [19]. Incubation of Hsp26 with 0.1 M (data not shown) and 0.5 M urea did not affect the sedimentation coefficient significantly (Fig. 1A). At 2 M urea, the sedimentation coefficient was decreased from ~ 24 to ~ 2 S, indicating that Hsp26 was completely dissociated into dimers under semi-equilibrium conditions (Fig. 1B). These conditions were used for refolding Hsp26_{S4C/S210C} in a two-step matrix-assisted approach.

3.2. Expression, refolding and purification of Hsp26_{S4C/S210C}

Expression analysis of Hsp26_{S4C/S210C} in *E. coli* BL21 (DE3) cells over 16 h revealed that the target protein was already synthesized efficiently after 1 h of induction and that the amount of target protein per cell was not increased significantly after 4 h (Fig. 2A). Separating the soluble and insoluble fractions by centrifugation after cell disruption and analysing both fractions by SDS-PAGE and western blotting showed that Hsp26_{S4C/S210C} was almost completely in the insoluble fraction (Fig. 2B and C). Incubation of the insoluble fraction with 5 M urea efficiently solubilized more than 95% Hsp26_{S4C/S210C} (Fig. 2B and C). The denatured fraction was then applied to a Q-Sepharose equilibrated in 5 M urea. No target protein was detected in the flow through or wash fraction (data not shown), demonstrating that unfolded Hsp26_{S4C/S210C} binds efficiently to the anion-exchange

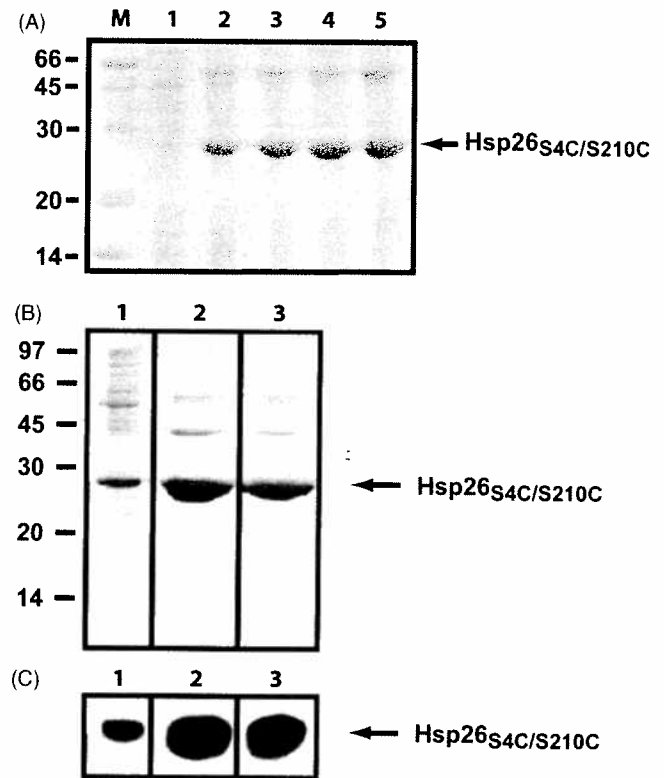


Fig. 2. Expression and solubility analysis of Hsp26_{S4C/S210C}. (A) Expression of Hsp26_{S4C/S210C} in *Escherichia coli* BL21 (DE3) cells at 37 °C was analysed by coomassie stained SDS-PAGE. Gene expression was induced with 1 mM IPTG. M: protein standard marker. Analysis of *E. coli* lysate before induction of gene expression (1), after 1 h (2), after 2 h (3), after 4 h (4) and after 16 h (5) of induction. (B) Solubility of Hsp26_{S4C/S210C} after cell disruption was analysed by coomassie stained SDS-PAGE and (C) western blotting. Cells were lysed and the soluble and insoluble fractions were separated by centrifugation. Analysis of the soluble fraction (1) and the insoluble fraction (2) after cell disruption. Insoluble fraction was treated with 5 M urea to resolubilize Hsp26_{S4C/S210C} (3).

matrix. Decreasing the urea concentration from 5 to 3 M to induce partial refolding of Hsp26_{S4C/S210C} did not elute the target protein (Fig. 3B). The protein eluted from the anion-exchange matrix at low ionic strength (~ 4.5 mS cm) with a

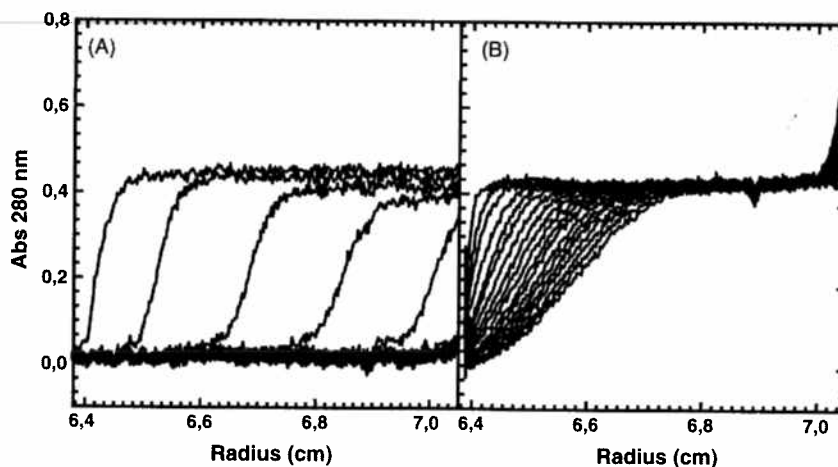


Fig. 1. Chemical-induced dimerization of Hsp26. Analytical velocity sedimentation ultracentrifugation profiles of 0.5 mg/ml Hsp26 at 20 °C. (A) In the presence of 0.5 M urea and (B) in the presence of 2 M urea.

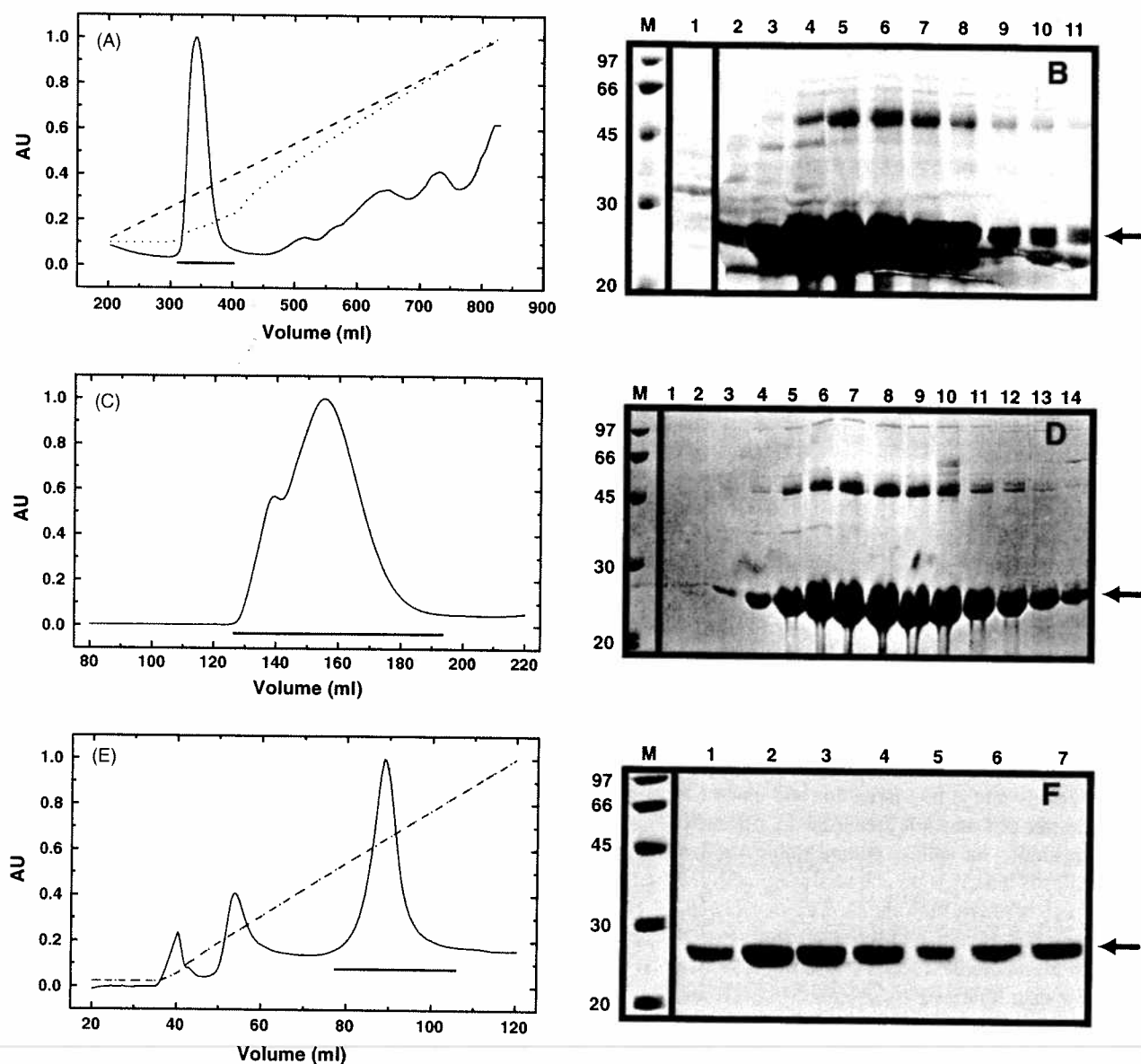


Fig. 3. Purification of Hsp26_{S4C/S210C}. Elution chromatograms and SDS-PAGE for quality control of the purification steps. Black bars in the chromatograms indicate the selected fractions analysed by coomassie stained SDS-PAGE. (A) Elution chromatogram of the Q-Sepharose FastFlow column, operating under denaturing conditions. (B) SDS-PAGE of selected fractions from the Q-Sepharose column. Protein standard (M), flow through fraction after partial refolding was induced by lowering the urea concentration to 3 M (1). Elution fractions containing Hsp26_{S4C/S210C} (2–11). (C) Chromatogram of the Superdex 200-pg operating under native conditions. (D) SDS-PAGE of the elution fractions of the Superdex 200-pg containing oligomeric Hsp26_{S4C/S210C}. (E) Elution profile of the ResourceQ column. (F) SDS-PAGE of selected ResourceQ fractions containing purified Hsp26_{S4C/S210C}.

relatively high mean protein concentration of ~ 2 mg/ml (Fig. 3A and B). No protein aggregation was detected when the combined were dialysed against 3 M Urea, indicating productive refolding of the Hsp26_{S4C/S210C} dimer (data not shown). To separate contaminants and degradation products from oligomeric Hsp26_{S4C/S210C}, the protein was loaded onto a Superdex 200-pg size exclusion column operating under native buffer condition, allowing oligomer reassembly. Hsp26_{S4C/S210C} eluted with a peak maximum at ~ 155 ml (Fig. 3C and D), indicative of the oligomeric state of Hsp26_{S4C/S210C}. A polishing step using a ResourceQ column removed all contaminants (Fig. 3E and F). Taken together, matrix-assisted refolding yielded high amounts of soluble Hsp26_{S4C/S210C}.

3.3. Structure and function analysis of Hsp26_{S4C/S210C}

sHsps share several key features; the most prominent one is the presence of the α -crystallin domain in the C-terminal part of the proteins. The α -crystallin domain appears to be structural conserved throughout the family of sHsps and adopts anti-parallel β -sheet structure [20,21]. Among this domain, sHsps have a mainly unstructured N-terminal region and C-terminal extension. In sHsps, the α -crystallin domain makes up the major part of the secondary structure. To test if Hsp26_{S4C/S210C} was refolded successfully using a matrix-assisted refolding approach its secondary structure was analysed by far-UV CD spectroscopy and compared to the Hsp26 wild type protein. For illustrative

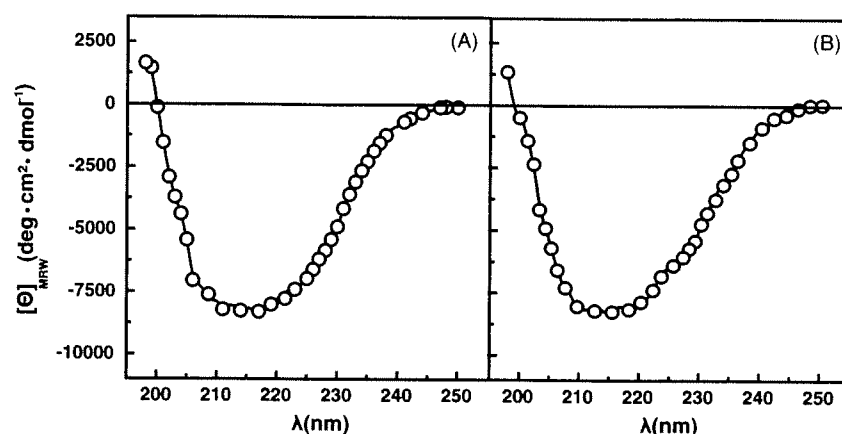


Fig. 4. Far-UV CD analysis of Hsp26_{S4C/S210C}. Far-UV CD spectra of (A) Hsp26 and (B) refolded Hsp26_{S4C/S210C} were recorded at a final concentration of 0.1 mg/ml from 250 to 198 nm in 10 mM potassium phosphate, pH 7.5 at 25 °C.

reasons, far-UV CD, analytical SEC and chaperone activity of Hsp26 wild type protein are shown, as described by Franzmann et al. [19].

Secondary structure analysis of Hsp26 by Far-UV CD spectroscopy revealed a minimum at ~214 nm with intensities of $-8500 \text{ mdeg cm}^2 \text{ dmol}^{-1}$ (Fig. 4A) [19]. About 17% α -helical content and ~45% β -sheet structure were predicted using the CDNN software [19]. The spectrum of Hsp26_{S4C/S210C} showed a minimum with intensities of $-8500 \text{ mdeg cm}^2 \text{ dmol}^{-1}$ similar to that of the wild type protein (Fig. 4B). For Hsp26_{S4C/S210C}, 16% α -helix and ~46% β -sheet content were predicted, indicating that the secondary structure of refolded Hsp26_{S4C/S210C} is comparable to that of the wild type protein.

sHsps adopt a distinct and dynamic quaternary structure. In the case of Hsp26 this oligomeric complex is composed of 24 subunits [22]. Consistent with previous studies at 25 °C, Hsp26 eluted as a single oligomer species from the analytical gel filtration column with an elution time of ~16.4 min. (Fig. 5A) [19]. To test for productive reassembly, refolded Hsp26_{S4C/S210C} was subjected to an analytical SEC. The elution

time for Hsp26_{S4C/S210C} was ~16.2 min (Fig. 5B), demonstrating that it was reassembled into a defined and stable oligomer complex.

Hsp26 is a molecular chaperone [22]. It can suppress heat- and chemical-induced aggregation of various substrates in vivo and in vitro [23,24]. Citrate synthase (CS) has been used as a model substrate to study the chaperone mechanisms of various molecular chaperones [25]. It aggregates quantitatively at temperatures above 38 °C [17] and co-incubation with Hsp26 efficiently suppresses CS aggregation and results to the formation of stable substrate complexes [24]. Equimolar concentrations reduced the aggregation signal significantly and aggregation was completely inhibited using a two-fold excess of Hsp26 (Fig. 6A) [19,22,24]. Testing Hsp26_{S4C/S210C} for chaperone activity revealed that substrate aggregation was reduced to ~50% at equimolar concentrations and completely inhibited using a two-fold excess of Hsp26_{S4C/S210C} (Fig. 6B). Taken together these results demonstrate that Hsp26_{S4C/S210C} purified from the insoluble fraction was successfully refolded using matrix-assisted refolding into its native oligomeric and chaperone-active conformation.

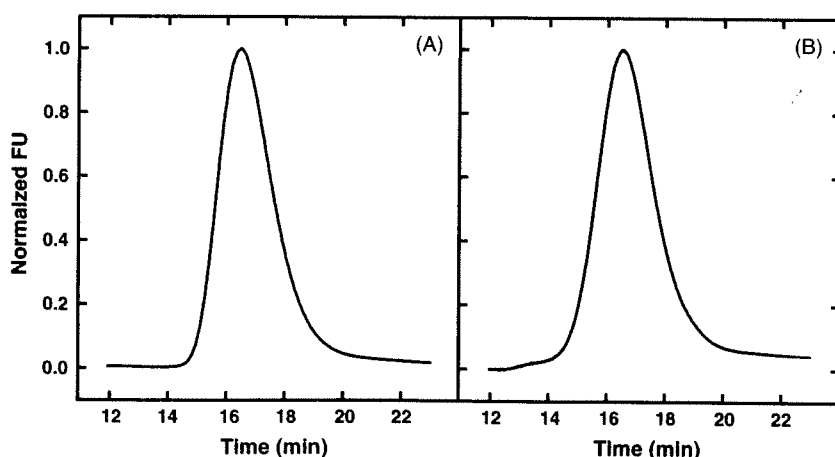


Fig. 5. Quaternary structure analysis of Hsp26_{S4C/S210C}. Analytical size exclusion chromatography was carried out using a Tosoh Biosciences TSK-G4000PW gel filtration column running in 40 mM HEPES, 150 mM KCl, pH 7.5 at 25 °C. (A) Elution profile of Hsp26 wild type protein and (B) of refolded Hsp26_{S4C/S210C}.

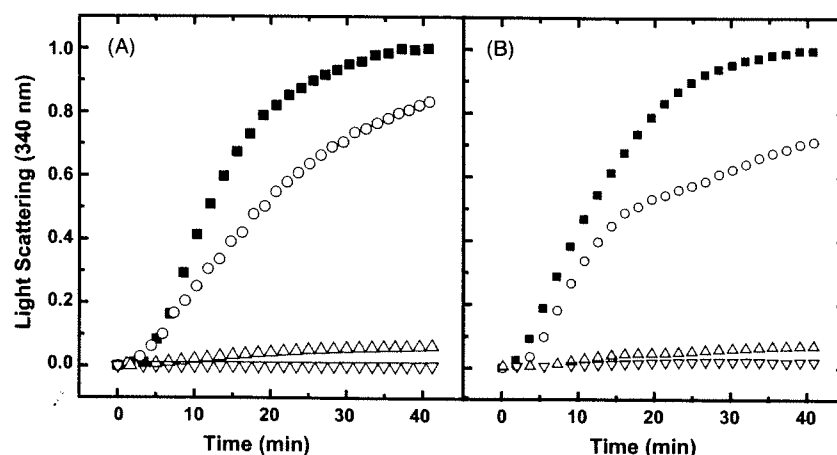


Fig. 6. Chaperone activity of Hsp26_{S4C/S210C}. Chaperone activity of refolded Hsp26_{S4C/S210C} was monitored using the CS aggregation assay. Aggregation of CS was induced by dilution to a final concentration of 1 μ M into the pre-heated cuvette at 44 °C. CS aggregation was followed at $\lambda = 340$ nm in 40 mM HEPES, pH 7.5. (A) CS aggregation in the absence (■) and presence of 1 μ M (○) and 2 μ M (△) and 4 μ M (▽) Hsp26 wild type protein. (B) CS aggregation in the absence (■) and presence of 1 μ M (○) and 2 μ M (△) and 4 μ M (▽) Hsp26_{S4C/S210C}.

4. Discussion

Protein aggregation is a frequent problem when proteins are produced at high levels in recombinant expression systems and *in vitro* protein refolding is required [8]. Typically, protein that is insoluble after protein synthesis is resolubilized using strong denaturants such as urea or guanidine and numerous strategies can be applied for purification and renaturation [26]. A prerequisite for productive protein refolding is the removal of the denaturant and the reduction of the protein concentration. Reducing the denaturant and protein concentration simultaneously by dilution often leads to productive refolding of polypeptide chains [5,10,17]. A disadvantage of this approach is the production of large reaction volume, which can be limiting and hard to handle. Especially in large scale production this procedure can exceed manageable volumes. Removal of denaturant can also be achieved by dialysis against native conditions. However, the speed of removal is limited by the diffusion of the denaturant; consequently refolding of the polypeptide chain is induced slowly and takes place at high protein concentrations facilitating irreversible protein aggregation. Another strategy to remove the denaturant is accomplished by buffer exchange while the protein remains immobilized and bound to a chromatographic matrix [12,27,28,14,29,13]. Matrix-assisted refolding of proteins offers different advantages over dilution or dialysis. The most important one is that intermolecular interactions between folding polypeptide chains are restricted. Importantly, during the initial folding process proteins expose hydrophobic surface, which supports protein aggregation. Matrix-assisted refolding reduces the entropic freedom and can therefore positively influence the folding pathway. A second advantage is that buffer exchange is quick and convenient. It can be automated for testing a variety of conditions. In the case of Hsp26_{S4C/S210C}, refolding of the stable dimer was induced by simply lowering the denaturant conditions in a step gradient. This resulted in productive folding of Hsp26_{S4C/S210C}, yet varying the gradient offers an additional option for influencing productive refolding of other proteins.

An interesting benefit of matrix-assisted refolding is the possibility to carry out multiple refolding steps sequentially, without the necessity of elution. The ionic properties of Hsp26_{S4C/S210C} were utilized to refold it by anion-exchange chromatography. Using a matrix-assisted two-step refolding strategy we were able to recover and refold Hsp26_{S4C/S210C} into its native, oligomeric and chaperone-active structure.

Acknowledgments

I thank Anja Osterauer, Bettina Richter and Helmut Krause for assistance with protein purification and mass spectrometry. Genomic DNA was a kind gift of Birgit Meinschmidt. I would also like to acknowledge Martin Hessling, Lin Römer, Otmar Hainzl and Sebastian Leptihn for discussion. I am thankful to Johannes Buchner for his support.

References

- [1] C.B. Anfinsen, *Science* 181 (1973) 223.
- [2] J. King, C. Haase-Pettingell, A.S. Robinson, M. Speed, A. Mitraki, *FASEB J.* 10 (1996) 57.
- [3] B. Bukau, E. Deuerling, C. Pfund, E.A. Craig, *Cell* 101 (2000) 119.
- [4] T. Kiefhaber, R. Rudolph, H.H. Kohler, J. Buchner, *Biotechnology (N. Y.)* 9 (1991) 825.
- [5] M.E. Goldberg, R. Rudolph, R. Jaenicke, *Biochemistry* 30 (1991) 2790.
- [6] G. Zettlmeissl, R. Rudolph, R. Jaenicke, *Biochemistry* 18 (1979) 5567.
- [7] F.A. Marston, *Biochem. J.* 240 (1986) 1.
- [8] R. Rudolph, H. Lilie, *FASEB J.* 10 (1996) 49.
- [9] M. Mayer, J. Buchner, *Meth. Mol. Med.* 94 (2004) 239.
- [10] De Bernardes, E. Clark, E. Schwarz, R. Rudolph, *Meth. Enzymol.* 309 (1999) 217.
- [11] M. Mayer, J. Buchner, *Meth. Mol. Med.* 94 (2004) 239.
- [12] Y. Berdichevsky, R. Lamed, D. Frenkel, U. Gophna, E.A. Bayer, S. Yaron, Y. Shoham, I. Benhar, *Protein Expr. Purif.* 17 (1999) 249.
- [13] J. Zouhar, E. Nanak, B. Brzobohaty, *Protein Expr. Purif.* 17 (1999) 153.
- [14] D.K. Saini, N. Pant, T.K. Das, J.S. Tyagi, *Protein Expr. Purif.* 25 (2002) 203.
- [15] G. Stempfer, B. Holl-Neugebauer, E. Kopetzki, R. Rudolph, *Nat. Biotechnol.* 14 (1996) 481.

- [16] G. Bohm, R. Muhr, R. Jaenicke, *Protein Eng.* 5 (1992) 191.
- [17] T. Kiefhaber, R. Rudolph, H.H. Kohler, J. Buchner, *Nat. Biotechnol.* 9 (1991) 825.
- [18] J. Buchner, H. Grallert, U. Jakob, *Meth. Enzymol.* 290 (1998) 323.
- [19] T.M. Franzmann, M. Wuhr, K. Richter, S. Walter, J. Buchner, *J. Mol. Biol.* 350 (2005) 1083.
- [20] K.K. Kim, R. Kim, S.H. Kim, *Nature* 394 (1998) 595.
- [21] R.L. van Montfort, E. Basha, K.L. Friedrich, C. Slingsby, E. Vierling, *Nat. Struct. Biol.* 8 (2001) 1025.
- [22] M. Haslbeck, S. Walke, T. Stromer, M. Ehrnsperger, H.E. White, S. Chen, H.R. Saibil, J. Buchner, *EMBO J.* 18 (1999) 6744.
- [23] M. Haslbeck, N. Braun, T. Stromer, B. Richter, N. Model, S. Weinkauff, J. Buchner, *EMBO J.* 23 (2004) 638.
- [24] T. Stromer, M. Ehrnsperger, M. Gaestel, J. Buchner, *J. Biol. Chem.* (2003).
- [25] H. Grallert, K. Rutkat, J. Buchner, *J. Biol. Chem.* 273 (1998) 33305.
- [26] R. Rudolph, G. Zettlmeissl, R. Jaenicke, *Biochemistry* 18 (1979) 5572.
- [27] C. Machold, R. Schlegl, W. Buchinger, A. Jungbauer, *J. Chromatogr. A* 1080 (2005) 29.
- [28] C. Machold, R. Schlegl, W. Buchinger, A. Jungbauer, *J. Biotechnol.* 117 (2005) 83.
- [29] R. Schlegl, G. Iberer, C. Machold, R. Necina, A. Jungbauer, *J. Chromatogr. A* 1009 (2003) 119.

Multiple Distinct Assemblies Reveal Conformational Flexibility in the Small Heat Shock Protein Hsp26

Helen E. White,¹ Elena V. Orlova,¹ Shaoxia Chen,^{1,4}
Luchun Wang,¹ Athanasios Ignatiou,¹ Brent Gowen,^{2,5}
Thusnelda Stromer,^{3,6} Titus M. Franzmann,³
Martin Haslbeck,³ Johannes Buchner,³
and Helen R. Saibil^{1,*}

¹Department of Crystallography
Birkbeck College
London WC1E 7HX
United Kingdom

²Department of Biological Sciences
Imperial College of Science, Technology and Medicine
London SW7 2AY
United Kingdom

³Department Chemie
Technische Universität
85747 Garching
München
Germany

Summary

Small heat shock proteins are a superfamily of molecular chaperones that suppress protein aggregation and provide protection from cell stress. A key issue for understanding their action is to define the interactions of subunit domains in these oligomeric assemblies. Cryo-electron microscopy of yeast Hsp26 reveals two distinct forms, each comprising 24 subunits arranged in a porous shell with tetrahedral symmetry. The subunits form elongated, asymmetric dimers that assemble via trimeric contacts. Modifications of both termini cause rearrangements that yield a further four assemblies. Each subunit contains an N-terminal region, a globular middle domain, the α -crystallin domain, and a C-terminal tail. Twelve of the C termini form 3-fold assembly contacts which are inserted into the interior of the shell, while the other 12 C termini form contacts on the surface. Hinge points between the domains allow a variety of assembly contacts, providing the flexibility required for formation of supercomplexes with nonnative proteins.

Introduction

The small heat shock proteins (sHsps) are thought to play a buffering role in preventing aggregation of nonnative proteins by binding them in stable complexes (Haslbeck, 2002; Narberhaus, 2002; van Montfort et al., 2002; Horwitz, 2003; Kappe et al., 2003; Haslbeck et al., 2005a). In the vertebrate eye lens, the small Hsp α -crystallin seems to be crucial for preventing aggregation that

would lead to cataract formation (Brady et al., 1997). In more dynamic tissues, the bound substrate proteins can eventually be released for refolding in cooperation with other chaperones such as the Hsp70 or Hsp100 systems (Veinger et al., 1998; Mogk et al., 2003; Cashikar et al., 2005; Haslbeck et al., 2005b; Lee et al., 2005). The mechanisms of substrate recognition and binding by small Hsps are still poorly understood.

sHsps share a conserved α -crystallin domain and a moderately conserved C terminus and have variable N-terminal regions, shown schematically in Figure 1. Crystal structures have been determined for archaeal (*M. jannaschii* Hsp16.5; Kim et al., 1998), plant (wheat Hsp16.9; van Montfort et al., 2001), and animal (tapeworm Tsp36; Stamler et al., 2005) sHsps. They show a β sandwich fold for the α -crystallin domain. The archaeal and plant α -crystallin domains are arranged as brick-shaped dimers linked by β strand exchange. In the archaeal structure, 12 of these dimers are arranged in a shell with octahedral symmetry (Kim et al., 1998). The small N-terminal domain of *M. jannaschii* Hsp16.5 is disordered and not seen in the crystal structure, but electron microscopy (EM) and spectroscopic data show that it is located inside the shell (Koteiche et al., 2005). The shell is held together by hydrophobic contacts between extended C-terminal tails and the adjacent α -crystallin domain dimers, and possibly by additional N-terminal contacts. In the wheat small Hsp, six α -crystallin domain dimers are arranged in two stacked rings of three dimers each (van Montfort et al., 2001). Half of the subunits have ordered N-terminal domains, with α -helical structure. These are essential, together with the C-terminal tail, for assembly of the dodecamer with D3 symmetry. In Acr1 (Hsp16.3) from *M. tuberculosis* (Kennaway et al., 2005), the 12 subunits are arranged in a hollow tetrahedral structure with disordered N domains that are probably located on the inner surface of the shell. In the plant, archaeal, and most likely mycobacterial (Acr1) sHsps, a conserved IXI motif on the C-terminal tail interacts with a hydrophobic region on an adjacent α -crystallin domain. EM studies of other sHsps show that their oligomeric structures are usually assembled as spherical shells or stacked rings of oligomers and that these are often polydisperse and poorly ordered (Lee et al., 1997; Haley et al., 1998, 2000; Bova et al., 2000; Stromer et al., 2003).

Hsp26, one of the two sHsps from yeast, forms well-defined 24-mers which are reversibly activated to bind nonnative substrate proteins at elevated temperatures (Haslbeck et al., 1999). A temperature-induced conformational change is necessary for substrate binding (Franzmann et al., 2005). The other small heat shock protein in the yeast cytosol, Hsp42, acts as a chaperone at normal and heat shock temperatures (Haslbeck et al., 2004a). Both are able to suppress aggregation of a variety of substrate proteins from different biochemical pathways in vivo and in vitro, suggesting that they have nonspecific binding properties. Deletion of Hsp26 or Hsp42 causes an abnormal cell shape phenotype in yeast (Haslbeck et al., 2004a).

*Correspondence: h.saibil@mail.cryst.bbk.ac.uk

⁴Present address: MRC Laboratory of Molecular Biology, Hills Road, Cambridge CB2 2QH, United Kingdom.

⁵Present address: Department of Biology, University of Victoria, Victoria, British Columbia V8W 3N5, Canada.

⁶Present address: TF Instruments GmbH, Im Neuenheimer Feld 515, 69120, Heidelberg, Germany.

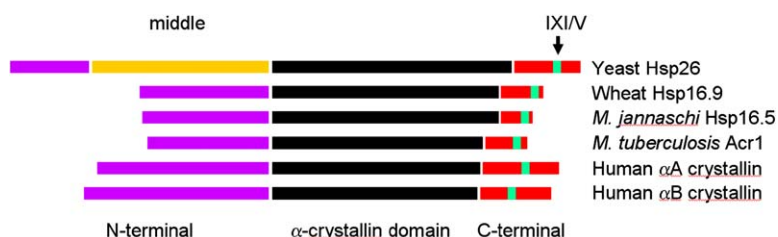


Figure 1. Domain Layout of Small Hsps

Sequence diagram of yeast Hsp26, archaeal Hsp16.5, plant Hsp16.9, *M. tuberculosis* Acr1, and α A and α B crystallins. The α -crystallin domain is highly conserved, but the N-terminal regions are variable. The location of the IXI or IXV sequence in the C terminus is indicated by the green bars.

Apart from Tsp36, little is known about the structure and function of N-terminal domains of small Hsps, which are very variable in size and sequence, as reflected in the subunit size variation of 16–40 kDa. Recent results suggest that the N-terminal region is involved in substrate binding (Giese et al., 2005). Hsp26 has a particularly large N-terminal region (residues 1–95), which appears to be subdivided into at least two domains by a short glycine-rich region at residues 25–31. A deletion variant lacking the first 30 residues, Hsp26 Δ N1-30 (Δ N30), forms destabilized oligomers and exhibits limited chaperone activity. Its complexes with nonnative protein are less stable than those of full-length Hsp26 (Haslbeck et al., 2004b). However, deletion of residues 1–95 produces dimers devoid of chaperone activity, indicating that residues 31–95 form a domain that is essential for oligomerization and chaperone activity (Stromer et al., 2004).

Here we present the cryo-EM structure of Hsp26. Our analysis resolves four distinct domains linked by flexible hinge regions in the Hsp26 monomer: N terminus, middle domain, α -crystallin domain, and C-terminal tail. Elongated dimeric units assemble into compact and expanded forms of a porous shell structure with assembly contacts made by the termini. Six different three-dimensional (3D) structures of Hsp26 oligomers of wild-type (wt) and N- and C-terminally modified forms reveal a remarkable degree of flexibility in the oligomeric assembly.

Results

Flexible Assembly of Hsp26

Raw cryo-EM images of wt Hsp26 showed round, oligomeric particles of apparently uniform size (Figure 2A), but subsequent image processing revealed the presence of two distinct populations. The structures are termed “compact” and “expanded”; they turned out to be only 5% different in external diameter but differed in their internal organization. Examples of averaged views of compact and expanded structures are shown in Figures 2B and 2C, including examples of their characteristic 2- and 3-fold symmetries. Both structures were found to have tetrahedral symmetry, as explained in the Experimental Procedures. Once we had two 3D models, the separation was refined by projection matching to both models. Classification of all images according to size variations led to a further improved separation into compact and expanded classes and ultimately to a successful refinement of both structures (Figures 2D and 2E). The resolution of the maps is \sim 11.0 Å at 0.5 Fourier shell correlation (Figure S1; see the Supplemental Data available with this article online). A larger set of class averages, with their corresponding reprojections, are shown in Figure S2. Because the structures

are so similar (diameters \sim 190 and 200 Å), the resolution is probably limited by our ability to sort the individual raw images into the correct structure and/or by the presence of intermediate structures.

The Hsp26 oligomers are formed of 12 elongated rods of density assembled into round, shell-like structures with holes of up to 40 Å (Figures 2D and 2E). The main structural element of the shell is an elongated, roughly dumbbell-shaped rod of density. The compact and expanded forms have a similar layout of their shells, but they differ significantly in their internal density arrangement. In the compact assembly, there is a single, central mass of density inside the shell (Figure 2F). In the expanded assembly, there are four densities inserted inside the shell, separated by a gap at the center (Figure 2G). Each of these inserted densities is a trimeric unit at a 3-fold position below an open region in the shell, connected by thin stalks to three equivalent shell regions. Only four of the eight 3-fold positions show this inserted density. The opposite four 3-folds are closed by additional density at the surface.

Tetrahedral Structures of the Δ N30 Variants

In order to determine the location of the N-terminal extension (residues 1–30) in the assembly, we performed a cryo-EM single particle analysis of the Δ N30 variant. The data set again revealed compact and expanded forms.

Example class averages of the Δ N30 maps with their corresponding reprojections are shown in Figures 3A and 3B. The compact structure has a similar size and surface arrangement to those of the compact wt form, but the inserted densities are separated as in the expanded wt structure (Figure 3C), possibly due to small changes in the angles of the surface domains. Unexpectedly, the expanded Δ N30 form showed completely different surface packing (Figure 3D). Since both structures have inserted domains, these domains cannot be formed by the N-terminal 30 residues of Hsp26. The resolution of the Δ N30 maps is \sim 14.2 Å at 0.5 Fourier shell correlation for the compact map and 14.5 Å for the expanded map.

We also examined the C-terminally His-tagged Δ N30 variant (Δ N30his), which gave the possibility of using the His-tag as a label for the C terminus. A set of class averages with their corresponding reprojections of the Δ N30his maps is shown in Figures 3E and 3F. Again, a compact form similar to the Δ N30 compact form was observed (Figure 3G) along with a different expanded assembly (Figure 3H). The inserted domains are present, but they are in different positions in the expanded form of the Δ N30his variant (Figure 3H). The expanded structures for both Δ N30 and Δ N30his variants have adopted new conformations. In the Δ N30his expanded variant (Figure 3H), some of the surface domains are located

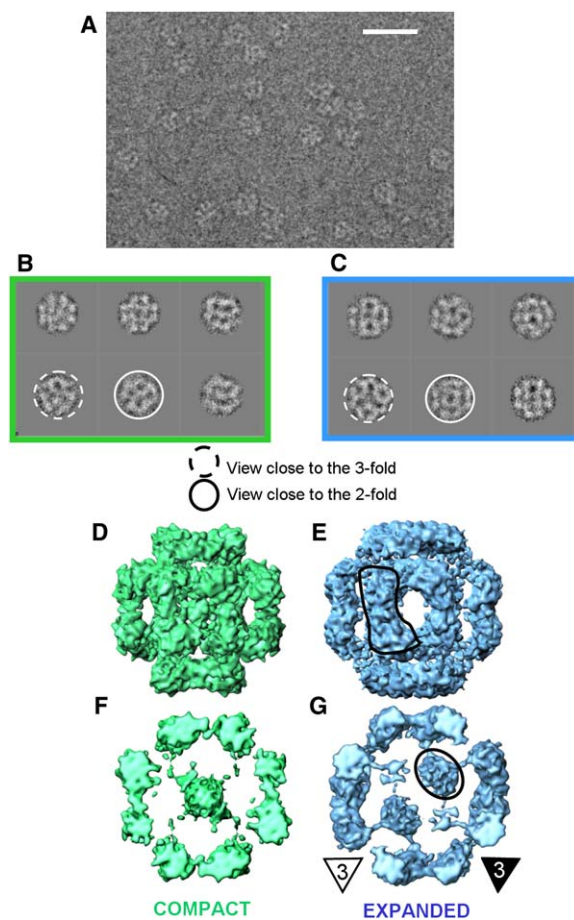


Figure 2. Structure Determination

(A) Cryo-EM image of wt Hsp26 complexes. In the raw images, it is impossible to discern which particles belong to the compact and expanded classes. Protein density is displayed as white. Scale bar, 500 Å.

(B and C) Examples of averaged views of the compact and expanded assemblies, after alignment and classification. Views along the symmetry directions are indicated. Resolution curves and a larger set of class averages, along with the corresponding reprojections of the 3D structures, are provided as [Supplemental Data \(Figures S1 and S2\)](#).

(D and E) Surface rendered views of the compact (green) and expanded (blue) maps of wt Hsp26. One surface assembly unit is outlined on (E).

(F and G) Sliced open views of the compact and expanded maps, showing the inserted densities. One of the four densities is circled in (G), and examples of an open and a closed 3-fold position are shown by open and closed triangles. There is additional density at the surface of the closed 3-folds. The 3D maps were rendered in Iris Explorer (NAG).

partly inside the shell. The resolution of the Δ N30his maps is ~ 12.6 Å at 0.5 Fourier shell correlation for the compact map and 14.5 Å for the expanded map.

Multiple Assemblies of the α -Crystallin Framework

For atomic structure docking, a homology model of the α -crystallin domain for yeast Hsp26 was built from the related archaeal and plant structures (36% identity to wheat Hsp16.9 and 23% identity to the archaeal Hsp16.5). No homologous structures were found for the N-terminal region by the sequence comparison

programs BLASTP (Altschul et al., 1997) and FASTA (Pearson, 1990). The α -crystallin domain dimer of wheat Hsp16.9 (Protein Data Bank code 1GME) was used to examine manually how it could fit into the wt maps. The elongated shape of the Hsp26 dimer and the tetrahedral symmetry of the assemblies restrict its possible location in each map to the extended region of density. Automated docking with URO (Navaza et al., 2000) gave a similar fit for both compact and expanded maps, leaving a region of unfilled density at either end of the α -crystallin domain dimer (Figures 4A–4D). The unfilled volumes are sufficient to accommodate structures containing most of the N-terminal residues in each of the two subunits. The use of threading programs suggested that an SH3-like fold could be formed by residues 30–82. This density is adjacent to the α -crystallin domain, so that the building block of the shell is a brick-shaped α -crystallin domain dimer, flanked by globular middle domains. Although the fold of the middle domain is unknown, the positions of these domains were approximated by using SH3 domains as models for fitting with URO. However, the positions of the α -crystallin domain dimers were not affected by the use of the SH3 model, which only serves as a place marker for the unknown middle domain.

The same approach was used for fitting the α -crystallin domain dimer and model SH3 domains into each of the variant maps. In the compact structures there was only one region where the α -crystallin dimer could be manually fitted (Figures 4E, 4F, 4I, and 4J). These were refined with URO. For both expanded variant maps, the α -crystallin dimer could be manually fitted in more than one location. Some positions were excluded on the basis of symmetry clashes when a complete 24-mer was generated. The remaining solutions were refined in URO and excluded if they showed symmetry clashes, poor match to the density for the α -crystallin domain dimer, or failure to converge in refinement (Figures S3 and S4). This led to one solution for each expanded variant (Figures 4G, 4H, 4K, and 4L).

The hand shown for the maps was chosen because it gave more consistent results for domain fitting with URO to the compact and expanded wt structures. With the other choice of hand, there were more differences between the fits to the two wt structures. In any case, the conclusions about domain structure and assembly contacts are not affected by the choice of hand in the maps.

Domain Rearrangements

In order to analyze the domain rearrangements in the different forms, we superposed low-resolution models of the subunit domains in the different assemblies (Figure 5). The fitted α -crystallin domain dimers are shown as smooth rods, and the middle domains (fitted SH3 positions) are represented as spheres. In the compact forms of Hsp26, the α -crystallin domain dimers of the wt (mid-green), Δ N30 (cyan), and Δ N30his (dark green) occupy very similar positions (Figure 5A). However, removal of the N terminus and addition of the His-tag result in dramatic rearrangements of subunit packing in the expanded variant forms (Figure 5B; wt, blue; Δ N30, light blue; Δ N30his, purple). Comparison of middle domain positions shows that the truncation causes the middle domains to move in toward the closed 3-fold

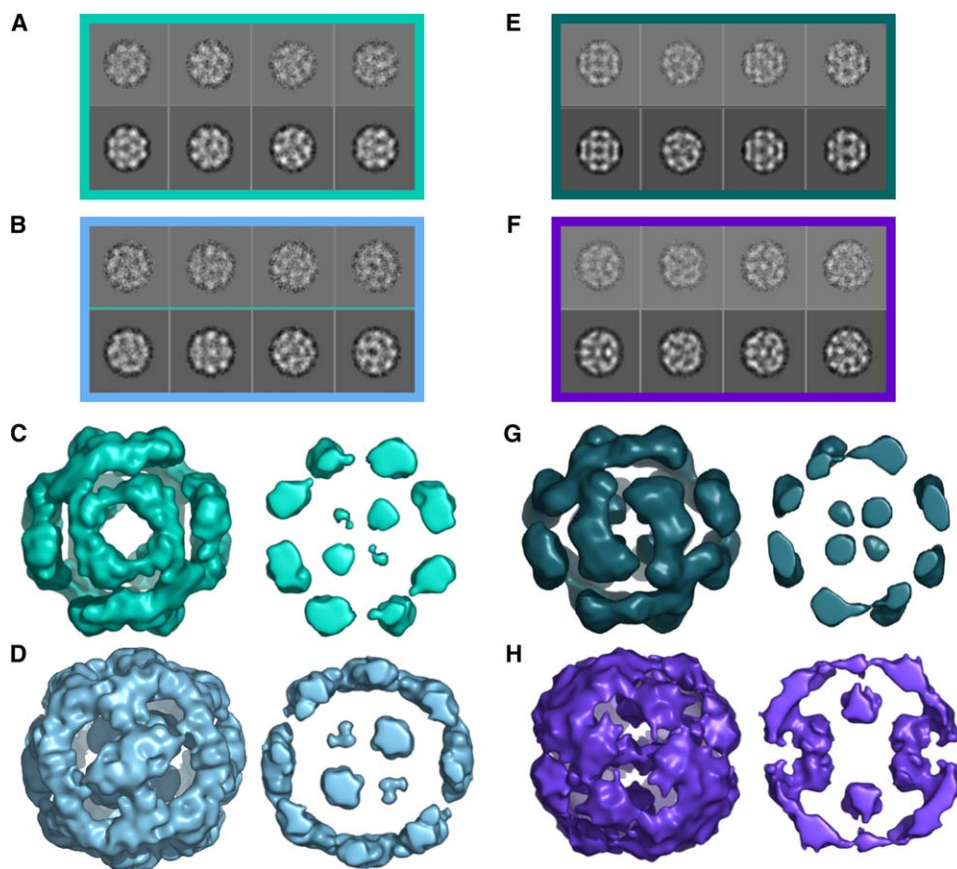


Figure 3. 3D Structures of Hsp26 Δ N30 Variant Complexes

(A) Δ N30 compact class averages (top) and reprojections (bottom).
 (B) Δ N30 expanded class averages (top) and reprojections (bottom).
 (C) 2-fold view and slice of Δ N30 compact (cyan).
 (D) Equivalent views of Δ N30 expanded (blue) maps.
 (E) Δ N30his compact class averages (top) and reprojections (bottom).
 (F) Δ N30his expanded class averages (top) and reprojections (bottom).
 (G) 2-fold view and slice of Δ N30his compact (dark green).
 (H) Δ N30his expanded (purple) maps.

This figure and all subsequent ones were produced with PyMOL (www.pymol.org).

and addition of the C-terminal His tag causes a further rotation of the middle domains (curved arrows, Figure 5).

We attempted to use gold labeling of cysteine mutants of Hsp26 to localize the termini in the oligomers. However, modification of either terminus by site-directed gold labeling of the mutants S4C and S210C resulted in even greater conformational variations. Nanogold labeling of the S4C mutant (Franzmann et al., 2005) produced oligomeric structures, but MSA analysis indicated that they had a different conformation to the wt or the Δ N30 variants (Figure S5A). Gold labeling at the C terminus (S210C) produced particles ranging in diameter from 90 to 200 Å (Figure S5B). It was therefore not possible to use these gold labels to determine the position of the N- and C termini by difference mapping of the six structures described here.

Difference Mapping of the N- and C-Terminal Regions

The terminal regions of Hsp26 subunits can be localized by comparison of the series of compact structures, since they are similar enough in structure to give inter-

pretable difference maps. The main effect of deleting residues 1–30, shown in difference maps of the full-length and Δ N30 compact structures, is a loss of density adjacent to the middle domains, indicating that the N-terminal extensions are located at the ends of the dimers around the 3-fold positions (Figure S6A). As mentioned above, the presence of the four inserted densities in the compact Δ N30 assembly shows that they are not formed by the N-terminal region. They adopt the same arrangement as in the wt expanded form and must be formed by a terminus of the protein chain, since they are connected to the shell by a thin extension that would only accommodate a single, connecting stretch of polypeptide chain. The difference between Δ N30his and Δ N30 variant maps shows the effect on the density of adding the C-terminal His tag (Figure S6B). In the His-tagged form, there has been some rearrangement of density at the closed 3-fold, indicating the likely involvement of 12 His-tagged C-terminal tails in this region, possibly in close proximity to the N termini. The larger inserted densities in the compact His-tagged structure are consistent with the notion that they are formed by

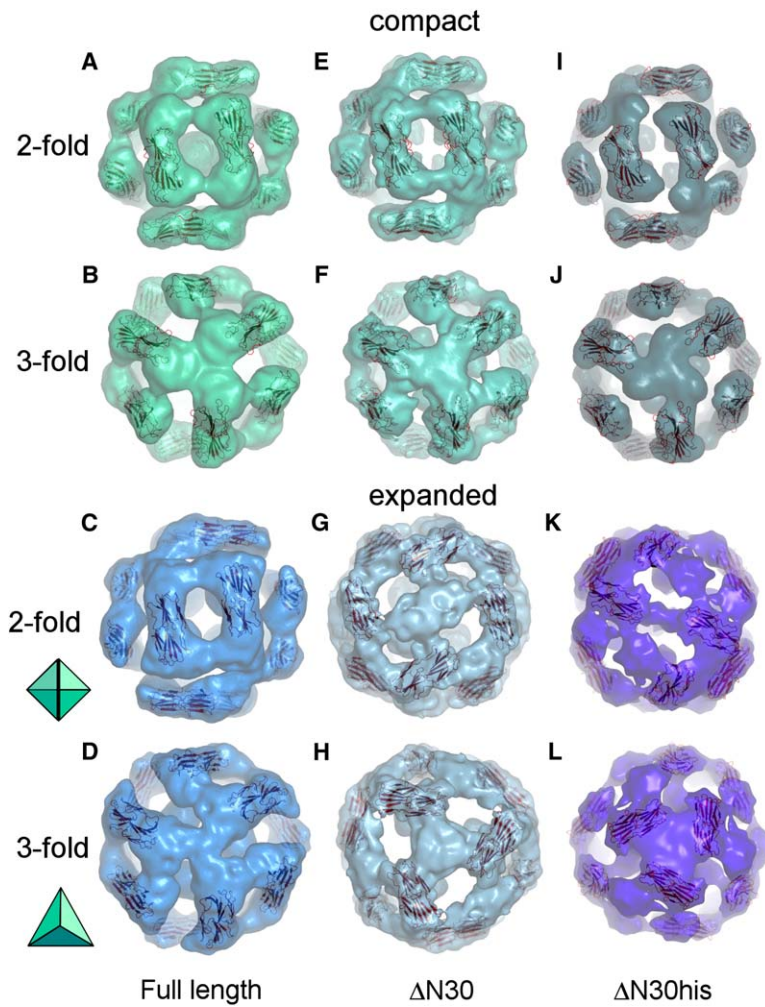


Figure 4. 2-Fold and 3-Fold Views of Hsp26 Oligomers with Fitted α -Crystallin Domain Dimers

(A and B) Views of wt Hsp26 compact structure (green).
(C and D) Expanded wt structure (blue).
(E and F) Compact Δ N30 structure (cyan).
(G and H) Expanded Δ N30 structure (pale blue).
(I and J) Compact Δ N30his structure (dark green).
(K and L) Expanded Δ N30his structure (purple).
Tetrahedra are shown in 2-fold and 3-fold views.

the other 12 C termini. The volumes of the inserted densities are compatible with trimers of C-terminal tails (3×24 residues) allowing for an extended region connecting the inserted domains to the α -crystallin domains in the shell.

Domain Assignments and Assembly Contacts

The overall organization revealed by the cryo-EM and domain fitting suggests that the α -crystallin domain dimers are assembled into 24-mers by 3-fold contacts involving both termini as well as the globular middle

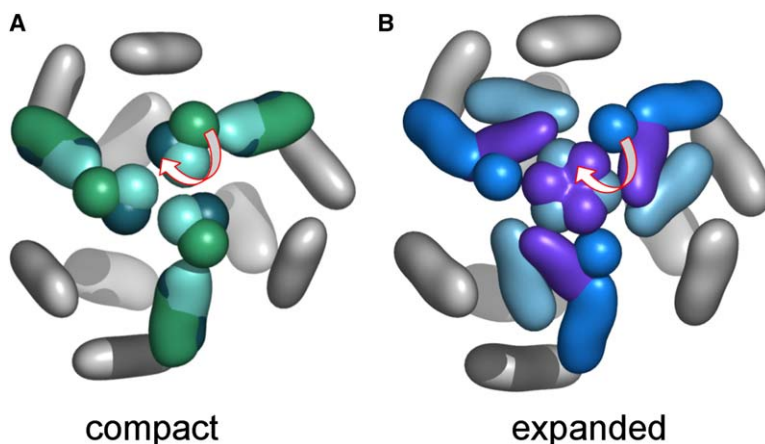


Figure 5. Overlays of Model Domain Densities in the Compact and Expanded Structures

Three-fold views of the fitted α -crystallin domain densities shown as smooth rods and the globular domains represented as spheres, overlaid for the compact (A) and expanded (B) Hsp26 structures. A set of α -crystallin domain dimers and middle domains are superposed in different colors around one 3-fold axis, with the remaining wt α -crystallin domain dimers shown in gray. (A) Wt (mid-green), Δ N30 (cyan), and Δ N30his (dark green) compact structures. The overlay shows that the α -crystallin domains have very similar positions in all three compact structures. Truncation of the N terminus causes the globular domains to move in toward the 3-fold axis, and addition of the His tag causes a further twist of their positions

(curved arrow). (B) Wt (blue) structure, Δ N30 (pale blue), and Δ N30his (purple) expanded structures. This overlay shows a dramatic rearrangement of α -crystallin domains caused by deletion of the N terminus (blue to light blue) and a smaller shift and rotation after tagging the C terminus (light blue to purple). The globular domains move in toward the 3-fold axis and rotate in a similar pattern as for the compact structures (curved arrow).

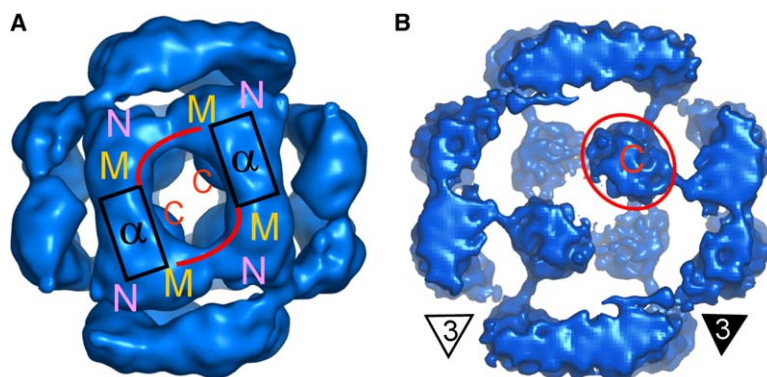


Figure 6. Location of the Domains in Hsp26

(A) Location of the N-terminal region ("N"), the middle globular domain ("M"), the α -crystallin domain (" α "), and the surface C-terminal tails ("C").

(B) Location of the inserted C-terminal trimers. The map in (A) has been smoothed for clarity.

domain. The domain layout is shown for two dimers of the wt expanded form in Figure 6. For the 12 C termini that remain in the outer shell, the length is sufficient for them to form a contact with the globular domain of the adjacent dimer related by the 2-fold symmetry (red curved line, Figure 6A). However, they are not long enough to reach the hydrophobic patch on the adjacent α -crystallin domain, which is ~ 60 Å distant. The other 12 C termini form the novel, trimeric insertions, one of which is circled in Figure 6B, in which the open and closed 3-fold positions are also indicated.

Discussion

In terms of methodology, this work addresses a common and important problem—the separation of mixed complexes. Many interesting biological samples contain mixtures of similar structures in different, functionally important states. In this case, the two wt forms of Hsp26 have the same subunit number and symmetry; they differ mainly in the packing of internal domains. They are almost identical in external diameters and features, and their separation required the development of new strategies for image processing (White et al., 2004). The variant forms also have the same symmetry, but they vary in their arrangement of subunits.

Assembly Contacts

Wt yeast Hsp26 assembles into 24-mers with tetrahedral symmetry. Each subunit has four domains: the N-terminal extension, a globular middle domain, the α -crystallin domain, and the C-terminal tail. The C terminus forms surface contacts at the closed 3-fold positions and inserted densities at the open 3-folds (Figure 6). A dimer of the α -crystallin and globular middle domains together forms a dumbbell-shaped unit constituting the bulk of the shell with the termini assembling the dimers into tetrahedral shells by trimeric contacts. One set of C termini penetrates inside the shell to form the inserted densities. The N-terminal domains are located around the 3-fold positions, and the observation that they can be cross-linked in the S4C mutant (Franzmann et al., 2005) supports the idea that they form 3-fold contacts. Their deletion destabilizes but does not abolish assembly (Haslbeck et al., 2004b). Modifications of the termini, as shown by the truncation, His-tagging, and gold labeling experiments, produce a variety of altered assemblies. However, deletion of both N-terminal and middle

globular domains ($\Delta 1-95$) results in dimers but not higher oligomers (Haslbeck et al., 2004b), showing that the globular middle domain of Hsp26 is essential for oligomeric assembly (Stromer et al., 2004).

In yeast Hsp26, the α -crystallin domain dimers are quite spaced out, with 40–50 Å gaps, unlike the case in the archaeal 24-mer and plant dodecamer in which the α -crystallin domain dimers are in direct contact through their C-terminal tails (Kim et al., 1998; van Montfort et al., 2001). The C-terminal tail forms a bridge between adjacent α -crystallin domain dimers in the archaeal and plant Hsp crystal structures (Kim et al., 1998; van Montfort et al., 2001). In the worm sHsp, the C-terminal tail is absent, and the hydrophobic region on the α -crystallin domain interacts with an IXI sequence in the N terminus (Stamler et al., 2005). In Hsp26, the C-terminal tail is partly conserved, with an IXV sequence. Because the α -crystallin domain dimers are so far apart in the large Hsp26 oligomers, this C-terminal tail cannot contact an adjacent α -crystallin domain in Hsp26. Our results suggest that it instead forms novel contacts in the inserted trimerization domains and with the middle domain (Figure 6).

Potential Chaperone Binding Sites

The effects of N-terminal and middle domain deletions on assembly are mirrored in their effects on chaperone activity. $\Delta N30$ shows some loss of stability of complexes with denatured proteins, but the deletion $\Delta 1-95$ abolishes chaperone activity, again showing that the middle domain is essential for this activity (Stromer et al., 2004). A temperature-induced conformational change is required for chaperone activity of Hsp26 (Haslbeck et al., 2004b; Franzmann et al., 2005). The N-terminally cross-linked variant is active in the oligomeric state (Franzmann et al., 2005), suggesting that there is a temperature-induced conformational change that exposes substrate binding sites. The N-terminal domain may provide unstructured regions with hydrophobic binding sites to form the large complexes observed with denatured substrates (Haslbeck et al., 1999; Stromer et al., 2003). The N-terminal region contains three occurrences of pairs of hydrophobic residues: phenylalanines at positions 6, 7, 9 and 10 and leucines at 23 and 24. It is clear in this case that the oligomeric assembly does not act as a protein binding cage, like for example the GroEL-GroES chaperonin system, since the internal cavity is occluded by the inserted domains. Binding of substrate

protein seems to further alter the domain arrangement, since the substrate complexes form much larger, heterogeneous assemblies which appear different in structure (Haslbeck et al., 1999).

In conclusion, the flexible, four-domain arrangement in an open shell assembly and exposure of potential binding sites by heating is likely to underlie the ability of Hsp26 to form extremely adaptable, large complexes with a wide variety of denatured substrate proteins (Stromer et al., 2003). The compact and expanded forms of the oligomer differ slightly in the hinge angles between subunit domains. In the compact form, the more central position of the inserted density means that the connecting region must be more extended, and the volume of the inserted domain is correspondingly less. The remarkable diversity in subunit assembly may provide a model for the polydispersity of other sHsp family members, including α -crystallin itself, but in this case there is a set of distinct, symmetrical assemblies.

Experimental Procedures

Sample Preparation

The yeast overexpressing strain was a kind gift from Dr S Lindquist, Whitehead Institute. Hsp26 and the Δ N30 variant were expressed and purified as described by Haslbeck et al. (1999). The Δ N30 variant with a C-terminal His-tag (GSRGHHHHH) was prepared by the protocol of Haslbeck et al. (2004b).

Electron Microscopy

The Hsp26 preparation, at 1 mg/ml in 40 mM HEPES, 50 mM NaCl, 2 mM EDTA, 1 mM DTT (pH 7.4) was vitrified on holey carbon grids, and low-dose images were collected on an FEI 200 kV FEG microscope at 38,000 \times magnification and digitized on a Zeiss SCAI scanner at a sampling of 1.86 Å/pixel at the specimen level (Figure 2A). The defocus ranged from 2 to 4 μ m. The microscope magnification was calibrated by comparisons of EM maps with known atomic structures. Cryo-electron micrographs for the Δ N30 variant (0.7–1 mg/ml in 20 mM HEPES/KOH, 50 mM KCl, 5 mM EDTA, 1 mM DTT [pH 7.5]) and the Δ N30his variant (1.3 mg/ml in 40 mM HEPES/KOH, 50 mM NaCl [pH 7.4]) were collected on a FEI 200 kV FEG microscope at 50,000 \times magnification and digitized on a Zeiss SCAI scanner at a sampling of 1.4 Å/pixel at the specimen level. The defocus ranged from 1.7 to 3.4 μ m.

Image Processing

A data set of ~15,000 images of Hsp26 was obtained from a total of 21 negatives. The defocuses were determined with the MRC program CTFIND2 and checked by comparison with theoretical curves in Imagic (van Heel et al., 1996). The images were corrected for the effects of the contrast transfer function by phase flipping. A high pass filter with a cut-off frequency related to the defocus of each negative was applied to make the weight of low frequencies the same in all images, after which the particle images were treated as a single data set. The assignment of individual images as expanded or compact was started by the recognition of a few classes, including 2-fold and 3-fold views, belonging to an expanded, tetrahedrally symmetric form. The observation of 2- and 3-fold views, combined with the knowledge that the structure is formed of 24 subunits in 12 dimers, is compatible with cubic, tetrahedral, and D3 point group symmetries. The only symmetry that ultimately gave consistent results, compatible with all views, was tetrahedral. Because the views of the expanded structure and its symmetry were most recognizable, it was reconstructed first. Image classes that appeared smaller and inconsistent with the expanded structure were initially assigned to the compact structure and were subjected to a separate structural analysis. Eventually, the images were sorted into expanded and compact structures by a combination of multivariate statistical analysis (MSA) and projection matching, using Imagic (van Heel et al., 1996). The 3D structures were separately determined for each group by angular reconstitution. The two 3D maps were then

used to refine the separation of the data set into the two forms by projection matching. The final data set for the compact structure had 5,000 images in 770 classes, and that for the expanded data set had 10,000 images grouped into 1300 classes. A general strategy for separation and refinement of structures of mixed size has been formulated (White et al., 2004). Reconstruction was done using the exact filter back projection algorithm in Imagic. Docking of atomic coordinates into the maps was done by density correlation, either in real space (DockEM; Roseman, 2000) or reciprocal space (URO; Navaza et al., 2000). A band pass filter from 25 Å to 6 Å was applied to both expanded and compact maps, enhancing components in that spatial frequency range by a factor of 7.5.

A data set of ~6000 images was obtained for the Δ N30 variant from 68 negatives, and one of ~6300 images was obtained from 48 negatives for the Δ N30his variant. These data sets were processed according to the same protocol as the wt, and compact and expanded forms were found in both. For the Δ N30 variant, 4300 images in the data set of the compact form were grouped into 625 classes while the 1600 images in the data set of the expanded form of the Δ N30 variant were grouped into 230 classes. For the Δ N30his variant, a data set of 4000 images of the compact form was grouped into 580 classes, and a data set of 2100 images for the expanded form was grouped into 300 classes.

Filters were designed to scale the maps to similar rotational power spectra. Maps were binarized at a density level corresponding to the molecular volume before difference maps were calculated between the three different compact structures.

Bioinformatics

The N-terminal half of the Hsp26 sequence was searched with psiblast (Altschul et al., 1997) but did not reveal any homologies to known structures. Once a potential domain boundary was identified within the N-terminal region (at residues 25–28), five different threading programs (123D+, Alexandrov et al., 1995; Predict Protein, Rost et al., 2004; Phyre, Kelley et al., 2000; Bioinbgu, Fischer, 2000; and Fugue, Shi et al., 2001) were used to search the putative middle domain sequence (residues 29–82).

Supplemental Data

Supplemental data, including six figures, are available with this article online at <http://www.structure.org/cgi/content/full/14/7/1197/DC1/>.

Acknowledgments

We thank Kerstin Kienlein for initial experiments, Christine Slingsby for helpful discussion at all stages of the work, Jorge Navaza and Alan Roseman for help with docking programs, Marketa Zvelebil for help with the threading analysis, Andrea Musacchio for helpful advice on SH3 domains, Nick Keep for comments on the manuscript, and Richard Westlake, David Houldershaw, and Steve Terrill for excellent computing support. This work was supported by grants from the BBSRC to H.R.S. and the DFG to J.B.

Received: March 27, 2006

Revised: May 26, 2006

Accepted: May 30, 2006

Published: July 18, 2006

References

- Alexandrov, N.N., Nussinov, R., and Zimmer, R.M. (1995). Fast protein fold recognition via sequence to structure alignment and contact capacity potentials. In Pacific Symposium on Biocomputing '96, L. Hunter and T.E. Klein, eds. (Singapore: World Scientific Publishing), pp. 53–72.
- Altschul, S.F., Madden, T.L., Schaffer, A.A., Zhang, J., Zhang, Z., Miller, W., and Lipman, D.J. (1997). Gapped BLAST and PSI-BLAST: a new generation of protein database search programs. *Nucleic Acids Res.* 25, 3389–3402.
- Bova, M.P., Mchaourab, H.S., Han, Y., and Fung, B.K.-K. (2000). Subunit exchange of small heat shock proteins: analysis of oligomeric formation of α A-crystallin and Hsp27 by fluorescence

- resonance energy transfer and site-directed truncations. *J. Biol. Chem.* **275**, 1035–1042.
- Brady, J.P., Garland, D., Douglas-Tabor, Y., Robison, W.G., Jr., Groome, A., and Wawrousek, E.F. (1997). Targeted disruption of the mouse α -A crystallin genes induces cataract and cytoplasmic inclusion bodies containing the small heat shock protein α -B crystallin. *Proc. Natl. Acad. Sci. USA* **94**, 884–889.
- Cashikar, A.G., Duennwald, M., and Lindquist, S.L. (2005). A chaperone pathway in protein disaggregation. Hsp26 alters the nature of protein aggregates to facilitate reactivation by Hsp104. *J. Biol. Chem.* **280**, 23869–23875.
- Fischer, D. (2000). Hybrid fold recognition: combining sequence derived properties with evolutionary information. In *Pacific Symp. Bio-computing, Hawaii* (Singapore: World Scientific Publishing), pp. 119–130.
- Franzmann, T.M., Wuhr, M., Richter, K., Walter, S., and Buchner, J. (2005). The activation mechanism of Hsp26 does not require dissociation of the oligomer. *J. Mol. Biol.* **350**, 1083–1093.
- Giese, K.C., Basha, E., Catague, B.Y., and Vierling, E. (2005). Evidence for an essential function of the N terminus of a small heat shock protein *in vivo*, independent of *in vitro* chaperone activity. *Proc. Natl. Acad. Sci. USA* **102**, 18896–18901.
- Haley, D.A., Horwitz, J., and Stewart, P.L. (1998). The small heat-shock protein, α B-crystallin, has a variable quaternary structure. *J. Mol. Biol.* **277**, 27–35.
- Haley, D.A., Bova, M.P., Huang, Q.-L., Mchaourab, H.S., and Stewart, P.L. (2000). Small heat-shock protein structures reveal a continuum from symmetric to variable assemblies. *J. Mol. Biol.* **298**, 261–272.
- Haslbeck, M. (2002). sHsps and their role in the chaperone network. *Cell. Mol. Life Sci.* **59**, 1649–1657.
- Haslbeck, M., Walke, S., Stromer, T., Ehrnsperger, M., White, H.E., Chen, S., Saibil, H.R., and Buchner, J. (1999). Hsp26: a temperature-regulated chaperone. *EMBO J.* **18**, 6744–6751.
- Haslbeck, M., Braun, N., Stromer, T., Richter, B., Model, N., Weikauf, S., and Buchner, J. (2004a). Hsp42 is the general small heat shock protein in the cytosol of *Saccharomyces cerevisiae*. *EMBO J.* **23**, 636–649.
- Haslbeck, M., Ignatiou, A., Saibil, H.R., Helmich, S., Franzl, E., Stromer, T., and Buchner, J. (2004b). A domain in the N-terminal part of Hsp26 is essential for chaperone function and oligomerization. *J. Mol. Biol.* **343**, 445–455.
- Haslbeck, M., Franzmann, T., Weinfurter, D., and Buchner, J. (2005a). Some like it hot: the structure and function of small heat-shock proteins. *Nat. Struct. Mol. Biol.* **12**, 842–846.
- Haslbeck, M., Meiss, A., Stromer, T., Walter, S., and Buchner, J. (2005b). Disassembling protein aggregates in the yeast cytosol. The cooperation of Hsp26 with Ssa1 and Hsp104. *J. Biol. Chem.* **280**, 23861–23868.
- Horwitz, J. (2003). Alpha-crystallin. *Exp. Eye Res.* **76**, 145–153.
- Kappe, G., Franck, E., Verschuure, P., Boelens, W.C., Leunissen, J.A., and de Jong, W.W. (2003). The human genome encodes 10 alpha-crystallin-related small heat shock proteins: HspB1–10. *Cell Stress Chaperones* **8**, 53–61.
- Kelley, L.A., MacCallum, R.M., and Sternberg, M.J.E. (2000). Enhanced genome annotation using structural profiles in the program 3D-PSSM. *J. Mol. Biol.* **299**, 499–520.
- Kennaway, C.K., Benesch, J.L., Gohlke, U., Wang, L., Robinson, C.V., Orlova, E.V., Saibil, H.R., and Keep, N.H. (2005). Dodecameric structure of the small heat shock protein ACR1 from mycobacterium tuberculosis. *J. Biol. Chem.* **280**, 33419–33425.
- Kim, K.K., Kim, R., and Kim, S.-H. (1998). Crystal structure of a small heat shock protein. *Nature* **394**, 595–599.
- Koteiche, H.A., Chiu, S., Majdoh, R.L., Stewart, P.L., and Mchaourab, H.S. (2005). Atomic models by cryo-EM and site-directed spin labeling: application to the N-terminal region of Hsp16.5. *Structure* **13**, 1165–1171.
- Lee, G.L., Roseman, A.M., Saibil, H.R., and Vierling, E. (1997). A small heat shock protein stably binds heat-denatured model substrates and can maintain a substrate in a folding-competent state. *EMBO J.* **16**, 659–671.
- Lee, U., Wie, C., Escobar, M., Williams, B., Hong, S.-W., and Vierling, E. (2005). Genetic analysis reveals domain interactions of Arabidopsis Hsp100/ClpB and cooperation with the small heat shock protein chaperone system. *Plant Cell* **17**, 559–571.
- Mogk, A., Deurling, E., Vorderwülbecke, S., Vierling, E., and Bukau, B. (2003). Small heat shock proteins, ClpB and the DnaK system form a functional triade in reversing protein aggregation. *Mol. Microbiol.* **50**, 585–595.
- Narberhaus, F. (2002). α -crystallin-type heat shock proteins: socializing minichaperones in the context of a multichaperone network. *Microbiol. Mol. Biol. Rev.* **66**, 64–93.
- Navaza, J., Lepault, J., Rey, F.A., Alvarez-Rua, C., and Borge, J. (2000). On the fitting of model electron densities into EM reconstructions: a reciprocal-space formulation. *Acta Crystallogr. D Biol. Crystallogr.* **58**, 1820–1825.
- Pearson, W.A. (1990). Rapid and sensitive sequence comparison with FASTP and FASTA. *Methods Enzymol.* **183**, 63–98.
- Roseman, A.M. (2000). Docking structures of domains into maps from cryo-electron microscopy using local correlation. *Acta Crystallogr. D Biol. Crystallogr.* **56**, 1332–1340.
- Rost, B., Yachdav, G., and Liu, J. (2004). The PredictProtein server. *Nucleic Acids Res.* **32**, W321–W325.
- Shi, J., Blundell, T.L., and Mizuguchi, K. (2001). FUGUE: Sequence-structure homology recognition using environment-specific substitution tables and structure-dependent gap penalties. *J. Mol. Biol.* **310**, 243–257.
- Stamler, R., Kappe, G., Boelens, W., and Slingsby, C. (2005). Wrapping the α -crystallin domain fold in a chaperone assembly. *J. Mol. Biol.* **353**, 68–79.
- Stromer, T., Ehrnsperger, M., Gaestel, M., and Buchner, J. (2003). Analysis of the interaction of small heat shock proteins with unfolding proteins. *J. Biol. Chem.* **278**, 18015–18021.
- Stromer, T., Fischer, E., Richter, K., Haslbeck, M., and Buchner, J. (2004). Analysis of the regulation of the molecular chaperone Hsp26 by temperature-induced dissociation: the N-terminal domain is important for oligomer assembly and the binding of unfolding proteins. *J. Biol. Chem.* **279**, 11222–11228.
- van Heel, M., Harauz, G., Orlova, E., Schmidt, R., and Schatz, M. (1996). A new generation of the IMAGIC image processing system. *J. Struct. Biol.* **116**, 17–24.
- van Montfort, R.L.M., Basha, E., Friedrich, K.L., Slingsby, C., and Vierling, E. (2001). Crystal structure of a eukaryotic small heat shock protein. *Nat. Struct. Biol.* **8**, 1025–1030.
- van Montfort, R.L.M., Slingsby, C., and Vierling, E. (2002). Structure and function of the small heat shock protein/ α -crystallin family of molecular chaperones. In *Protein Folding in the Cell: Advances in Protein Structure, Volume 59*, A. Horwich, ed. (San Diego: Academic Press), pp. 105–156.
- Veinger, L., Diamant, S., Buchner, J., and Goloubinoff, P. (1998). The small heat-shock protein ibpb from *Escherichia coli* stabilizes stress-denatured proteins for subsequent refolding by a multichaperone network. *J. Biol. Chem.* **273**, 11032–11037.
- White, H.E., Saibil, H.R., Ignatiou, A., and Orlova, E.V. (2004). Recognition and separation of single particles with size variation by statistical analysis of their images. *J. Mol. Biol.* **336**, 453–460.

Accession Numbers

The EM maps have been deposited in the EM databank (European Bioinformatics Institute) with accession codes for wt compact (1226), wt expanded (1221), Δ N30 compact (1227), Δ N30 expanded (1230), Δ N30his compact (1229), and Δ N30his expanded (1228). The fitted α -crystallin domain dimers for the wild-type structures have been deposited as EM models in the PDB, with accession codes 2H53 (wt compact) and 2H50 (wt expanded).

Activation of the Chaperone Hsp26 Is Controlled by the Rearrangement of Its Thermosensor Domain

Titus M. Franzmann,¹ Petra Menhorn,¹ Stefan Walter,¹ and Johannes Buchner^{1,*}

¹Department Chemie, Center for Integrative Protein Science Munich, Technische Universität München, 85747 Garching, Germany

*Correspondence: johannes.buchner@ch.tum.de

DOI 10.1016/j.molcel.2007.11.025

SUMMARY

Cells respond to a sudden increase in temperature with the transcription of a special set of genes, a phenomenon known as the heat shock response. In the yeast *S. cerevisiae*, the molecular chaperone Hsp26 is one component of the heat shock response. Hsp26 has the remarkable ability to sense increases in temperature directly and can switch from an inactive to a chaperone-active state. The underlying principle of this temperature regulation has remained enigmatic. Hsp26 variants with altered spectroscopic properties allowed us to identify structural elements controlling this activation process. We show that temperature sensing by Hsp26 is a feature of its middle domain that changes its conformation within a narrow temperature range. This structural rearrangement allows Hsp26 to respond autonomously and directly to heat stress by reversibly unleashing its chaperone activity. Thus, the Hsp26 middle domain is a thermosensor and intrinsic regulator of chaperone activity.

INTRODUCTION

The native structure of proteins is sensitive to changes in the cellular environment. In particular, proteins can unfold and aggregate when cells are exposed to thermal or chemical stress. To reduce the potentially fatal effects of stress on the proteome, cells express a set of proteins, termed molecular chaperones, that rescue other proteins from aggregation and mediate their renaturation (Lindquist and Craig, 1988). Small heat shock proteins (sHsps) represent a ubiquitous class of molecular chaperones. Their distinguishing feature is the presence of a conserved α -crystallin domain, named after the most renowned member of sHsps, the α -crystallin of the vertebrate eye lens (Horwitz, 1992). The importance of sHsps in preventing protein aggregation has been demonstrated in vitro (Horwitz, 1992; Jakob et al., 1993) and in vivo. Knockout mice lacking α A-crystallin develop cataracts early in life (Brady et al., 1997), and dysfunctions of α B-crystallin and Hsp27 were found to be involved in the development of a number of neurodegenerative disorders, including Alzheimer's and Creutzfeldt-Jakob disease (Krueger-Naug et al.,

2002; Lowe et al., 1992; Renkawek et al., 1992). In *S. cerevisiae*, the deletion of Hsp26 causes an abnormal cell shape and accumulation of protein aggregates under stress conditions (Haslbeck et al., 2004a).

According to their cellular function as chaperones, sHsps bind nonnative polypeptides and maintain them in a refolding-competent state (Ehrensperger et al., 1997; Lee et al., 1997; Stromer et al., 2003). The substrate binding site on sHsps is unknown, but the N-terminal region of sHsps seems to play an important role in substrate recognition (Giese et al., 2005; Haslbeck et al., 2004b). Although sHsps themselves lack refolding activity, trapped polypeptides can be renatured with the assistance of ATP-dependent chaperones such as Hsp70 and Hsp100 (Cashikar et al., 2005; Ehrensperger et al., 1997; Haslbeck et al., 2005; Lee et al., 1997; Mogk et al., 2003).

sHsps associate into large oligomers that in most cases contain either 12 or 24 subunits (Kennaway et al., 2005; Stamler et al., 2005; White et al., 2006). In the sHsp monomer, the α -crystallin domain is flanked by a divergent N-terminal region and a short and moderately conserved C-terminal extension. While the α -crystallin domain mediates dimerization of sHsp monomers, the C-terminal extensions establish oligomer formation through contacts with adjacent α -crystallin domains (Kim et al., 1998; van Montfort et al., 2001). Little is known about the structure of the N-terminal domain (NTD). In the case of Hsp16.9 from wheat, the resolved N termini from opposite subunits adopt α -helical structure and stabilize the dodecamer by pairwise intertwining (van Montfort et al., 2001). In vitro, sHsps exchange subunits between oligomers, a process whose biological significance is currently under debate (Bova et al., 1997; Haslbeck et al., 1999; Sobott et al., 2002). However, recent findings show that, for some sHsps, oligomer dissociation and subunit exchange (SX) do not correlate with chaperone activity (Aquilina et al., 2005; Franzmann et al., 2005).

Hsp26 is the principal sHsp of *S. cerevisiae* (Susek and Lindquist, 1989). It forms shell-like particles composed of 24 subunits (Bentley et al., 1992; White et al., 2006). One of the most remarkable features of Hsp26 is that its activity is temperature dependent (Haslbeck et al., 1999). At 25°C, Hsp26 does not interact with nonnative proteins, while it does display a strong affinity for unfolded polypeptides under conditions of thermal stress, e.g., at 45°C (Franzmann et al., 2005). The molecular basis of this temperature regulation is unknown, but it was shown recently that a conformational rearrangement within the oligomer is responsible for the activation of Hsp26 (Franzmann et al., 2005).

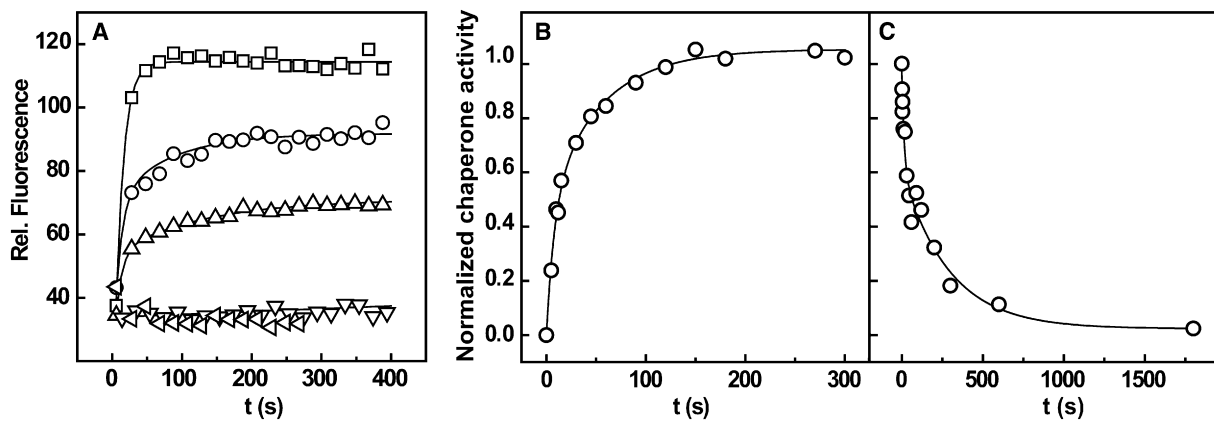


Figure 1. Activation of Hsp26 Chaperone Function by Temperature

(A) Hsp26 chaperone activity was assessed at 25°C by its capability to suppress the aggregation of 200 nM chemically denatured GDH. The formation of light scattering aggregates was monitored at 350 nm in a fluorometer. Hsp26 that was not temperature activated adopts an inactive conformation and cannot reduce GDH aggregation (\square). Increasing times of preincubation at 36°C (\circ , 5 s; \triangle , 10 s; ∇ , 5 min) results in an increasing Hsp26 activity. In a control, heat-activated Hsp26 was tested in the absence of GDH (\triangle , 5 min).

(B) Kinetics of Hsp26 chaperone activation was analyzed in dependence of its preincubation time at 36°C. Activation follows a double exponential function with an overall half life of 9 s.

(C) Hsp26 was heat activated for 10 min at 45°C and then shifted back to 25°C, and the residual chaperone activity was determined. Inactivation follows a double exponential function with an overall half-life of 100 s.

The primary structure Hsp26 reveals an exceptionally long N-terminal region that can be divided into an NTD and a middle domain (MD) (Haslbeck et al., 2004b; White et al., 2006). Whereas NTD appears to play a critical role for oligomer stability and substrate recognition, the function of MD was unknown up to now.

Here, we analyzed the thermodynamic and kinetic characteristics of structural changes that govern the transition from the inactive to the active chaperone by fluorescence spectroscopy. We provide compelling evidence that the activation of Hsp26 correlates with a distinct rearrangement of its MD. Upon activation, we observed major changes in the efficiency of fluorescence resonance energy transfer (FRET) of labels attached to MD, supporting the notion that MD serves as a thermosensor and intrinsic regulator of chaperone activity.

RESULTS

Hsp26 Chaperone Function Is Thermally Controlled

Molecular chaperones prevent the irreversible aggregation of polypeptides and assist in protein refolding after heat stress. Most chaperones exploit ATP binding and hydrolysis to cycle between states with different affinities for their polypeptide substrates (Beissinger and Buchner, 1998; Bukau and Horwich, 1998; Hendrick and Hartl, 1993; Walter and Buchner, 2002). Hsp26 from *S. cerevisiae*, a member of the class of small Hsps, differs from these chaperones in that its transition from the low- to the high-affinity state is controlled by temperature itself (Franzmann et al., 2005; Haslbeck et al., 1999). Only after exposure to elevated temperature is Hsp26 able to bind unfolded polypeptides and prevent their aggregation. This activity can be determined experimentally using assays in which the chaperone suppresses the formation of light scattering aggregates by a suitable protein, such as glutamate dehydrogenase (GDH).

When we tested Hsp26 for chaperone function at 25°C, it did not prevent GDH aggregation, demonstrating that Hsp26 adopts a conformation that is unable to interact with unfolded polypeptides (Figure 1A). However, when Hsp26 was heat activated at 36°C for just 10 s and then shifted back to 25°C prior to the addition of GDH, the extent of aggregation was already reduced by half. When preincubation at 36°C was extended to 5 min, GDH aggregation was suppressed completely, demonstrating that heat treatment of Hsp26 unleashes its chaperone activity. The conversion from the inactive to the active chaperone is a time-dependent process and follows a double exponential function with 55% of the amplitude corresponding to the fast phase (Figure 1B).

To test whether activation is reversible, Hsp26 was first incubated at 45°C for 10 min to induce full chaperone activity. Subsequently, the sample was shifted back to 25°C, and its residual chaperone activity was assayed after different times. Indeed, the activity of Hsp26 decreased upon incubation at 25°C, and again the kinetics can be described by a double exponential function with 60% of the amplitude corresponding to the fast phase (Figure 1C). In contrast to temperature activation that has a half life of 6 s for the fast reaction and 36 s for the slow phase, Hsp26 inactivation is a relatively slow process with half times of 10 s and 194 s for the fast and slow phase, respectively. This may be a consequence of the different reaction temperatures, as, in general, kinetics are faster at higher temperature.

Temperature Activation of Hsp26 Induces a Conformational Change in Its Middle Domain

We next investigated how the active conformation of Hsp26 differs from the inactive. Site-directed mutagenesis was used to introduce single Cys residues in the three domains, NTD (Hsp26_{S4C}), MD (Hsp26_{S82C}), and CTE (Hsp26_{S210C}) (Figure 2). The Cys residues

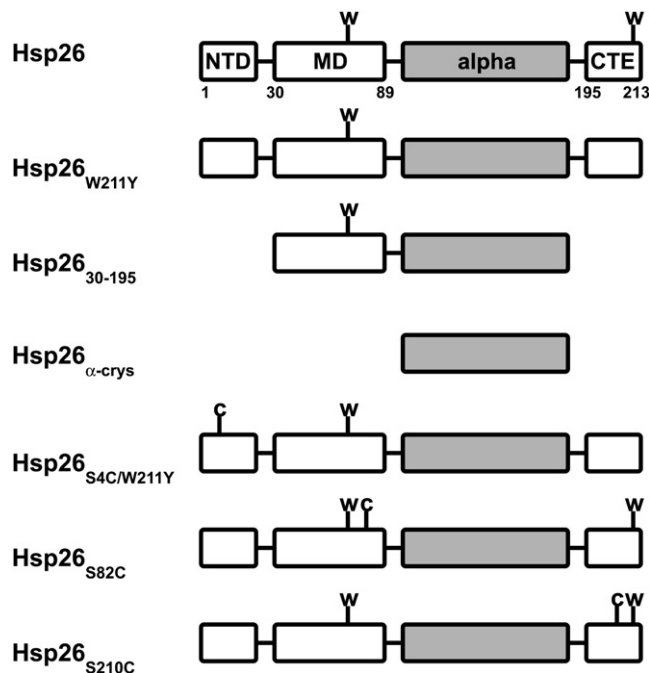


Figure 2. Hsp26 Domain Structure

Hsp26 consists of an NTD, an MD, the conserved α -crystallin domain (alpha), and a C-terminal extension (CTE). The domain structures of Hsp26 variants are aligned to the WT protein. Amino acids are indicated by single letter code.

were then modified with the fluorescent dyes AIAS (donor dye) or LYI (acceptor dye) for subsequent FRET analysis. Note that WT Hsp26 does not contain Cys residues. The structural and functional properties of the Cys variants were indistinguishable from those of the WT protein (see Figure S1 available online).

As expected, the six labeled proteins themselves did not show FRET (data not shown). When a donor-labeled protein was mixed with acceptor-labeled protein, FRET could be observed. Hsp26 oligomers are dynamic and exchange subunits (dimers) with each other, resulting in the formation of FRET-active oligomers (Figure 3A). Thus, the extent of FRET between the three domains of Hsp26 could be determined by pairwise mixing of the appropriate proteins. First, FRET was recorded at 25°C, i.e., for the inactive state of Hsp26. Subsequently, samples were shifted to 45°C to induce the chaperone active state. If the conformation of Hsp26 changes during the activation process, this should lead to a change in the FRET signal. In general, changes in FRET efficiency (E_T) can result from spectral shifts, changes in dipole-dipole orientation of the fluorophors, in donor quantum yield, or in donor-acceptor distance. Control experiments showed that the first two possibilities can be ruled out (Figures S2 and S3). In our analysis, signals were corrected for the decreased donor quantum yield at 45°C, and thus changes in E_T primarily arise from changes in fluorophor distance.

For all combinations of domain pairs, FRET could be observed, demonstrating that each domain of a dimeric subunit is in proximity to at least one NTD, MD, and CTE from a neighboring dimer. Figure 3B shows an example in which Hsp26_{S82C-AIAS} and

Hsp26_{S82C-LYI} were used to measure the FRET efficiency between MDs. In the inactive chaperone, the FRET efficiencies between the various domains delivered values in the range of 1–1.3 R_0 (Figure 3D, note that $r = 1 R_0$ means that 50% of the donor signal is lost by FRET). When we analyzed the thermally activated state of Hsp26, r between NTD and NTD or between CTE and CTE was barely affected (Figure 3D, Figure S2). This supports our previous conclusion about the oligomeric nature of the activated state (Franzmann et al., 2005), since all FRET interactions would have been lost if the dimer would constitute the active species. However, temperature treatment caused a strong decrease in FRET between MDs (Figure 3C). At the same time, we observed pronounced changes in E_T between MD and NTD or CTE (Figure 3D). Cooling and reheating Hsp26 produced identical results, demonstrating that the structural changes are reversible. It appears that activation of Hsp26 causes a distinct rearrangement of the MD, which in turn reduces the efficiency of FRET from a given MD to neighboring subunits. One could argue that these differences in E_T may simply reflect changes in the oligomer composition rather than changes in domain distances. Since SX is significantly slower than temperature-induced conformational changes within the oligomer (see below), this possibility can be ruled out.

Additional evidence for a major conformational change in MD came from fluorescence-quenching experiments. Dynamic quenching depopulates the excited state of a fluorophor upon encounter with quencher molecules and thus decreases fluorescence intensity (Lakowicz, 1999). The quenching coefficient expresses the degree of accessibility of the fluorophor to the quencher. In inactive Hsp26, quenching of NTD- and CTE-labeled Hsp26 was fairly efficient (Figure 3E). In contrast to the terminal regions, MD displayed a 3- to 5-fold lower quenching coefficient (Figure 3E). Upon temperature activation, the quenching coefficient for MD was increased almost 3-fold, whereas the quenching coefficients for the NTD and CTE increased only slightly (Figure 3E). These results support the notion that temperature increase induces a specific conformational change in MD, whereas the N- or C-terminal regions remain largely unchanged in the activated oligomer.

Tryptophan 72 Reports on Structural Changes of the Middle Domain

To directly monitor changes in MD, we used tryptophan fluorescence. The intrinsic fluorescence of Trp is sensitive to its environment and thus can be used to monitor transitions between conformational states of a protein. Hsp26 possesses two tryptophan residues, W72 in MD and W211 in CTE (Figure 2). To simplify spectroscopic analysis, single Trp variants were designed by replacing W72 or W211 with Tyr. Hsp26_{W72Y} proved to be insoluble and inactive and was not investigated further (data not shown). Hsp26_{W211Y} was soluble, and its behavior was indistinguishable from WT Hsp26 (Figure S1). In addition, we generated a truncation variant (Hsp26₃₀₋₁₉₅) consisting only of MD and α -crystallin domain (Figure 2). This protein also lacks W211. In contrast to Hsp26_{W211Y}, its assembly stops on the level of a dimer, and it does not exhibit chaperone activity (Figure S1). Thus, Hsp26_{W211Y} allowed us to specifically follow changes in W72 fluorescence (and hence in the structure

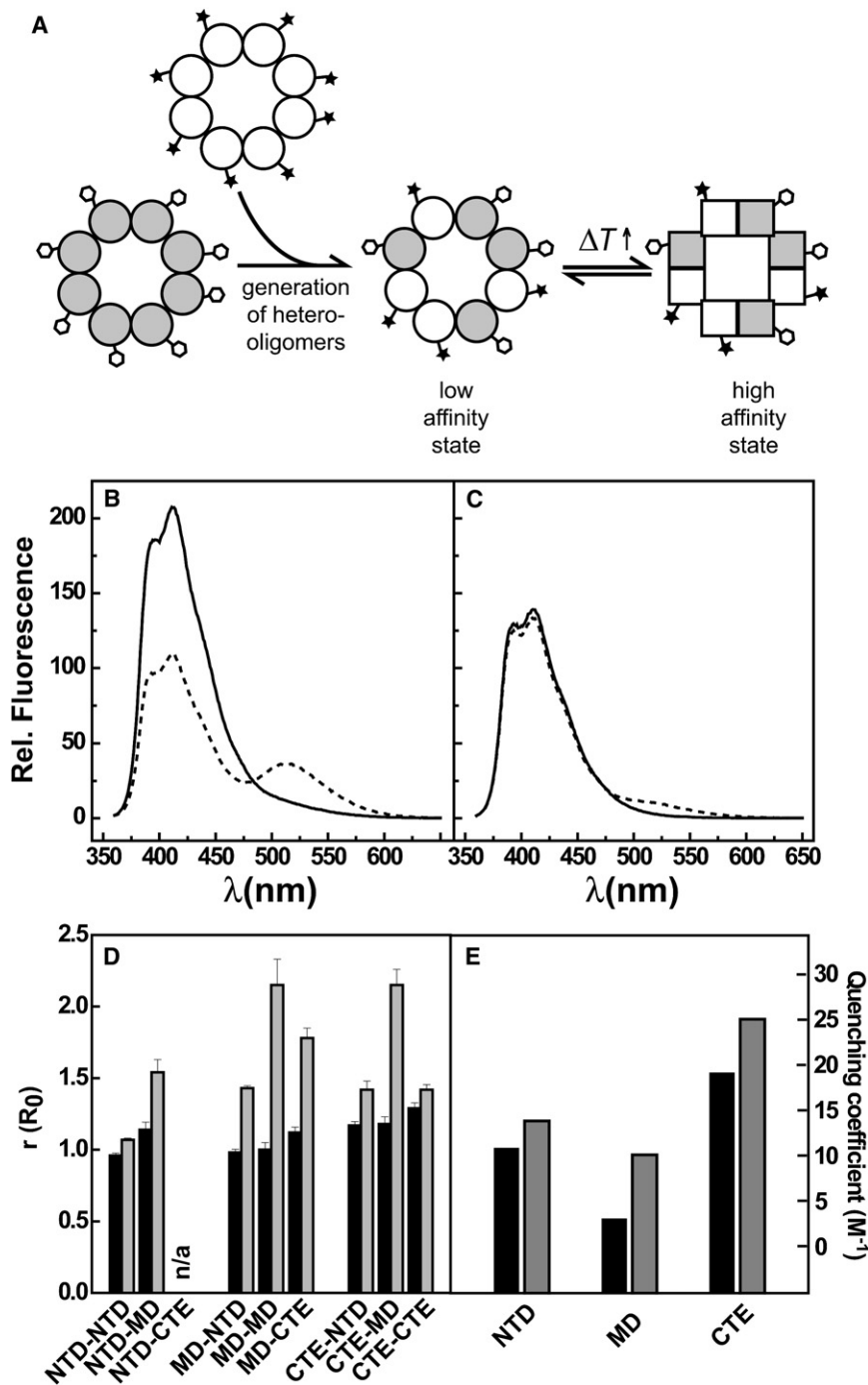


Figure 3. Site-Specific Conformational Changes in Hsp26 Determined by FRET

(A) To generate FRET-active hetero-oligomers, donor-labeled Hsp26 (gray) was mixed with the acceptor-labeled Hsp26 (white) and incubated until SX had reached equilibrium. Hetero-oligomers were then subjected to FRET analysis to determine FRET efficiencies between donor and acceptor fluorophores in the inactive and chaperone active states.

(B) Fluorescence spectra of Hsp26_{S82C-AIAS} (donor) in the absence (straight line) and presence (dotted line) of Hsp26_{S82C-LY1} (acceptor). Residue 82 is located in the MD.

(C) Fluorescence spectra of thermally activated Hsp26_{S82C-AIAS} in the absence (straight line) and presence (dotted line) of Hsp26_{S82C-LY1}. All spectra were recorded at 25°C.

(D) FRET distances between distinct sites within inactive (black bars) and active Hsp26 (gray bars). Standard deviations were determined from at least three individual experiments.

(E) Solvent accessibility of NTD, MD, and CTE determined by NaI quenching of inactive (black bars) and active Hsp26 (gray bars).

showing that activation of Hsp26 is associated with a structural change in MD and indicates that W72 becomes more solvent accessible in the activated state. For comparison, we tested the effect of temperature on the spectral properties of free N-acetyl tryptophan amide (data not shown). Between 25°C and 45°C, the fluorescence intensity was reduced by only 16%, while the position of the maximum at 355 nm was unaffected. Hence, the spectral changes in W72 fluorescence cannot be explained by a general temperature effect on Trp fluorescence.

The emission spectrum of WT Hsp26 showed a maximum at 324 nm at 25°C (Figure 4B). Heating WT Hsp26 to 45°C shifted the fluorescence maximum to 355 nm. Due to the presence of W211, fluorescence intensities at both temperatures are significantly increased in comparison to Hsp26_{W211Y}. Upon transition to the active state, the fluorescence intensity at 340 nm decreases by 40 units

of MD) within the context of the 24-mer, whereas Hsp26₃₀₋₁₉₅ allowed monitoring changes in MD within the simpler dimeric system.

To assess whether the local environment of W72 changes upon Hsp26 activation, fluorescence spectra were recorded. At 25°C, the single Trp variant Hsp26_{W211Y} exhibited an emission maximum of 314 nm, which increased to 343 nm at 45°C (Figure 4A). This pronounced red shift is consistent with our model

in Hsp26_{W211Y} but by more than 120 units in the case of the WT protein. Hence, fluorescence properties of WT Hsp26 are dominated by W211. This in turn suggests that not only the environment of W72 but also that of W211 changes during thermal activation. The C-terminal region of Hsp26 is involved in oligomer formation, and spectroscopic changes observed for W211 likely are related to the increased rates of SX at elevated temperature (see below).

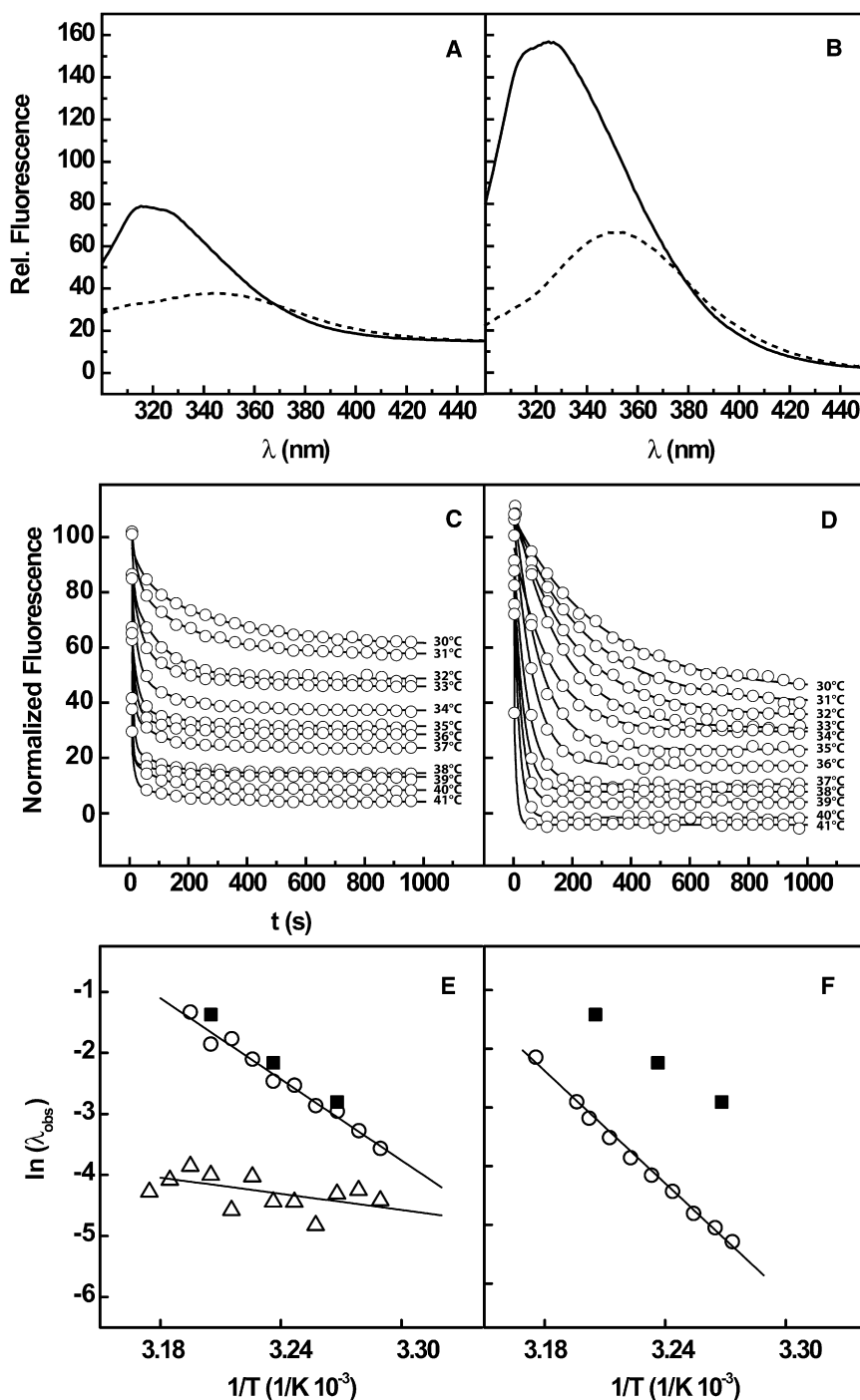


Figure 4. Temperature-Induced Changes in Hsp26 Tryptophan Fluorescence

(A and B) (A) Fluorescence spectra of Hsp26_{W211Y} at 25°C (straight line) and 45°C (dotted line) and (B) of WT Hsp26 at 25°C (straight line) and 45°C (dotted line).

(C) Traces of the changes in Hsp26_{W211Y} fluorescence upon temperature shift. W72 fluorescence decreases double exponentially with time.

(D) For WT Hsp26, changes in fluorescence follow a single exponential function.

(E) The logarithm of each rate constant (\circ , λ_1 ; Δ , λ_2) observed for Hsp26_{W211Y} depends linearly on the reciprocal temperature.

(F) The logarithm of the rate constant observed for WT Hsp26 (\circ , λ_{WT}) depends linearly on the reciprocal temperature, suggesting one rate-limiting step. The rates for Hsp26 chaperone activation at 33°C, 36°C, and 45°C (\blacksquare) are shown in comparison to the rate determined by fluorescence.

experiments, we also investigated the temperature dependence of the reaction rates. According to transition state theory, the logarithm of a rate constant λ depends linearly on the reciprocal temperature. From these Arrhenius plots ($\ln[\lambda]$ versus $1/T$), the activation energy (E_A) can be calculated. If two processes show superimposing Arrhenius plots, i.e., their rates match over the tested temperature range, it is likely that they are controlled by the same rate-limiting step.

Figure 4C shows the kinetic traces for the changes in Hsp26_{W211Y} fluorescence upon shift from 25°C to higher temperature. The amplitude for the changes in W72 fluorescence increases with temperature, indicating an increased number of molecules undergoing a structural rearrangement of MD. The kinetics could only be described by a double exponential equation (Figure S4A). The logarithm of each rate constant, λ_1 and λ_2 , depends linearly on the reciprocal temperature (Figure 4E). λ_1 is large and strongly affected by changes in the temperature, indicating a large activation energy of $E_A = 150 \text{ kJ mol}^{-1} \pm 10 \text{ kJ mol}^{-1}$. λ_2 is

Chaperone Activity of Hsp26 and Changes in MD Are Controlled by the Same Process

Although our results show that MD undergoes a structural rearrangement when Hsp26 is thermally activated, this does not necessarily mean that both processes are mechanistically connected. To gain more information about the structural rearrangements of Hsp26, we determined how fast the structure of MD changes upon temperature increase and how fast the activation of chaperone function occurs. By varying the temperature between our

small and depends weakly on the temperature, resulting from a small intrinsic reaction rate with a small activation energy ($E_A = 20 \text{ kJ mol}^{-1} \pm 10 \text{ kJ mol}^{-1}$). Next, we determined how fast Hsp26 gains chaperone activity when temperature is increased from 25°C to higher values. After Hsp26 was heat activated for various times at 33°C, 36°C, or 45°C, the chaperone was shifted back to 25°C, and its activity was assessed by the capability to suppress GDH aggregation. The rate constants for chaperone activation are similar to the rates obtained for the changes in

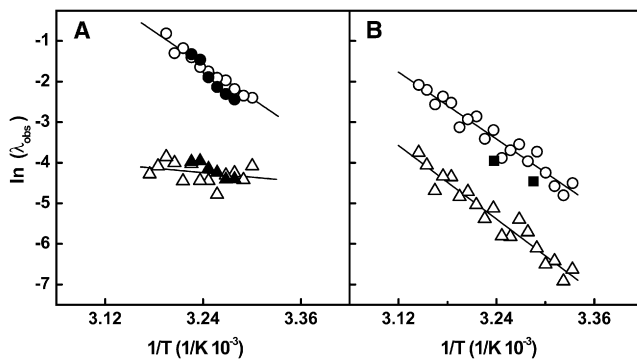


Figure 5. Kinetic Analysis of Mutant Hsp26

(A) Kinetic analysis of changes in W72 fluorescence in Hsp26₃₀₋₁₉₅ revealed two rate constants (●, λ₁; ▲, λ₂). For comparison, the rates for the changes in W72 fluorescence determined for Hsp26_{W211Y} (○, λ₁; △, λ₂) are shown. The rates observed for dimeric Hsp26₃₀₋₁₉₅ and their temperature dependence superimpose with values obtained for oligomeric Hsp26_{W211Y}. Thus, W72 is an intrinsic probe for the conformational state of MD.

(B) Kinetic analysis of MD rearrangement in oxidized Hsp26_{S4C/W211Y}. Both rates (○, λ₁; △, λ₂) are slowed down by one order of magnitude compared to Hsp26_{W211Y}. Importantly, also the rates for chaperone activation determined at 33°C, 36°C, and 45°C (■) are slowed down by one order of magnitude, demonstrating that Hsp26 activation is coupled to the structural rearrangement of MD.

W72 fluorescence (λ₁) (Figure 4E, Table S2). This argues that the gain of chaperone activity and the structural changes in MD occur in the same process. Due to the poor signal-to-noise ratio of the assay at 33°C (only few active Hsp26 species exist) and the fast activation reaction at 45°C, only the fast phase of the kinetics with its large amplitude was analyzed.

A similar analysis with the WT protein yielded a different picture. Here, the decrease in fluorescence signal occurred in a single exponential function (Figure 4D, Figure S4B). The corresponding rate constant, λ_{WT}, strongly increases with temperature, and its logarithm depends linearly on the reciprocal temperature within the tested temperature range (E_A 250 kJ mol⁻¹ ± 10 kJ mol⁻¹) (Figure 4F). However, the kinetics measured for the gain of chaperone activity did not match the energetic profile determined for the temperature-induced changes in W211 fluorescence observed with WT Hsp26 (Figure 4F). We conclude that W72 and W211 report on different structural changes in Hsp26 and are controlled by individual energy barriers.

To confirm that W72 is a specific probe for the conformational state of MD, we analyzed dimeric Hsp26₃₀₋₁₉₅, which consists only of MD and α-crystallin domain (Figure 2). Because the structure of the α-crystallin domain is stable within the tested temperature range (Stromer et al., 2004), all changes in W72 fluorescence result from conformational changes in MD. As in the case of Hsp26_{W211Y}, kinetics observed with Hsp26₃₀₋₁₉₅ upon temperature shift decreased double exponentially with time (data not shown). Each of the rates depends linearly on the reciprocal temperature (Figure 5A) and is independent of the protein concentration (data not shown). Comparison of dimeric Hsp26₃₀₋₁₉₅ to oligomeric Hsp26_{W211Y} reveals that both the rates and their temperature dependence are identical (Figure 5A). Thus, W72 fluorescence is not affected by other regions of Hsp26, namely

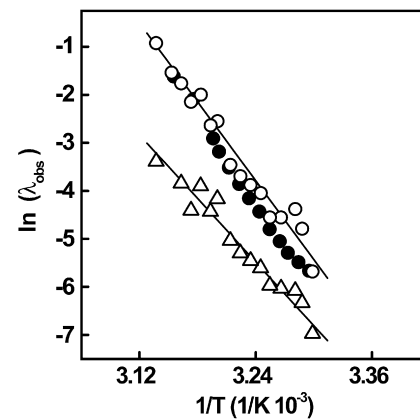


Figure 6. Subunit Exchange of Hsp26 Is Controlled by a Large Energy Barrier

Hsp26 SX was analyzed by FRET, mixing donor (AIAS)- and acceptor (LYI)-labeled Hsp26_{S4C/W211Y}. Analysis of SX revealed two rate constants (○, λ_{SX-1}; ●, λ_{SX-2}). Temperature dependence of changes in W211 fluorescence is shown as (●).

NTD or CTE, or the oligomeric structure and is an intrinsic probe for the conformational state of MD.

If the chaperone activity of Hsp26 is controlled by a conformational change in MD, one would expect that mutations that alter the dynamics of this conformational change directly affect the kinetics of activation. To prove that the gain of chaperone function is strictly coupled to MD rearrangement, we determined the kinetic properties for the oxidized Hsp26_{S4C/W211Y} variant (Figure 2). By introduction of a Cys residue in the Hsp26_{S4C/W211Y} variant, neighboring subunits can be crosslinked by disulfide bridges (Franzmann et al., 2005). As in the case of Hsp26_{W211Y}, the temperature-induced conformational changes of this Cys variant follow a double exponential function (Figure S4). However, the rate constants are reduced by one order of magnitude (Figure 5B) compared to Hsp26_{W211Y}. Importantly, the kinetics for chaperone activation are slowed down by one order of magnitude as well, and hence the conformational change in MD occurs again with the same rate as the increase in chaperone activity (Figure 5B).

Subunit Exchange Does Not Correlate with the Activation of Hsp26

As shown above, thermal activation of Hsp26 is associated with a decrease in the fluorescence of W72. Although the signal for the C-terminal Trp (W211) also decreases, our kinetic analysis demonstrates that this change is not correlated with the gain of chaperone function. We tested if W211 fluorescence could be instead related to SX. In vitro, Hsp26 oligomers exchange subunits (Franzmann et al., 2005). As a prerequisite for SX, the Hsp26 oligomer must disassemble. This process may depend on structural changes in the C-terminal extensions, which were suggested to stabilize the Hsp26 oligomer (White et al., 2006).

To measure SX, donor- and acceptor-labeled Hsp26_{S4C/W211Y} were mixed at various temperatures, and the formation of FRET-active oligomers was monitored over time. Figure 6 shows that the SX kinetics and the change in tryptophan fluorescence in

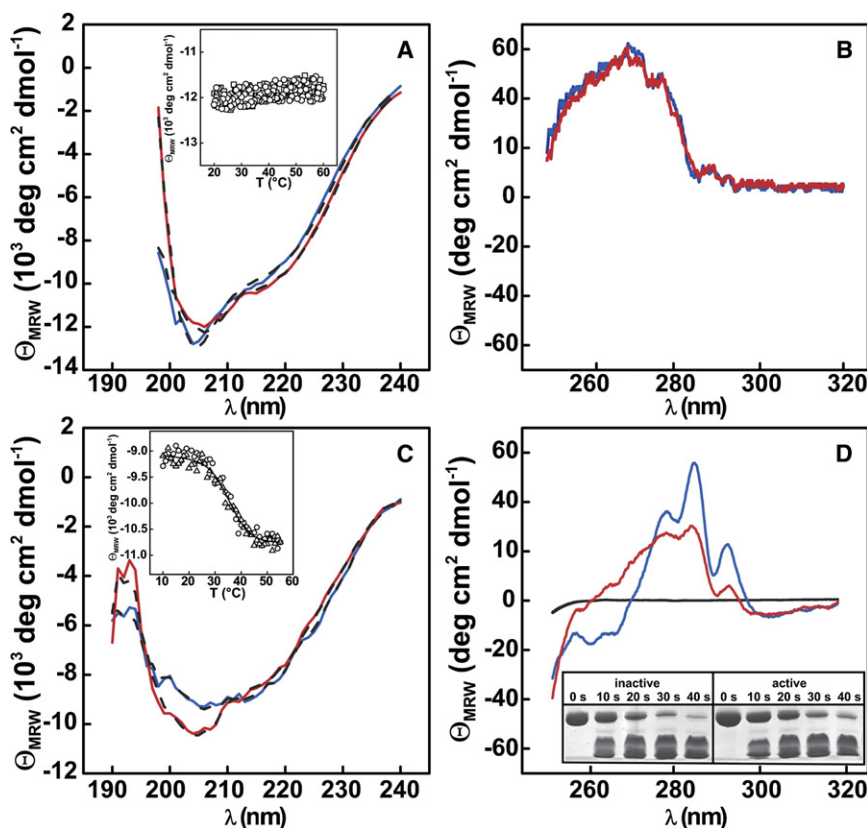


Figure 7. Conformational Changes of MD

(A) Far UV CD spectra of the Hsp26 α -crystallin domain at 25°C (blue) and 45°C (red). Fit of the CD spectra is shown in dashed lines. (Inset) Thermal unfolding (\circ) and refolding (\square) monitored by CD at 205 nm. (B) Near UV CD spectra of the Hsp26 α -crystallin domain at 25°C (blue) and 45°C (red). (C) Far UV CD spectra of Hsp26_{30–195} at 25°C (blue) and 45°C (red). Fit of the CD spectra is shown in dashed lines. (Inset) Thermal unfolding (\circ) and refolding (Δ) monitored by CD at 205 nm. (D) Far UV CD spectra of Hsp26_{30–195} at 25°C (blue), 45°C (red), and 85°C (black). (Inset) Proteolytic stability of inactive and thermally activated Hsp26_{30–195} against chymotrypsin.

creased susceptibility to proteolytic degradation. As Figure 7D (inset) shows, this was not the case. Apparently, MD adopts a β sheet structure that remains compact and folded during activation and exhibits tertiary structure that undergoes a defined and reversible rearrangement.

DISCUSSION

sHsps are oligomeric chaperones that specifically bind unfolded polypeptides to prevent their aggregation (Horwitz,

1992; Jakob et al., 1993; Kim et al., 1998; van Montfort et al., 2001; White et al., 2006). Some sHsps were found to be activated at elevated temperature, among them Hsp26 from yeast (Haslbeck et al., 1999). Apparently, these proteins are able to sense thermal stress directly and respond to it by an increase in antistress activity. In the case of Hsp26, the gain of activity is associated with global changes in the secondary and the tertiary structure, while its oligomeric status is maintained (Franzmann et al., 2005). To obtain a detailed understanding of the underlying regulatory mechanism, we analyzed the structural features of inactive and active Hsp26 and determined the kinetic barrier that separates these functionally distinct states.

The Tertiary Structure of MD Changes upon Hsp26 Activation

What is the nature of the thermosensor rearrangements that occur in Hsp26 upon chaperone activation? To address this, we analyzed Hsp26_{30–195}, which is comprised of MD and the α -crystallin domain in parallel to the isolated Hsp26 α -crystallin domain by CD spectroscopy. For the α -crystallin domain, which lacks the thermosensor, no significant differences between 25°C and 45°C were detected (Figures 7A and 7B), indicating that the α -crystallin domain does not participate in the activation reaction. The CD spectra of Hsp26_{30–195} suggest minor changes on the level of secondary structure, while its tertiary structure appears to be significantly altered at 45°C (Figures 7C and 7D). It has been shown previously that tryptophan residues also contribute to the CD of proteins in the far-UV region (Andersson et al., 2001). Therefore, we think the differences in the far-UV spectra do not reflect changes in the secondary structure of MD but changes in the local environment of W72. We also tested whether the proteolytic stability of Hsp26_{30–195} against chymotrypsin changes upon activation. If the structure of MD becomes significantly unfolded upon activation, this would lead to an in-

crease in proteolytic susceptibility. As Figure 7D (inset) shows, this was not the case. Apparently, MD adopts a β sheet structure that remains compact and folded during activation and exhibits tertiary structure that undergoes a defined and reversible rearrangement.

The Middle Domain Changes Its Conformation in Response to Temperature

Based on the data presented here, the structural changes occurring in Hsp26 during its activation can be assigned to the conformational rearrangement of a distinct part of the N-terminal region, the so-called middle domain (MD). The FRET efficiency between MD and its environment decreases significantly upon Hsp26 activation, indicating a major conformational change. Analysis of the activated state by CD and fluorescence spectroscopy suggests that MD remains compact and folded. The wavelength of the fluorescence maximum and the quenching coefficients do not match the values expected for a fully unfolded polypeptide. Based on CD spectra, MD consists of $\sim 55\%$ β structure and $\sim 12\%$ α helices, and this composition does not change upon activation. Apparently, temperature activation leads to a rearrangement of

MD with altered tertiary structure without perturbation of the secondary structure. These changes are only local and do not have major consequences for the overall Hsp26 structure. Dynamic light scattering experiments did not reveal large differences in the hydrodynamic radius of Hsp26 between 25°C and 45°C (data not shown), and the changes detected in FRET efficiency between the terminal contacts (NTD and CTE) were only minor. Neither MD nor the isolated α -crystallin domain interact with unfolded polypeptides (Figure S1 and data not shown). We conclude that an intramolecular rearrangement of the MD controls the accessibility to the substrate binding site within the Hsp26 oligomer and establishes a mechanistic link between thermal stress and Hsp26 chaperone activity. This might be achieved, e.g., by either twisting a buried substrate binding site (supposedly located within NTD) onto the surface of the oligomer or by breaking an inhibitory interaction of MD with the substrate binding site.

A Large Energy Barrier Controls the Position of the Thermoswitch

According to our kinetic analysis, temperature activation of Hsp26 is a fast and biphasic process. Two models can account for this behavior. On a sequential pathway, partially active Hsp26 molecules are generated in a first, fast step. Chaperone activity of this intermediate increases during a second slower phase. An inactive intermediate can be excluded, since binding-competent Hsp26 species are generated during the fast phase. In a parallel pathway model, two distinct populations become activated directly through either of the two reactions. The latter explanation takes into account that two structurally different species have been observed by cryo EM (White et al., 2006). The kinetic barrier separates inactive from active oligomers and allows Hsp26 to persist in the chaperone-inactive state at low temperature. Without this barrier, both states would be kinetically indistinguishable, and a cooperative activation could not be achieved.

Confinement of the flexibility of the NTD through a disulfide bridge increases the kinetic barrier for chaperone activation, indicating that NTD and MD are functionally communicating with each other and that N-terminal flexibility accelerates the displacement of the MD and allows fast activation. It is tempting to speculate that rigid mutants with considerably increased energy barriers may no longer be able to reach the active state. In agreement with this hypothesis, some mutants of a thermally regulated sHsp from *Synechocystis spec.* exhibit increased oligomer stability in vitro and fail to mediate thermotolerance in vivo (Giese et al., 2005; Giese and Vierling, 2002). This illustrates the importance of the controlled transition between the inactive and active states in vivo.

Such a distinct regulation puts Hsp26 in an exceptional position. The activity of most heat shock proteins is regulated by binding of cochaperones and on the level of transcription. The latter is also true for Hsp26, but in addition its activity is subject to an intrinsic conformational regulation that directly responds to thermal stress. Because of the thermoswitch, inactive Hsp26 molecules can be stored in the cytosol. Temperature shifts the conformational equilibrium of Hsp26 from the inactive toward the active conformation, and the height of the energy barrier between both states controls the rate of conversion. This mech-

anism allows the precise autoregulation of Hsp26 without the necessity of regulatory cofactors.

Subunit Exchange Does Not Correlate with Chaperone Activity

sHsps continuously exchange subunits between oligomers in vitro (Aquilina et al., 2005; Bova et al., 2002; Franzmann et al., 2005; Sobott et al., 2002). Previous experiments showed that a temperature increase accelerates SX and unleashes Hsp26 chaperone activity. Our data, however, demonstrate that SX and chaperone activation are two distinct processes that are not related. This becomes most evident at 36°C, where chaperone activation is ten times faster than SX. Thus, SX cannot be a prerequisite for chaperone activity. The energy barriers of SX and of chaperone activation do not match, emphasizing that both processes are controlled by different structural changes. SX was found to be a biphasic process. Both phases have similar large activation energies ($230 \text{ kJ mol}^{-1} \pm 15 \text{ kJ mol}^{-1}$ and $180 \text{ kJ mol}^{-1} \pm 11 \text{ kJ mol}^{-1}$) and similar temperature dependencies, suggesting that they originate from two distinct Hsp26 populations with different structural properties (Figure 6). This is in good agreement with the observation of two distinct populations by cryo EM that differ in the degree of packing of the C termini in the Hsp26 particle (White et al., 2006). The involvement of the C-terminal extensions in SX would explain why changes in the fluorescence of W211 correlate with SX.

Hsp26 in the Cell

Precise regulation of protein function plays a key role for the integrity of the cell in response to changing environmental conditions. Molecular chaperones assist protein folding and prevent unspecific aggregation of polypeptides. To this end, binding and release of target proteins must be controlled. Commonly, ATP binding and hydrolysis are utilized to switch from a high- to low-affinity state, which in turn releases the substrate from the chaperone and allows its refolding (Bukau and Horwich, 1998; Hartl, 1996; Walter and Buchner, 2002). However, as long as the stress conditions persist, this ATP-dependent cycling may not be productive because polypeptides are released into an environment detrimental to folding. sHsps could help the cell to manage this problem, since they act independently of ATP and form stable substrate complexes with unfolded polypeptides (Cashikar et al., 2005; Ehrnsperger et al., 1997; Friedrich et al., 2004; Haslbeck et al., 1999, 2005; Mogk et al., 2003; Stromer et al., 2003). Thus, they separate the binding from the refolding process. Hsp26 activation by temperature is fast and independent of other proteins such as transcription factors. Due to its fast activation, Hsp26 will be first chaperone to encounter unfolded polypeptides generated by stress. Hsp26 functionally interacts with the molecular chaperone Hsp104 (Cashikar et al., 2005; Haslbeck et al., 2005). This ATP-driven disaggregase dissolves protein aggregates after heat shock and plays a crucial role in mediating thermotolerance in yeast (Bosl et al., 2006; Parsell et al., 1994). Deletion of both Hsp26 and Hsp104 from yeast cells reduces the survival rate after severe heat shock 5-fold (Cashikar et al., 2005). It appears that polypeptides can be recovered more efficiently from complexes with Hsp26 than from pure protein aggregates (Cashikar et al., 2005; Haslbeck et al., 2005). Although the deletion of Hsp26

from yeast does not affect thermotolerance, it seems that trapping unfolded proteins on sHsps simplifies refolding and is beneficial to the cell on an evolutionary scale.

Why should Hsp26 be inactive under non-heat shock conditions? sHsps bind substrate proteins tightly, and substrate complexes can persist for a long time in vitro (Ehrensperger et al., 1997; Stromer et al., 2003). Its high affinity for unfolded polypeptides makes Hsp26 a very potent chaperone in suppressing protein aggregation. However, uncontrolled binding of Hsp26 to newly synthesized proteins might interfere with fundamental processes and folding pathways. It may unnecessarily route polypeptides through a chaperone- and ATP-dependent folding pathway. The regulation through its thermoswitch restricts Hsp26 activity to heat shock conditions and ensures its instantaneous availability when required.

EXPERIMENTAL PROCEDURES

Aggregation of Chemically Denatured GDH

GDH (Roche, Germany) was denatured in 5 M guanidinium chloride, and aggregation was induced by diluting GDH to a final concentration of 200 nM. Aggregation was followed in a SPEX FluoroMax-1 fluorescence spectrometer (Jobin Yvon, Germany) monitoring light scattering at 350 nm. To monitor the kinetics of chaperone activation, Hsp26 was incubated for various times at elevated temperature (33°C, 36°C, or 45°C) and then shifted back to 25°C. GDH aggregation was induced and the aggregation was monitored for 400 s. The amplitudes were plotted in dependence of the Hsp26 activation time. For the inactivation of Hsp26, 10 μM Hsp26 was heat activated at 45°C for 10 min and then diluted 1:10 into a cuvette at 25°C. After various times, GDH aggregation was induced as described above, and the amplitudes were plotted in dependence of the inactivation time. The kinetics were fitted with a double exponential equation or estimated from the half-life of the reaction. All experiments were carried out in 40 mM HEPES, 1 mM EDTA (pH 7.5).

FRET Measurements

Hsp26_{S4C}, Hsp26_{S82C}, and Hsp26_{S210C} were labeled with AIAS and LYI, respectively. Labeling was carried out as described by the manufacturer's protocol and as described elsewhere (Franzmann et al., 2005). AIAS- and LYI-labeled Hsp26 were mixed in a 1:1 ratio to generate FRET-active oligomers at a final concentration of 10 μM. After mixing, the sample was diluted 1:10 into a 500 μl cuvette at 25°C, and fluorescence spectra were recorded. Excitation was at 336 nm. The remaining sample was incubated until SX reached equilibrium. Then, another sample was diluted 1:10 and analyzed as described above. The sample was then incubated for 10 min at 45°C to allow for Hsp26 activation and thereafter quenched 1:10 into the cuvette at 25°C. To test for the reversibility of the reaction, heat-treated samples were further incubated at 25°C to allow Hsp26 inactivation and analyzed. The same procedure was also carried out without acceptor to determine the donor fluorescence intensities.

The FRET efficiency (E_T) was derived from the donor fluorescence in the presence of acceptor, F_{DA} , and in its absence, F_D . The distance r given in units of Forster radius (R_0) was calculated from Equations 1 and 2.

$$E_T = 1 - \frac{F_{DA}}{F_D} \quad (1)$$

$$r = R_0 \cdot \sqrt[6]{\frac{1 - E_T}{E_T}} \quad (2)$$

Fluorescence Spectroscopy

Hsp26 fluorescence was monitored with a SPEX FluoroMax-1 fluorescence spectrometer (Jobin Yvon, Germany) equipped with a water bath. Fluorescence was excited at 275 nm, and spectra were recorded from 295 to 450 nm. All spectra were buffer corrected. For kinetics, Hsp26 was kept at 25°C and

diluted into the preheated 1.5 ml stirring cuvette to a final concentration of 0.5 μM. Fluorescence was excited at 275 or 295 nm, respectively, and fluorescence traces were recorded at 340 nm. No differences were detected when exciting Hsp26 fluorescence at 275 or 295 nm, yet the amplitude was larger at 275 nm, allowing better determination of the reaction rates.

Analysis of the Reaction Kinetics and Activation Barriers

The traces for WT Hsp26 were fitted with the single exponential Equation 3.

$$F = F_0 + A \cdot \exp^{-\lambda \cdot t} + m \cdot t \quad (3)$$

Kinetics for Hsp26_{W211Y} and Hsp26₃₀₋₁₉₅ were fitted with the double exponential Equation 4.

$$F = F_0 + A_1 \cdot \exp^{-\lambda_1 \cdot t} + A_2 \cdot \exp^{-\lambda_2 \cdot t} + m \cdot t \quad (4)$$

The factor m corrects for photo bleaching. Calculation of the activation energy was carried using Equation 5,

$$\ln(\lambda_{obs}) = -\frac{E_A}{R} \cdot \frac{1}{T} + \ln(A), \quad (5)$$

in which T is the absolute temperature, R the gas constant, E_A the activation energy in J mol⁻¹, and A the pre-exponential factor.

Subunit Exchange of Hsp26

SX was monitored by FRET at a final concentration of 1 μM labeled Hsp26_{S4C/W211Y}, monitoring the time-dependent changes of the donor and acceptor signals, respectively (Franzmann et al., 2005). The exchange rates were determined using Equation 4.

Supplemental Data

Supplemental Data include Supplemental Experimental Procedures, four figures, three tables, and Supplemental References and can be found with this article online at <http://www.molecule.org/cgi/content/full/29/2/207/DC1/>.

ACKNOWLEDGMENTS

We thank W. Palm, A. Osterauer, and H. Krause for experimental assistance and mass spectrometry, respectively. S. Weinkauff and N. Neumaier are acknowledged for assistance with dynamic light scattering. This work was supported by grants from the Deutsche Forschungsgemeinschaft (SFB594) to S.W. and J.B.

Received: June 20, 2007

Revised: September 18, 2007

Accepted: November 5, 2007

Published: January 31, 2008

REFERENCES

- Andersson, D., Carlsson, U., and Freskgard, P.O. (2001). Contribution of tryptophan residues to the CD spectrum of the extracellular domain of human tissue factor: application in folding studies and prediction of secondary structure. *Eur. J. Biochem.* 268, 1118–1128.
- Aquilina, J.A., Benesch, J.L., Ding, L.L., Yaron, O., Horwitz, J., and Robinson, C.V. (2005). Subunit exchange of polydisperse proteins: mass spectrometry reveals consequences of alphaA-crystallin truncation. *J. Biol. Chem.* 280, 14485–14491.
- Beissinger, M., and Buchner, J. (1998). How chaperones fold proteins. *Biol. Chem.* 379, 245–259.
- Bentley, N.J., Fitch, I.T., and Tuite, M.F. (1992). The small heat-shock protein Hsp26 of *Saccharomyces cerevisiae* assembles into a high molecular weight aggregate. *Yeast* 8, 95–106.
- Bosl, B., Grimminger, V., and Walter, S. (2006). The molecular chaperone Hsp104—a molecular machine for protein disaggregation. *J. Struct. Biol.* 156, 139–148.

- Bova, M.P., Ding, L.L., Horwitz, J., and Fung, B.K. (1997). Subunit exchange of alphaA-crystallin. *J. Biol. Chem.* 272, 29511–29517.
- Bova, M.P., Huang, Q., Ding, L., and Horwitz, J. (2002). Subunit exchange, conformational stability, and chaperone-like function of the small heat shock protein 16.5 from *Methanococcus jannaschii*. *J. Biol. Chem.* 277, 38468–38475.
- Brady, J.P., Garland, D., Douglas-Tabor, Y., Robison, W.G., Jr., Groome, A., and Wawrousek, E.F. (1997). Targeted disruption of the mouse alpha A-crystallin gene induces cataract and cytoplasmic inclusion bodies containing the small heat shock protein alpha B-crystallin. *Proc. Natl. Acad. Sci. USA* 94, 884–889.
- Bukau, B., and Horwich, A.L. (1998). The Hsp70 and Hsp60 chaperone machines. *Cell* 92, 351–366.
- Cashikar, A.G., Duennwald, M., and Lindquist, S.L. (2005). A chaperone pathway in protein disaggregation. Hsp26 alters the nature of protein aggregates to facilitate reactivation by Hsp104. *J. Biol. Chem.* 280, 23869–23875.
- Ehmsperger, M., Graber, S., Gaestel, M., and Buchner, J. (1997). Binding of non-native protein to Hsp25 during heat shock creates a reservoir of folding intermediates for reactivation. *EMBO J.* 16, 221–229.
- Franzmann, T.M., Wuhr, M., Richter, K., Walter, S., and Buchner, J. (2005). The activation mechanism of Hsp26 does not require dissociation of the oligomer. *J. Mol. Biol.* 350, 1083–1093.
- Friedrich, K.L., Giese, K.C., Buan, N.R., and Vierling, E. (2004). Interactions between small heat shock protein subunits and substrate in small heat shock protein-substrate complexes. *J. Biol. Chem.* 279, 1080–1089.
- Giese, K.C., and Vierling, E. (2002). Changes in oligomerization are essential for the chaperone activity of a small heat shock protein in vivo and in vitro. *J. Biol. Chem.* 277, 46310–46318.
- Giese, K.C., Basha, E., Catague, B.Y., and Vierling, E. (2005). Evidence for an essential function of the N terminus of a small heat shock protein in vivo, independent of in vitro chaperone activity. *Proc. Natl. Acad. Sci. USA* 102, 18896–18901.
- Hartl, F.U. (1996). Molecular chaperones in cellular protein folding. *Nature* 381, 571–579.
- Haslbeck, M., Walke, S., Stromer, T., Ehmsperger, M., White, H.E., Chen, S., Saibil, H.R., and Buchner, J. (1999). Hsp26: a temperature-regulated chaperone. *EMBO J.* 18, 6744–6751.
- Haslbeck, M., Braun, N., Stromer, T., Richter, B., Model, N., Weinkauff, S., and Buchner, J. (2004a). Hsp42 is the general small heat shock protein in the cytosol of *Saccharomyces cerevisiae*. *EMBO J.* 23, 638–649.
- Haslbeck, M., Ignatiou, A., Saibil, H., Helmich, S., Frenzl, E., Stromer, T., and Buchner, J. (2004b). A domain in the N-terminal part of Hsp26 is essential for chaperone function and oligomerization. *J. Mol. Biol.* 343, 445–455.
- Haslbeck, M., Miess, A., Stromer, T., Walter, S., and Buchner, J. (2005). Disassembling protein aggregates in the yeast cytosol. The cooperation of Hsp26 with Ssa1 and Hsp104. *J. Biol. Chem.* 280, 23861–23868.
- Hendrick, J.P., and Hartl, F.U. (1993). Molecular chaperone functions of heat-shock proteins. *Annu. Rev. Biochem.* 62, 349–384.
- Horwitz, J. (1992). Alpha-crystallin can function as a molecular chaperone. *Proc. Natl. Acad. Sci. USA* 89, 10449–10453.
- Jakob, U., Gaestel, M., Engel, K., and Buchner, J. (1993). Small heat shock proteins are molecular chaperones. *J. Biol. Chem.* 268, 1517–1520.
- Kennaway, C.K., Benesch, J.L., Gohlke, U., Wang, L., Robinson, C.V., Orlova, E.V., Saibil, H.R., and Keep, N.H. (2005). Dodecameric structure of the small heat shock protein Acr1 from *Mycobacterium tuberculosis*. *J. Biol. Chem.* 280, 33419–33425.
- Kim, K.K., Kim, R., and Kim, S.H. (1998). Crystal structure of a small heat-shock protein. *Nature* 394, 595–599.
- Krueger-Naug, A.M., Plumier, J.C., Hopkins, D.A., and Currie, R.W. (2002). Hsp27 in the nervous system: expression in pathophysiology and in the aging brain. *Prog. Mol. Subcell. Biol.* 28, 235–251.
- Lakowicz, J. (1999). *Principles of Fluorescence Spectroscopy*, Second Edition (New York: Kluwer Academic and Plenum Publishers).
- Lee, G.J., Roseman, A.M., Saibil, H.R., and Vierling, E. (1997). A small heat shock protein stably binds heat-denatured model substrates and can maintain a substrate in a folding-competent state. *EMBO J.* 16, 659–671.
- Lindquist, S., and Craig, E.A. (1988). The heat-shock proteins. *Annu. Rev. Genet.* 22, 631–677.
- Lowe, J., McDermott, H., Pike, I., Spendlove, I., Landon, M., and Mayer, R.J. (1992). alpha B crystallin expression in non-lenticular tissues and selective presence in ubiquitinated inclusion bodies in human disease. *J. Pathol.* 166, 61–68.
- Mogk, A., Deuerling, E., Vorderwulbecke, S., Vierling, E., and Bukau, B. (2003). Small heat shock proteins, ClpB and the DnaK system form a functional triad in reversing protein aggregation. *Mol. Microbiol.* 50, 585–595.
- Parsell, D.A., Kowal, A.S., Singer, M.A., and Lindquist, S. (1994). Protein disaggregation mediated by heat-shock protein Hsp104. *Nature* 372, 475–478.
- Renkawek, K., De Jong, W.W., Merck, K.B., Frenken, C.W., van Workum, F.P., and Bosman, G.J. (1992). alpha B-crystallin is present in reactive glia in Creutzfeldt-Jakob disease. *Acta Neuropathol. (Berl.)* 83, 324–327.
- Sobott, F., Benesch, J.L., Vierling, E., and Robinson, C.V. (2002). Subunit exchange of multimeric protein complexes. Real-time monitoring of subunit exchange between small heat shock proteins by using electrospray mass spectrometry. *J. Biol. Chem.* 277, 38921–38929.
- Stamler, R., Kappe, G., Boelens, W., and Slingsby, C. (2005). Wrapping the alpha-crystallin domain fold in a chaperone assembly. *J. Mol. Biol.* 353, 68–79.
- Stromer, T., Ehmsperger, M., Gaestel, M., and Buchner, J. (2003). Analysis of the interaction of small heat shock proteins with unfolding proteins. *J. Biol. Chem.* 278, 18015–18021.
- Stromer, T., Fischer, E., Richter, K., Haslbeck, M., and Buchner, J. (2004). Analysis of the regulation of the molecular chaperone Hsp26 by temperature-induced dissociation: the N-terminal domain is important for oligomer assembly and the binding of unfolding proteins. *J. Biol. Chem.* 279, 11222–11228.
- Susek, R.E., and Lindquist, S.L. (1989). hsp26 of *Saccharomyces cerevisiae* is related to the superfamily of small heat shock proteins but is without a demonstrable function. *Mol. Cell. Biol.* 9, 5265–5271.
- van Montfort, R.L., Basha, E., Friedrich, K.L., Slingsby, C., and Vierling, E. (2001). Crystal structure and assembly of a eukaryotic small heat shock protein. *Nat. Struct. Biol.* 8, 1025–1030.
- Walter, S., and Buchner, J. (2002). Molecular chaperones-cellular machines for protein folding. *Angew. Chem. Int. Ed. Engl.* 41, 1098–1113.
- White, H.E., Orlova, E.V., Chen, S., Wang, L., Ignatiou, A., Gowen, B., Stromer, T., Franzmann, T.M., Haslbeck, M., Buchner, J., and Saibil, H.R. (2006). Multiple distinct assemblies reveal conformational flexibility in the small heat shock protein hsp26. *Structure* 14, 1197–1204.